Fakultät für Medizin
Institut für Klinische Chemie und Pathobiochemie
Klinikum rechts der Isar

Balanced signaling strength in chronic lymphocytic leukemia

Veronika Ecker

Vollständiger Abdruck der von der Fakultät für Medizin der Technischen Universität München zur Erlangung des akademischen Grades eines
Doktors der Naturwissenschaften (Dr. rer. nat.)
genehmigten Dissertation.

Vorsitzender: Prof. Dr. Percy A. Knolle
Prüfer der Dissertation:
1. TUM Junior Fellow Dr. Maike Buchner-Mayr
2. Prof. Dr. Bernhard Küster

Die Dissertation wurde am 24.04.2020 bei der Fakultät für Medizin der Technischen Universität München eingereicht und durch die Fakultät für Medizin am 6.10.2020 angenommen.

Zusammenfassung

Veränderungen in der B-Zell-Signaltransduktion können Immundefizienz, Autoimmunität oder eine maligne Transformation verursachen, indem bestimmte Kontrollmechanismen der Zelle umgangen werden. Im ersten Teil dieser Arbeit haben wir untersucht, ob eine B-Zellspezifische Expression und Aktivierung des RANK-Rezeptors (Rezeptoraktivator von NF-κB) zu Transformation von B-Zellen führt. Vorherige Arbeiten haben gezeigt, dass Mäuse mit B-zellspezifischer Expression, der RANK(K240E)-Mutation, welche beim diffusen großzelligen B-Zelllymphom (DLBCL) nachgewiesen wurde, eine Autoimmunerkrankung mit spezifischen Merkmalen des systemischen Lupus erythematodes (SLE) entwickeln. Im Fokus dieser Arbeit stand die Frage ob Mäuse mit einer RANK(K240E)-Mutation, die trotz ihrer Autoimmunität länger als 10 Monate überlebten, eine maligne B-Zell-Transformation entwickeln. In der Tat haben wir eine starke Anreicherung von RANK(K240E)-getriebenen B1a-Zellen in diesen gealterten RANK-transgenen Mäusen gefunden. Die $CD5^+$ RANK-getriebenen B-Zellen, sind nach der Transplantation in immunkompetente Empfängermäuse angewachsen, klonal expandiert und waren weiterhin von RANKL abhängig, um zu überleben. Der Phänotyp der transformierten RANK-getriebenen B-Zellen ähnelte stark der monoklonalen, indolenten Krankheit chronische lymphatische Leukämie (CLL), einer der häufigsten malignen B-Zellerkrankungen in westlichen Ländern. Wir konnten außerdem zeigen, dass sowohl die von transgenen TCL1-Mäusen stammenden murinen CLL und von Patienten stammenden humane CLL-Zellen für ein optimales Wachstum und Überleben *in vitro* und *in vivo* von RANKL abhängig sind. Zusammenfassend konnten wir die RANK/RANKL-Achse als kritisch für die CLL-Entwicklung und -Progression identifizieren und schlagen eine RANKL-Intervention durch Blockierung mit dem klinisch zugelassenen Medikament Denosumab, als mögliche neue therapeutische Option für CLL vor.

Im zweiten Teil dieser Arbeit haben wir eine neuartige, unkonventionelle Strategie getestet, um negative Regulatoren wichtiger Signalwege in der CLL zu hemmen und durch die resultierende Hyperaktivierung Zelltod zu induzieren. Der MAPK-Signalweg spielt eine entscheidende Rolle bei der CLL-Pathogenese. Klinische Versuche zur therapeutischen Intervention dieses Signalwegs sind jedoch bisher gescheitert. Im Rahmen dieser Arbeit wurde die Auswirkung der Inhibierung der Phosphatasen DUSP1/6, welche ERK, JNK und p38 dephosphorylieren, in CLL-Zellen untersucht. Die durch den niedermolekularen Inhibitor BCI vermittelte Hemmung von DUSP1/6 führte zu einer selektiven Zelltodinduktion in primären CLL-Zellen sowie CLL-Zelllinien. In einem genetischen Modell konnten wir diese Effekte durch die gezielte Ausschaltung von *DUSP1* und *DUSP6* in MEC-1-CLL-Zellen bestätigen. Eine Phosphoproteom-Analyse von Patienten- und MEC-1-CLL-Zellen nach BCI-Behandlung ergab eine signifikante Deregulierung der MAPK- und B-Zell-Rezeptor-Signatur, begleitet von den Merkmalen der Apoptose und der Induktion einer DNA-Schadensantwort. Die Aktivierung der Phosphorylierung von ATF2 und c-JUN wurde als potenzieller Auslöser der Zelltodinduktion ermittelt.

Zusammenfassend ergab unsere Studie, dass die Hemmung von DUSP1/6 und dadurch die Hyperaktivierung von MAPK ein potenziell nützlicher Ansatz für die Behandlung von CLL ist. Einen weiteren interessanten Angriffspunkt bietet der PI3K-Signalweg, der Überlebenssignale in CLL-Zellen steuert und bereits als therapeutisches Ziel genutzt wird. Die starke Toxizität dieser PI3K-Hemmung begrenzt jedoch die klinische Anwendung. Als neuen Therapieansatz haben wir die Auswirkungen der Hyperaktivierung des PI3K-Signals in der CLL durch Hemmung des negativen Regulators SHIP1 untersucht. Wir konnten die selektive Induktion des Zelltods in CLL-Zellen nach SHIP1-Hemmung durch die niedermolekularen Inhibitoren 3AC (*in vitro*) und K118 (*in vivo*) beobachten. Die genetische *SHIP1*-Deletion in MEC-1-CLL-Zellen bestätigte die Ergebnisse des zytotoxisch- und antiproliferativ-wirkenden Inhibitors. Interessanterweise spiegelte die akute Aktivierung von AKT, den Verlust der SHIP1-Funktion in CLL-Zellen wieder, und verzögerte das Fortschreiten der Erkrankung. Sowohl die SHIP1-Hemmung als auch die AKT-Hyperaktivierung in CLL-Zellen verminderte den bestehenden immunsuppressiven Charakter der CLL-Zellen und förderte die T-Zell-Aktivierung. Desweiteren konnte die Beteiligung von Nekroptose,

einer immunogenen Form des Zelltods, in Folge der SHIP1-Hemmung in CLL-Zellen gezeigt werden mit Calreticulin-Exposition und Freisetzung von HMGB1 und ATP. Klinisch relevante, neu auftretende BTK-Resistenzen gehen mit einer erhöhten PI3K-Signalübertragung einher und wir konnten zeigen, dass Kinase-Inhibitor-resistente MEC-1-CLL-Zellen eine erhöhte Sensitivität gegenüber SHIP1-Inhibition aufweisen. Zusammenfassend konnten wir aufzeigen, dass SHIP1 eine entscheidende limitierende Rolle bei der AKT-Signalübertragung spielt, um das Überleben der CLL-Zellen und die Immunsuppression zu fördern. Daher schlagen wir eine vorübergehende SHIP1-Hemmung, mit einem hohen Potenzial zur Wiederherstellung einer T-Zell-Immunantwort, als neuartigen Therapieansatz für die CLL vor.

Zusammenfassend hebt unsere Studie die Bedeutung von intermediären Signalstärken für das Überleben von CLL-Zellen und das Fortschreiten der Krankheit hervor. Einerseits benötigen CLL-Zellen Signale aus ihrer Umgebung, und unsere Arbeit ergab, dass RANK ein neuartiger entscheidender Vermittler dieser Aktivierung ist. Therapeutische Inhibition von RANK führte zu einer Verringerung der Signalübertragung und des CLL-Überlebens. Andererseits konnten wir zeigen, dass die Signalhyperaktivierung eine attraktive neue Strategie für die CLL-Therapie darstellt, mit der sich auch Resistenzen, die aus der Kinasehemmung entstehen, behandeln lassen.

Abstract

Aberrant B cell signaling can result in immunodeficiency as well as autoimmunity or malignant transformation by evading specific control checkpoints. In the first part of this work, we focused on how altered signaling downstream of the receptor RANK (Receptor Activator of NF-κB) in B cells results in malignant B cell transformation. Previous work has revealed that mice with B cell specific expression of the diffuse large B-cell lymphoma (DLBCL)-derived RANK(K240E) mutation develop an autoimmune disease with specific features of systemic lupus erythematosus (SLE). In this study, we evaluated whether RANK(K240E) induces malignant B cell transformation in mice that survived for longer than 10 months despite their autoimmunity. Indeed, we detected a striking enrichment of RANK(K240E)-driven B1a cells in these aged RANK-transgenic mice. The $CD5^+$ RANK-driven B cells clonally engrafted and expanded upon transplantation in immunocompetent recipients, and they still relied on RANKL for survival. The phenotype of the transformed RANK-driven B cells closely resembled the monoclonal, indolent disease chronic lymphocytic leukemia (CLL), one of the most prevalent B cell malignancies in Western countries. Importantly, we also showed that murine CLL, derived from TCL1 transgenic mice, and patient-derived human CLL cells depend on RANKL for optimal growth and survival *in vitro* and *in vivo*. Taken together, we identified the RANK/RANKL axis to be critical for CLL development and progression and propose RANKL intervention by blocking antibodies, with the clinically approved drug Denosumab, as a potential novel therapeutic option for CLL.

In the second part of this thesis, we tested a novel, unconventional strategy to inhibit negative regulators of important signaling pathways in CLL to induce activation-induced cell death. The MAPK signaling pathway plays a critical role in CLL pathogenesis. However, until now clinical attempts for therapeutic intervention of

this pathway have failed. Here, we evaluated the effects of hyperactivation of MAPK signaling in CLL cells by inhibition of the phosphatases DUSP1/6 via small molecule inhibitor BCI. We found selective cell death induction upon DUSP1/6 inhibition in primary CLL cells as well as the MEC-1 cell line model. We could confirm the effects of the inhibitor by genetic knockout of *DUSP1* and *DUSP6* in MEC-1 CLL cells. Phosphoproteome analysis of patient and MEC-1 CLL cells upon BCI treatment revealed a significant deregulation of the MAPK and BCR signature, accompanied by the features of apoptosis and induction of a DNA damage response. Activating phosphorylation on ATF2 and c-JUN were detected as potential mediators of cell death induction. Taken together, our study revealed small molecule inhibition of DUSP1/6 and hyperactivation of MAPK as a potentially useful approach for the treatment of CLL.

The PI3K signaling pathway is another important survival mediator for CLL cells and is therapeutically exploited for CLL. However, strong toxicities towards PI3K inhibition limit the clinical use. Here, we tested a novel approach to target the PI3K network and evaluated the effects of hyperactivation of PI3K signaling in CLL, by inhibition of the negative regulator SHIP1. We observed the selective induction of cell death in CLL cells upon SHIP1 inhibition by the small molecule inhibitors 3AC (*in vitro*) and K118 (*in vivo*). Genetic *SHIP1* deletion in MEC-1 CLL cells confirmed the cytotoxic and antiproliferative inhibitor results. Interestingly, loss of SHIP1 function in CLL cells was functionally equivalent to acute activation of AKT and delayed the disease progression. Both SHIP1 inhibition and AKT hyperactivation in CLL cells reverted the immunosuppressive character of CLL cells and promoted T cell activation. We found the involvement of necroptosis, an immunogenic form of cell death, upon SHIP1 inhibition in CLL cells. In line, Calreticulin exposure and release of HMGB1 and ATP were upregulated upon SHIP1 inhibition. Clinically relevant, emerging BTK resistances are associated with increased PI3K signaling and we show here that kinase inhibitor resistant MEC-1 CLL cells responded with increased sensitivity towards SHIP1 inhibition. In summary, we have shown that SHIP1 has a critical role to limit AKT signaling to promote CLL cell survival and immunosurveillance. Therefore, we propose transient SHIP1 inhibition as novel therapeutic approach in CLL, with high potential to restore T cell responses.

Taken together, our study highlights the importance of intermediate signaling levels for CLL cell survival and disease progression. On the one hand, CLL cells rely on signals derived from their environment and our study revealed RANK as a novel crucial mediator of this activation. Targeting RANK resulted in reduced signaling and CLL survival. On the other hand, we show that signal hyperactivation downstream of the BCR provides an attractive novel strategy for CLL therapy, with potential to treat resistances developed from kinase inhibition.

Abbreviations

3AC	3-a-aminocholestane
4-OHT	4-hydroxytamoxifen
ActB	beta-actin
AID	activation-induced deaminase
AKT	protein kinase B
AKT(E17K)	AKT glutamine to lysine mutation at position 17
ALL	acute lymphoblastic leukemia
allo-SCT	allogeneic hematopoietic stem cell transplantation
AML	acute myeloid leukemia
AMPK	5 -adenosine monophosphate (AMP)-activated protein kinase
AnxV	annexin-V
AP-1	activator protein 1
APC	antigen presenting cell
APRIL	a proliferation-inducing ligand
ATG	autophagy-related
ATM	ataxia telangiectasia tutated
BAD	Bcl-2-antagonist of cell death

BAFF	B-cell activating factor
BAFF-R	B-cell activating factor receptor
Bam32	B lymphocyte adapter protein
BCAP	phosphoinositide-3-kinase adaptor protein
BCI	(E)-2-benzylidene-3-(cyclohexylamino)-2,3-dihydro-1H-inden-1-one
BCI-HCl	BCI hydrochloride
BCL2	B-cell lymphoma 2
BCL6	B-cell lymphoma 6
BCMA	B-cell maturation antigen
BCR	B-cell receptor
BLIMP-1	B lymphocyte-induced maturation protein-1
BLK	B lymphocyte kinase
BLNK	B-cell linker
BMDC	bone marrow-derived dendritic cell
BMK1	big mitogen-activated protein kinase 1
BSA	bovine serum albumin
BTK	bruton‘s tyrosine kinase
CALR	calreticulin
CAR	chimeric antigen receptor
CBM	CARD11-BCL10-MALT1
cDNA	complementary deoxyribonucleic acid
CDR3	complementarity-determining region 3

CD40L	CD40 ligand
CFSE	carboxyfluorescein succinimidyl ester
CHK1	checkpoint-kinase 1
CK2	casein kinase 2
CLL	chronic lymphocytic leukemia
CLP	common lymphoid precursor
CMV	cytomegalovirus
CR	complement receptor
CRISPR/Cas9	clustered regularly interspaced short palindromic repeats/CRISPR associated protein 9
DAG	diacylglycerol
DAMP	damage-associated molecular pattern
DAPI	4 ,6-diamidin-2-phenylindol
DDR	DNA damage response
DNA	deoxyribonucleic acid
dNTP	deoxynucleotide triphosphate
DLBCL	diffuse large B-cell lymphoma
Dok	docking protein
DUSP	dual specificity protein phosphatase
E17K	glutamate to lysine at position 17
EBF	early B cell factor 1
EPR	enhanced permeability and retention
ERK	extracellular-signal regulated kinase

eIF2α	eukaryotic translation initiation factor 2A
FBS	fetal bovine serum
FcγRIIB	Fcγ receptor IIB
FDA	food and drug administration
Fe-IMAC	iron immobilized metal ion affinity chromatography
FISH	fluorescence in situ hybridization
Flt3-L	Fms-like tyrosine kinase 3 ligand
GC	germinal center
GEP	gene expression profiling
GFP	green fluorescent protein
GM-CSF	granulocyte macrophage colony stimulating factor
Grb2	growth factor receptor-bound protein 2
GSK3	glycogen synthase kinase 3
HePTP	hematopoietic protein tyrosine phosphatase
HMGB1	high-mobility-group-protein B1
HpH-RP	nuclear localization sequence high pH reverse phase separation technique
HPLC	high performance liquid chromatography
HRP	horseradish peroxidase
HSC	hematopoietic stem cell
ICD	immunogenic cell death
Ig	immunoglobulin
IgH	immunoglobulin heavy chain

IgL	immunoglobulin light chain
IgVH	immunoglobulin variable heavy chain region
IKAROS	IKAROS family zinc finger protein 1
IL	interleukin
i.p.	intraperitoneal
IP3	inositol-1,4,5-trisphosphate
IRES	internal ribosomal entry site
IRF8	interferon regulatory factor 8
ITAM	immunoreceptor tyrosine-based activation motif
ITIM	immunoreceptor tyrosine-based inhibitory motif
ITAMi	inhibitory ITAM
i.v.	intravenous
JNK	c-Jun N-terminal kinase
K240E	lysine to glutamic acid at position 240
ko	knockout
LCA-2	lymphoid 2 progenitor
LN	lymph node
LPS	lipopolysaccharid
Luc	luciferase
LYN	Lck/Yes novel tyrosine kinase
MACS	magnetic-activated cell sorting
MAPK	mitogen-activated protein kinase
MAP3K	MAP kinase kinase kinase

MAPKp38 mitogen-activated protein kinase

MBL monoclonal B lymphocytosis

mCAT1 mouse cationic amino acid transporter 1

MCL1 myeloid cell leukemia 1

MDM2 mouse double minute 2 homolog

MDSC myeloid-derived suppressor cell

MEC-1 Eco MEC-1 expressing ecotropic receptor Slc7a

MEK mitogen-activated protein kinase kinase

MFI mean fluorescent intensity

MHC major histocompatibility complex

mIg membrane immunoglobulin

miR microRNA

MLKL mixed lineage kinase domain-like protein

MPP multipotent progenitor cell

MPS mononuclear phagocyte system

mRNA messenger RNA

MS mass spectrometry

MSCV murine stem cell virus

mTORC1 mechanistic target of rapamycin complex 1

mTORC2 mechanistic target of rapamycin complex 2

myrAKT myristoylated AKT

NFAT nuclear factor of activated T-cells

NF-κB nuclear factor kappa-light-chain-enhancer of activated B-cells

NLC	nurselike cell
NLS	nuclear localization signal
NSG	NOD.Cg-Prkdcscid Il2rgtm1WjI/SzJ
OS	overall survival
p	phosphorylated
PAMP	pattern recognition receptor
PARP	poly(ADP-ribose)-polymerase 1
Pax5	paired box gene 5
PB	peripheral blood
PBMC	peripheral blood mononuclear cell
PBS	phosphate-buffered saline
PCR	polymerase chain reaction
PD-1	programmed cell death protein 1
PDK1	phosphoinoisitide dependent kinase 1
PEA15	phospho-enriched protein in astrocytes 15 kDa
PenStrep	penicillin-streptomycin
PH	pleckstrin homology
PI-4,5-P2	phosphatidylinositol (4,5)-bisphosphate
PI-3,4-P2	phosphatidylinositol (3,4)-bisphosphate
PI-3,4,5-P3	phosphatidylinositol (3,4,5)-trisphosphate
PI3K	phosphoinositide 3-kinase
PK	pharmacokinetic
PKC-β	protein kinase C beta

PLCγ2	phospholipase C gamma 2
PM	polymeric micelle
pMIG	plasmid MSCV IRES GFP
Poly (I:C)	polyinosinic:polycytidylic acid
PP2	protein phosphatase 2
PRR	proline-rich region
PS	phosphatidylserine
PTEN	phosphatase and tensin homolog
PTP-SL	protein tyrosine phosphatases SL
RAF	rapidly accelerated fibrosarcoma
RAG1/2	recombinase activating genes 1 and 2
RAS	rat sarcoma
RasGRP3	RAS guanyl releasing protein 3
RANK	receptor activator of nuclear factor-κ B
RANKL	RANK ligand
RIP1	receptor-interacting serine/threonine-protein kinase 1
RIP3	receptor-interacting serine/threonine-protein kinase 3
RNA	ribonucleic acid
SASP	senescence-associated secretory phenotype
Ser473	serine site at postion 473
sgRNA	single guide ribonucleic acid
SH2	Src homology 2
SH3	Src homology 3

Shc	Src homology 2 domain containing
SHIP1	Src homology 2 (SH2) domain containing inositol polyphosphate 5-phosphatase 1
SHP-1	Src homology region 2 domain-containing phosphatase-1
shRNA	short hairpin ribonucleic acid
SLC	surrogate light chain
SLE	systemic lupus erythematosus
SLL	small lymphocytic lymphoma
SPK	stress-activated protein kinase
sSHIP	stem cell-restricted SHIP
STAT	signal transducer and activator of transcription
STEP	striatal-enriched protein tyrosine phosphatase
SYK	spleen tyrosine kinase
TACI	transmembrane activator and CAML interactor
TAM	tamoxifen
TAPP	tandem-pleckstrin-homology-domain-containing protein
TBS-T	tris-buffered saline with tween20
TCL1	T cell leukemia/lymphoma protein 1
TD	thymus dependent
TdT	terminal deoxynucleotidyl transferase
tg	transgenic
Thr308	threonine site at position 308
TI	thymus independent

TLR	toll-like receptor
TMT	tandem mass tag
TNFRSF	tumor necrosis factor receptor superfamily
TRAF	TNF receptor-associated factor
Treg	regulatory T cell
TSC1/2	tuberous sclerosis proteins
USP7	ubiquitin-specific-processing protease 7
VH	heavy-chain variable
VL	light-chain variable
WES	whole exome sequencing
wt	wildtype
Y643H	tyrosine to histidine at position 643
ZAP-70	zeta-chain (TCR) associated protein kinase 70kDa

Contents

Zusammenfassung **II**

Abstract **IV**

Abbreviations **VIII**

Table of Contents **XVIII**

1 Introduction **1**

1.1 Immune system and adaptive immunity 1

1.1.1 B cell development 2

1.1.2 B cell selection 7

1.1.3 TNFRSF family 8

1.2 Chronic lymphocytic leukemia 10

1.2.1 CLL pathogenesis and cellular origin 11

1.2.2 The role of BCR signaling in CLL 13

1.2.3 CLL and microenvironment co-evolution 21

1.2.4 CLL prognosis and treatment options 22

1.2.5 Drug delivery and release 24

2 Research Aims and Objective **27**

3 Material **31**

3.1 Chemicals and reagents . . . 31

3.2 Antibodies . . . 31

3.2.1 Western Blot antibodies . . . 31

3.2.2 Therapeutical antibody . . . 33

3.2.3 Flow cytometry antibodies . . . 33

3.3 Cell stimulation / binding reagents . . . 35

3.4 Inhibitors . . . 35

3.5 Primer . . . 36

3.5.1 Genotyping . . . 36

3.5.2 Ig Clonality PCR . . . 36

3.5.3 CRIPR/Cas9 sgRNA oligonucleotides . . . 37

3.5.4 Amplification and sequencing of CRISPR/Cas9 targeted DNA segments . . . 38

3.6 Cell lines . . . 39

3.7 Patient samples . . . 40

3.8 Mouse models . . . 40

3.9 Transfection reagents . . . 42

3.10 Plasmids . . . 42

3.11 Kits . . . 43

3.12 Buffer . . . 44

4 Methods **47**

4.1 Polymerase Chain Reaction . . . 47

4.2 DNA isolation . . . 52

4.3 Bacterial transformation . . . 53

4.4 Nucleofection-based transient transfection 53
4.5 Virus production and stable transduction 54
4.6 Cell selection upon nucleofection or viral manipulation 56
4.7 Cell Culture 56
4.8 Cell Lysate preparation and Western Blot 61
4.9 Fe-IMAC phosphopeptide enrichment 62
4.10 Flow Cytometry 63
4.11 Fluorescence-activated cell sorting (FACS) 65
4.12 ATP measurement by luminescence-based assays 66
4.13 Transplantation experiments 66
4.14 RANK-RANKL interference *in vivo* 67
4.15 Negative feedback inhibition *in vivo* 67
4.16 Regular blood draws 69
4.17 IVIS bioimaging 69
4.18 Data analysis 70

5 Results **71**

5.1 Pathological RANK signaling in CLL 71
5.1.1 RANK(K240E) expression drives a CLL-like disease in aged mice 71
5.1.2 RANK/RANKL signaling is important for CLL cell survival 77
5.2 DUSP1/6 inhibition in CLL as novel therapeutic approach 81
5.2.1 DUSP1 and DUSP6 are readily expressed and may have prognostic value 81

5.2.2 Inhibition of DUSP1/6 by small molecule inhibitor BCI induces cell death in CLL 83

5.2.3 Validation of distinct BCI-nanoparticle formulations to improve the *in vivo* application 86

5.2.4 Genetic deletion of *DUSP1/6* confirms small molecule inhibitor (BCI) effects 90

5.2.5 Mechanism of cell death induction by DUSP1/6 inhibition 92

5.2.6 DUSP1/6 inhibition in drug-resistant CLL 98

5.3 SHIP1 is critical for CLL progression and immunosurveillance 99

5.3.1 SHIP1 is expressed and active in CLL 99

5.3.2 Inhibition of SHIP1 phosphatase activity reduces CLL cell survival and disease progression 99

5.3.3 Genetic confirmation of small molecule inhibitor (3AC) effects 108

5.3.4 SHIP1 phosphatase activity is critical for CLL immunosurveillance 118

5.3.5 SHIP1 inhibition in drug-resistant CLL 122

6 Discussion **124**

7 Summary and Outlook **138**

Bibliography **141**

8 Acknowledgements **i**

Chapter 1

Introduction

1.1 Immune system and adaptive immunity

B cells represent, together with T cells, the components of the adaptive immune system that provides specific and long enduring immune responses against pathogens in the human body. In contrast, the innate immunity comprising cells of the myeloid lineage, such as macrophages, neutrophils, and dendritic cells, provides a rapid, less specific response to invading foreign organisms. Thereby, innate immunity initiates inflammation and bridges from the innate to the adaptive immune response through the presentation of processed antigens to lymphoid B and T cells. Adaptive lymphoid immune cells are highly antigen-specific and capable of forming a memory against previous encountered antigens to provide sustained protection [Janeway et al., 1996]. To fulfill this antigen specificity, lymphoid cells express a specific antigen receptor (B cell receptor/T cell receptor) on the cell surface. It is generated by a highly diverse process of somatic gene rearrangements during the early development of both B and T cells. Both cell types emerge from common lymphoid progenitors in the bone marrow, however T cells follow a distinct developmental path via migration into the thymus, whereas B cell remain in the bone marrow for proper antigen receptor rearrangement. Immature lymphoid cells then migrate into the secondary lymphoid organs, such as lymph node and spleen, in order to encounter antigen provided by antigen presenting cells (APCs) in the microenvironment. Upon intact antigen recognition and with help of cytokine secretion from the microenvironment, B cells initiate humoral responses

by antibody secretion, which contributes to antigen elimination. T cells, in contrast to B cells, can only recognize phagozytosed and processed antigens presented on major histocompatibility complex (MHC) (I/II) molecules on the cell membrane of APCs, can exert direct lytic cell-mediated responses. CD8 positive T cells are the subtype that fulfill such cytotoxic actions (MHC I), whereas CD4 positive T cells (MHC II) secrete cytokines and thus contribute to other cellular responses to result in antigen elimination. [Janeway et al., 1996]. Consequently the functional and protective end point is antibody production by terminally differentiated plasma B cells.

1.1.1 B cell development

Alterations in B cell development and selection can result in autoimmunity or other hematological malignancies such as CLL and the detailed development of B cells is described in the following section and comprises "conventional" B2 B cells as well as B1 B cells.

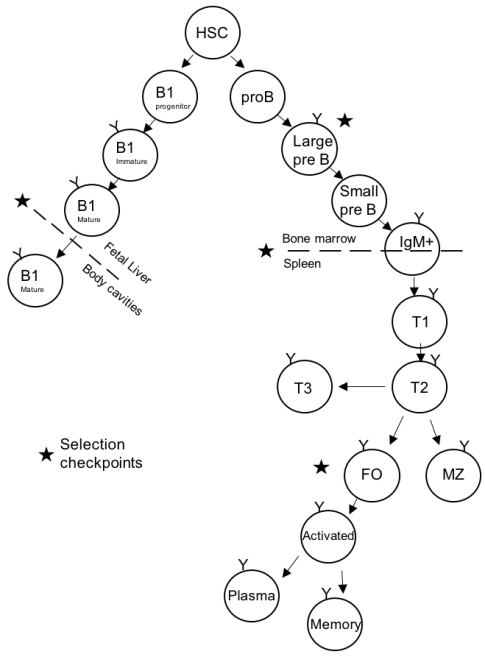

Figure 1.1: Schematic overview of B1 and B2 cell development. HSC: hematopoietic stem cell, T: transitional B cells, FO: follicular B cell, MZ: marginal zone B cell.

1.1.1.1 B2 cell development

Conventional B cell development is initiated by migration of multipotent progenitor cells (MPPs) first into the fetal liver and then into the bone marrow throughout life. MPPs further differentiate into the common lymphoid precursor (CLP) which produces the lymphoid 2 progenitor (LCA-2), responsible for the B cell lineage [LeBien and Tedder, 2008]. Signals from the bone marrow stroma, such as interleukin (IL)-7 and Fms-like tyrosine kinase 3 ligand (Flt3-L) and transcription factors including PU.1, IKAROS family zinc finger protein 1 (IKAROS), E2A, early B cell factor 1 (EBF), paired box gene 5 (Pax5), and interferon regulatory factor 8 (IRF8) further induce B cell development [Tobón et al., 2013]; [Melchers, 2015]. The critical step of clonal B-cell receptor (BCR) formation is then initiated in B cell progenitor cells. To note, the heavy and light chain loci of immunoglobulins (Igs) comprise a multitude of V (variable), several D, (diversity - only on heavy chain gene), J (joining), and C (constant region) exons. Gene rearrangement and nucleotide insertions at junctions are mediated by VDJ recombinase, which is a diverse collection of enzymes [Tonegawa, 1983]; [Alt et al., 1984]. Terminal deoxynucleotidyl transferase (TdT) and recombinase activating genes 1 and 2 (RAG1/2) are essential during this process, and become induced in response to bone marrow stroma cell-derived cytokines. As initial event D and J gene segments are joined on the heavy chain chromosome (D-JH) resulting in early pro-B cells. In the late pro-B cell stage an additional V segment is joined to the D-JH gene segment and following successful VHDJH recombination; the pre-B cell stage begins. By pairing of the resulting heavy chain with the so-called surrogate light chain (SLC), which consists of $\lambda 5$ and VpreB, the pre-BCR (expressed on the cell surface) is formed, which includes the intracellular association of Ig-α and Ig-β signaling modules. Pre-BCR signaling further drives B cell development and downregulates RAG1/2 levels, which results in increased proliferation, marking the large pre-B cell stage [Kitamura et al., 1992]. Finally, large pre-B cells halt proliferation and RAG1/2 proteins are expressed again, which marks the small pre-B cell stage and induces light chain rearrangement at either the Ig-κ or -λ light chain loci. The correctly assembled BCR is then expressed as IgM on the surface of immature B cells. To note, B cell development in the bone marrow is similar in mouse and human, however only murine pro-and pre-B cells depend on

IL-7 signaling for survival and differentiation and human B cells are IL-7-independent [Nuñez et al., 1996]; [LeBien, 2000].

Within several days, those immature B cells will then enter the circulation as transitional B cells, subdivided into three groups, namely T1, T2, and T3 B cells, respective their surface marker expression and function [Palanichamy et al., 2009]. T1 cells mature into T2 B cells via B-cell activating factor (BAFF)/BAFF receptor, a proliferation-inducing ligand (APRIL), transmembrane activator and CAML interactor (TACI), and B-cell maturation antigen (BCMA) signaling (Naradikian et al. 2014). This occurs primarily in the spleen and T2 cells reside in the follicles, where antigen-based selection processes are continued to select for low-avidity to self antigens, whereas high affinity self-antigen recognizing B cells are deleted [Chung et al., 2002]. Afterwards T2 B cells either circulate until they encounter their respective antigen and organize in so called germinal centers (GCs), associated with somatic hypermutation to allow the generation of high affinity antigen receptors, or do not circulate and stay in the marginal zones [Tobón et al., 2013]. Antigen-selected B cells leave the GC and turn into memory B cells or plasmablasts.

There are two routes to B cell activation and initiation of the humoral immune response, which depend on the nature of the antigen. Non-protein antigens such as lipids, nucleic acids and glycoproteins stimulate antibody production in the absence of T cells and are referred to as thymus independent (TI) antigens. TI responses are often of shorter duration and comprise typically IgM with low affinity for the antigens. TI antigens can further be divided in type I antigens (lipopolysaccharid (LPS), CpG, polyinosinic:polycytidylic acid (Poly (I:C))) that induce B cell activation in immature and mature cells via toll-like receptors, and type II antigens that are generally polysaccharides and act by crosslinking the BCRs of mature B cells that are specific for antigens [Janeway et al., 1996]. Typically within 2-3 weeks, most of those plasma cells die, however, some persist long term and also memory B cells can be formed [Obukhanych and Nussenzweig, 2006].

In contrast, the antibody response to protein antigens requires both B and T cell involvement and these antigens are described as thymus dependent (TD) antigens. This T cell-dependent B cell activation occurs in two spaciotemporaly distinct phases, at the interface of T cell area and primary follicles and in the GCs within lymphoid

follicles. Upon 1-2 days of antigen exposure, naïve $CD4^+$ T cells become activated through recognition of antigens presented by APCs in the T cell area of lymphoid organs. At the same time, B cells recognize the same antigen and move from the follicle into the T cell area upon activation. The T and B cell interaction at this interface occurs 3-7 days upon antigen exposure. In detail, when B cells bind antigens via their Ig receptors, the expression of co-stimulatory receptors on B cells is increased. B cells then internalize the antigen bound receptor via endocytosis and process it into peptide fragments that can be presented on the cell membrane via MHC Class II molecules to cognate $CD4^+$ T cells. This interaction is further enhanced by binding of CD28 on the T cells to B7-1 and B7-2 on B cells, which results in T cell proliferation. Upon activation, T cells express CD40 ligand (CD40L) which further binds CD40 on B cells, resulting in transcription of Ig genes, the release of T cell cytokines, and B cell proliferation. Cytokines direct the process of isotype class switching that leads to the production of antibodies with heavy chains of different classes. Mechanistically, the VDJ gene segment recombines with a downstream C region gene and deletes the intervening section, resulting in a switch recombination. Some proliferating B cells differentiate into effector antibody secreting cells with antibodies of the same specificity as the initial antigen recognizing Ig receptor and reside in extrafollicular sites of lymphoid tissue, or they can migrate to the bone marrow 2-3 weeks after antigen exposure.

The late phase of T cell-dependent B cell activation occurs during GC formation. Within 4-7 days of antigen exposure, clusters of proliferating B cells center at the borders of B cell follicles and T cell zones in the lymph nodes and spleen and build temporary structures, named GCs [Nieuwenhuis and Opstelten, 1984]; [Jacob et al., 1991]. There, particularly affinity maturation takes place, which enables the formation of memory B cells and long-lived plasma cells. In detail, GCs contain cells derived from only one or a few antigen-specific B cell clones. Follicular dendritic cells, found only in lymphoid follicles, express complement receptors (CRs) (CD35/CR1, CD21/CR2, CD11b/CD18 (CR3)), Fc receptors, and CD40L, which stimulate GC B cell proliferation and accumulation in the basal dark zone of the GC. The generation of high affinity antigen specific antibodies is mediated through somatic mutations in Ig genes followed by selective survival of B cells producing

antibodies with highest affinity. Somatic hypermutation induces point mutations into the V(D)J region of the rearranged gene loci. The gene activation-induced deaminase (AID) is crucial as it mediates both somatic hypermutation and isotype class switching [Muramatsu et al., 2000]. After successful GC reaction, some of the antigen activated B cells develop into memory B cells that can fulfill rapid antibody response upon secondary exposure to an antigen.

1.1.1.2 B1 cell development

In contrast to classical B2-type B cells, B1-type B cells comprise a unique subset of B cells, present in mice and humans, yet less well characterized in the latter. B1 cells are further subdivided in B1a, which express CD5 and contribute to a more innate type of immune response and B1b, which lack CD5 expression and can fulfill more adaptive immune responses [Berland and Wortis, 2002]; [Hardy, 2006]. In the mouse, they comprise the main cell population in the peritoneal and pleural cavities and are found rarely in the spleen or lymph nodes [Montecino-Rodriguez and Dorshkind, 2012]. They derive from the fetal liver and are sustained in the periphery by self-renewal with slow turn-over rates [Godin et al., 1993]. It is controversially discussed whether B1 and B2 B cells derive from a common progenitor, whereas two distinct possibilities are facing each other: the antigen-dependent selection (the selection model), or instead the development from distinct precursors of separate lineages (the lineage hypothesis), whereas remarkable evidence was collected for the latter [Hardy, 2006]. B1 cell development strongly depends on BCR activation and subsequent nuclear factor kappa-light-chain-enhancer of activated B-cells (NF-κB) signaling. B1 cells may preferentially follow the TI, non-follicular activation pathway, as they appear to be much less dependent on T cell help [Tarlinton, 2006]. It was shown that the heavy chain V segments used by B1 B cells are more restricted compared to B2 B cells, resulting in a less diverse B cell repertoire [Rowley et al., 2007]. B1 cells are cross-reactive to self-antigens and B1 cell responses to BCR as well as toll-like receptor (TLR) ligation are tightly regulated. The general polyreactivity and secretion of low-affinity antibodies (mostly IgM) against antigens expressed by apoptotic cells and several pattern recognition receptors (PAMPs) ensures sustained BCR signaling and allows the B cells to escape negative selection during development

[Martin et al., 2001]; [Hogquist et al., 2003]. At the same time, several negative regulators limit the expansion of these polyreactive cells [Berland and Wortis, 2002]. CD5, and its associated immunoreceptor tyrosine-based inhibitory motif (ITIM) motif, plays a major role in the B1a compartment and also regulation via Lck/Yes novel tyrosine kinase (LYN), Src homology region 2 domain-containing phosphatase-1 (SHP-1), CD22, and Siglec G receptors as well as CD19 occur. In addition, the production of IL-10 is high in B1 B cells [Sindhava and Bondada, 2012]. B1 B cells are capable of class switching into any antibody *in vitro*, whereas *in vivo*, they preferentially switch to IgA [Baumgarth, 2011]. As mentioned, a population of $CD5^+$ B cells has also been discovered in adult humans, however, they do not reside in the peritoneal cavity as a distinct cell population. Although B1 B cells have various roles in tissue maintenance and pathogen elimination, their self-reactivity provides pathological potential and B1 B cells have been implicated in human and mouse autoimmune diseases, and elimination of B1 cells by genetic deficiency reduced autoimmunity in mouse models [Hayakawa et al., 1983]; [Duan and Morel, 2006].

1.1.2 B cell selection

When B cells respond to their specific antigen, the output can be proliferation, anergy, or apoptosis. The longterm goal of a B cell however is to develop into a highly selective antigen recognizing cell. The complex process of gene segment rearrangement is prone to errors. To ensure proper B cell development and functional BCR arrangement, several checkpoints exist to direct B cell selection [Melchers, 2015]. The first checkpoint occurs during assembly of the pre-BCR, where immunoglobulin heavy chain (IgH) fitness is probed during its assembly with the SLC. The second checkpoint tests the pre-BCR for autoreactivity of the IgH chain. And only if immunoglobulin light chain (IgL) chains with light-chain variable (VL) regions are expressed that fit the pre-expressed heavy-chain variable (VH) region of the IgH chain, IgM is displayed as BCR on immature B cells, with each B cell expressing monoclonaly one BCR. Thus a large repertoire of BCRs is required to ensure the selectivity and specificity of the adaptive immune response. The newly generated VH/VL repertoires of immature B cells then go through the next checkpoint, where

they encounter autoantigens. B cells with high-affinity autoreactive BCRs are deleted at this step, whereas B cells expressing low-affinity autoreactive BCRs are positively selected to exit the bone marrow and enter the periphery as B1-type B cells (gut- and lung-associated lymphoid tissues). In contrast conventional B2-type B cells do not recognize autoantigens, enter the periphery, and are directed to the spleen and lymph nodes. Importantly, more than 85% of the newly formed immature B cells in the bone marrow die as a consequence of high autoantigen recognition. Finally in the periphery, namely the spleen a fourth checkpoint controls the transition from immature to mature B cells. The antigen-presenting microenvironment drives proliferation and hypermutation and thus enables the development of a large repertoire of highly specific B cells, whereas autoreactive B cells upon hypermutation are eliminated or supressed [Melchers, 2015].

1.1.3 TNFRSF family

Cell surface receptors of the tumor necrosis factor receptor superfamily (TNFRSF) play very important roles in the regulation of B cell survival, selection, and expansion [Kawabe et al., 1994]; [Lesley et al., 2004]; [Luo et al., 2018]. Most important members are the B-cell activating factor receptor (BAFF-R), BCMA, as well as CD40 [Huang et al., 2011]; [Mackay and Schneider, 2009]. They are all well described to regulate normal B cell immunity and gain- and loss-of-function alterations in these TNFRSFs have been associated with various immunodeficiencies, autoimmune diseases, and B cell malignancies [Batten et al., 2004]; [Rickert et al., 2011]; [Smulski and Eibel, 2018]. Another additional TNFRSF with emerging roles in B cell pathology is receptor activator of nuclear factor-κ B (RANK), also termed TNFRSF11A. Several cell types including activated T cells, osteoblasts, and bone marrow stromal cells can produce its ligand RANK ligand (RANKL), also named TNFSF11. RANKL is available both as soluble and membrane-bound form. Upon binding to RANKL, RANK receptors trimerize and recruit TNF receptor-associated factors (TRAFs) 2,3,5 and 6 to their cytoplasmic tail to activate mitogen-activated protein kinases (MAPKs), the canonical and non-canonical NF-κB pathways, and the phosphoinositide 3-kinase (PI3K) pathway, which mediate depending on the

cell type multiple biological effects and are also well described to be active in CLL cells [scheme 1.2]; [Wada et al., 2006]; [Walsh and Choi, 2014]. RANK is normally expressed on multiple tissue types, particularly on osteoclast precursors, medullary thymic epithelial cells, lymphoid tissue inducer cells, mammary epithelial cells, and on dendritic cells [Anderson et al., 1997]; [Figgett et al., 2014]. On normal B cells, CD40L stimulation is described to induce RANK expression [Anderson et al., 1997]; [Yun et al., 1998] and RANK knockout mice show abnormalities in B cell development. In line with that, human patients with a mutation in the RANK gene possess B cell defects that represent as hypogammaglobulinemia and impaired antibody responses [Guerrini et al., 2008]. However, the analysis of B cell specific RANK knockout mice revealed that these abnormalities stem from a disturbed microenvironment in the bone marrow where B cells develop rather than from B cell intrinsic alterations [Perlot and Penninger, 2012]. Nevertheless, there is evidence emerging for roles of the RANK-RANKL signaling axis in B cell-mediated immune pathology. In Hodgkin's lymphoma, Hodgkin and Reed Sternberg cells co-express RANK and RANKL on their surface, leading to a positive feedback loop that enhances cell survival. Furthermore, multiple myeloma cells express RANKL or induce bone marrow stromal cells to overexpress RANKL, contributing to the development of bone lesions in myeloma patients [Fiumara et al., 2001]; [Michigami et al., 2000]; [Schmiedel et al., 2013]. In addition, CLL B cells have increased surface expression of RANK and RANKL, which leads to the induction of IL-8 secretion in CLL cells and a reduction in apoptosis [Schmiedel et al., 2013]; [Secchiero et al., 2006].

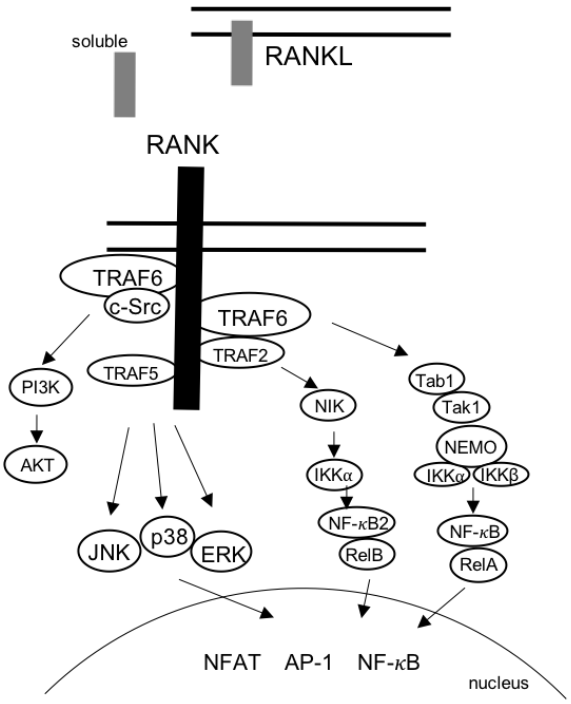

Figure 1.2: Schematic depiction of RANK/RANKL activation and downstream signaling.

Furthermore, a somatically acquired point mutation leading to a change of lysine to glutamic acid at position 240 (K240E) in the intracellular domain of RANK is recurrently detected in patients with DLBCL and has been suggested to be a gain of function alteration [Compagno et al., 2009]; [Davis et al., 2010]; [Wilson et al., 2015]. Nevertheless, despite these intriguing findings that suggest pathophysiological functions of aberrant RANK signaling in B cell pathology, the functional consequences of deregulated RANK signaling in B cells *in vivo* remain unclear.

1.2 Chronic lymphocytic leukemia

Chronic lymphocytic leukemia (CLL) is one of the most common hematologic malignancies in adults in the Western world. In Germany every year 7.4/100,000 males and 4.8/100,000 females get newly diagnosed with CLL and the median age of diagnosis is 70 to 75 years. However it is not unusual that younger individuals (30 to 39 years of age) are affected, whereas the incidence increases massively with age [Sabattini et al., 2010].

CLL is characterized as a disease of neoplastic B cells and is distinguished from small

lymphocytic lymphoma (SLL) by its leukemic manifestation. It is often preceded by an undiagnosed, clinically asymptomatic pre-stage with proliferation of clonal B cells, which are referred to as monoclonal B lymphocytosis (MBL). In >5% of over 60 year old individuals, an MBL is detectable. The risk of progression to a CLL requiring treatment is about 1% per year [Chiorazzi et al., 2005]. When $\geq$5x10e^9 B lymphocytes per liter are present in the peripheral blood, sustained for at least 3 months, it is no longer considered as MBL and the diagnosis of CLL is further confirmed. CLL B lymphocytes are of monoclonal character, which is determined by immunoglobulin light chain restriction (κ or λ). Besides, CLL cells appear as characteristically small and mature lymphocytes and present with a narrow border of cytoplasm and a dense nucleus lacking discernable nucleoli and partially aggregated chromatin [Hallek et al., 2018]. Immunophenotypically, CLL cells co-express the T cell surface antigen CD5 together with B cell antigens CD19, CD20 and CD23. Besides, low levels of surface Igs (IgM, IgD), intermediate B220, as well as low CD20 and CD79b are characteristic [Hallek et al., 2018]. Clinical manifestations comprise a blood lymphocytosis, which is often detected during regular blood checks in an asymptomatic stage. As the disease progresses, lymphadenopathy, spleno- and hepatomegaly, signs of bone marrow failure, and possibly autoimmune cytopenias occur. Clinical complaints can also present as 'B symptoms', namely fatique, night sweat, and unintentional weight loss, as well as an increased susceptibility to infections [Hallek et al., 2018].

1.2.1 CLL pathogenesis and cellular origin

Despite critical for the understanding of its pathogenesis, the cellular origin of CLL is still under debate. The fact that two distinct types of CLL exist, depending on the mutational status of the immunoglobulin variable heavy chain region (IgVH), increases the complexity. The IgVH gene can have rare and no mutations ("unmutated") or be clonally rearranged with 2% or more IgVH mutations ("mutated" CLL) [Oscier et al., 1997]; [Fais et al., 1998]. Investigation of CLL versus normal B cell subset transcriptomics from human blood and spleen revealed that IgVH unmutated CLL derives from unmutated mature CD5$^+$ B1-type cells and mutated CLL derives

from a distinct, previously unrecognized $CD5^+CD27^+$ post–germinal center B cell subset [Seifert et al., 2012]. Stereotypical V gene rearrangements are increased among $CD5^+$ B cells, providing independent evidence for a $CD5^+$ B cell origin. To note, those $CD5^+$ B cell populations comprise oligoclonal expansions, which can already be found in young healthy individuals and might represent an early phase before MBL occurs [Seifert et al., 2012]. In contrast to that hypothesis, detailed gene expression profiling (GEP) of CLL and normal human B cell subsets surprisingly indicated that mutated and unmutated CLL are both similar to memory B cells, but not $CD5^+$ B cells [Klein et al., 2001]. This further indicates that both CLL subsets originate from antigen-experienced B cells [Klein et al., 2001]; [Rosenwald et al., 2001]. The fact that 30% of CLL cases show highly similar IgV genes that can be grouped into >150 sets of stereotyped receptors, provides further support for specific antigen recognition [Stamatopoulos et al., 2007]; [Murray et al., 2008]. This strongly suggests that such CLL recognize common antigens and consequently B cell receptor (BCR) specificity plays an essential role in CLL pathogenesis.

Generally, the pathogenesis of CLL is charactrized by the inhibition of apoptosis and dysregulation of proliferation in B cells. Specific genetic alterations and their impact on signaling pathways contribute to the disease pathogenesis. There is evidence that mutations already occur in hematopoietic stem cells (HSCs), as HSCs isolated from CLL patients possess a lymphoid-lineage gene priming and produce a high number of polyclonal B cell progenitors [Kikushige et al., 2011]. In line, it was shown that CLL develops from pre-leukemic multipotent hematopoietic progenitors that carry somatic CLL-specific mutations [Damm et al., 2014]. Whole exome sequencing (WES) studies comparing CLL samples to matched germline DNA samples, have identified several distinct driver mutations in CLL that result in accelerated BCR, MAPK, PI3K, and NF-κB signaling and are involved in ribonucleic acid (RNA) processing/export and MYC activity [Landau et al., 2015]; [Puente et al., 2015]. Besides, associated with frequent TP53 and ataxia telangiectasia tutated (ATM) mutations, the DNA damage response (DDR) is frequently altered [Frenzel et al., 2016]. Taken together, those whole exome sequencing (WES) analysis showed a high degree of genetic variability among CLL patients, although the overall somatic mutation rate was significantly lower than in solid tumors [Pleasance et al., 2010]; [Fabbri et al., 2011];

[Puente et al., 2011]; [Wang et al., 2011].
Until now, the question in which stage of B cell development CLL B cells evolve is not fully solved, yet a very important role of the BCR during CLL pathogenesis is very well recognized and described in the following [Buchner and Müschen, 2014].

1.2.2 The role of BCR signaling in CLL

B cell activation via interaction between the BCR and specific antigens plays a crucial part in the immune system since it regulates development, proliferation, differentiation, and consequently humoral immune response [Cambier et al., 1994]. Thereby, BCR signaling allows for the expansion of selected, foreign antigen-specific B cells, and deletion of unwanted, self-reactive B cells. Because mature B cells express only one type of BCR for a specific antigen (clonal BCR distribution), a large repertoire of BCRs is required to ensure the selectivity and specificity of the adaptive immune response.
B cell receptor signaling has a central pathogenic role in CLL, which is reflected by the striking success of BCR signaling inhibitors for CLL therapy
[Ten Hacken and Burger, 2016]. According to the current view, both CLL types (IgVH mutated and unmutated) derive from antigen-experienced cells. Based on the finding that the IgVH repertoire is highly restricted (1% with nearly identical complementarity-determining region 3 (CDR3) region) and biased (20% with biased IgVH segment usage), as compared to the normal adult B-cell repertoire, it has been hypothesized that CLL cells are selected by some sort of antigenic pressure [Mauerer et al., 2005]; [Messmer et al., 2004]. This is in line with the absence of activating pathway mutations, as they occur for example in DLBCL. In CLL either autoantigens or antigens derived from apoptotic cells or pathogens are essential to trigger CLL pathogenesis [Kil et al., 2012]. Recent studies raise an additional target of BCR recognition, which is the binding of an intrinsic IgVH motif [Dühren-von Minden et al., 2012].

1.2.2.1 BCR activation

The BCR complex comprises a multiprotein complex with membrane bound antibody structure, which consists of a ligand binding moiety, the antigen-binding trans-membrane immunoglobulin (mIg), and its intracellularly associated Igα/Igβ heterodimers (CD79A/CD79B) crucial for signal transduction. After antigen-dependent membrane movement and aggregation of the BCR, Src kinases (LYN, Fyn, B lymphocyte kinase (BLK)) phosphorylate the immunoreceptor tyrosine-based activation motifs (ITAMs) in the cytoplasmic tails of CD79A and CD79B. As mentioned, in CLL also ligand-independent (autonomous BCR signaling) is described [Dühren-von Minden et al., 2012]. Phosphorylated ITAMs recruit then the spleen tyrosine kinase (SYK), which becomes activated by phosphorylation of tyrosines, and propagates further downstream signaling networks. Activation of SYK is critical, as it induces further targets comprising the adaptor proteins, such as CD19, B-cell linker (BLNK), and bruton's tyrosine kinase (BTK), and signaling enzymes, such as phospholipase C gamma 2 (PLCγ2), protein kinase C beta (PKC-β), PI3K, and the guanine nucleotide exchange factor Vav [Benkisser-Petersen et al., 2016]; [Buchner et al., 2009]. Signals evolving from those signalosomes initiate and regulate further downstream signaling systems including signal transducer and activator of transcription (STAT) signaling, the rat sarcoma (RAS)/rapidly accelerated fibrosarcoma (RAF)/mitogen-activated protein kinase kinase (MEK)/extracellular-signal regulated kinase (ERK) pathway and CARD11-BCL10-MALT1 (CBM)-mediated NF-κB, which activate transcription factors that are significant for B cell fate decisions, such as proliferation, survival, differentiation, cytoskeleton rearrangement, internalisation of BCR antigen complexes, and cell death [Su et al., 1999]; [Turner et al., 2000]. As mentioned, CLL B cells vary in their signaling capacity in response to BCR stimulation depending on their mutational status (increased BCR signaling in more aggressive unmutated CLL), whereas in general, CLL cells show diminished responses towards BCR stimulation [Lankester et al., 1995].

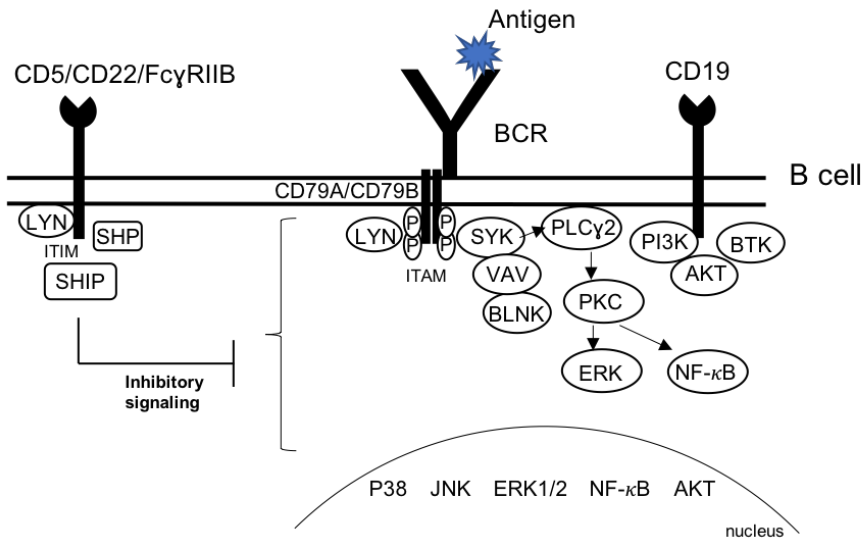

Figure 1.3: Overview of BCR activation and signaling including respective stimulatory and inhibitory co-receptors.

Not only the BCR itself controls normal B cell development, but also dedicated co-receptors integrate cues from the B cell microenvironment [Bannard and Cyster, 2017]; [Kwak et al., 2019]; [Nemazee, 2017]. During physiological BCR activation, the magnitude and duration of signaling is tightly controlled by a dynamic interplay between activating and inhibiting mechanisms that act in complex processes. Transmembrane receptors possess ITAM or ITIM cytoplasmic domains and serve as docking platforms for several stimulatory or inhibitory molecules that can accelerate or terminate BCR signalosomes. Recently, the discrimination has become less stringent between ITAM and ITIM motifs with the identification of inhibitory ITAM (ITAMi) sequences [Getahun and Cambier, 2015].

1.2.2.2 Stimulatory and inhibitory BCR feedback regulation

B cells recognize antigen often in the form of a complex ligand, which connects the BCR and other cell-surface receptors. For example upon BCR activation, LYN-mediated phosphorylation of tyrosine kinases, such as SYK, can phosphorylate tyrosines in the cytoplasmic domain of the positive regulator CD19, which then further serves as docking site for Vav or PI3K and thus accelerates downstream

signaling [DeFranco, 1996].

In addition, several signals from inhibitory co-receptors are integrated upon BCR activation and they downmodulate the BCR signaling by setting a signaling threshold that prevents B cell overstimulation. Activation of these inhibitory co-receptors (e.g. CD5, CD22, Fcγ receptor IIB (FcγRIIB)) takes place by phosphorylation of their intracellular ITIMs and subsequent recruitment of phosphatases (e.g. SHP-1, Src homology 2 (SH2) domain containing inositol polyphosphate 5-phosphatase 1 (SHIP1)) [Tsubata, 2012]; [Nitschke, 2005]. LYN is the major player to phosphorylate such ITIM motifs and thus serves as both positive and negative regulator during BCR signaling, reflecting the complexity of regulation.

For example CD5, which is aberrantly expressed on CLL cells, is physiologically known to rescue B1 subtype B cells from apoptosis and prevent their differentiation towards autoantibody producing plasma cells by decreasing the activating signal [Ochi and Watanabe, 2000]. In CLL, constitutive activation of the BCR pathway is strictly required during its pathogenesis, however, the negative regulation of BCR activation suggests the selection for intermediate and controllable BCR signal during disease evolution.

1.2.2.3 MAPK activation and negative regulation

Aberrant activation of MAPK signaling and its interactions with other cellular signaling pathways has been identified to be involved in the pathogenesis of CLL. Upon BCR activation, SYK induces PLCγ2, which leads to the hydrolysis of phosphatidylinositol (4,5)-bisphosphate (PI-4,5-P2) into inositol-1,4,5-trisphosphate (IP3) and diacylglycerol (DAG), further inducing the release of intracellular calcium and activation of the PKC-β. Active PKC-β then triggers the activation of MAPK signaling, comprising the four members ERK1/2, c-Jun N-terminal kinase (JNK)/stress-activated protein kinase (SPK), mitogen-activated protein kinase (MAPKp38), and ERK5/big mitogen-activated protein kinase 1 (BMK1). Apart from activation via the PLCγ2 pathway upon BCR stimulation, ERK can also be induced directly by RAS. It was shown that RAS guanyl releasing protein 3 (RasGRP3) can directly bind to RAF-1, the MAP kinase kinase kinase (MAP3K) in the ERK pathway and that activated RAF-1 subsequently phosphorylates MEK1/MEK2, which both in turn activate

ERK1/2. Phosphorylated ERK1 and ERK2 dimerize, which is essential for nuclear translocation and initiation of regulatory gene transcription. MAPK signaling is very well studied to be important for the regulation of a subset of genes responsible for cell proliferation, survival, and differentiation. In particular upon BCR activation in B cells, both pro-survival and apoptotic processes can be initiated following ERK1/2 activation [Eeva and Pelkonen, 2004]; [Limnander et al., 2011]. This complex signaling network is regulated by distinct mechanisms of negative feedback regulation. Those feedback loops can be divided into two main categories: direct posttranslational modification of pathway components (e.g. Raf proteins, MEK1/2, adapter proteins) and the induction of *de novo* gene synthesis of specific pathway inhibitors (Sprouty and dual specificity protein phosphatases (DUSPs)) [Lake et al., 2016]. Both threonine and tyrosine of ERK1/2 need to be phosphorylated for full kinase activity. Apart from type 1/2 serine/threonine phosphatases (protein phosphatase 2 (PP2)A, PP2C) and protein tyrosine phosphatases (striatal-enriched protein tyrosine phosphatase (STEP), hematopoietic protein tyrosine phosphatase (HePTP) and protein tyrosine phosphatases SL (PTP-SL)), the largest and most studied group of phosphatases that specifically regulate MAPK activity and dephosphorylate both threonine and tyrosine residues, are the DUSPs, which comprise in total 10 members, divided in 3 distinct groups [Lake et al., 2016]; [Caunt and Keyse, 2013]. They differ in substrate specificity (ERK, JNK, p38), subcellular localization, tissue distribution, and inducibility by certain stimuli. Group 1 includes the nuclear proteins DUSP1 (JNK, p38 > ERK1/2) , DUSP2 (ERK1/2) and DUSP5 (ERK1/2), whereas group 2 comprises phosphatases located in the cytoplasm, namely DUSP6, DUSP7 and DUSP9, which are all ERK1/2 specific, whereas the third group contains the p38/JNK-specific regulators, DUSP8, DUSP10 and DUSP16 that can be found in the nucleus and cytoplasm [Lake et al., 2016]; [Caunt and Keyse, 2013]. For DUSP1 and DUSP6 potential small molecule inhibitors have been identified for therapeutic intervention [He et al., 2013]. (E)-2-benzylidene-3-(cyclohexylamino)-2,3- dihydro-1H-inden-1-one (BCI) was identified in a transgenic zebrafish chemical screen and inhibits both DUSP1/6 [Molina et al., 2009].

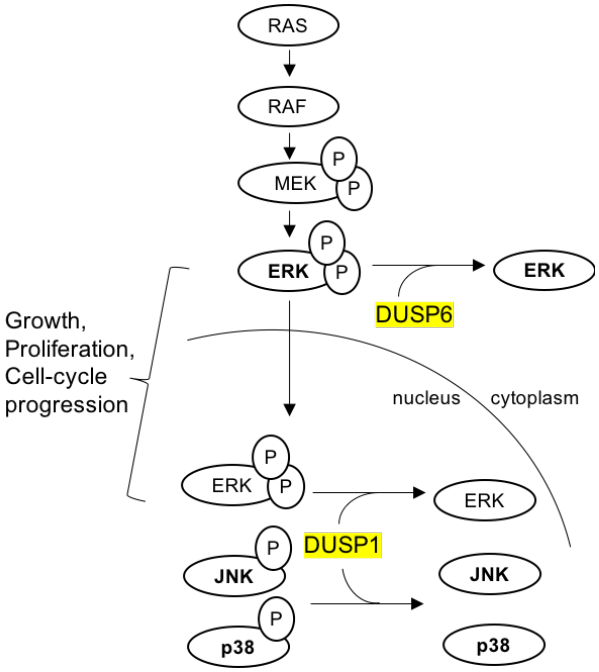

Figure 1.4: DUSP1 and DUSP6 dephosphorylate ERK. DUSP1 has a higher specificity for JNK and p38 MAPK. Both phosphatases provide negative regulation upon MAPK activation.

1.2.2.4 PI3K activation and negative regulation

PI3K phosphorylates phosphatidylinositols and phosphoinositides on the 3 position hydroxyl group of the inositol ring. It comprises a conserved family consisting of eight different PI3K isoforms that can be divided in three classes I, II and II, depending on structure and substrate preference, whereas class I is the most studied one. PI3Ks are heterodimeric enzymes that contain a regulatory and a catalytic (p110α, p110β and p110δ) subunit, whereas p110δ is preferentially expressed in leukocytes [Chantry et al., 1997]; [Vanhaesebroeck et al., 1997]. Activation of PI3K signaling downstream the BCR requires distinct signals. LYN-dependent phosphorylation of CD19 is essential. Besides activation of phosphoinositide-3-kinase adaptor protein (BCAP) by SYK, in turn recruits PI3K to the plasma membrane via binding of its Src homology 2 (SH2) domains to phosphorylated docking proteins. This induces phosphorylation of PI-4,5-P2 to phosphatidylinositol (3,4,5)-trisphosphate (PI-3,4,5-P3) and recruitment of pleckstrin homology domain containing proteins, such as phosphoinoisitide dependent kinase 1 (PDK1), protein kinase B (AKT), and BTK that are activated via binding to PI-3,4,5-P3 [Lemmon and Ferguson, 2000]. AKT is

the most important downstream effector described, involved in regulation of anti-apoptotic genes (B-cell lymphoma 2 (BCL2), Bcl-2-antagonist of cell death (BAD)) via NF-κB activation, tuberous sclerosis proteins (TSC1/2), mouse double minute 2 homolog (MDM2), as well as in glucose metabolism by inactivating glycogen synthase kinase 3 (GSK3), thus directing cell survival and apoptosis, translation, cell cycle, and glucose metabolism [Song et al., 2005]; [Chalhoub and Baker, 2009]. To ensure proper termination and negative regulation of the activated PI3K pathway, a complex network of phosphatases exists. It comprises the ubiquitously expressed 54-kDa tumor suppressor phosphatase and tensin homolog (PTEN), which hydrolyzes PI-3,4,5-P3 to PI-4,5-P2, whereas the 145-kDa hematopoietic-restricted SHIP1, the 104-kDa stem cell-restricted SHIP (sSHIP), and the more widely expressed 150-kDa SHIP2 break it down to phosphatidylinositol (3,4)-bisphosphate (PI-3,4-P2) [Sly et al., 2003]. With respect to BCR signaling in CLL cells, in particular PTEN and SHIP1 are of interest. To note PTEN function is described to be impaired in CLL, due to several regulatory circuits, such as PTEN targeting microRNAs (miRs), casein kinase 2 (CK2)-mediated phosphorylation, or overexpression of the deubiquitinase ubiquitin-specific-processing protease 7 (USP7), which results in PTEN inactivation [Zou et al., 2015]; [Shehata et al., 2010]; [Carrà et al., 2017].

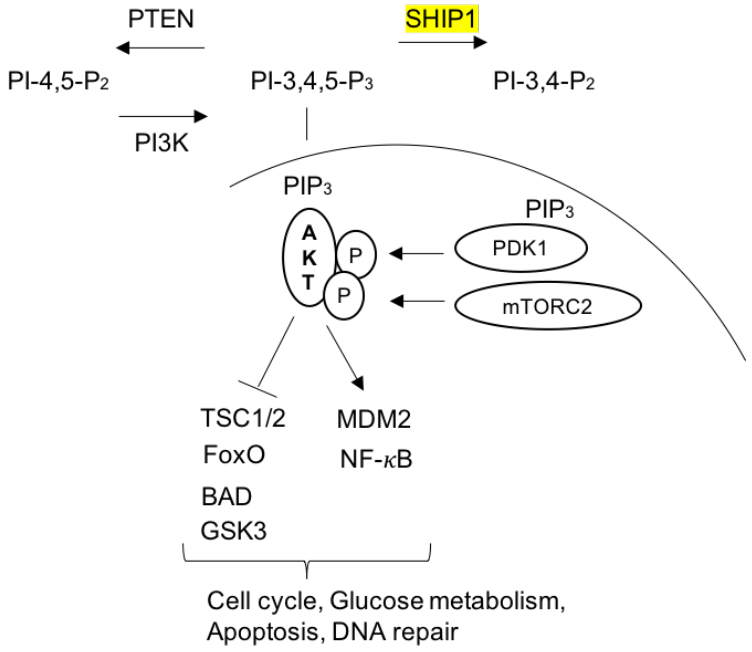

Figure 1.5: SHIP1 dephosphorylates PI-3,4,5-P3 to PI-3,4-P2 and thus negatively regulates PI3K signaling and AKT activation.

In strong contrast, SHIP1 is active and functional in CLL, yet its precise role is not very well studied. In general those phosphatases regulate the retention of signaling molecules at the inner plasma cell membrane. Reduction of PI-3,4,5-P3 levels lowers the binding of pleckstrin homology (PH) domains specific for PI-3,4,5-P3, such as PLCγ2 and AKT. At the same time, increased PI-3,4-P2, resulting from e.g. SHIP1 activity, promotes activity of tandem-pleckstrin-homology-domain-containing protein (TAPP)1, TAPP2, B lymphocyte adapter protein (Bam32), and their respective PI-3,4-P2 specific PH domains. TAPP proteins are important for maintenance of B cell tolerance and negatively regulate B cell activation, whereas in contrast Bam32 rather supports B cell activation [Allam and Marshall, 2005]. The structure of SHIP1 and its separation into distinct functional domains allows its interaction with other signaling proteins and controls the function. It contains a N-terminal SH2 domain and two NPXY domains, which allow interaction with phosphorylated docking protein (Dok) family proteins, Src homology 2 domain containing (Shc), ITIMs, and ITAMs. Besides, the C-terminal proline-rich region (PRR) enables interaction with adaptors like growth factor receptor-bound protein 2 (Grb2) via their Src homology 3 (SH3) domains, and the resulting Grb2 association promotes SHIP1 binding to

phosphorylated FcγRIIB. Importantly, a PH-like domain was identified within SHIP1 that allows direct localization to the PI-3,4,5-P3 phosphatase domain and a C2 domain can associate with the SHIP1 phosphatase product PI-3,4-P2. It is suggested that this interaction provides an additional positive feedback loop for further SHIP1 activation [Pauls and Marshall, 2017]. The small molecule inhibitor 3AC and its water-soluble derivate K118 have been identified to inhibit SHIP1 for therapeutic targeting [Brooks et al., 2010]; [Brooks et al., 2015].

1.2.3 CLL and microenvironment co-evolution

There is growing evidence that CLL evolves through a process of clonal evolution, involving genetically distinct subclones that compete over resources and adapt to external pressures [Greaves and Maley, 2012]; [Purroy and Wu, 2017]. In this context, interaction with the CLL microenvironment plays a very important role and is further described in the following. On the one hand, CLL cells are highly dependent on interactions with the tissue microenvironment for survival, as they proliferate in secondary lymphoid organs, such as lymph nodes and spleen, where (auto-)antigens and/or autonomous mechanisms activate BCR and downstream signaling processes. Major players of the CLL microenvironment comprise monocyte-derived nurselike cells (NLCs), T cells, NK cells, and stromal cells. The communication takes place via a complex network of chemokine receptors, adhesion molecules, tumor necrosis factor family members, and soluble factors. Stromal cells are frequently experimentally used to simulate a protective effect on CLL cells *in vitro*. On the other hand, CLL is characterized by immunosupression during all disease stages. This is mediated by increased numbers of immunosuppressive cell populations, like myeloid-derived suppressor cells (MDSCs), regulatory T cells (Tregs), and direct inhibitory effects of the malignant CLL cells on T cells [Jitschin et al., 2014]; [Christopoulos et al., 2011]. This complex interplay between CLL cells and the microenvironment is described as the co-evolution of CLL and its microenvironment [Purroy and Wu, 2017]. Usually, in a process called tumor immune surveillance, the immune system identifies aberrant tumor cells and eliminates them before they can be harmful. If this first phase of elimination is incomplete, a temporary state of equilibrium develops between the

immune system and developing cancer cells. During this phase, tumor cells can be dormant or continue to progress and accumulate further alterations (e.g. DNA mutations or gene expression changes), which can modify the tumor-specific antigen or stress induced antigen expression. Consequently, during this process, the immune system puts a selective pressure on distinct tumor clones that reciprocally shapes tumor immunogenicity, leading to success or failure of immunosurveillance. In case of incomplete tumor elimination, certain fit clones that resist, avoid, or suppress the antitumor immune response and can escape and initiate progressive growth [Schreiber et al., 2011]; [Swann and Smyth, 2007].

1.2.4 CLL prognosis and treatment options

Based on previous reports that revealed no benefit for early treatment, CLL diagnosis is usually followed by the "watch and wait" strategy, often over long periods of time. However, CLL shows a variable clinical course in between patients, with some surviving for many years without therapy and eventually succumbing to unrelated diseases, and with others having a fast and aggressive course despite extensive therapies. The relative survival for patients at age 40-59 years is 69.9% versus 38.1% for patients greater than 80 years of age. Thus, prognostic markers are important to help predict which patients require treatment and when to start therapy.

Treatment start is based on two established systems for CLL stratification: Rai (based on lymphocytosis) and Binet (classified by the number of affected lymphoid tissue groups and whether anemia or thrombocytopenia occur). Briefly, a Rai stage of III/IV (defined as lymphocytosis; enlarged (IV) or not enlarged (III) lymph nodes, spleen, or liver; normal (III) or low (IV) red blood cell or platelet counts), or a Binet stage C (anemia and/or thrombocytopenia; enlarged number of lymphoid tissue areas) results in therapy initiation [Hallek et al., 2018]. However, within the individual stages there is still a great level of variability. Other prognostic markers are important to further guide treatments and predict outcomes. Those comprise, the mutational status of IgVH, whereas patients with unmutated BCR tend to have an aggressive, more rapidly fatal course [Damle et al., 1999]; [Hamblin et al., 1999]. Besides 80% of CLL cases carry at least one of four commonly recurrent chromosomal aberrations, which are rou-

tinely detectable by fluorescence in situ hybridization (FISH) [Döhner et al., 2000]. Deletion of chromosome 13q14.3 (del[13q]), occurring in more than 50% of patients over time, is the most common alteration. It is associated with favorable prognosis and contains the DLEU2/MIR15-16 cluster, which regulates B cell apoptosis and cell cycle [Klein et al., 2010]. Other common events are del(11q), trisomy 12, and del(l7p), which occur in 18%, 16%, and 7% of patients, respectively. A more advanced disease and rapid disease progression is associated with del(17p), as it disrupts the expression of the tumor suppressor TP53, or del(11q), which targets the ATM locus [Zenz et al., 2010]; [Savitsky et al., 1995]. Additionally, CD38 and zeta-chain (TCR) associated protein kinase 70kDa (ZAP-70) expression correlate with more aggressive disease [Furman, 2010]; [Ibrahim et al., 2001]; [Rassenti et al., 2004]. High ZAP-70 expression also correlates with unmutated CLL cases, although its prognostic value was also shown independently of IgVH status. Overall, those prognostic factors help to divide CLL cases in slow and fast growing malignancies and steer treatment choices. Treatment options for CLL patients have remarkably changed in recent years. For decades, it was based on alkylating agents and similar DNA damaging drugs with modest efficacy and no major impact on survival. The introduction of fludarabine and other purine analogues brought significant advancement [Keating et al., 1991]; [Rai et al., 2000], which was further improved by the application of monoclonal antibodies, particularly those targeting CD20 [Hallek et al., 2010], which are constantly further enhanced by novel generations [Wierda et al., 2010]; [Goede et al., 2014]. Recently, treatment choices were remarkably raised with the development of modern targeted therapies, comprising immune modulators [O'Brien, 2008], BCL2 antagonists [Ng and Davids, 2014], the BTK inhibitor Ibrutinib [Byrd et al., 2013], and PI3K inhibitors Idelalisib and Duvelisib [Furman et al., 2014]. However, despite the promising effects, these kinase inhibitors do not eliminate the malignant clone and resistance occurs in a significant fraction of these patients [Woyach and Johnson, 2015]. Upon Ibrutinib treatment, resistant clones arise due to mutations in BTK(C481S) or PLCγ2 (R665W and L845F) [Furman et al., 2014]; [Woyach et al., 2014]. Ibrutinib-resistant CLL patients lack further treatment options and have very poor clinical outcome with a median overall survival (OS) of 3 - 23 months, varying at distinct clinical sites [Pinilla-Ibarz and Chavez, 2015]; [Woyach, 2017]. Consequently, novel

targeted approaches are urgently needed and the restoration of proper immune responses will be essential. Until now, the only curable treatment modality was allogeneic stem cell transplantation, which is however only available for a small group of fit patients based on the high level of treatment-related mortality [Dreger et al., 2010]. The majority of patients with relapsed, refractory CLL are however not candidates for allogeneic hematopoietic stem cell transplantation (allo-SCT). A very promising novel therapy, shown to be highly effective in for example Ibrutinib refractory CLL, is chimeric antigen receptor (CAR) T cell therapy [Bair and Porter, 2019]. This adoptive therapy is based on extraction of T cells from patient‘s blood, introduction of the CAR gene into the cells‘ genome, replication of the modified T cells, and reintroduction of CAR T cells into the patient. Targeting CD19 B cells, CAR T cells were successfully first described in 2011 and induced complete remission in CLL [Porter et al., 2011]. Since then, several trials were undertaken to improve adverse effects, such as cytokine release syndrome [Bair and Porter, 2019]. Although very potent, this treatment modality is not applicable in daily use, mostly due to high costs and reflects again the requirement of novel targets and the restoration of an effective T cell response [Hay and Cheung, 2019].

1.2.5 Drug delivery and release

Dose-related toxicity is frequently present in tumor therapy, since high drug dosage and frequent administration to reach therapeutic levels at the tumor site, are required. Drug delivery systems can help to achieve circulation for prolonged periods of time in the blood to be able to reach the tumor sites. To obtain prolonged circulation times in plasma, nanomedicine systems need to be small (<100 nm) and present stealth properties (polyethylene glycol corona) to prevent opsonization and recognition by the mononuclear phagocyte system (MPS). [Gref et al., 2000]. The most extensively studied nanomedicine systems are lipid-based nanoparticles and polymeric nanoparticles, schematically depicted in figure 1.6.

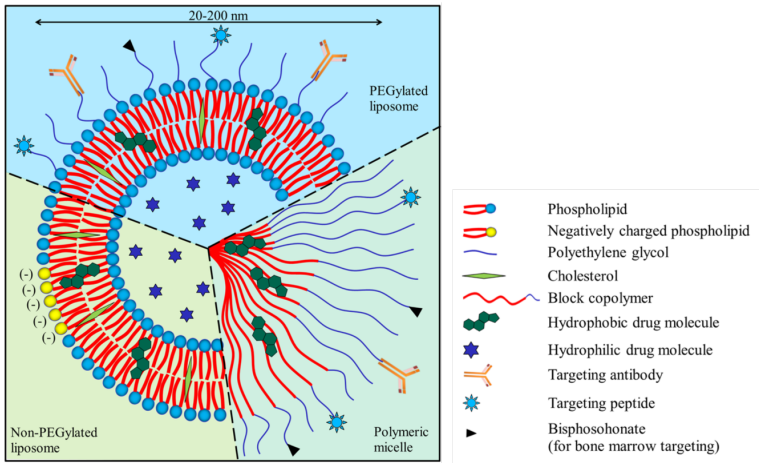

Figure 1.6: Liposomal and polymeric nanoparticles (scheme is taken from [Deshantri et al., 2018]). Liposomes consist of membrane forming phospholipids and cholesterol. Once in aqueous solution, metastable spherical structures are built, whereas a lipid bilayer surrounds an inner aqueous compartment. Stabilization is provided by hydrophobic interactions and hydrogen bonds, van der Waals forces and electrostatic interactions. This offers the encapsulation of a wide range of hydrophobic, and hydrophilic drug molecules in the lipid bilayer or in the aqueous compartment, respectively. Polimeric micelles (PMs) are built with block copolymers of amphiphilic nature and enable loading of hydrophobic compounds into the core. Also, PMs form spontaneously in aqueous solution and the core is stabilized by hydrophobic interactions between the building blocks, whereas the hydrophilic chain engages with H-bridges with water and forms the shell of the micelles. This core-shell structure enables loading of hydophobic compounds in the core, whereas the hydophilic shell provides colloidal stability and prolonged *in vivo* circulation. Moreover, the small average diameter of PMs (10-100 nm) and a near neutral surface charge are advantageous for efficient accumulation in target tissues by means of the enhanced permeability and retention (EPR) effect [Deshantri et al., 2018].

Nanoparticles are beneficial for poorly soluble substances and specifically accumulate in tumors. Great success was achieved in solid tumors: since vessels are leaky, the permeation is increased and in addition, also the retention is elevated at tumor sites, due to poor lymphatic drainage [Stylianopoulos, 2013]. In contrast to solid tumors, in hematological malignancies this EPR effect is not very much appreciated. However, increased angiogenesis, microvessel density and infiltration of inflammatory cells into the bone marrow is present in many hematological malignancies, including CLL [Peterson and Kini, 2001]. In particular in CLL, where proliferation of the malignant cells takes place in secondary lymphoid organs, inflammation is present and activation of the proinflammatory transcription factor NF-κB is involved and critical for CLL

engraftment and disease progression [Lutzny et al., 2013]. Since nanomedicines *per se* accumulate in organs of the MPS such as liver, spleen, and bone marrow, this approach seems in particular attractive to target CLL cells that preferentially reside and proliferate in those organs.

Chapter 2

Research Aims and Objective

Altered signaling throughout different B cell developmental stages can result in diverse pathological outcomes such as autoimmune disorders or lymphoid malignancies. At the same time, once diseases are manifested, altered signaling networks of tumor cells compared to healthy counterparts can provide attractive therapeutic targets and selective intervention can reflect the tumor‘s achilles‘ heel.

CLL is a malignancy of mature, monoclonal B cells with active BCR signaling [Burger and Chiorazzi, 2013]. Extensive research during the last years has shown that BCR signaling, comprising for example downstream PI3K and MAPK pathway activation, is crucial for the survival of CLL cells. Besides elevated RANK signaling was reported for Hodgkin‘s lympoma, multiple myeloma and also CLL, yet its precise contribution during pathogenesis is unknown [Schmiedel et al., 2013]. Despite promising therapeutic approaches, to date CLL is not curable by standard treatments and treatment options, that restore an intact immune response are lacking. These, however, are urgently needed since patients possess strong immunosuppression, mostly with respect to impaired T cell functions.

To identify potential novel targets, this study addresses the following aims:

1) Characterization of RANK signaling in driving CLL pathogenesis and progression.

2) DUSP1/6 inhibition to increase MAPK signaling and induce CLL activation induced cell death.

3) SHIP1 inhibition and AKT hyperactivation to increase PI3K signaling and eliminate malignant CLL cells, yet promote T cell responses.

RANK, a receptor important for both osteoclastogenesis and adaptive immune system activation, is mutated in 8% of ABC-DLBCL cases with characteristics of constitutive active NF-κB [Davis et al., 2010]. One recurrent mutation described is the RANK A756G (K240E) [Compagno et al., 2009]. Since the role of an altered RANK/RANKL axis during B cell pathogenesis has not been studied previously, we aimed to study the consequences of enforced RANK signaling in early B cells and their potential transformation, in the first part of this thesis (5.1).

A mouse model to study the functional role of enforced RANK signaling, by Rosa26 locus targeted expression of the human DLBCL-derived Rank(K240E) in CD19 positive B cells was generated in this laboratory (Doctoral thesis Begüm Alankus). Those mice developed a lymphoproliferative autoimmune disease with specific features of SLE. Whether enforced RANK signaling can contribute to malignant transformation, has however not been studied so far.

In the first part of this thesis, we therefore set off to further investigate the consequences of RANK signaling in terms of B cell transformation. Our analysis comprised the phenotypic characterization of RANK(K240E) driven B cells derived from aged RANK mice, their clonality status and engraftment potential as well as their dependence on RANK ligand *in vitro*. Based on the close resemblance of the malignancy CLL, we further investigated whether this pathway is relevant in other CLL mouse models as well as human patient cells.

The objective of this first part focusing on B cell pathogenesis therefore was to characterize the consequences of enforced RANK signaling and its potential to induce a CLL-like B cell malignancy. Furthermore, these insights provide a rationale for therapeutic intervention with RANKL blocking antibodies, e.g. Denosumab (first FDA approval 2010; [Jules et al., 2010]), which was finally tested in this chapter, in *in vitro* experiments as well as preclinical *in vivo* models. In the second part of this thesis we focused on the characterization of novel therapeutic targets that interfere with BCR signaling (5.2). Up to date, targeted therapeutic approaches in clinical application comprise BCR downstream kinase inhibitors, such as Ibrutinib, an inhibitor of BTK, or Idelalisib and Duvelisib, two PI3K inhibitors. Although the concept of kinase inhibition, which decreases the BCR signaling strength, has revealed great success, severe side effects and toxicities, particularly for PI3K inhibitors, and

resistances occur and the recurrent disease is challenging to treat [Falchi et al., 2016]; [Woyach and Johnson, 2015]; [Mato et al., 2016].

CLL cells are characterized by high levels of BCR-derived signals [Burger and Chiorazzi, 2013]. Such activation signals through the BCR, induce a negative feedback response in the cell to limit the activity of activating signaling molecules in a spatiotemporal manner. We hypothesize, that CLL cells select only intermediate BCR signals during CLL development, as negative feedback regulators are present and active during pathogenesis. Thus, hyperactivation upon negative feedback inhibition, might result in activation induced CLL cell death. At the same time, T cells, that suffer strong immunosuppression might rather be stimulated and re-activated upon negative feedback inhibition.

MAPK signaling was found to play a central role in CLL by whole exome sequencing and identification of driver mutations affecting this pathway [Landau et al., 2015]. Upon activation, MAPK induces a negative feedback loop that regulates the level of phosphorylation of target proteins via upregulation of phosphatases, namely DUSP1 and DUSP6. These provide negative feedback by dephosphorylating ERK1/2 (DUSP6 and, to a lesser extent, DUSP1) and also JNK and p38 (mainly regulated by DUSP1) [Lake et al., 2016]. In order to evaluate the potential relevance of DUSP1 and DUSP6 in CLL, we characterized the expression in CLL, applied small molecule inhibition (BCI), generated genetic knock-out CLL cell lines, and studied the mechanism of DUSP1/6 inhibition by a global phosphoproteome approach. In a side project, by nanoparticle application, we aimed to optimize BCI drug delivery, which is challenging due to the structure of the BCI molecule. Taking together, in the second part of this thesis we investigated the potential of DUSP1/6 inhibition to induce activation induced cell death in CLL.

Idelalisib and Duvelisib are in clinical application, and point to an important role of PI3K signaling in CLL cells [Ortiz-Maldonado et al., 2015]. We focused on SHIP1, as it is readily expressed in CLL, a phosphatase that dephosphorylates PI-3,4,5-P3 toPI-3,4-P2 at the plasma membrane and thereby provides negative feedback for the PI3K pathway and important downstream signaling molecules such as AKT. Using small molecule inhibitors as well as genetic strategies to reduce the expression or delete *SHIP1* in CLL, we evaluated its functional relevance *in vitro* and *in vivo*. We

further characterized the mode of cell death and analyzed the consequences on other immune cells, namely the T cell compartment. To summarize, the objective of the the last part focused on activation-induced cell death in CLL via SHIP1 inhibition, in order to target the malignant clones on the one hand but on the other hand stimulate the immune system to restore a proper long enduring immune surveillance of the disease (5.3).

In summary, we focused in the first part on the role of enforced RANK signaling in B cells and its contribution to CLL pathogenesis (5.1), while we characterized the role of negative regulators of CLL cell signaling in the second and third part of the thesis (5.2 and 5.3).

Chapter 3

Material

3.1 Chemicals and reagents

All chemicals and reagents were purchased from Sigma-Aldrich, unless stated otherwise. A more detailed description of reagents and their origin, is noted in the Chapter "Methods".

3.2 Antibodies

Antibodies were applied for distinct purposes: during Western Blot-mediated protein detection, flow cytometric visualization of surface markers and as therapeutical approach.

3.2.1 Western Blot antibodies

All primary Western Blot antibodies were derived from rabbit, polyclonal and diluted 1:1000 and all secondary antibodies coupled to horseradish peroxidase (HRP) 1:2000 in 5% bovine serum albumin (BSA) in tris-buffered saline with tween20 (TBS-T), if not stated otherwise.

Name	**Company**
α-phospho-Akt Ser473	Cell Signaling Technology 9271
α-phospho-Akt T308	Cell Signaling Technology 9275
α-Akt	Cell Signaling Technology 9272
α-DHX9	Proteintech Europe
α-DUSP1 (monoclonal)	Abcam ab195261
α-DUSP6	Cell Signaling Technology 3058
α-phospho-ATF2 Thr71 (11G2, monoclonal)	Cell Signaling Technology 5112
α-ATF2 (20F1, monoclonal)	Cell Signaling Technology 9226
α-phospho-c-jun Ser63	Cell Signaling Technology 9261
α-phospho-p44/42 MAPK (Erk1/2) Thr202/Tyr204	Cell Signaling Technology 0101
α-PARP	Santa Cruz sc7150
α-SHIP1 (C40G9)	Cell Signaling Technology 2727
α-HMGB-1	Abcam ab18256
α-Calreticulin	Cell Signaling Technology 2891
α-HSP70	Cell Signaling Technology 4872
α-β-Actin (mouse, monoclonal IgG), 1:60000	PeproTech
α-β-Actin (8H10D10, mouse, monoclonal IgG) 1:2000	Cell Signaling Technology 3700
α-mouse IgG HRP-linked (horse polyclonal IgG)	Cell Signaling Technology 7076
α-rabbit IgG HRP-linked (goat polyclonal IgG)	Cell Signaling Technology 7074
α-phospho-SAPK/JNK Thr183/Tyr185	Cell Signaling Technology 9251
α-phospho-p38 MAPK Thr180/Tyr182 (D3F9, monoclonal)	Cell Signaling Technology 4511
α-phospho-SHIP1 Tyr1020	Cell Signaling Technology 3941

3.2.2 Therapeutical antibody

Name	Company
Neutralizing antibody purified mouse α-RANKL	eBioscience

3.2.3 Flow cytometry antibodies

Flow cytometry antibodies listed below were conjugated to respective fluorochromes as listed: phycoerythrin (PE), phycoerythrin cyanin 7 (PE-Cy7), allophycocyanin (APC), APCeFluor780 (APC Cy7), AmCyan, PerCP-Cy5.5, Fluorescein isothiocyanate (FITC). Purified α-mouse CD16/32 and purified Human Fc Receptor Binding Inhibitor Polyclonal Antibody were used for Fc receptor blocking. Besides, α-human Calreticulin (rb) CALR Antibody (Center) was used unconjugated and detected with secondary donkey α-rabbit IgG FITC.

Name	**Company**
Annexin V (APC) Apoptosis Detection Kit	eBioscience
CFSE Cell Proliferation dye	Invitrogen
Zombie Aqua™ Fixable Viability Kit	BioLegend
α-mouse B220 PE-Cy7 (RA3-6B2)	BioLegend
α-mouse CD5 PE (53-7.3)	eBioscience
α-mouse CD5 APC (53-7.3)	eBioscience
α-mouse CD8 APC (53-6.7)	eBioscience
α-mouse CD16/32 (93), purified	eBioscience
α-mouse CD19 APCeFluor780 (1D3)	eBioscience
α-mouse CD19 AmCyan (6D5)	Biolegend
α-mouse CD45 PE (30-F11)	Invitrogen
α-mouse IgD PE (11-26)	eBioscience
α-mouse IgM PE (II/41)	eBioscience
α-mouse PD1 APC/AF647 (29F.1A12)	BioLegend
α-mouse IL-10 APC/AF647 (JES5-16E3)	eBioscience
α-human CD5 PE-Cy7 (L17F12)	BioLegend
α-human CD19 APC (HIB19)	BioLegend
α-human CD45 PerCP-Cy5.5 (2D1)	Invitrogen
Human Fc Receptor Binding Inhibitor Polyclonal Antibody	eBioscience
α-human Calreticulin (rb)	
CALR Antibody (Center)	ABGENT.COM
Rabbit IgG-UNLB	Southern Biotech
Donkey (α-rabbit IgG FITC (Poly4064)	BioLegend

3.3 Cell stimulation / binding reagents

Name	Company
Functional grade purified α-mouse CD3e (145-2C11)	eBioscience
Ovalbumin	Sigma Aldrich
mouse recombinant RANKL	R&D systems
RetroNectin® Recombinant Human Fibronectin Fragment	Takara T100B
Cell Activation Cocktail (with Brefeldin A)	BioLegend

3.4 Inhibitors

Name	target	Company
3AC	SHIP1	Sigma Aldrich
BCI	DUSP1/6	Axon Medchem
BCI hydrochloride	DUSP1/6	Axon Medchem
K118	SHIP1	Echelon Biosciences
Idelalisib	PI3Kdelta	Selleckchem
Ibrutinib	BTK	LKT Laboratories
Oxaliplatin	Platinum derivative (cytostatica)	Selleckchem
Doxorubicin	Anthracycline (cytostatica)	Selleckchem
PD0325901	MEK	Selleckchem
LY2603618	CHK1	Cayman Chemical
Compound C	AMPK	Selleckchem
Nec-1s	RIP1	Bio Vision
GSK-843	RIP3	MedChemExpress
z-VAD	pan-caspase	Adooq Bioscience
QVD-ODH	pan-caspase	R&D Biosciences
Emricasan	pan-caspase	Selleckchem
IETD	caspase-8	BD Biosciences
Necrosulfonamide (NSA)	MLKL	Cayman Chemical

3.5 Primer

All primers were synthesized by Eurofins. All previously unpublished primers were designed with the freeware ApE (version 2.0.47).

3.5.1 Genotyping

Name	**5'-3' sequence**
Cre7	TCAGCTACACCAGAGACGG
CD19c	AACCATTCAACACCCTTCC
CD19d	CCAGACTAGATACAGACCAG
RANKgeno	ACACTGGCTAGGAGAGATTCCTTC
Longgeno	ACTCGGGTGAGCATGTCTTTAATC
Shortgeno	GTGATCTGCAACTCCAGTCTTTCTA
IRESgeno	ATACGCTTGAGGAGAGCCATTTG
Mb1CreERT2 fw	ACAAAGGGGAAAGGGAAGAA
Mb1CreERT2 rev	CATGTTTAGCTGGCCCAAAT
TCL1tg fw	AGTGGTAAATATAGGGTTGTCTACACG
TCL1tg rev	CCCGTAACTGTAACCTATCCTTTA
AKT 35	TACAAGGACGACGACGACAAG
AKT 39	CTGCCGCTTCTGAAGTCCA

3.5.2 Ig Clonality PCR

Name	**5'-3' sequence**
JH4	AAAGACCTGCAGAGGCCATTCTTACC
DSF	AGGGATCCTTGTGAAGGGATCTACTACTGTG

3.5.3 CRIPR/Cas9 sgRNA oligonucleotides

human DUSP1	**targeted gRNA 5'-3' sequence**
hDusp1avana guide 1 FW	caccgTGGTGTTGCTGGACGAGCG
hDusp1avana guide 1 RV	aaacGCGCTCGTCCAGCAACACCAc
hDusp1avana guide 2 FW	caccgCGCAAGTCTTCTTCCTCAAA
hDusp1avana guide 2 RV	aaacTTTGAGGAAGAAGACTTGCGc
hDusp1avana guide 3 FW	caccgCTGAGTACTAGCGTCCCTGA
hDusp1avana guide 3 RV	aaacTCAGGGACGCTAGTACTCAGc
hDusp1avana guide 5 FW	accgCGCCGTGGTGTTGCTGGACG
hDusp1avana guide 5 RV	aaacCGTCCAGCAACACCACGGCGc
human DUSP6	**targeted gRNA 5'-3' sequence**
hDusp6guide 1 FW	caccgGTGCGCGCGCTCTTCACGCG
hDusp6guide 1 RV	aaacCGCGTGAAGAGCGCGCGCACCc
hDusp6avana guide 2 FW	caccgCAGGAGCTATACGAGTCGTC
hDusp6avana guide 2 RV	aaacGACGACTCGTATAGCTCCTGc
hDusp6guide 3 FW	caccgCATCGAGTCGGCCATCAACG
hDusp6guide 3 RV	aaacCGTTGATGGCCGACTCGATGc
hDusp6avana guide 4 FW	caccgAATGGCGATCAGCAAGACGG
hDusp6avana guide 4 RV	aaacCCGTCTTGCTGATCGCCATTc
human SHIP1	**targeted gRNA 5'-3' sequence**
hSHIP1 guide 1 FW	caccgCAGGCATTGCAAACACACTG
hSHIP1 guide 1 RV	aaacCAGTGTGTTTGCAATGCCTGc
hSHIP1 guide 2 FW	caccgCTGACACACCACGTGCACCA
hSHIP1 guide 2 RV	aaacTGGTGCACGTGGTGTGTCAGc
hSHIP1 guide 3 FW	caccgGCTCTGGAACATCCGCATCG
hSHIP1 guide 3 RV	aaacCGATGCGGATGTTCCAGAGCc
hSHIP1 guide 4 FW	caccgGTGGCTGTTGACGAACCCTA
hSHIP1 guide 4 RV	aaacTAGGGTTCGTCAACAGCCACc
hSHIP1 guide 5 FW	caccgCAACATCACCCGCTCCAAGG
hSHIP1 guide 5 RV	aaacCCTTGGAGCGGGTGATGTTGc

3.5.4 Amplification and sequencing of CRISPR/Cas9 targeted DNA segments

3.5.4.1 Amplification of gene segments

To amplify human *DUSP1*, the whole gene segment from start to stop codon (Exon 1 to Exon 4), with an expected size of 2191 bp was amplified. For amplification of human *DUSP6*, the whole gene segment from start to stop codon (Exon 1 to Exon 3), with an expected size of 2786 bp was amplified. Due to the large size of *SHIP1*, spanning 27 exons, different primer pairs were applied, to amplify respective exon regions, where sgRNAs are expected to cut: Amplification of a 214 bp fragment of Exon 1 (targeted by guide 5), a 601 bp fragment of Exon 13 (targeted by guide 1, 3), a 436 bp fragment of Exon 18 (targeted by guide 2) and a 310 bp fragment of Exon 14 (targeted by guide 4), were performed.

Name	**5'-3' sequence**
hDusp1 amplif FW	ggcctcgagccaccATGGTCATGGAAGTGGGCACCCTG
hDusp1 amplif RV	gccgaattcTCAGCAGCTGGGAGAGGTCGTAATGG
hDusp6 amplif FW	ggcctcgagccaccATGATAGATACGCTCAGACCCG
hDusp6 amplif RV	gccgaattcTCACGTAGATTGCAGAGAGTCC
hInpp5d amplif Exon 1 FW	ggcctcgagccaccATGGTCCCCTGCTGGAACCATG
hInpp5d amplif Exon 1 RV	GAACAACCCATCTCAAAGCTGGG
hInpp5d amplif Exon 13 FW	GATTACAGACAGGATACCCCATACCC
hInpp5d amplif Exon 13 RV	CTTTCCTGCAAAAGTTGGCCAATGC
hInpp5d amplif Exon 18 FW	GAAGTAGTCAGGAGGATATGTGAGG
hInpp5d amplif Exon 18 RV	GACACATCAACAGACTGAAGCCC
hInpp5d amplif Exon 14 FW	TTGCCAGCTCCTCACTCACTG
hInpp5d amplif Exon 14 RV	CAAAGGCAGGAGCTGAGC

3.5.4.2 Sequencing

Upon amplification of respective deoxyribonucleic acid (DNA) segments, DNA was isolated from agarose gels and sent to Eurofins for sequencing with the following

primers in separate reactions: For sequencing of *DUSP1* amplified DNA, primers spanning Exon 1 (targeted by guide 1, 2, 5) and Exon 2 (targeted by guide 3) were applied. For sequencing of *DUSP6* amplified DNA, primers spanning Exon 1 (targeted by all guides) were used and for *SHIP1*, the following primers spanning Exon 1 (targeted by guide 5), 13 (targeted by guide 1, 3), 14 (targeted by guide 4), 18 (targeted by guide 2) were applied.

Name	**5'-3' sequence**
hDusp1 Exon 1 guide FW Seq	CCATGGGCCTGGAGCACATCGTG
hDusp1 Exon 1 guide RV Seq	GAGCCAGGGGTACCGGGCAAAAC
hDusp1 Exon 2 guide FW Seq	GAAGCGTTTTCGGCTTCCTGC
hDusp1 Exon 2 guide RV Seq	CCCTGGCACTACTCTTCCATGC
hDusp6 Exon 1 guide FW Seq	ATGATAGATACGCTCAGACCCG
hDusp6 Exon 1 guide RV Seq	CTCGTCCTTGAGCTTCTTGAG
hInpp5d Exon 1 guide RV Seq	GAACAACCCATCTCAAAGCTGGG
hInpp5d Exon 13 guide FW Seq	GATTACAGACAGGATACCCCATACCC
hInpp5d Exon 14 guide FW Seq	TTGCCAGCTCCTCACTCACTG
hInpp5d Exon 18 guide RV Seq	GACACATCAACAGACTGAAGCCC

3.6 Cell lines

Cell line	**origin**
HEK293T, ST-2, HUT78	kindly provided by Jürgen Ruland
MEC-1 and EHEB	DSMZ, Braunschweig (Germany)
MEC-1 (Slc7a) Eco	kindly provided by Ingo Ringshausen
MEC-1 luciferase $(Luc)^+$ cells	Generated by introduction of pCL6-Luc-GFP into MEC-1 Eco
HBL-1, Bal17, SUDHL6, BJAB	kindly provided by Markus Müschen
Jurkat	kindly provided by Garry P. Nolan
NFAT-GFP T cell hybridoma	kindly provided by Konstantin Neuman [Neumann et al., 2014] adapted from [Bot et al., 1996]

3.7 Patient samples

Primary CLL samples were obtained from the peripheral blood (PB) of patients at the National Center for Tumor Diseases, Heidelberg, Germany. Data for IgVH status, BRAF and KRAS status, DUSP6 and SHIP1 expression and time to first treatment were taken from the clinical records and analyzed by Junyan Lu (DKFZ Heidelberg; [Zenz et al., 2019]). In addition Klinikum München Schwabing (Clemens Wendtner) and Tumor Therapy Center of Klinikum rechts der Isar (Christian Bogner) provided peripheral blood of CLL patients for xeno-transplantation approaches and *in vitro* experiments. The local ethics committee approved patient sampling and all patients gave informed consent.

3.8 Mouse models

All animal work was conducted in accordance with German Federal Animal Protection Laws and approved by the Institutional Animal Care and Use Committee at the Technical University of Munich.

3.8.0.1 RANK(K240E)$^{\text{CD19-Cre}}$

RANK(K240E)$^{\text{CD19-Cre}}$ mice were generated as previously described (Doctoral thesis Begüm Alankus: urn:nbn:de:bvb:19-245118) and used to study the role of enforced Rank signaling in B cells and during CLL development. They were kindly provided by Jürgen Ruland.

3.8.0.2 TCL1tg

As CLL mouse model the commonly applied T cell leukemia/lymphoma protein 1 (TCL1)transgenic (tg) line was applied [Bichi et al., 2002]. Mice develop CLL upon 12-16 months, that strongly resembles the human indolent CLL disease and also possesses dysfunctional T cell responses [Hofbauer et al., 2011].

3.8.0.3 PKC-$\beta^{-/-}$

To investigate the involvement of microenvironmental inflammation in CLL we applied PKC-$\beta^{-/-}$ as recipients for TCL1tg splenocyte transplantation. Mice were kindly provided by Marc Schmidt Supprian (TUM) [Holler et al., 2009]; [Saijo et al., 2002].

3.8.0.4 AKTtg x TCL1tg x MB1CreERT2

To study constitutive AKT activation in primary CLL cells and mimic a therapeutical setting with inducible AKT activation *in vivo* and within the immunocompetent microenvironment we applied triple transgenic AKTtg x TCL1tg x MB1CreERT2 mice. The glutamate to lysine at position 17 (E17K) AKT mutation is originally found in solid tumors. A cDNA encoding AKT(E17K) together with an IRES-GFP preceded by a loxP-flanked (FL) STOP cassette was introduced into the ubiquitously expressed murine ROSA26 locus (Doctoral thesis Stefan Wanninger: http://nbn-resolving.de/urn/resolver.pl?urn:nbn:de:bvb:91-diss-20141107-1192175-0-0). By crossing AKT(E17K)tg mice to the Mb1CreERT2 strain, the STOP cassette is excised upon tamoxifen treatment and specifically in the B cell-lineage and AKT(E17K) expression is indicated by green fluorescent protein (GFP) expression [Hug et al., 2014]. After crossing the AKT(E17K) Mb1CreERT2 line to the TCL1tg CLL model, we obtained triple transgenic mice. AKT(E17K)tg mice were kindly provided by Jürgen Ruland.

3.8.0.5 OT-I

Homozygous OT-I mice contain transgenic inserts for mouse Tcra-V2 and Tcrb-V5 genes. The transgenic T cell receptor is designed to recognize ovalbumin residues 257-264 in the context of H2Kb and is used to study the role of peptides in positive selection and the response of $CD8^+$ T cells to antigen. The mice were kindly provided by Hendrik Poeck (TUM). Mice were used to isolate $CD8^+$ T cells and study the interaction with CLL cells (and bone marrow-derived dendritic cells) with respect to T cell activation in the context of immunogenic cell death.

3.8.0.6 C57BL/6 and NOD.Cg-Prkdcscid Il2rgtm1WjI/SzJ (NSG)

C57BL/6 (Janvier Labs) wt immunocompetent mice were used as recipients for TCL1tg and RANK(K240E)$^{CD19\text{-}Cre}$ derived splenocytes and NSG (The Jackson Laboratory) immunosupressed mice served as recipients for the human CLL cell line MEC-1 and for patient-derived isolated CLL peripheral blood cells. NSG mice carry two mutations on the NOD/ShiLtJ genetic background; severe combined immune deficiency (scid) and a complete null allele of the IL2 receptor common gamma chain (IL2rgnull), which renders the mice, B and T as well as functional NK cell deficient.

3.9 Transfection reagents

Name	Company
Lipofectamine 2000	Invitrogen
Nucleofection Kit V	Lonza Bioscience
FuGene HD	Roche

3.10 Plasmids

pCL6-Luc-GFP:
kindly provided by Ingo Ringshausen
pLKO.1 sh RNA SHIP1:
Knockdown1 (KD1) / knockdown2 (KD2) / scramble (scr): kindly provided by Manfred Jücker
phit60 and phit123:
kindly provided by Markus Müschen
pCMV delta R8.2:
Addgene Plasmid 12263
pMSCV modified with U6 Sp6 (derived from Px458) for sgRNA entry:
kindly provided by Paul König; the cloning of respective human guide RNA sequences into pMSCV is described in the subsection "CRIPR/Cas9 cloning" and oligos are listed in the section "Material"
MSCV Cas9 IRES GFP:

kindly provided by Tim Wartewig

pSpCas9(BB)-2A-GFP (Px458):

Addgene Plasmid 48138

pSpCas9(BB)-2A-Puro (Px459):

Addgene Plasmid 48139

pMIG-emtpy and pMIG-myrAKT:

kindly provided by Hassan Jumaa [Abdelrasoul et al., 2018]. pMIG is a MSCV based vector, carrying an internal ribosomal entry site (IRES)-GFP sequence

3.11 Kits

Amersham™ ECL™ Western Blotting Detection Reagents:	
Luminol Solution	
Peroxide Solution	GE Healthcare
Pierce® BCA Protein Assay Kit	Thermo Fisher Scientific
Pierce® ECL Western Blotting Substrates:	
Detection Reagent 1: Peroxide Solution	
Detection Reagent 2: Luminol Enhancer Solution	Thermo Fisher Scientific
Expand Long Template PCR System	Roche
Wizard DNA isolation Kit	Promega
DNA spin Plasmid DNA Purification Kit	iNtRON Beiotechnology
NucleoBond Xtra Maxi from	Macherey Nagel
Nucleo Spin Gel and PCR Clean-up	Macherey Nagel
TMT10plex™ Isobaric Label Reagent Set	Thermo Fisher
$CD8a^+$ T Cell Isolation Kit, mouse	Miltenyi Biotec
B Cell Isolation Kit, mouse	Miltenyi Biotec
B Cell Isolation Kit II, human	Miltenyi Biotec
Cell Titer Glo	Promega
ATP Enliten	Promega
Fixation/Permeabilization Solution Kit	BD Biosciences

3.12 Buffer

Name	Company
PBS	Sigma-Aldrich
4X LDS Sample Buffer diluted in H_2O	NuPAGE Invitrogen
10X Sample Reducing Agent diluted in H_2O	NuPAGE Invitrogen
4-12% Bis/Tris Gels	NuPAGE Invitrogen
20X MES buffer diluted in H_2O; for-LDS Bis/Tris Gels	NuPAGE Invitrogen
cOmplete™ EDTA-free Protease Inhibitor Cocktail	Roche
Phosphatase Inhibitor Cocktails 1-3	Roche
AnnexinV Binding buffer	BD Biosciences

Self-made buffer:

6X Laemmli buffer:

12 g SDS, 60 mg bromphenolblue, 47 ml glycerol, 12 ml 0.5 M Tris, pH6.8, add to in total 90 ml MilliQ H_2O (heat at 60 °C if necessary)

10X TBS:

20 mM Tris, 137 mM NaCl, pH 7.4

10X TBS-T:

20 mM Tris, 137 mM NaCl, Tween20, pH 7.4

1X TBS-T:

10X TBS, 0.1% Tween 20, diluted in VE-H_2O

10X Transfer buffer:

58.2 g 480 mM Tris, 29.4 g 390 mM Glycine, 1.6 ml 20% SDS, add to in total 1 l H_2O

1X Transfer buffer:

10% 10X Transfer buffer, 20% Methanol, 70% H_2O

10X Running buffer:

30.2 g 25 mM Tris pure, 144 g glycine, 50ml 20% SDS, add to in total 1 l H_2O

1X Running buffer:

for SDS-Bis/Tris Gels: 10X Running Buffer diluted in H_2O

APS 10%:

1 g ammonium persulfate in 10 ml H_2O

Blocking buffer:

5% BSA in 1X TBS-T

CHAPS Lysis buffer: 6 ml 1 M Tris/HCl pH 7.5, 1.75 g (150 mM) NaCl, 1% (2 g) CHAPS, add to in total 200 ml H_2O. Freshly added (both 1:100): Protease inhibitor and Phosphatase inhibitor (500 mM NaF, 100 mM NaPervanadate)

Urea Lysis buffer:

8 M urea, 40 mM Tris / HCl, pH 7.6, Protease Inhibitor and Phosphatase Inhibitor Cocktails 1-3 (both Roche)

Stripping buffer:

6.25 ml 1 M Tris pH 6.5, 20 ml 10% SDS, 0.7 ml 13.4 M beta-mercaptoethanol, 73.1 ml H_2O

MACS buffer:

PBS, 0.5% BSA, 2mM EDTA

1X TAE buffer:

50X TAE buffer diluted in H_2O

50X TAE buffer:

242 g Tris, 37.2 g EDTA, dilute in 800 ml H_2O, 57.1 ml acetic acid, pH 8, add to in total 1 l H_2O

LB plates:

20 g agar, 10 g NaCl, 10 g Trypton, 5 g yeastextract, add to in total 1 l H_2O

LB medium:

10 g NaCL, 10 g trypton, 5 g yeast extract, add to in total 1 l H_2O

Freezing media:

FBS + 10% DMSO

10% Polyacrylamide gel:

reagent	**stacking gel 4%**	**running gel 10%**
30%Acrylamide-Bisacrylamide	8.4 ml	48 ml
1.5 M Tris/HCl (pH 8.8)	-	30 ml
0.5 M Tris/HCl (pH 6.8)	14.4 ml	-
H_2O	36.3 ml	41.4 ml
20% SDS	300 μl	600 μl
10% APS	300 μl	600 μl
TEMED (add last)	60 μl	60 μl

Chapter 4

Methods

4.1 Polymerase Chain Reaction

The polymerase chain reaction (PCR) is used to amplify nucleotide sequences of interest. Forward and reverse primers that bind to the single-stranded DNA in the desired region of the genome and a DNA polymerase to synthesize the desired fragment are applied. A PCR consists of three phases: First, DNA is denaturated at high temperatures to obtain single-stranded DNA. Next, annealing takes place to allow primers to bind the region of interest at a lower temperature. Last, extension takes place, where the DNA polymerase synthesizes the DNA fragment of interest, by adding templated nucleotides from the primer-binding site on. To maximize the yield of the reaction, these three steps are repeated as several cycles, typically 30 to 35 times [Garibyan and Avashia, 2013]. Unless stated otherwise, the amplification reactions were set up with 0.2 mM deoxynucleotide triphosphate (dNTP) (Bioline), 0.2 μM of each primer, 50 ng template, 0.04 U/μl of Phire HotStart II DNA polymerase (ThermoFisher Scientific) in reaction buffer (ThermoFisher Scientific). Reaction volumes were chosen to be 20 or 50 μl, depending on the application.

Here, we used PCRs for several purposes, such as genotyping mice, determining the clonality of the B cell repertoire of RANK(K240E) mice and molecular cloning for clustered regularly interspaced short palindromic repeats/CRISPR associated protein 9 (CRISPR/Cas9) approaches as well as amplification of CRISPR/Cas9 targeted sequences for sequencing. All reactions were implemented in a PCR thermocycler

(Bio-Rad). Further specifications of reactions for different applications are given in the respective sections. PCR products were separated by agarose gel electrophoresis, with 1-2% agarose gels, run in TAE buffer for 20-40 min at 120V. Bands were visualized by UV exposure using the Intas Science Imaging gel documentation system.

4.1.0.1 Genotyping PCR

Transgene-specific sequences of RANK(K240E) and CD19-Cre alleles were amplified as follows. The ROSA26$^{\text{loxSTOPlox-RANK(K240E)}}$ allele was detected by a 4-primer PCR (long, short, IRES, RANK genotyping primers), capable of amplifying both the sequence of the recombined locus with the IRES-RANK primer pair and the wildtype locus with the long-short primer pair. The recombinant locus yields at 570 base-pair (bp) band, whereas the wildtype locus yields a 300 bp band. The Cre allele of CD19-Cre mice was detected utilizing a 3-primer PCR with CD19c/CD19d/Cre7 primers. The recombinant and wiltype loci yield bands of size 715 bp and 492 bp, respectively. The human T-cell leukemia/lymphoma protein 1 TCL1 transgene, and human AKT(E17K) were amplified by specific forward and reverse primers spanning a 250 bp and 388 bp fragment, respectively. Mb1CreERT2 was detected by amplification of a specific 500 bp sequence.

The PCR conditions for the distinct genotyping PCRs are the same except for alterations in the annealing temperatures, as follows:

RANK genotyping PCR

Phire HotStart activation	30”, 98°C
35 cycles	denaturation: 5”, 98°C
	annealing: 5”, 62°C
	extension: 15”, 72°C
End elongation:	1’, 72°C

CD19-Cre genotyping PCR

	annealing: 5”, 57°C

TCL1tg genotyping PCR

annealing: 5”, 59°C

AKT tg genotyping PCR

annealing: 5”, 73°C

Mb1CreERT2 genotyping PCR

annealing: 5”, 59°C

4.1.0.2 Ig Clonality PCR

The clonality of the B cell repertoire in mice was determined by PCR, as described previously [Pennycook et al., 1993]. Briefly, DNA was isolated from peripheral blood or splenocytes of RANK(K240)$^{\text{CD19-Cre}}$ mice, TCL1tg mice or C57BL/6 wildtype mice respectively. B cell genomic DNA was isolated using Wizard SV Genomic DNA Purification System Kit (Promega), according to the manufacturer's instructions. CLL content in RANK(K240E) and TCL1tg mice was >70% and wt B cells were MACS purified prior to PCR. A clonality PCR with the primer pair DFS-JH_4 was implemented using the Expand Long Template PCR System (Roche), according to the manufacturer's instructions. DFS primer hybridizes to the 5' recombination signaling sequence of all murine DH segments, whereas JH4 hybridizes downstream of the JH4 segment, leading to the amplification of four possible DJH recombinations with a “ladder” appearance on the agaorse gel in a polyclonal B cell repertoire. The conditions of the PCR reaction are:

94°C	2’
35 cycles of:	
94°C	1’
60°C	90”
68°C	2’ (3” increment)
68°C	10’

4.1.0.3 CRISPR/Cas9 cloning and sequencing

Oligonucleotides (described in "Material") were ordered from Eurofins. DUSP1 and DUSP6 avana sequences were taken from [Doench et al., 2016]. To clone respective sequences into vectors (Px458 or murine stem cell virus (MSCV) U6 Puro) Golden Gate Cloning was applied.

4.1.0.4 Oligo Annealing and Phosphorylation

0.5 μl fwd Primer (100 μM)
0.5 μl rev Primer (100 μM)
0.5 μl T4 Ligation Buffer (10x)
0.5 μl T4 Kinase
3 μl H_2O

PCR condition:

37°C	30'
95°C	5'
cool down until 25 °C	
with 5 °C/min,	
hold at 8 °C	

4.1.0.5 Golden Gate Cloning

0.5 μl vector (Px458 or MSCV U6 Puro) (100 ng)
1 μl Oligos (diluted 1:200)
1 μl Tango Buffer (10x)
0.5 μl DTT (10mM)
0.5 μl ATP (10mM)
0.5 μl FD BpiI
0.5 μl T4 ligase
5.5 μl H_2O

PCR condition:

37°C	5’
21°C	5’
6 cycles, hold at 8 °C	

4.1.0.6 Plasmid Safe Ligation

5.5 μl Ligation
0.75 μl Plasmid Safe Buffer (10x)
0.75 μl ATP (10mM)
0.5 μl PlasmidSafe exonuclease
PCR condition:

37°C	30’
70°C	30’

In order to validate successfully generated CRISPR/Cas9 knockouts in MEC-1 cells, DNA was isolated from 2x10e^6 cells and forward and reverse primer (depicted in section “Material”) spanning the respective Cas9 targeted sequences were applied in the following PCR reaction:
50-100ng template
10 μl HF Buffer (5x)
2 μl dNTP‘s (2.5 mM)
1 μl DMSO
1 μl Primer forward
1 μl Primer reverse
1 μl Phusion Polymerase
H_2O (in total 50 μl reaction)
PCR condition:

98°C	45”
5 cycles of:	
98°C	20”
72°C	2.5’
5 cycles of:	
98°C	20”
68°C	30”
72°C	2.5’
5 cycles of:	
98°C	20”
65°C	30”
72°C	2.5’
72°C	5’
hold 4°C	

Upon PCR, the amplified reactions were loaded on 2% agarose gels and respective amplified DNA sequences were isolated, purified and sent for sequencing with respective sequencing primers (depicted in “Material”).

4.2 DNA isolation

For genotyping of mice, clonality PCRs and sequencing of CRISPR/Cas9 manipulated cells, DNA was isolated by using the Wizard SV Genomic DNA Purification System Kit. DNA was isolated from the tails of 3-week old mice for genotyping. For clonality experiments with RANK(K240E)$^{\text{CD19-Cre}}$ or TCL1tg mice, whole blood cells were lysed with RBC buffer, as described (“Cell purification and isolation”), prior to DNA isolation. As clonality comparison wildtype B cells were isolated and MACS purified (“Cell purification and isolation”) from C57BL/6 splenocytes and DNA was isolated. For sequencing of generated *DUSP1*, *DUSP6* and *SHIP1* knockouts in MEC-1 cells, 1x10e^6 cells were applied for DNA isolation.

For isolation of plasmid DNA, DNA spin Plasmid DNA Purification Kit was applied, according to manufacturer‘s instruction. The day before, Stabl3 competent bacteria

were inoculated with respective plasmid DNA as described ("Bacterial transformation"). To amplify plasmid DNA, NucleoBond Xtra Maxi Kit, from Macherey Nagel was used according to manufacturer's instruction. For isolation of DNA out of agarose gels, Nucleo Spin Gel and PCR Clean-up was applied, as described by Macherey Nagel. DNA was quantified by NanoDrop 2000/2000c Spectrophotometer (Thermo Scientific).

4.3 Bacterial transformation

Competent bacteria are used for plasmid replication. Transformation is initiated by careful addition of 2 μl (100 ng) plasmid DNA to Stabl3 chemically competent bacteria (25 μl) and subsequent incubation for 10 min on ice, followed by a heat shock for 30 seconds at 42 °C and additional 2 min on ice. Then, 100-200 μl SOC media were added and bacteria were incubated for 15 to 60 minutes at 37 °C during shaking (650 rpm), and then plated on LB plates with ampicillin resistance over night at 30 °C. The next day, colonies were picked and inoculated in 6-200 ml LB media with ampicillin at 30 °C over night during shaking and DNA was isolated the next day applying DNA spin Plasmid DNA Purification Kit or NucleoBond Xtra Maxi, respectively.

4.4 Nucleofection-based transient transfection

Electroporation is based on permeabilization of the cell membrane by applying an electrical pulse and thereby allowing molecules to enter into the cell via the electrical field. As this method induces high toxicity, Amaxa improved the NucleofectorTM Technology using a specific combination of optimized electrical parameters and cell type specific solutions to enable entry directly into the cell nucleus, leading to independency from target cell proliferation (Lonza Bioscience).
For transient transfection of Cas9 plasmids (Px458) containing certain single guide ribonucleic acids (sgRNAs) (insertion described in subsection "CRIPR/Cas9 cloning"; oligonucleotides are listed in the section "Material") the Amaxa nucleofection (Lonza

Bioscience) system was applied, according to manufacturer‘s instructions. In detail, Amaxa Nucelofector Kit V was applied and 2x10e^6 MEC-1 cells were transfected with 5-20 μg plasmid by application of the program X-001. 48 h post transfection, cells were sorted for GFP expression.

4.5 Virus production and stable transduction

Via retroviral and lentiviral transduction, nonviral genes can be introduced into a mammalian cell through a virus. The introduced DNA sequence is integrated into the genome of the cellular host, therefore leading to stable gene expression [Soneoka et al., 1995]; [Schambach et al., 2006]. To this end HEK293T cells were used to produce the retroviral and lentiviral particles carrying the gene of interest. All experiments were undertaken with MEC-1 Eco cells, stably expressing the murine Slc7a (mouse cationic amino acid transporter 1 (mCAT1)) receptor. This enables high titer retroviral virus production applying the cytomegalovirus (CMV) driven packaging components, pHIT60 (gag-pol) and ecotropic pHIT123 (env) [Soneoka et al., 1995]. For lentiviral virus production pHIT123 and pCMV delta R8.2 were applied [Schambach et al., 2006]. Details are described in the following.

4.5.0.1 Retroviral approach

Retroviral introduction was applied for all MSCV based plasmids. On the first day 1.8x10e7 HEK cells were seeded in 100 cm dishes in DMEM growth media. On the second day HEK cells were transfected as follows:

1. reaction in 3.75 ml DMEM plain: 20 μg retrovirus + 20 μg pHIT60 + 5 μg pHIT123

2. reaction in 3.75 ml DMEM plain: 80 μl Lipofectamine 2000 (incubate 5 min at room temperature)

3. mix reaction 1+2 and incubate for 20 min at room temperature

Media was removed from HEK cells and reaction mix carefully added drop-wise on HEK cells. Additionally, 7 ml plain media were added. Upon 3 h incubation at 37 °C, 15 ml HEK growth medium was added. On day 3 medium was removed from

HEK cells and sodium butyrate was added for 6-8 h in HEK growth media, then removed and HEK cells cultivated with 15 ml HEK growth media. 24 h after media exchange virus supernatants were harvested by centrifugation, to separate detached cells, and filtered through 0.45 μm filter units. Virus was used freshly or frozen at -80 °C. Additional HEK growth media was added to HEK cells to continue virus production and harvested as described upon 24 h additional incubation.
Retronectin was dissolved in sterile water at 1 mg/ml and filtered through a 0.22 μm filter and stored at -20 °C. Prior to use, retronectin was further diluted to 50 μg/ml in PBS. This stock was re-used for up to 5 times. For spin infections, non-tissue culture treated 6 well plates were coated over night at 4 °C with retronectin (2 ml/well). Then retronectin was removed and wells were blocked with 2% sterile BSA in PBS for 30 min at RT and then washed once with 2 ml PBS. 2-3.5 ml virus supernatant were applied per well and plates were centrifuged for 2 h at 2000x g and 32 °C. Afterwards virus was discarded without drying of the wells and 1-2x10e^6 MEC-1 cells were added per well and centrifuged 30 min at 600x g at 32 °C. Cells were incubated for 2 d in the incubator or until confluent. 3 days upon spin infection puromycin selection or GFP sorting was initiated.

4.5.0.2 Lentiviral approach

Lentiviral spin infections were performed for introduction of SHIP1 targeted and mock short hairpin ribonucleic acids (shRNAs) and to generate stable Luciferase positive MEC-1 cells. HEK cells were seeded at 1.2x10e^7 cell/plate on day 0 to reach 70-80% confluence on day 1. 30 min prior to transfection, media on HEK cells was replaced with OptiMEM, 5% FCS, 1x Chloroquinone (50 ml OptiMEM + 5 ml FCS + 50 μl Quloroquinone). In 2 ml OptiMEM 17 μg pCMV delta R8.2, 10 μg Phit123 and 10 μg vector (pLKO.1 backbone) were added. Then 100 μl FuGene HD was added and carefully vortexed and incubated for 30 min at room temperature. Thereafter the mix was added drop wise to HEK cells, which were removed from media beforehand, and incubation took place for 6 h at 37 °C. Cells were then once rinsed with 10 ml OptiMEM and 15 ml new OptiMEM was added onto 15 cm plates. 24 h upon transfection, on day 2, virus supernatants were harvested by centrifugation for 400x g at 4 °C for 5 min. Another 15 ml OptiMEM were added onto plates for

virus collection upon 48 h. To concentrate virus supernatants the Centricon Plus 70 filters were applied according to manufacturer‘s instructions. Virus was spun at 3500x g for 15 min at 4 °C and collected at 1000x g for 2 min at 4 °C. 10 ml virus supernatant were concentrated and used for 1 well of a retronectin coated 6 well plate (2 ml/well). Not directly processed virus supernatants were frozen in liquid nitrogen and stored at -80 °C. Spin infection was undertaken as described previously. 5 days upon spin infection, Puromycin selection was initiated. For generation of Luc positive MEC-1 cells, GFP positive cells were sorted thereafter.

4.6 Cell selection upon nucleofection or viral manipulation

Upon electroporation and retroviral or lentiviral spin infections, cells were either sorted as bulk or single cell for GFP expression (see section “FACS”) or selected with puromycin. Selection of pMSCV plasmids was performed with 2 μg/ml Puromycin and was completed upon 2 days and confirmed by flow cytometric analysis of viability (4 ,6-diamidin-2-phenylindol (DAPI)). Prior to selection, different puromycin doses were tested on MEC-1 cells, and 2 μg/ml puromycin was identified to entirely kill non-manipulated MEC-1 cells.

4.7 Cell Culture

4.7.0.1 Maintainance

The murine B cell lymphoma cell line BAL17, the murine bone marrow-derived ST-2 cell line and freshly isolated primary murine B and T cells were cultured in RPMI-1640 Glutamax medium supplemented with 10% fetal bovine serum (FBS), 1% penicillin-streptomycin (PenStrep), and 0.1% 2-mercaptoethanol. Patient- and healthy donor-derived CLL and B cells were cultured in RPMI-1640 Glutamax medium supplemented with 10% FBS and 1% PenStrep. CLL cell lines MEC-1 were cultivated in IMDM medium supplemented with 10% FBS and 1% PenStrep and

EHEB cells were kept in RPMI medium, with 10% FBS and 1% pen/strep. HEK293T cells for virus production were grown in DMEM supplemented with 10% FBS and 1% PenStrep. B cell lymphoma cell lines (BJAB, HBL-1, SUDHL6) and T cell lymphoma lines (Jurkat, HUT78) were cultivated in RPMI 10% FBS and 1% PenStrep. Bone marrow-derived dendritic cells (BMDCs) were differentiated and cultured in RPMI with 10%FBS, 1% PenStrep, 1% L-glutamine, 0,1% 2-mercaptoethanol, 20 ng/ml granulocyte macrophage colony stimulating factor (GM-CSF).
B lymphoma, T lymphoma and MEC-1 cell lines cells were split 1:10 in suspension every 3 days, and EHEB cells were split 1:3 every 3 days. Adherent cell lines ST-2 and HEK293T cells were split 1:10 every three days by trypsinizing (1% Trypsin/EDTA), to detach the cells. BMDC were differentiated and cultured in RPMI with 10% FBS, 1% PenStrep, 1% L-glutamine, 0,1% 2-mercaptoethanol, 20 ng/ml GM-CSF, as described ("BMDC generation").
All cells were cultured under standard cell culture conditions; at 37 °C, 5% CO_2 and 95% humidity. The cells were frozen for conservation in FBS supplemented with 10% DMSO (Sigma-Aldrich). Cells were thawed again by quick resuspension in 50 ml PBS (400x g, 4°C, 5 min) and subsequent resuspension in respective culture medium. Prior to further experimental processing, cells were recovered for 2 hours upon thawing in culture media at 37 °C. All media and supplements were purchased from Gibco, unless stated otherwise.

4.7.0.2 BMDC generation

Femur and tibia of both sides from C57BL/6 mice were isolated, and single cell suspensions prepared, as described ("Cell Purification"). 5x10e^6/ml cells in 10 ml BMDC media were seeded in 10 cm plates and incubated at 37 °C, 5% CO^2 and 95% humidity. On day 2 and day 5 upon isolation, 5 ml fresh BMDC media were added. BMDCs were applied for OT-I co-culture experiments on day 9-10 upon differentiation.

4.7.0.3 Cell counting

Cells were counted with Trypan Blue Stain (0.4%; Gibco) to discriminate live and dead cells. Based on estimated cell counts, cell suspensions were diluted 1:10 in Trypan Blue. 10 μl were then pipetted in a Neubauer counting chamber (0.0025mm^2; 0.100 mm Depth; HBG Germany) and viable Trypan Blue negative cells were counted. According to the layer thickness of the applied counting chamber the cell number per ml was determined as follows: (Number of viable count cells / number of count squares) x dilution factor (10) x 10e^4.

4.7.0.4 CLL and stroma cell co-culture

To simulate protective effects from the microenvironment, human or murine primary CLL cells and MEC-1 cells were co-cultivated with murine bone marrow-derived ST-2 stroma cells at a ratio of 10:1 (96 well format: 1x10e^4 ST-2 cells). ST-2 cells were pre-seeded over night to allow adherence. Before analysis, stroma cell contamination in subsequent separated CLL samples, was evaluated by flow cytometric analysis and size discrimination of CLL and stroma cells. Contamination of CLL cells with ST-2 cells $< 2\%$ was accepted.

4.7.0.5 CLL (and BMDC) and T cell co-culture

Complex co-culture experiments were applied to study a potential induction of immunogenic cell death (ICD). CLL cells were fed with 0.2, 0.4 and 1 μg/ml Ovalbumin over night, washed the following day and treated with inhibitors for 48 h as described ("Cell stimulation"). Cell death was confirmed by flow cytometric analysis of DAPI exclusion. BMDCs were generated from murine bone marrow as described (section 4.7 "BMDC generation"). Upon MACS isolation of CD8$^+$ T cells from OT-I mice (section 4.7 "Cell purification and isolation"), co-culture was started with 1x10e^5 (dead) CLL cells, 2.5x10e^4 BMDCs and 5x10e^4 cytotoxic T cells. Prior to co-culture, CLL cells were treated and killed with 3AC or respective chemotherapeutics (section 4.7 cell "stimulation and treatments") and T cells were carboxyfluorescein succinimidyl ester (CFSE)-labeled as follows: Cells were washed once with phosphate-buffered

saline (PBS) and then resuspended in 5 μM CFSE diluted in PBS and incubated for 10 min at 37 °C, 5% CO^2 and 95% humidity, then washed with PBS, containing 10% FBS and resuspended in culture medium. Flow cytometric analysis of T cell proliferation in the co-culture was performed upon 72 h of co-culture. Cells were stained with anti-CD8 (APC) and DAPI.

4.7.0.6 Competition assay

We applied competition assays to study the growth behaviour of generated *DUSP1*, *DUSP6* and *SHIP1* knockouts in MEC-1 cells. 5x10e^5 knockout cells, that in addition were GFP-positive, were mixed with equal amounts of MEC-1 wildtype, GFP-negative cells. The percentage of GFP over time was followed by flow cytometric analysis.

4.7.0.7 Generation of drug-resistant MEC-1 cells

In order to generate drug-resistent MEC-1 cells, drugs (Ibrutinib 5-20 μM and Idelalisib 0.5-2 μM) were added, first weekly and then twice per week with increased doses over a period of 6 month. Simultanously, untreated MEC-1 cells were split similarly over the same time period. Before treatment, MEC-1 wt and drug-resistant cells were kept Ibrutinib/Idealisib-untreated for 1 week, washed, and synchronized at 1x10e^6/ml over night in fresh medium. Cells were then treated as described ("Cell stimulation and treatments").

4.7.0.8 Cell purification and isolation

Primary murine cells from spleen and lymph nodes were isolated by mashing organs through 70 μm filters in PBS. Bone marrow cells were isolated by flushing the marrow out of the bone with the help of a needle and PBS, and mashing through a 70 μm filter. Spleen and bone marrow samples underwent a red blood cell lysis procedure, and were resuspended in 1 ml red blood cell lysis buffer (G-DEX11, Intron Biotechnology) for 1 minute, and washed thereafter with PBS (400x g, 4°C, 5 min). For analysis of murine peripheral blood derived cells, 15 μl peripheral whole blood cells were lysed in 700 μl red blood cell lysis buffer for 7 minutes and washed

thereafter twice with 1 ml PBS.

Primary human cells from peripheral blood were isolated by ficoll density gradient (400x g, 20°C, 30 min, no brakes). In detail 15 ml ficoll solution (Ficoll Paque plus; GE Healthcare), was slowly overlaid with 15 ml whole blood, pre-diluted with 15 ml PBS. Upon centrifugation the peripheral blood mononuclear cell (PBMC) layer was carefully isolated and washed with PBS. Cells were counted and further processed freshly or cryopreserved in freezing media.

Murine and human B cells or $CD8^+$ murine T cells were enriched by negative magnetic labeling, as described by manufacturer‘s instructions (Miltenyi Biotec). In this system of magnetic-activated cell sorting (MACS), the cells of interest accumulate in the flow-through, untouched and therefore unactivated. The flow-through containing the cells of interest was centrifuged at 400x g for 5 minutes to collect the cells. Cells were washed with respective medium, counted, and used for further analysis.

4.7.0.9 Cell stimulation and treatments

NFAT GFP reporter T cell hybridoma cells were stimulated with α-CD3. 96 well flat bottom plates were pre-coated with 0.156-1 μg/ml α-CD3 (in PBS) over night at 4 °C and washed the next day twice with PBS. Afterwards, 3-5x10e^5 cells were plated per well. 5 μM 3AC were added and upon 6 h incubation, T cell activation was measured by flow cytometric analysis of GFP expression and DAPI exclusion.

Cells derived from RANK(K240E)$^{\text{CD19-Cre}}$ mice or primary murine and human CLL cells were stimulated with 100 ng/ml (final concentration) mouse recombinant RANKL (R&D systems). To block the RANK/RANKL axis, the following day 2 μg (final concentration) neutralizing antibody purified mouse α-RANKL (eBioscience) was added and viability was monitored after 48 h and up to 10 days by flow cytometric exclusion of DAPI.

Murine TCL1tg splenocytes (>70% CLL), primary patient-derived CLL cells (>70% CLL) and healthy peripheral blood MACS-isolated B cells were seeded at 2x10e^5 in 96 well plates and then treated with BCI/3AC/K118 for 48 hours and viability was analyzed by flow cytometry and DAPI exclusion. In combinatorial treatment experiments with distinct inhibitors (PD0325901: 1 μM, Compound C: 1 μM, LY2603618: 1 μM, GSK2399872A: 1 μM, Nec-1s: 30 μM, NSA: 1 μM, IETD: 10 μM, QVD-ODH: 5

μM, Emricasan: 5 μM) cells were pre-treated for 1 h, followed by addition of 1.25-10 μM BCI / 2.5-20 μM 3AC / 1.25-10 μM K118 for 48 h and analysis of cell viablity. Distinct murine and human cell lines (MEC-1, EHEB, HBL-1, Jurkat, HUT78, Bal17, SUDHL6) were synchronized by cell count and resuspended at 1x10e^6 cells/ml in culture medium 1 day prior to treatment. Cell lines were then count again and treated with BCI and 3AC at 1x10e^5/well as described above.

4.7.0.10 Cre-mediated recombination *in vitro*

TAT-Cre recombinase is a recombinant cell-permeant fusion cre-recombinase protein consisting of a TAT sequence, a nuclear localization signal (NLS) and it is known to catalyze the site specific recombination event between two loxP DNA sites. TAT-Cre (Excellgen) was diluted in Opti-MEM and AKTtg x TCL1tg isolated splenocytes were washed twice in Opti-MEM and then resuspended in Opti-MEM containing TAT-Cre at a final concentration of 2 μM. for 1 h at 37 °C, 5% CO_2 and 95% humidity. Afterwards cells were washed again twice in culture media.
4-hydroxytamoxifen (4-OHT) is used as an activator of CreER recombinase in conditional mouse systems. Triple transgenic AKTtg x TCL1tg x MB1CreERT2 isolated splenocytes were induced with 500 ng/ml 4-OHT for 48 h and then washed, to avoid toxicity. The induction of the AKT transgene was analyzed daily by flow cytometric measurement of GFP percentage and DAPI exclusion.

4.8 Cell Lysate preparation and Western Blot

Whole cell lysates for protein analysis were prepared upon washing cells twice in ice cold PBS. All subsequent steps were performed on ice. If CLL cells were co-cultivated with ST-2 stroma cells, they were carefully separated from the stroma layer and stroma contamination was analyzed by flow cytometric measurement and size discrimination between CLL and stroma cells. Per sample 2x10e^6 cells (cell lines) or 1x10e^7 cells (primary material) were lysed in ice cold CHAPS buffer, supplemented with phosphatase inhibitors (50 mM NaF, 0.1 mM Na^3VO^4) and protease inhibitors (EDTA free Protease Inhibitor Cocktail Tablets, Roche Diagnostics) for 15 min

on ice. Afterwards lysates were spun at maximal speed (>14000x g) for 15 min. Concentrations of lysates were determined by absorbance measurement, with the BCA Protein Assay Kit (Pierce), according to the manufacturer's instructions. The lysates were then denatured in SDS sample buffer at 95 °C for 5 minutes before loading onto the polyacrylamide gel. PageRuler pre-stained protein ladder (Thermofisher) was used as molecular weight marker. For simultanous detection of proteins >150kDa and <20kDa, 4-12% gradient gels from Invitrogen, NuPage were applied according to manufacturer‘s instructions. Polyacrylamide gel electrophoresis method separates proteins across an electrically charged field based on their molecular weight and charge. Gels were run 20 min at 70 Volt, for all proteins to equally cross the stacking gel, followed by 120 Volt for 1-2 hours to separate all proteins according to their size in the running gel. The separated proteins were transferred onto a nitrocellulose membrane (Amersham Protran, GE Healthcare) by a wet-blott electrophoresis in transfer buffer for 2 hours at 300 mA. Following transfer, membranes were blocked in 5% BSA in TBST and incubated overnight with specific primary antibodies diluted 1:1000 in 5% BSA in TBST. HRP-conjugated secondary antibodies (1:2000 in 5% BSA in TBST) were added the next day upon washing the membranes with TBST for 10 minutes, 3 times. For chemiluminescent detection, the detection systems LumigenTM TMA-6, Solution A+B (GE Healthcare) or Detection Reagent 1+2/Peroxid Solution (Thermo Scientific, Pierce) were utilized.

For analysis of CLL cell secreted factors, the supernatants of treated cells were taken upon 48 h drug, or combinatorial inhibitor and drug treatment and directly mixed with SDS sample buffer before freezing at -80 °C. Samples were further processed as described above. The antibodies and buffers used for Western blotting are listed in “Material” (3.2.1 and 3.10).

4.9 Fe-IMAC phosphopeptide enrichment

Iron immobilized metal ion affinity chromatography (Fe-IMAC) columns enable selective, comprehensive, and reproducible enrichment of phosphopeptides out of complex lysates in an high performance liquid chromatography (HPLC) column format [Ruprecht et al., 2015]. This technique was applied by our collaboration

partners (Piero Giansanti, Bernhard Küster). Primary CLL cells were treated with 2 μM BCI for 3 and 10 minutes freshly after purification from the peripheral blood of CLL patients using a ficoll density gradient. MEC-1 cells were incubated for 24 hours at a cell density of 1x10e^6/ml and then treated with 5 μM BCI for 15 and 45 minutes. After the treatment period, cells were immediately transferred to ice-cold PBS and centrifuged (400x g, 4°C, 10 min). The cell pellets were lysed on ice for 10 minutes in urea lysis buffer and centrifuged again (21,000x g, 4°C, 60 min). All subsequent steps were done by our collaboration partners. Protein concentration was determined by Bradford assay (according to manufacturer‘s instruction) and protein reduction and alkylation were achieved by treatment with dithiothreitol and 2-chloroacetamide. Trypsin digestion was carried out overnight and desalting of the peptides was done using SepPak cartridges. tandem mass tag (TMT) reagent labeling (ThermoFisher Scientific, Waltham, MA) was performed according to the manufacturer's instructions. After desalting, phosphopeptide enrichment was performed using ProPac IMAC 10 columns. After another desalting step, nuclear localization sequence high pH reverse phase separation technique (HpH-RP) chromatography was performed to fractionate the peptides and mass spectrometry (MS) measurement using a phospho-gradient.

4.10 Flow Cytometry

Flow cytometry method is based on computer-processed light scatter and fluorescent signals received from a fluorescently-labeled single cell suspension after laser excitation. Cells in a suspension fluid are injected into the flow cytometer instrument and ideally one cell at a time flows through a laser beam which results in scattered light, characteristic to the cells components. This enables to determine the size and granularity of cells, as well as expression of surface markers, which can be fluorescently-labeled using antibodies against certain epitopes of surface molecules conjugated to fluorescent molecules. This results in light absorbance that is then emitted in a band of wavelengths. Flow cytometry can also be used for detection of intracellular proteins, after proper cell fixation and permeabilization methods are applied.

4.10.0.1 Immunophenotyping

In this study, flow cytometry was used to perform immunophenotyping of lymphocytes isolated from peripheral blood, spleen, lymph nodes, bone marrow of mice and also from peripheral blood of CLL patients. In addition distinct cell lines were analyzed. After cells were prepared as explained in section 4.7 ("Cell purification and isolation") and counted ("Cell counting") , they were resuspended and washed in PBS (400x g, 4°C, 5 min) and incubated with 1:200 diluted murine CD16/32 or human Fc Receptor Binding Inhibitor Polyclonal Antibody , to block free F_c receptors, washed in PBS again and incubated for 20 min at 4°C with respective fluorescently conjugated antibodies against surface molecules. The antibodies were diluted 1:100 to 1:400. All antibodies were diluted in PBS. The cells were acquired using a FACSCantoII flow cytometer (BD Bioscience).

4.10.0.2 AnnexinV stain

Primary human CLL cells were thawed and treated with BCI and 3AC for 24 h or 48 h as previously described. Cells were washed once in PBS and then in annexin-V (AnxV) Binding Buffer, diluted 1:10 in sterile water (400x g, 4°C, 5 min). AnxV (APC) was diluted 1:40 in AnxV Binding Buffer and 20 μl were applied per sample, for 15 min at room temperature, protected from light. Afterwards, 50 μl AnxV Binding buffer, supplemented with 1:1000 diluted DAPI (1 mg/ml), were added and cells were characterized as viable ($AnxV^-$, $DAPI^-$), apoptotic ($AnxV^+$, $DAPI^-$), late apoptotic ($AnxV^+$, $DAPI^+$) and necrotic cells ($AnxV^-$, $DAPI^+$) by flow cytometry.

4.10.0.3 Calreticulin stain

Primary human CLL cells were thawed and treated with 3AC and K118 for 4 h as previously described. To stain calreticulin (CALR) on the cell surface, Human Fc Receptor Binding Inhibitor Polyclonal Antibody was added to the cells together with 1:40 diluted (PBS) α-human Calreticulin (rb) CALR Antibody (Center). As isotype control Rabbit IgG-UNLB was used at 0,625 μg per $1x10e^6$ cells. Upon 45 min at 37°C cells were washed twice in PBS (400x g, 4°C, 5 min) and secondary donkey

α-rabbit IgG FITC was added, diluted 1:200 in PBS, for 30 min at 37°C. Cells were washed again twice in PBS, DAPI was added directly and cells were analyzed by flow cytometry.

4.10.0.4 Intracellular stain

To stain IL-10 and PD1 in murine lymphnode-derived cells, 1x10e^6 cells were incubated in Cell Activation Cocktail with Brefeldin A (BioLegend) for 3 h at 37°C, 5% CO_2. Afterwards cells were stained for live/dead discrimination with BV510 Zombie, according to manufacturer's instruction and washed with PBS thereafter. Upon fixation and permeabilization according to the Fixation/Permeabilization Solution Kit (BD), IL-10 and PD-1 were stained in separate reactions (1:200 diluted).

4.11 Fluorescence-activated cell sorting (FACS)

Cell sorting is a method to purify distinct cell populations based on the presence or absence of specific characteristics, such as fluorescent labeling or expression of fluorescent markers. In flow cytometers with sorting capabilities, such as FACS Aria III, the instrument detects cells using parameters including cell size, morphology, fluorescent labeling and protein expression, and then droplet technology to sort cells and recover the subsets for post-experimental use [Kamentsky et al., 1965].
The FACS method was implemented to sort and enrich MEC-1 cells that were previously manipulated to stably express GFP. All sorting experiments were performed on a FACS Aria III sorter and viable, GFP expressing cells were sorted directly into filtered sterile FBS. CRISPR/Cas9 *DUSP1*, *DUSP6* and *SHIP1* knockouts were sorted as single cells into 96 well plates whereas pMIG-myrAKT and pMIG-emtpy, Cas9-GFP and Luciferase-GFP expressing cells were sorted as GFP high expressing bulk population into 15 ml falcons. Upon sorting, cells were spun (400x g, 4°C, 5 min) and resuspended in culture media (RPMI, 10% FBS, 1%PenStrep).

4.12 ATP measurement by luminescence-based assays

To measure the release of ATP, patient-derived CLL cells were treated for 4 h with 3AC as described and supernatants were analyzed with the ATP Enliten Kit (Promega), according to manufacturer‘s instructions. For detection of luminescence the GloMax® Discover platereader was applied (Promega).

4.13 Transplantation experiments

4.13.0.1 RANK(K240)$^{\text{CD19-Cre}}$ transplantation

Since malignancy of cells can be determined by their property to engraft in an immunocompetent recipient of the same background, transplantation experiments were used to study the malignant potential of aged, diseased RANK(K240E) CLL-like cells derived from mice >12 month. Splenocytes were isolated (Section 4.7 “Cell purification”) and upon flow cytometric characterization (section 4.10 “Flow Cytometry”) 1x10e^7-2x10e^7 were injected intravenous (i.v.) in C57BL/6 recipients. Regular blood draws and flow cytometric analysis were performed upon transplantation to monitor engraftment and progression (CD19$^+$ CD5$^+$) in recipients.

4.13.0.2 TCL1tg transplantation

To study CLL in an *in vivo* setting, the TCL1tg mouse model is commonly applied. Since development of CLL takes up to 8-12 month in this model and underlies heterogeneity, we used a transplantation approach with diseased splenocytes to obtain a homogenous cohort of CLL mice for treatment. 2x10e^7 isolated splenocytes (Section 4.7 “Cell purification”) with >70% CLL content were i.v. injected in C57BL/6 recipients. Engraftment was evaluated by flow cytometric PB (CD19$^+$ CD5$^+$) analysis over time. In addition, AKTtgxTCL1tgxMb1CreERT2 triple transgenic mice were transplanted as described above.

4.13.0.3 MEC-1 xeno-transplantation

1x10e^6-2x10e^6 MEC-1 cells were injected intravenously into NSG mice (8-12 weeks old, female, n=5 per group). Engraftment was studied by flow cytometric analysis of CLL content in PB and by bioimaging (section 4.16).

4.13.0.4 Patient CLL xeno-transplantation

1x10e^8 isolated patient CLL cells (>70% CLL in ficoll isolated PBMCs) were injected i.v. into age- and sex-matched NSG mice. Engraftment was studied by flow cytometric analysis of PB.

4.14 RANK-RANKL interference *in vivo*

To study the RANK/RANKL signaling axis, on day 8 post transplantation of MEC-1 cells into NSG, the mice were separated into two groups and received 5 mg/kg anti-Rank ligand, or PBS twice per week intraperitoneal (i.p.). The mice were sacrificed upon clear signs of disease according to the animal protocol guidelines.

4.15 Negative feedback inhibition *in vivo*

Negative feedback regulators were inhibited by small molecule inhibitors or genetically manipulated as described in the following.

4.15.0.1 DUSP1/6 inhibition

To inhibit DUSP1/6 *in vivo*, BCI micelles or BCI HCl liposomes were applied due to poor BCI solubility. Treatment of TCL1tg-transplanted mice was conducted 3 times a week with 40 mg/kg BCI micelles (n=7) or empty micelles (n=7) by i.v. injection. Treatment was initiated at day 8 upon transplantation and in total 6 doses were applied. 1 day after the last treatment (d21) organs were harvested to analyze CLL infiltration. In addition TCL1tg-transplanted mice were treated with BCI HCl liposomes with 6 mg/ml daily (due to low loading capacity) starting at day

12 upon transplantation for 9 days and organs were harvested on day 24. Treatment of patient-derived xenotransplanted cells (n=2, different CLL patient donor) was initiated at day 1 in both independent experiments and mice received either (n=5) 4 doses BCI micelles (40 mg/kg) or empty micelles (n=5) during 11 days or 7 doses during 18 days (n=4 each group) depending on the engraftment of donor cells.

4.15.0.2 *DUSP1* knockout

DUSP1 knockout was studied *in vivo* by transplantation of 1x10e^6 *DUSP1* ko (n=2) versus wt MEC-1 cells (N=2) into NSG mice. Mice were sacrificed upon neurological symptoms and weight loss.

4.15.0.3 SHIP1 inhibition

NSG mice xenotransplanted with MEC-1 Luc CLL cells were treated with 10 mg/kg K118 or H_2O, starting at day 2 upon transplantation, daily for a total of 10 doses. Engraftment and progression of MEC-1 Luc cells was followed by IVIS bioimaging. Mice were sacrificed when the following end criteria were reached: weight loss of more then 25% compared to the initial maximal weight and paralysed hind limbs.
Patient-derived xenotransplanted cells were similarly treated with 10 mg/kg K118 or H_2O, starting at day 1 upon transplantation. PB analysis determined the end point and organs were harvested when <10% human CLL cells were detected in the PB, upon 4-9 daily doses.
In the murine Tcl1tg model, treatment was initiated at day 11 upon transplantation when CLL content was on average 60% in the PB. Mice were treated daily with K118 or H_2O for 4 days, and upon 2 days another treatment cycle was continued for 4 days. Organs were harvested on day 22 and analyzed for CLL content by flow cytometry.

4.15.0.4 SHIP1 knockdown

SHIP1 knockdown in MEC-1 cells versus scramble control setting were transplanted at 1x10e^6 into NSG mice and CLL engraftment and progression was followed by bioimag-

ing. The mice were sacrificed upon clear signs of disease, comprising neurological symptoms and weight loss, as described before.

4.15.0.5 AKT hyperactivation via Cre-mediated recombination *in vivo*

To hyperactivate AKT *in vivo*, mice transplanted with above described triple transgenic splenocytes, were induced to express AKT(E17K) by providing tamoxifen-enriched chow or control chow for two weeks upon transplantation. CLL content in the peripheral blood was followed by flow cytometry and upon 2 month, mice were sacrificed and organs harvested.

4.16 Regular blood draws

To characterize the engraftment and progression of CLL upon transplantation or in genetic models 10-30 μl blood were taken by vene puncture on a regular basis and analyzed by flow cytometry (CD19, CD5). Mice were pre-warmed for 5 min with red light and during the vene puncture mice were fixed using a restrainer.

4.17 IVIS bioimaging

Bioimaging uses external cameras to detect *in vivo* light generated in mice. The most widely utilized reporter is the firefly luciferase gene that is stably introduced into the cells. The principle of bioluminescence imaging is based on the light-emitting properties of the biochemical process, where luciferase-mediated oxidation of the molecular substrate luciferin results in light production [Fleiss and Sarkisyan, 2019]. 1 hour upon transplantation of Luciferase expressing MEC-1 cells into NSG mice, 2 mg Luciferin were applied per mouse (i.p.) and after a 10 min integration time, mice were captured using the IVIS Lumina imaging system (PerkinElmer) and exposed for 10 sec, 1 min and 5 min. Bioimaging was performed weekly during leukemia progression.

4.18 Data analysis

As primary CLL cells undergo spontaneous apoptosis in *in vitro* culture, we calculated the % of specific cell death upon drug treatment. The formula for calculation is: specific cell death (%)= 100*((%dead cells-%baseline dead cells)/(100%-%baseline dead cells)). Analysis of flow cytometry data was done with FACS Diva (Becton Dickinson) and FlowJo (Treestar, Inc.) software. For the analysis of bioimaging data the Living Image software (Perkin Elmer) was applied. Primers were designed with the help of the freeware ApE (A plasmid Editor; version 2.0.47; Copyright © 2004-2011 M. Wayne Davis). Statistical significance for the results was analyzed with paired or unpaired two-tailed Student's t test as indicated, ordinary one-way ANOVA or Log-Rank (Mantel Cox), using Prism Version 7.0, Graphpad Software Inc. Differences between analyzed groups were labeled as significant if p-value < 0.05.

Chapter 5

Results

5.1 Pathological RANK signaling in CLL

5.1.1 RANK(K240E) expression drives a CLL-like disease in aged mice

To study the effects of enforced RANK signaling, a mouse model with conditional RANK (DLBCL-derived K240E mutation) expression in B cells was generated and the initial phenotype was analyzed by Begüm Alankus as part of her doctoral thesis. In this mouse model, the human RANK(K240E) mutation, preceded by a loxP-flanked transcriptional and translational STOP cassette, was targeted into the ubiquitously expressed murine ROSA26 locus. By crossing those mice to the CD19-Cre strain, RANK(K240E) is expressed specifically in B cells from the early pro B cell stage on and CD19 positive B cells express RANK(K240E) together with GFP [Rickert et al., 1997]. As shown by Begüm Alankus, those mice exhibited B cell activation and proliferation with an expansion of the B1 B cell subset and the development of an autoimmune disease with specific features of SLE. As a result, the majority of these mice succumbed within the first 6-8 months of age with splenomegaly and lymphadenopathy, accompanied by kidney failure due to immunoglobulin complex accumulation (figure 5.1, shared data with Begüm Alankus).

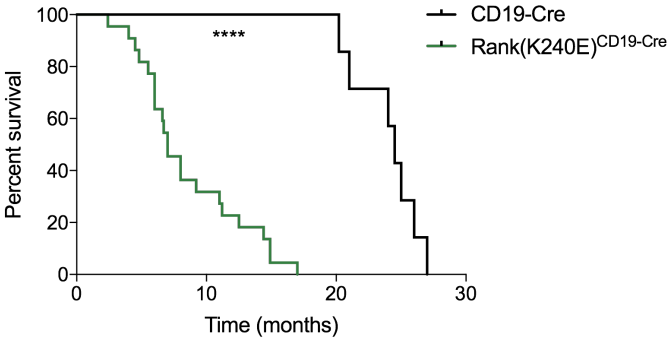

Figure 5.1: Shortened survival of RANK(K240E)$^{\text{CD19-Cre}}$ mice. Kaplan–Meier curve of CD19-Cre and RANK(K240E)$^{\text{CD19-Cre}}$ mice (n=7 CD19-Cre and n=22 RANK(K240E)$^{\text{CD19-Cre}}$). For statistical analysis, Log-Rank (Mantel Cox) analysis was performed. ****, p<0.0001.

However, several mice survived longer (over 10 month, figure 5.1), despite the autoimmune phenotype. Analysis of the spleens of those aged mice revealed further enrichment of RANK(K240E)-driven, GFP-expressing, CD19^{+}CD5^{+} B cells comprising between 10 and 73% viable splenocytes (figure 5.2). CD19^{+}CD5^{+} expression is characteristic to B1a cells in mice and they comprise the origin of the malignancy CLL [Seifert et al., 2012]. We therefore compared peripheral blood of aged RANK(K240E)$^{\text{CD19-Cre}}$ to TCL1tg-derived PB cells and indeed found high similarity (figure 5.2).

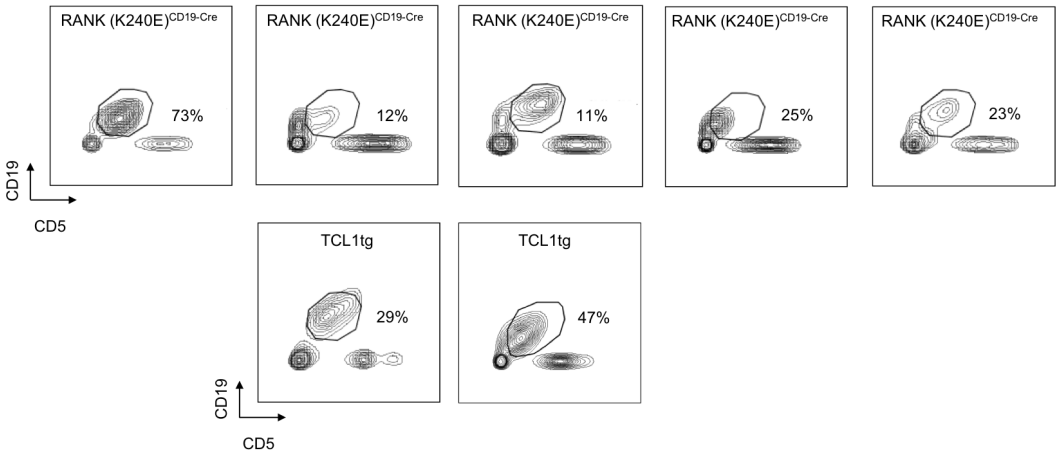

Figure 5.2: CLL-like RANK (K240E)$^{\text{CD19-Cre}}$ cells resemble TCL1tg CLL cells. Flow cytometric analysis for CD19 and CD5 expression of RANK(K240E)$^{\text{CD19-Cre}}$ and TCL1tg mice older than 12 months.

To study the malignant potential of aged RANK(K240E)$^{CD19\text{-}Cre}$ CD19$^+$, CD5$^+$, GFP$^+$ cells, we further set off to study their engraftment potential in immunocompetent C57BL/6 recipient mice. We injected, depending on donor mice cell counts, 1x10e^7-2x10e^7 splenocytes, comprising 20-73% GFP$^+$ cells (n=3 donor mice) into C57BL/6 wildtype (wt) mice and followed the engraftment and progression of GFP$^+$ CD19$^+$, CD5$^+$ cells in the recipients over time in the blood by flow cytometric analysis. As shown in figure 5.3, CD19$^+$ CD5$^+$ GFP$^+$ cells expanded, indicating the expression of RANK(K240E).

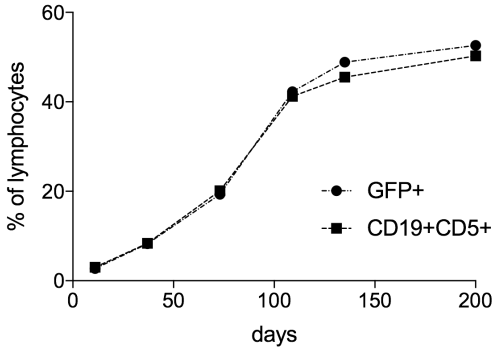

Figure 5.3: Transplantation of RANK(K240E)$^{CD19\text{-}Cre}$ splenocytes into C57BL/6 wt mice results in engraftment and progression in recipient mice. Isolated splenocytes of one representative for 5 of 7 mice analyzed >12 months of age were transplanted. After injection of 2x10e^7 splenocytes in wt recipients, the percentage of GFP$^+$ and CD19$^+$ CD5$^+$ cells was detected in the PB via regular blood draws. The engraftment of one of three different RANK(K240E)$^{CD19\text{-}Cre}$ donor mice is shown as representative.

Interestingly, GFP$^+$ yet CD5$^-$ negative B cells that were still present in two donor splenocytes were not detectable upon engraftment in C57BL/6 wt mice (figure 5.4 left pannel). All transplanted Rank(K240)$^{CD19\text{-}Cre}$ splenocytes revealed engraftment and progression of CD19$^+$CD5$^+$GFP$^+$ cells in the PB of wt recipient mice upon 3 month of transfer (figure 5.4 right graph).

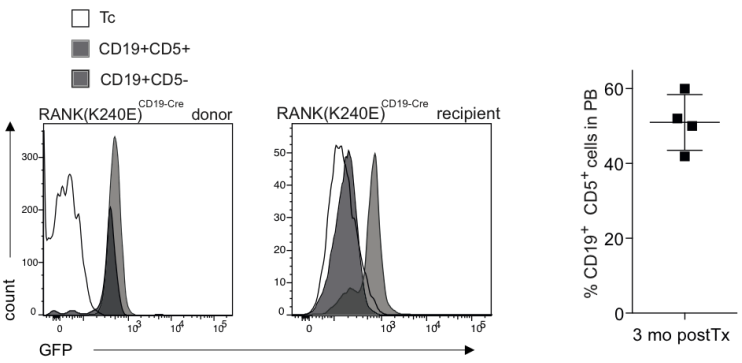

Figure 5.4: Exclusively CD5$^+$ RANK(K240)$^{\text{CD19-Cre}}$ cells engraft and progress in wt recipients (left pannel). In total n=3 different aged RANK(K240)$^{\text{CD19-Cre}}$ splenocytes were transplanted in wt recipients and all mice showed engraftment and progression in the PB upon 3 month (right pannel). Depicted is the PB flow cytometric analysis of recipients, stained for CD19 and CD5.

Based on these indications for malignant transformation of RANK(K240E) expressing B cells, we further characterized their phenotype and compared it to the classical CLL mouse model driven by the TCL1 transgene. We found low expression of B220 and low IgD on the cell surface as compared to normal wt B cells in the recipient mice. IgM levels were variable on RANK(K240E) expressing CLL-like cells. To be noted, a similar expression pattern was detected on the TCL1 oncogene driven murine CLL cells (figure 5.5). Figure 5.6 depicts the quantification of mean fluorescent intensity (MFI) for B220, IgD, and IgM of the analyzed RANK(K240E)$^{\text{CD19-Cre}}$ CLL-like mice.

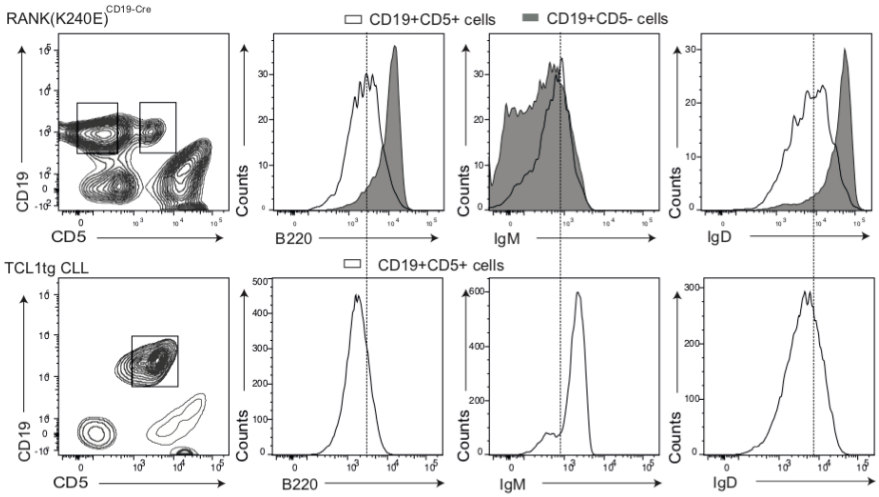

Figure 5.5: RANK(K240E)$^{\text{CD19-Cre}}$ CLL-like cells express similar amounts of B220, IgD, and variable IgM compared to TCL1-driven CLL cells. CLL phenotypic analysis was performed in wt mice retransplanted with cells from 3 independent donor RANK(K240E)$^{\text{CD19-Cre}}$ mice and compared to classical TCL1-derived splenocytes. Flow cytometric analysis and the gating strategy is depicted.

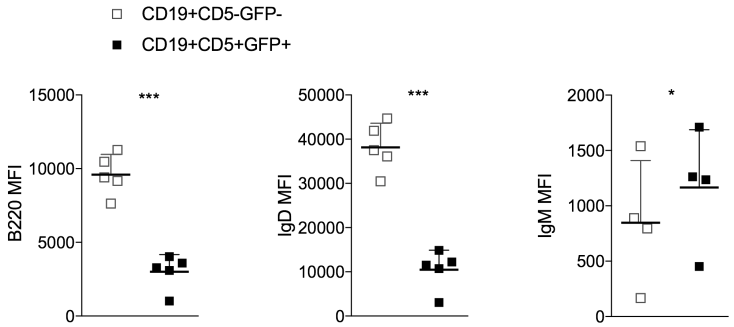

Figure 5.6: Quantification of B220 low, IgD low and and variable IgM expression levels in RANK(K240E)$^{\text{CD19-Cre}}$ mice. MFI values of B220, IgD, and IgM from 3 different donors with CLL-like cells in different wt recipients is shown. For statistical analysis, Student's t-Test with paired analysis was performed. ***, $p<0.001$; *, $p<0.05$.

Next, we analyzed the clonality of the BCR repertoire in the peripheral blood in primary and secondary recipients of aged RANK(K240E)-driven CD19^{+} cells. RANK(K240E) mice with autoimmune phenotype and shortened life span have previously been shown to contain a polyclonal BCR repertoire (Doctoral thesis Begüm Alankus). Interestingly, we found a prominent dominant clone in the donor mouse and in all recipient mice (figure 5.7 left gel, further clones from RANK-driven

B1 cells are shown on the right gel), again, strongly resembling the CLL monoclonal phenotype. In the analysis of BCR repertoires we also included wt and TCL1tg driven CLL samples. Whereas wt purifed B cells showed all four possible rearrangements, the exemplary CLL sample possessed one single rearrangement as expected.

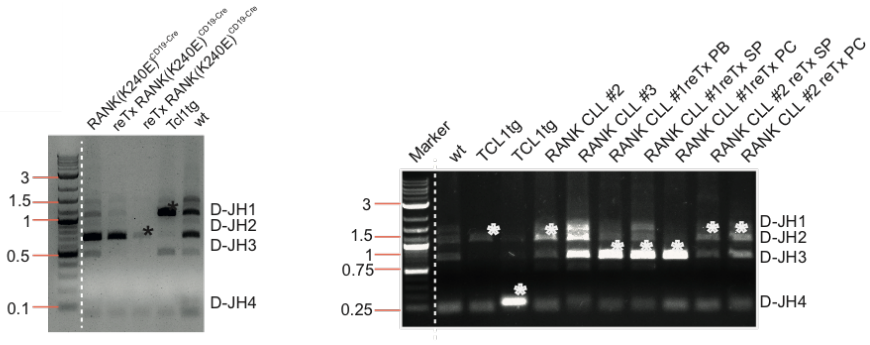

Figure 5.7: CLL-like RANK(K240E)$^{\text{CD19-Cre}}$ cells possess monoclonality. Ig clonality analysis from genomic DNA isolated from PB of wt mice transplanted with splenocytes from an aged RANK(K240E)$^{\text{CD19-Cre}}$ mouse. Isolated PB derived wt B and TCL1tg peripheral blood cells containing 70% CLL cells serve as reference.

As it could be shown by Begüm Alankus in her doctoral thesis, RANK(K240E)-driven B cells are ligand dependent and RANKL is provided by T cells and stroma cells in the bone marrow (Doctorall thesis, Begüm Alankus). Finally, we evaluated the dependency on RANKL of the transformed B1 cells and found that addition of recombinant murine RANKL resulted in a significant survival benefit of CLL-like cells, confirming the dependency on RANKL *in vitro*. This effect could be largely blocked by addition of a RANKL blocking antibody, administered 24 hours after RANKL culture (figure 5.8). Since we observed that RANK(K240E) expression contributes to malignant transformation of B1a cells, which closely resemble the phenotype of CLL, and most importantly the dependency towards RANKL remains during disease course, interference with the RANK-RANKL axis by blocking antibody might be an attractive therapeutic intervention in CLL.

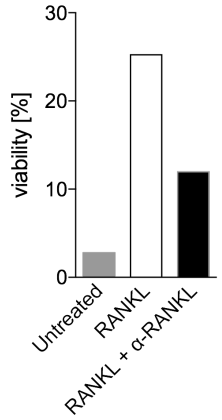

Figure 5.8: CLL-like RANK(K240E)$^{\text{CD19-Cre}}$ cells do still respond to RANKL stimulation and anti-RANKL inhibition. Depicted is the *in vitro* survival (day 10) of CLL-like cells derived from the PB of a re-transplanted wt mouse with aged RANK(K240E)GFP^{+} cells in the presence and absence of RANKL and simultaneous RANKL blocking antibodies as described.

5.1.2 RANK/RANKL signaling is important for CLL cell survival

Based on these indications for RANK signaling in CLL pathogeneisis, we set off to investigate this further. First, the expression levels on Tcl1-driven CLL were analyzed and revealed that CLL cells from TCL1-transgenic mice express significantly higher RANK levels compared to wt CD19^{+} B cells (Begüm Alankus, manuscript in preparation). We then used co-culture experiments of murine CLL cells with RANKL expressing ST-2 stromal cells and added RANKL blocking antibodies to analyze the effect on CLL cell viability. Indeed, we found decreased viability of CLL cells upon RANKL blocking antibody treatment (figure 5.9).

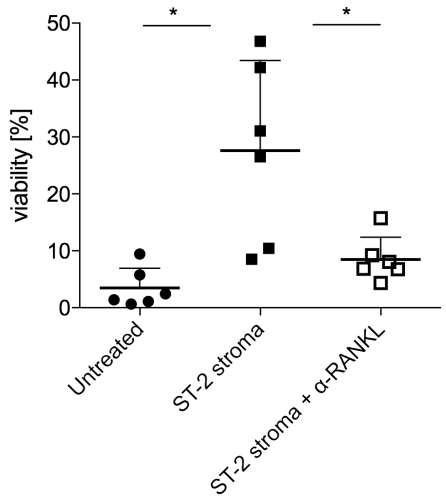

Figure 5.9: Anti-RANKL treatment of murine CLL cells in co-culture with ST-2 stromal cells decreases CLL viability. Survival of murine CLL cells *in vitro*, in the presence and absence of the RANKL expressing stroma cell line ST-2 with concomitant RANKL blocking antibody is shown upon 48 hours by flow cytometric analysis of viability. Depicted are n=6 different murine CLL samples, analyzed by flow cytometric DAPI exclusion. For statistical analysis paired Student's t-Test was applied. *, $p<0.05$.

To confirm the relevance of the RANK-RANKL axis in CLL *in vivo*, Begüm Alankus (manuscript in preparation) performed an *in vivo* experiment where TCL1tg CLL splenocytes were transplanted into C57BL/6 recipients. Mice were randomized into two groups and treated with anti-RANKL or PBS for 4 weeks. A significant reduction of CLL cells in the spleens and bone marrow of anti-RANKL treated mice was observed. Based on the enhanced RANK/RANKL expression on malignant cells derived from CLL patients [Schmiedel et al., 2013], we further set off and tested patient-derived CLL cells for anti RANKL sensitivity. Again, CLL cells were co-cultivated with ST-2 cells and blocking antibody for 48 h. We could confirm a decrease in viability upon RANKL blockade in human patient-derived CLL cells.

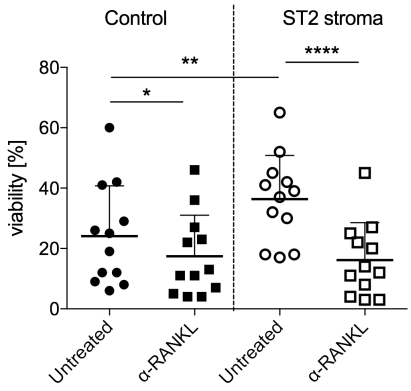

Figure 5.10: Anti-RANKL treatment of human CLL cells in co-culture with ST-2 stromal cells decreases CLL viability. Human patient-derived CLL cells (n=12 patients) were co-cultivated with the RANKL expressing stromal cell line ST-2 in the presence, and absence of RANKL blocking antibody. Viability is shown as determined by DAPI exclusion via flow cytometry and paired Student‘s t-Test was applied. *, $p<0.05$; **, $p<0.01$ ****; $p<0.0001$.

To proof the relevance of RANK signaling in human CLL *in vivo*, we used a xenograft approach with the CLL-like cell line MEC-1. 2x10e^6 MEC-1 cells were transplanted by i.v. injection into 10 immunocompromized NSG mice. 8 days post injection, anti-RANKL treatment was started in one group (n=5) while the control group received the vehicle (n=5). All control group mice showed overt signs of illness, accompanied by paralysis of the hind limps and weight loss on day 24 post injection and had to be sacrificed. Blocking murine RANKL significantly resulted in enhanced symptom-free survival and, interestingly, prevented neural symptoms (figure 5.10). Taken together, we could confirm the functional relevance of RANK/RANKL signaling in human CLL and thus support the therapeutic opportunity of this prosurvival pathway.

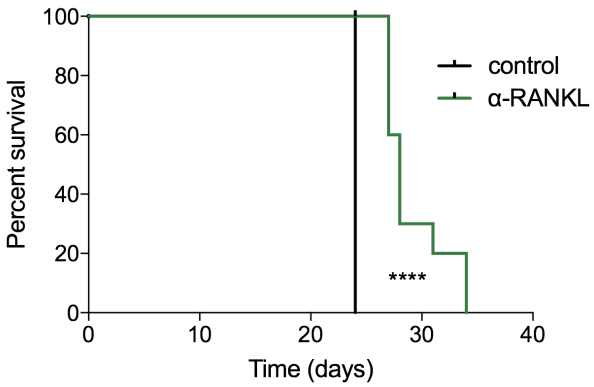

Figure 5.11: MEC-1 xenografted NSG mice show increased survival upon anti-RANKL treatment. 2x10e^6 CLL-derived MEC-1 cells were transplanted in NSG mice and on day 8, anti-RANKL treatment was initiated twice a week. Kaplan-Meier end analysis is shown and for statistical analysis Log-Rank (Mantel Cox) analysis was performed. ****, $p<0.0001$.

5.2 DUSP1/6 inhibition in CLL as novel therapeutic approach

Aberrant immune cell signaling contributes to the development of CLL. The impact of negative regulators of the MAPK signaling pathway, which is known to play an important role for CLL survival, has not been studied in CLL so far.

5.2.1 DUSP1 and DUSP6 are readily expressed and may have prognostic value

To investigate the role of the phosphatases DUSP1 and DUSP6 in CLL, we first analysed DUSP1/6 expression levels in PBMC-derived CLL samples compared to healthy donor-derived B cells by Western Blot. Figure 5.12 shows variable expression levels of both DUSP1 and DUSP6 in CLL samples, yet no significant differences compared to healthy B cells. Also with regard to the prognostic marker of mutated and unmutated IgVH region of the BCR of the CLL samples, we could not detect significant differences in expression levels; however importantly all of the analyzed CLL samples confirmed DUSP1/6 expression. Since BCR signaling is enriched in secondary lymphoid organs, we hypothesized to find enriched feedback regulation and thus increased DUSP1/6 expression levels in lymph nodes (LNs) compared to PB of CLL patients [Herishanu et al., 2011]. We analyzed DUSP1/6 messenger RNA (mRNA) data of CLL patients and indeed found significant increased DUSP1/6 levels in LNs compared to PB. (5.13; [Gutierrez et al., 2010]). To mimic increased BCR signaling in CLL niches, we co-cultivated patient-derived CLL cells with stromal ST-2 cells and found DUSP1 and DUSP6 up regulation upon stromal contact, starting upon 4 hours of CLL-stroma culture (figure 5.14). Interestingly, when looking into available patient data, we found DUSP6 to be elevated in BRAF and KRAS mutant patient samples (figure 5.15). Besides, the time to treatment was decreased in patients with high DUSP6 expression (figure 5.15).

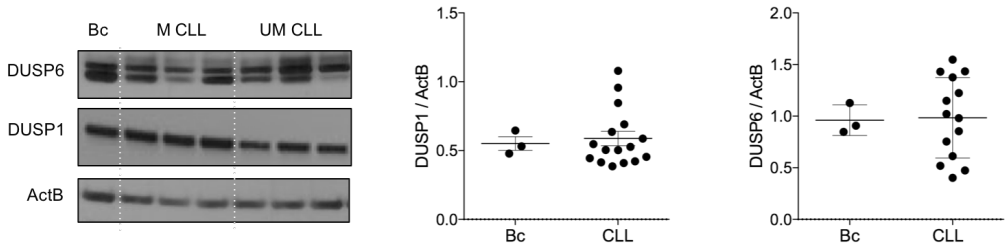

Figure 5.12: DUSP1 and DUSP6 are expressed in CLL. PBMC-derived CLL samples (n=3 mutated BCR-M; n=8 unmutated BCR-UM) compared to (n=3) healthy donor-derived B cells (Bc) were analyzed by Western Blot. DUSP1/6 and beta-actin (ActB) expression was analyzed and quantified with ImageJ.

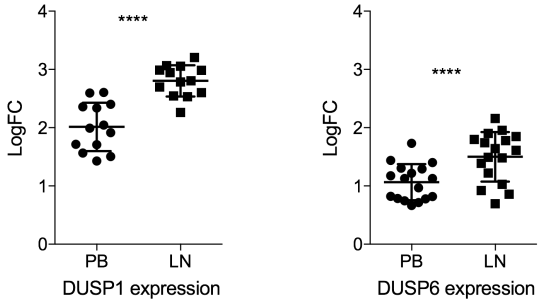

Figure 5.13: DUSP1/6 is upregulated in CLL LNs compared to PB. Published patient CLL mRNA data [Gutierrez et al., 2010] was analyzed for DUSP1/6 expression in matched LNs compared to PB. Student's paired t-Test was applied. ****, $p<0.0001$ for both DUSP1 and DUSP6.

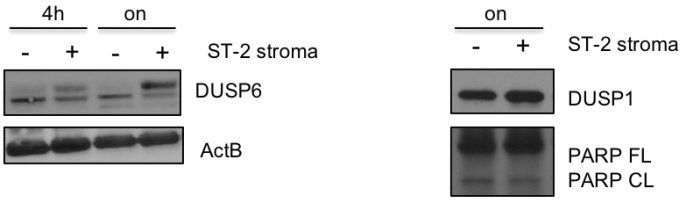

Figure 5.14: DUSP1/6 is upregulated in CLL cells upon stromal co-culture. Patient-derived CLL cells were co-cultivated with ST-2 cells for the indicated period of time (on: overnight). CLL cell lysates were prepared for subsequent Western Blot analysis of DUSP1/6. For each phosphatase n=2 patient samples were tested and one representative example is depicted.

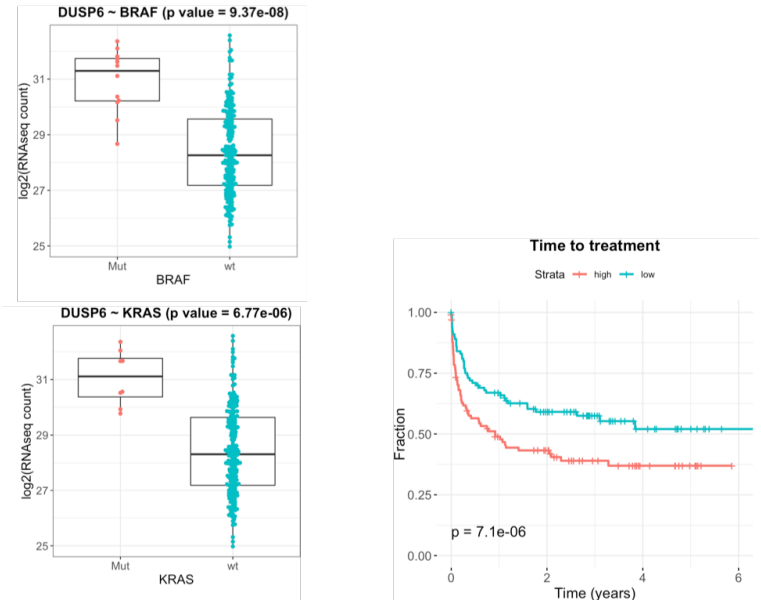

Figure 5.15: DUSP6 is upregulated in BRAF and KRAS mutant CLL samples and high DUSP6 expression correlates with decreased time to treatment and decreased overall survival. Depicted is RNA sequencing data analyzed by Junyan Lu (DKFZ Heidelberg; [Zenz et al., 2019])

5.2.2 Inhibition of DUSP1/6 by small molecule inhibitor BCI induces cell death in CLL

As both DUSP1 and DUSP6 are expressed and upregulated in secondary lymphoid organs where CLL cells proliferate, we propose a functional role of both phosphatases in CLL. Thus, we studied the effects of DUSP1/6 inhibition on CLL cell survival. We made use of the small molecule inhibitor BCI, stated to inhibit both DUSP1/6 ([Molina et al., 2009]; Axonmedchem BCI-NSC 150117). Primary human PBMC-derived CLL cells were incubated with different concentrations of BCI for 48 h. Figure 5.16A shows a strong dose-dependent increase in specific cell death upon BCI addition. Interestingly, when healthy PBMC-derived isolated B cells (n=4) and distinct B cell lymphoma cell lines (BJAB, SUDHL6, Bal17) were simultanously treated with BCI, no striking differences in viability could be detected. However, two CLL-like cell lines (MEC-1 and EHEB) confirmed the selectivity of BCI towards CLL cells with a strong induction of specific cell death (figure 5.16B). To further validate this selectivity, we measured the kinetics of the CLL cell line MEC-1 treated with different doses of BCI over a time period of 24-72 hours and compared its viability to

three non-CLL cell lines, namely HBL-1 (DLBCL), Jurkat, and HUT-78 (both T cell lymphoma). We could confirm a strong selectivity for the induction of cell death in the CLL MEC-1 cells (figure 5.16 C) during all time points, whereas non-CLL cell lines weakly responded towards DUSP1/6 inhibition and recovered over time. Since CLL cells strongly depend on their microenvironment, we mimicked the interaction with bystander cells, with co-culture experiments of ST-2 stroma and CLL cells treated with BCI for 48 hours. As expected, the stromal co-culture induced a very strong protective effect and elevated the viability of CLL cells, however with higher doses (10 μM) of BCI this protection could be overcome. To explore DUSP1/6 inhibition in an *in vivo* setting, several attempts to increase BCI pharmacokinetics (PKs) and biodistribution were undertaken, described in the following section.

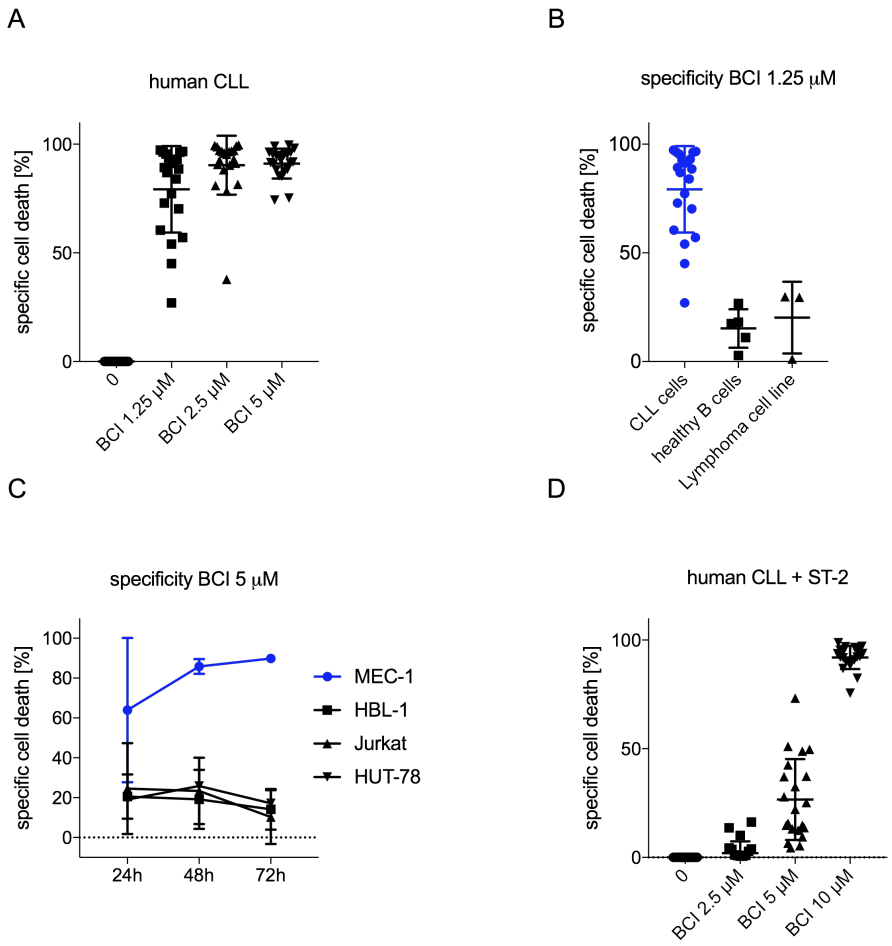

Figure 5.16: DUSP1/6 inhibition by small molecule inhibitor BCI induces cell death in CLL cells and is more specific for CLL cells. A) Patient-derived CLL cells (n=21) were treated with BCI at the indicated concentrations and viability was measured upon 48 h. B) CLL patient-derived cells, CLL cell lines, healthy B cells, and B cell lymphoma cell lines were treated with 1.25 µM BCI for 48 hours. B lymphoma cell lines were applied at suboptimal condition to mimic spontaneous CLL apoptosis *in vitro*. C) MEC-1, HBL-1, Jurkat, and HUT-78 cells were synchronized over night and then treated with 5 μM BCI. Cell viability was determined after 24, 48, and 72 hours. D) Patient-derived CLL cells were co-cultivated with ST-2 stroma cells and treated with BCI at indicated concentrations. Upon 48 h, CLL cells were carefully separated from stroma cells and viability was measured. In all experiments viability was analyzed by flow cytometric measurement of DAPI exclusion and is depicted as % specific cell death.

5.2.3 Validation of distinct BCI-nanoparticle formulations to improve the *in vivo* application

Due to the poor solubility of BCI, *in vivo* application is challenging. To overcome this, we collaborated with a research group of nanoparticle experts from University Medical Center Utrecht (Marcel Fens, Aida Varela-Moreira). A certain group of Nanomedicines, namely polymeric micelles, can accomodate poorly soluble small molecules and are known to accumulate specifically in solid tumors, due to the EPR effect within the tumor mass resulting from rapid angiogenesis and inflammation [Jain and Stylianopoulos, 2010]; [Deshantri et al., 2018]. Whether nanoparticles are suitable for hematological malignancies and in particular CLL therapy is not very well understood, as it is not very extensively studied. Thus, to investigate whether nanoparticles possess prolonged circulation times in blood and consequently accumulate in CLL-infiltrated organs, we performed several *in vivo* studies using micellar particles with fluorescent labeled polymer. We chose the TCL1tg mouse as commonly applied CLL model and compared the accumulation of micelles in the spleen as the main site of infiltration in this model. Figure 5.17A shows in two independent experiments a spleen infiltrated with CLL (about 10% CLL of splenocytes) and in figure 5.17B a fully infiltrated spleen with about 70% CLL is depicted. In both cases, we observed an accumulation of the Cy7 polymer in CLL-infiltrated spleens regardless of CLL stage. As a control for equal micellar injection, the kidneys of the respective mouse are shown, in which no CLL infiltration took place. The murine CLL cells transplanted in the experiment shown in figure 5.17B also strongly infiltrated the liver and we analyzed the liver tissue for micellar accumulation by IVIS bioimaging and found elevated accumulation. The non-CLL-infiltrated kidneys, on the other hand, showed reduced fluorescence intensity, presumably due to the high accumulation in CLL-infiltrated organs (figure 5.17B). Since it is known that CLL cells grow only in the presence of the signal PKC-β in the recipient animal and this seems to be critical, so that CLL cells can form their (inflammatory) niche, we have included PKC-β knockout animals in the study [Lutzny et al., 2013]. Strikingly, these showed no micellar accumulation in liver and spleen despite splenohepatomegaly after CLL injection, as shown by Cy7 quantification of the entire organs after IVIS measurement

(figure 5.17B). Based on the increased enrichment of micelles in inflamed CLL organs, we continued to test the loading of BCI into micelles. First, we analyzed the plasma levels of BCI after injection of the free compound. Our collaboration partners found, using HPLC, that no measurable levels of BCI were detectable in plasma of mice as early as 1 minute after injection of the free drug (figure 5.17C). When BCI micelle formulations were injected, the BCI detection was prolonged. Most of the BCI had already dropped below 40% of the injected dose after 1 hour, while the Cy7-polymer was still detectable at higher percentage (figure5.17D). Initial therapeutic trials with these micelles (40 mg/kg) showed that this increase in bioavailability of BCI was, though increased to free drug, still insufficient to induce a significant reduction in CLL progression. To study this, we transplanted murine diseased TCL1tg splenocytes in wt recipients and one cohort received 6 doses of BCI micelles and was compared to vehicle control (i.e. micelles without BCI). At day 6 (upon the first 3 doses), we detected a decline of CLL cells in the PB (figure 5.18A). However on day 21 upon treatment start, organs were harvested to analyze CLL infiltration and revealed no differences in CLL content. In addition, experiments with xenografted patient-derived CLL cells from 3 different donors were performed (n=3). In one xenograft experiment (xenograft 1), we could detect a transient decrease of CLL cells in the peripheral blood (figure 5.18B). Figure 5.18B (xenograft 2) shows a trend for reduced CLL content in the spleen and remarkably, an increase in human T cells. Another xenograft experiment revealed no significant differences.

Based on the fast release of BCI from the micelles *in vivo*, we then set off to to obtain more stable encapsulation and decreased BCI release *in vivo*. For this, our collaboration partners loaded BCI hydrochloride (BCI-HCl), a less hydrophobic version of BCI, into liposomes. However, this approach was limited by the amount of BCI-HCl that could be loaded inside liposomes and we could not detect a significant reduction in CLL burden in the TCL1tg model by application of 6 mg/kg BCI-HCl liposomes that were injected daily for 9 days. Besides, PK studies revealed again insufficient retentionof the BCI-HCl inside the liposomes upon injection. However, despite poor PK, during the treatment course we found again a transient, yet not significant increase of T cells in the PB (figure 5.18C). Taken together, we could show that nanomedicines, and in particular polymeric micelles, are in principle a

promising approach to deliver CLL targeting therapeutics; however, for BCI delivery, further improvements will be essential to achieve sufficient BCI *in vivo*, in order to cross the upper tolerable signaling strength.

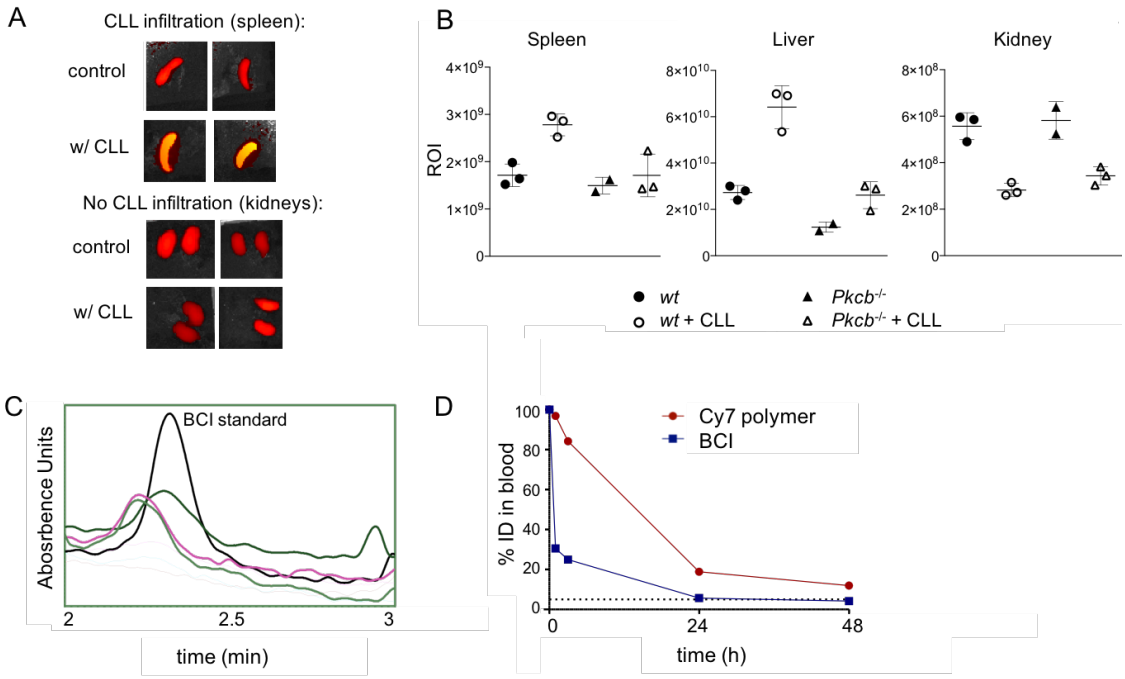

Figure 5.17: BCI micelles improve the delivery of BCI *in vivo*, yet further improvements are required. A) Accumulation of Cy-7-labeled micelles in CLL infiltrated spleen and non CLL infiltrated kidneys were measured by IVIS bioimaging 24 h upon i.v. injection. B) Quantification of Cy-7 with regard to CLL infiltration in the respective organs. ROI: Region of Interest. C) HPLC analysis of BCI plasma concentration was measured 1 min upon i.v. injection of free BCI. Black line shows the lowest detectable concentration of the BCI standard curve. D) Measurement of BCI and Cy-7 polymer at indicated time points in PB upon i.v. injection of micelles in C57BL/6 mice shows premature release of BCI, whereas polymer is more stable. ID: Internal Diameter.

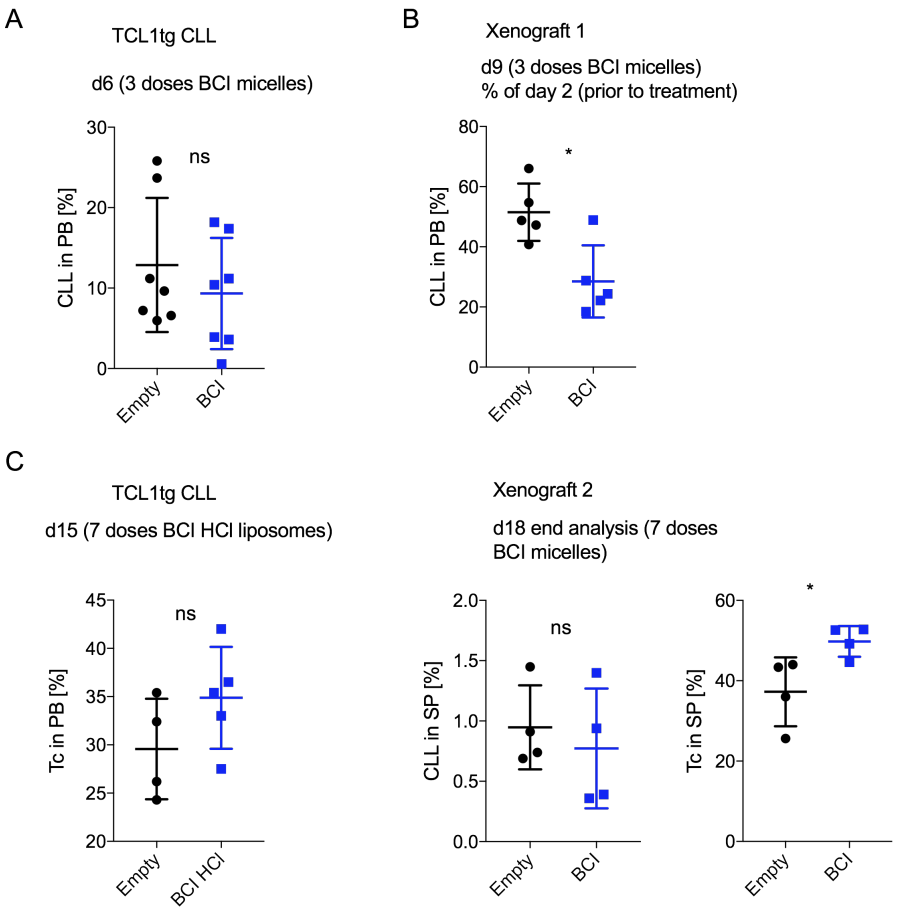

Figure 5.18: BCI micelle application *in vivo* transiently decreases CLL burden and increases the percentage of T cells. A) 6 doses of BCI micelles compared to vehicle control were applied in the TCL1-driven CLL model *in vivo*. On day 21 upon treatment start, organs were harvested to analyze CLL infiltration and revealed no differences. Depicted is a transient decline of CLL cells in the PB analyzed on day 6, upon 3 doses, by flow cytometric analysis of $CD19^{+}CD5^{+}$ viable cells. B) One (out of 3) xenograft experiments (Xenograft 1) revealed a significant decline of CLL cells in the peripheral blood at day 9 during BCI micelle treatment upon the third dose. In total 4 doses at day 3, 6, 8, 10 were injected. End analysis at d 11 revealed no differences in spleens (data not shown). Another independant approach (Xenograft 2) shows the end analysis of spleens with a trend towards reduction in CLL cells and a significant increase in human T cells. Treatment schedule comprised 7 doses, on day 1, 3, 5, 7, 10, 12, 15 at 40 mg/kg. End analysis was performed at day 18. Depicted are murine $CD45^{-}$, human $CD45^{+}$, human $CD19^{+}$, and $CD5^{+}$ cells (CLL) and murine $CD45^{-}$, human $CD45^{+}$, human $CD19^{-}$, and $CD5^{+}$ cells (T) analyzed by flow cytometry. C) BCI-HCl liposomes were tested in the murine TCL1tg model. Depicted is an increase of T cells on day 15 upon 7 doses in the PB, measured by flow cytometric detection of murine $CD5^{+}$ viable cells. In total 9 doses were applied and on day 20 no significant differences could be detected in the harvested organs. A-C) For statistical analysis unpaired Student‘s t-Test was performed. *, $p<0.05$.

5.2.4 Genetic deletion of *DUSP1/6* confirms small molecule inhibitor (BCI) effects

To address the specificity of BCI to inhibit DUSP1/6, we aimed to generate *DUSP1* and *DUSP6* single knockouts. We used the CLL cell line MEC-1 Eco and used two distinct experimental setups to generate genetic knockout lines. First, we generated stable Cas9-GFP-expressing MEC-1 cells by retroviral manipulation and then introduced different guide sequences. Four different sgRNA were tested for *DUSP1*, and upon Puromycin selection, single cells were sorted into 96 well plates. Since the knockouts are expected to be lethal or provide a growth disadvantage, outgrowth of potential knockouts was attentively followed. Figure 5.19A depicts two successful knockouts for *DUSP1*. In order to investigate the proliferative capacity of the *DUSP1* knockouts, we performed competition assays with wt MEC-1 cells. On day 0, we mixed equal amounts of MEC-1 wt (GFP^-) and *DUSP1* knockout cells (GFP^+) and followed the percentage of GFP over time. Strikingly, both knockouts tested had a selective growth disadvantage compared to the wt counterpart. Figure 5.19B shows one knockout (ko) compared to *DUSP1* wt cells. Importantly, *DUSP1* wt cells (MEC-1 Cas9 GFP^+) cells did not alter the ratio of GFP over time when mixed with wt MEC-1 (GFP^-) cells. To confirm a functional relevance of DUSP1 *in vivo*, we transplanted NSG mice (n=2 each group) with either MEC-1 *DUSP1* ko or wt cells. We observed a trend towards prolonged survival (5 days) in mice injected with *DUSP1* ko cells. Further *in vivo* experiments will be essential to proof the functional relevance of both DUSP1/6. In a second CRIPSR/Cas9 approach, we introduced Cas9 and the respective sgRNAs simultanously via electroporation (vector Px458 Addgene Plasmid 48138; containing distinct sgRNAs), leading to transient expression of both components [Ran et al., 2013]. 2 days upon electroporation, GFP^+ cells were single cell sorted in 96 well plates. Figure 5.19D depicts successful knockouts for both *DUSP1* and *DUSP6*. In order to investigate the proliferative capacity of the *DUSP1/6* knockouts, we performed again competitor assays with wt MEC-1 GFP^+ cells, since knockouts were GFP^- in this setting. We could confirm a growth disadvantage of both *DUSP1/6* knockouts (figure 5.19E right graph), whereas again wt GFP^- cells mixed with GFP^+ cells grew in constant ratios over time (figure

5.19E left graph). To note, an attempt to generate *DUSP1/6* double knockouts was not successful. Whether indeed combined knockout is lethal or toxicity of the electroporation approach resulted in the failure of double knockout generation needs further investigation.

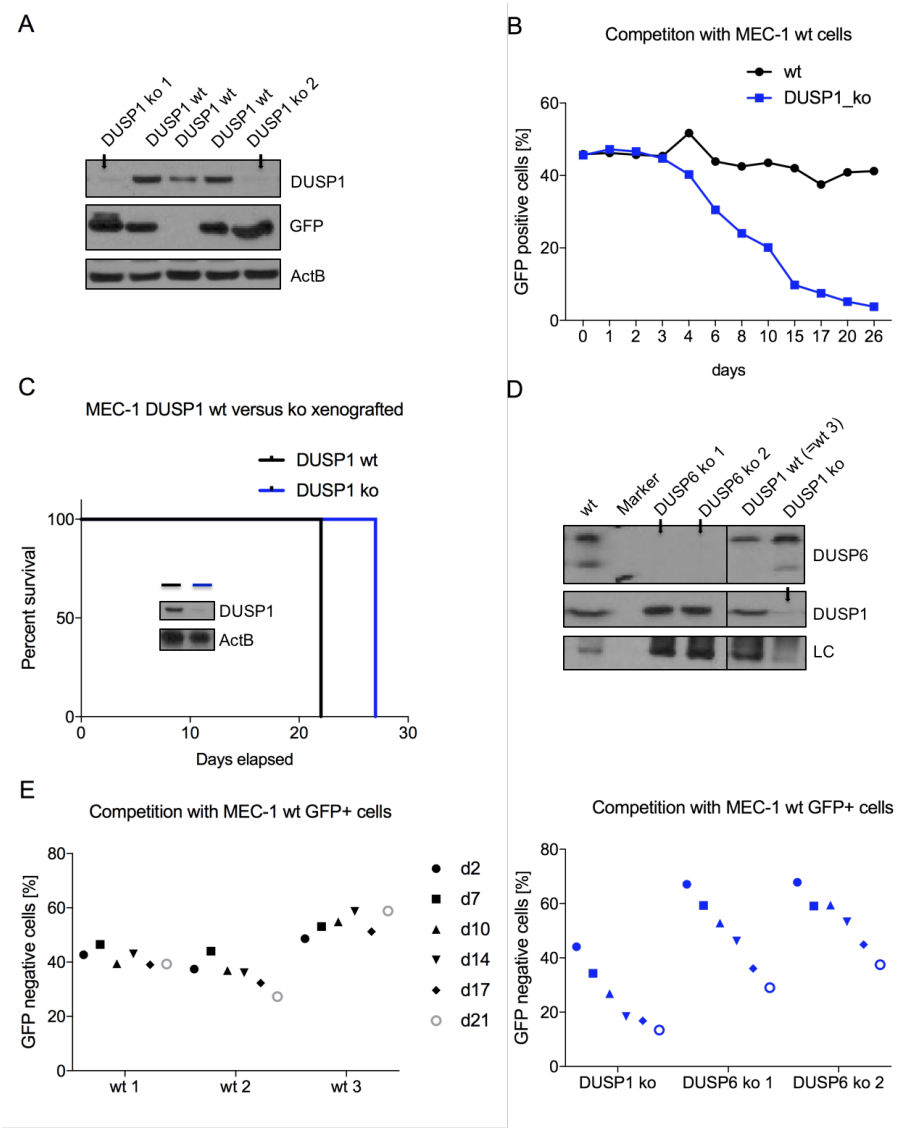

Figure 5.19: *DUSP1* and *DUSP6* knockout in MEC-1 cells leads to a growth disadvantage. A) *DUSP1* CRISPR/Cas9 knockouts (MSCV-based approach) were validated by Western Blot. B) Competitor assays of *DUSP1* ko with MEC-1 wt cells analyzed by flow cytometry. C) Kaplan Meier survival curve of mice xenotransplanted with *DUSP1* wt versus *DUSP1* ko MEC-1 cells. Western Blot shows DUSP1 protein level of injected MEC-1 wt and ko cells. D) *DUSP1/6* CRISPR/Cas9 knockouts (Amaxa electroporation-based approach) were validated by Western Blot E) Competitor assays of *DUSP1* ko and *DUSP6* ko with MEC-1 wt GFP^+ cells analyzed by flow cytometry. The legend is representative for both graphs (wt and ko cells).

5.2.5 Mechanism of cell death induction by DUSP1/6 inhibition

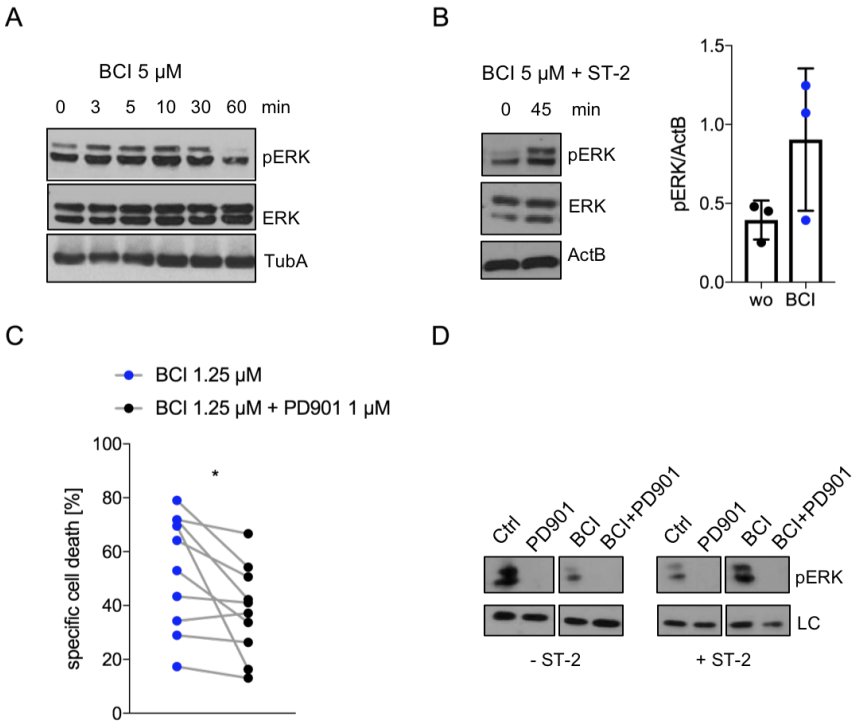

Figure 5.20: DUSP1/6 inhbition increases phosphorylated ERK (pERK) and inhibition of MEK partially reverts the induction of specific cell death by BCI. A) Primary patient-derived CLL cells were treated for the indicated time with BCI and protein lysates were analyzed by Western Blot. B) Primary patient CLL cells were cultivated with ST-2 stroma cells for 5 h and then treated with 2.5 μM BCI for 45 min. One representative Blot is shown and quantification was performed for n=3 patients with ImageJ. C) Primary patient-derived CLL cells (n=8) were pre-treated for 1 h with the MEK inhibitor PD0325901 (PD901), then BCI was added for 48 h. Viability was analyzed by DAPI stain and flow cytometry. Depicted is the induction of specific cell death and statistical analysis was performed by paired Student's t-Test. **, $p<0.01$. D) Western Blot analysis of patient-derived CLL cells treated with indicated drugs (2,5 μM BCI and 1 μM PD901) and combinations in ST-2 co-culture as described in B).

To understand how inhibition of DUSP1/6 induces cell death in CLL cells, we performed Western Blot analysis of the direkt downstream targets pERK1/2. We found a slight and transient increase in both ERK1/2 as early as 3 to 10 min upon BCI addition with a quick and strong decrease between 30 and 60 min. When we co-cultivated CLL cells on stroma cells and thus provided a protective effect, the increase of pERK was still present upon 45 min of BCI treatment (figure 5.20B).

To further confirm on-target effects, we added a MEK inhibitor to interfere with MAPK signaling. Pre-treatment of human CLL cells with the MEK inhibitor (PD901) partially reversed the induction of specific cell death by BCI treatment after 48 h (figure 5.20C). This was also reflected in a decrease in pERK upon combinatorial MEK and DUSP1/6 inhibition, as shown by Western Blot (figure 5.20D). To better dissect the complex downstream signaling networks, we further performed a global phosphoproteome analysis of CLL cells treated with BCI (collaboration with Bernhard Küster, Piero Giansanti; TUM).

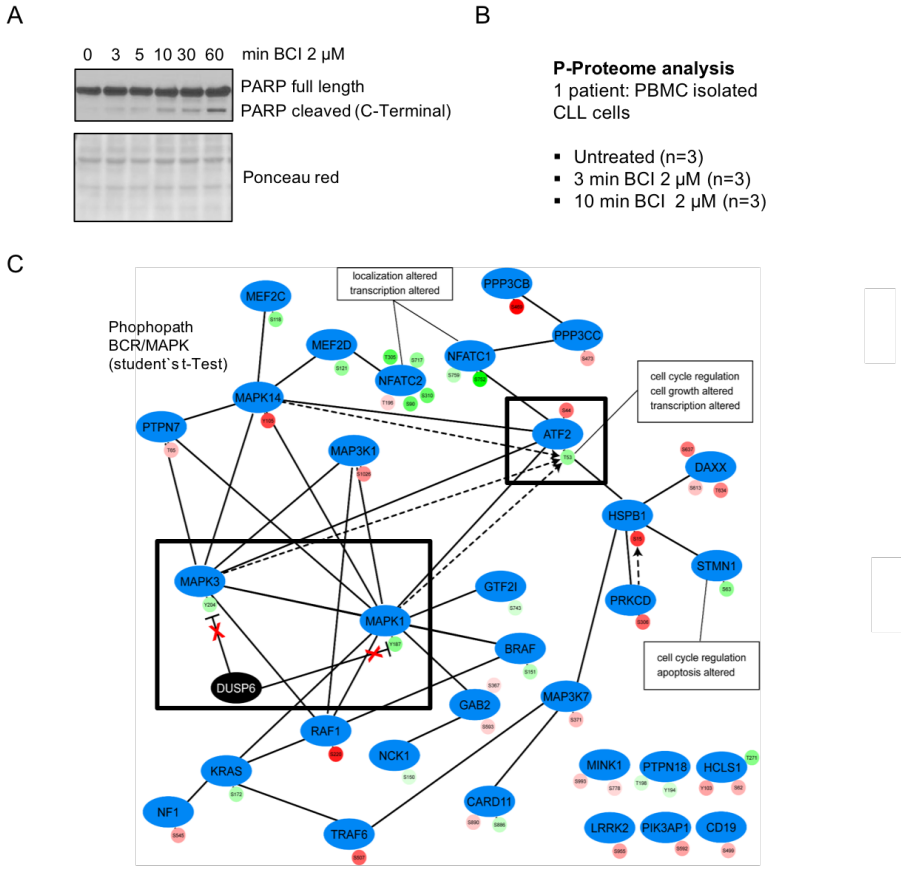

Figure 5.21: CLL phosphoproteome analysis of patient-derived CLL cells upon BCI treatment. A) DUSP1/6 inhbition induces PARP cleavage upon 3 min. CLL patient cells were treated with 2 μM BCI and protein lysates were analyzed by Western Blot. B) Parameters for phopshoproteome analysis upon DUSP1/6 inhibition in patient-derived CLL. C) Network analysis upon 10 min BCI treatment compared to untreated primary CLL cells.

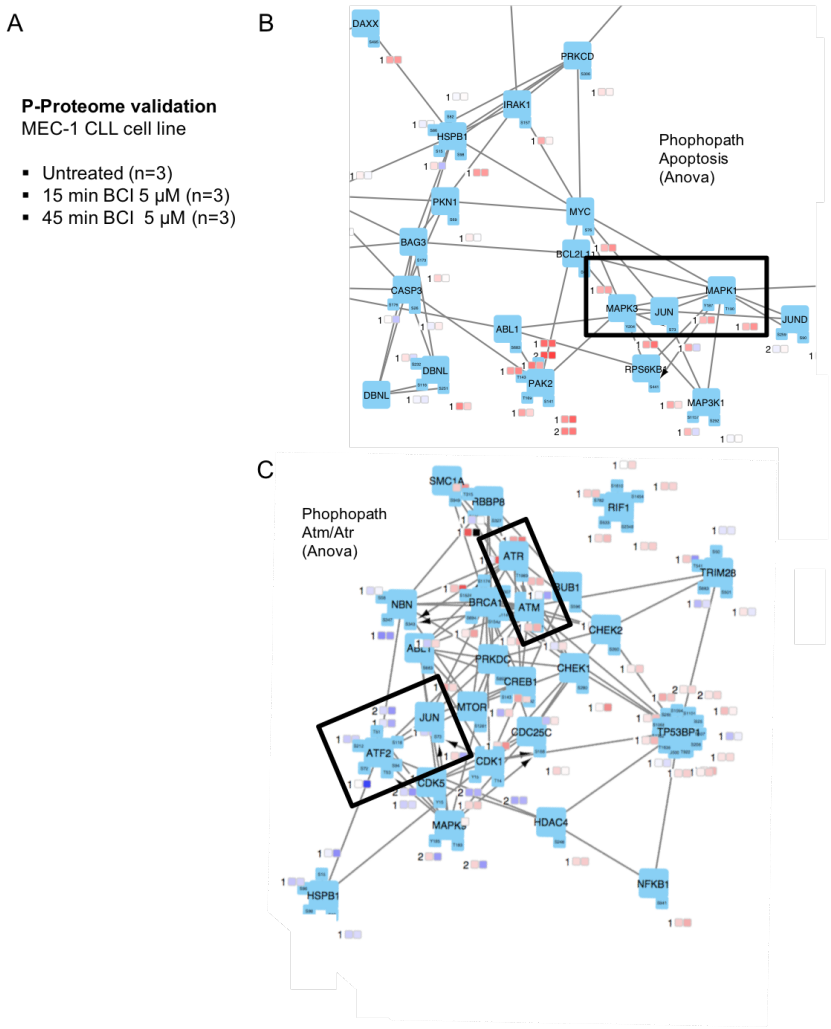

Figure 5.22: CLL phosphoproteome analysis of MEC-1 CLL cells upon BCI treatment. A) Parameters for phosphoproteome analysis upon DUSP1/6 inhibition in MEC-1 CLL cells. B) PhosphoPath Network analysis upon 45 min BCI treatment compared to untreated MEC-1 CLL cells, depicting an apoptosis network. C) PhosphoPath Network analysis comprising Atm/Atr networks. For statistical analysis Anova comparison was performed. Data was analyzed by Piero Giansanti (TUM).

In order to avoid interference with secondary events, such as apoptosis induction, we first performed Western Blot analysis of PARP cleavage induction upon BCI treatment. As PARP cleavage occurred as early as 3 min upon BCI addition, we decided to measure phosphoproteome changes upon 3 and 10 min BCI treatment

in one primary CLL sample (figure 5.21A+B). However, only upon 10 min BCI treatment significant alterations in phospho sites were detected. We found among the most significant regulated pathways BCR and MAPK signaling, which further confirmed on target activity of BCI on both ERK1 and ERK2 (figure 5.21C). One interesting event was the increase of pATF2 (figure 5.21C), a master regulator of cell cycle, proliferation, and apoptosis. Validation of its regulation by Western Blot confirmed the increase of activated ATF2 in several patient-derived CLL cells (figure 5.23A). Moreover, the CLL cell line MEC-1 confirmed specific upregulation of pATF2 in CLL, which was absent in DLBCL and two T cell lines treated simultanously (figure 5.23B). PD901 treatment was used to confirm that ATF2 phosphorylation is not an unspecific, apoptosis-related event in CLL upon cell death induction. Along with increased pATF2, we also found an increase in p-c-JUN and pJNK together with slightly elevated pMAPK38 (figure 5.23A+C). Since primary CLL cells derived from patients underly strong heterogenity, we decided to use the MEC-1 cell line to validate our results with a second phosphoproteome analysis upon treatment (figure 5.22A). We used the kinetics of pATF2 and p-c-JUN to determine appropriate time points for BCI treatment of MEC-1 cells, via Western blot (figure 5.23B+C). To detect further downstream effects of BCI, we used a 15 and 45 min timepoint for the analysis (figure 5.21B). Overall the results of treated MEC-1 cells confirmed the above described events in one patient-derived CLL sample. Moreover, several apoptosis related kinases (ATM, ATR) were predicted to be involved and motif prediction revealed amongst other sites, associations with 5 -adenosine monophosphate (AMP)-activated protein kinase (AMPK) . In order to determine whether the implicated AMPK activation is critical for BCI-mediated cytotoxicity, we co-treated CLL cells with Compound C (Comp C), an AMPK inhibitor, and BCI. However, we observed increased cell death by the combination of the two substances, implying AMPK is activated as a potential rescue strategy of the cell (figure 5.23D). We also tested whether checkpoint-kinase 1 (CHK1) inhibiton alters BCI-induced cell death and found trends for reduced specific cell death upon CHK1 inhibition, by LY2603618 (LY260). This implies that BCI mediates cell death partially via activation of the DNA damage response pathway (figure 5.23D). To validate apoptosis induction that is implicated by activation of apoptosis related kinases, we performed AnxV stainings

24 h upon BCI treatment in patient-derived CLL cells (5.23E). We confirmed the exposure of phosphatidylserine (PS) on the outer membrane, which could be partially reverted by pre-incubation with a pan-caspase inhibitor (z-VAD). Taken together, we could confirm on target effects comprising MAPK and BCR signaling upon DUSP1/6 inhibition and in particular found phosphorylation of ATF2 and c-JUN, which points towards the involvement of a DDR response during caspase mediated cell death induction with apoptotic features.

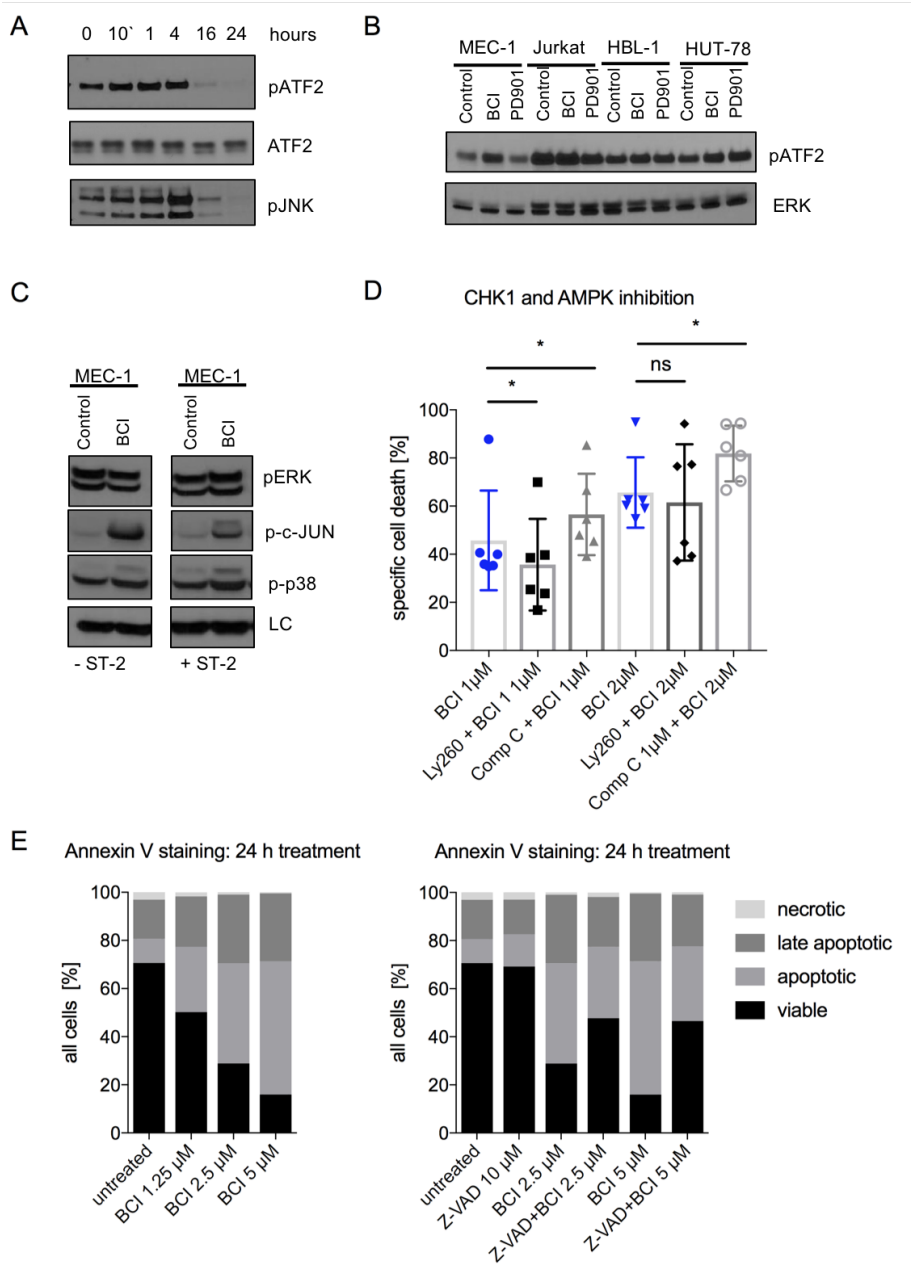

Figure 5.23: Validation of phopshoproteome results. A) DUSP1/6 inhibition increases pATF2, p-c-JUN, and pJNK in patient-derived CLL cells treated with 2 μM BCI. Upon BCI treatment for the indicated time, protein lysates and Western Blots were performed. B) Increase of pATF2 in MEC-1 cells compared to Jurkat, HBL-1, and HUT-78 cells upon BCI treatment for 10 min. C) Kinetics of pERK, p-c-JUN, and p-p38 in MEC-1 cells treated with BCI for 45 min in presence and absence of stroma cells. D) Inhibition of AMPK prior to BCI treatment increases specific cell death in patient-derived cells (n=6) whereas CHK1 inhibition slightly reverses cell death. Viability was analyzed by flow cytometric exclusion of DAPI and for statistical analysis paired Student's t-Test was performed. *, $p<0.05$. E) Analysis of apoptosis induction and involvement of caspases upon BCI treatment in patient-derived CLL cells (n=6). 24 h upon BCI treatment samples were stained with AnxV and DAPI and analyzed by flow cytometry.

5.2.6 DUSP1/6 inhibition in drug-resistant CLL

Since resistances are emerging in clinical patient care and are very challenging to treat, we aimed to analyze the effect of DUSP1/6 inhibition in Idelalisib and Ibrutinib resistant cells. To this end, we generated Idelalisib and Ibrutinib resistant MEC-1 cells by respective drug treatment over a period of 6 months, twice weekly, with increasing doses over time. Untreated MEC-1 cells were cultured in parallel and served as controls. Both cell types were left untreated at equal cell count overnight and then treated with BCI for 48 h. Strikingly, we found a strong increase in the induction of specific cell death in Idelalisib resistant cells (figure 5.24 left pannel). Also in Ibrutinib resistant cells, we found similar trends (figure 5.24 right pannel), although the Ibrutinib resistance was not evident from our drug testing. To proof a clinical relevance for this observation, the treatment of patient-derived Ibrutinib and Idelalisib resistant CLL cells is of future interest.

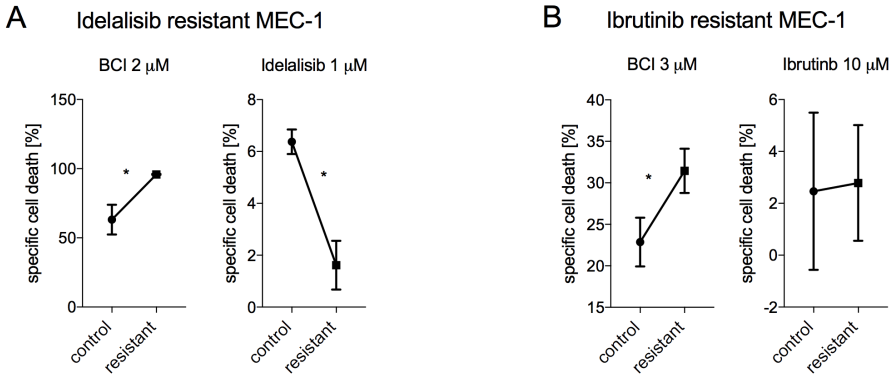

Figure 5.24: MEC-1 Idelalisib/Ibrutinib-resistant cells appear more sensitive for DUSP1/6 inhibition. A) Idelalisib-resistant MEC-1 cells and wt cells were treated with BCI for 48 h and viability was measured by flow cytometry and DAPI exclusion. Treatment with Idelalisib proves the generation of resistance over time. B) Ibrutinib-resistant MEC-1 cells and wt cells were treated and analyzed as described in A). For statistical analysis, paired Student‘s t-Test was performed on technical triplicates. *, $p<0.05$. Depicted is one example each, representative for two independent experiments with similar results.

5.3 SHIP1 is critical for CLL progression and immunosurveillance

5.3.1 SHIP1 is expressed and active in CLL

Another very important BCR downstream signaling branch is PI3K/AKT activation and here we assessed the functional role of the negative PI3K regulator SHIP1, which is in contrast to PTEN described to be active in CLL. To investigate the role of the phosphatase SHIP1 in CLL we analyzed PBMC-derived healthy B cells and patient-derived CLL cells for SHIP1 protein expression by Western Blot. We found SHIP1 to be expressed in all CLL cell samples at variable levels with no significant difference to healthy B cells. Interestingly, by using a phospho-specific Tyr1020 SHIP1 antibody, to detect phosphorylated (p)SHIP1, we found partially high phosphorylation levels in CLL samples, suggesting active SHIP1 in CLL (5.25).

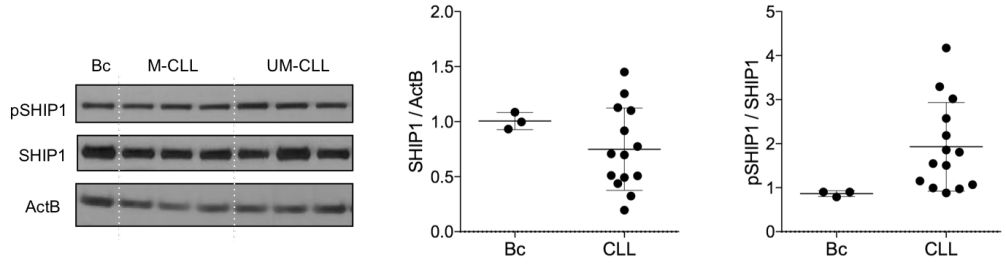

Figure 5.25: SHIP1 is expressed and active in CLL. PBMC-derived CLL samples (n=3 mutated BCR-M; n=8 unmutated BCR-UM) compared to healthy (n=3) B cells (Bc) were analyzed by Western Blot. SHIP1 and ActB expression were analyzed and quantified with ImageJ.

5.3.2 Inhibition of SHIP1 phosphatase activity reduces CLL cell survival and disease progression

In order to test a potential functional role of SHIP1 in CLL, we next evaluated the effects of a small molecule inhibitor named 3-a-aminocholestane (3AC) to inhibit SHIP1 in CLL cells [Brooks et al., 2010].

5.3.2.1 Small molecule inhibition of SHIP1 *in vitro* induces CLL cell death with necroptotic features and is accompanied by a transient increase in pAKT.

We started to evaluate the effects of SHIP1 inhibition on CLL cell viability *in vitro* and found dose-dependent cytotoxicity at 2.5-20 μM 3AC, as depicted by an increase in specific cell death (figure 5.26A). The IC50 of 3AC for SHIP1 inhibition in a cell-free assay is described as 10 μM (Calbiochem). Interestingly, by implementing different B cell lymphoma cell lines and also healthy PBMC-derived B cells, we found a strong selectivity for CLL cells to respond to 3AC treatment with a reduction in cell viability. Since the viability of primary CLL cells is reduced upon standard cell culture conditions we cultured the B lymphoma cell lines at suboptimal condition and found that some non-CLL cell lines, in strong contrast to CLL samples, benefit from 3AC treatment. However, two CLL-like cell lines MEC-1 and EHEB responded, similarly to CLL primary samples, with a strong induction of 3AC-mediated specific cell death (figure 5.26B). To further unravel the mode of cell death, we performed AnxV stainings to measure PS exposure, one hallmark of apoptosis, on the outside of the cell membrane. We found no consistent induction of PS. Only 1 (human CLL 3) out of 4 different patient samples tested showed increased PS levels that could be partially reverted by co-treatment of CLL cells with a pan-caspase inhibitor (z-VAD) 1 h prior to 3AC treatment for 48 h (figure 5.27). In addition, we tested several other pan-caspase inhibitors (Emricasan and QTD) and a specific caspase-8 inhibitor (Z-IETD). Only QTD could partially restore the induction of specific cell death by 3AC treatment (figure 5.28A). Next, the involvement of necroptosis was evaluated by use of a receptor-interacting serine/threonine-protein kinase 1 (RIP1) (Nec1s) and receptor-interacting serine/threonine-protein kinase 3 (RIP3) (GSK-843) inhibitor. Both RIP1 and RIP3 inhibition 1 h prior to 3AC treatment significantly reverted the induction of specific cell death (figure 5.28B). We also tested a mixed lineage kinase domain-like protein (MLKL) inhibitor and found no significant alteration of CLL cell viability (figure 5.28B). As SHIP1 dephosphorylates PIP3 to PIP2 at the plasma membrane and its inhibition is hypothesized to induce AKT activation as one of the critical downstream events, we investigated the pAKT status early upon 3AC treatment. Figure 5.29 shows a fast increase in pAKT on the serine site at

postion 473 (Ser473) in patient-derived CLL cells (one representative for n=4). In the CLL cell line MEC-1, AKT was found to be phosphorylated at later time-points as shown upon 3 hour 3AC treatment. Taken together, we found a strong decline in viability, specifically in CLL cells, upon SHIP1 inhibition. The mode of cell death is accompanied by the induction of necroptosis, whereas caspases seem to be rarely involved. In addition, a fast increase of pAKT, an important direct downstream modulator, can be observed upon SHIP1 inhibition.

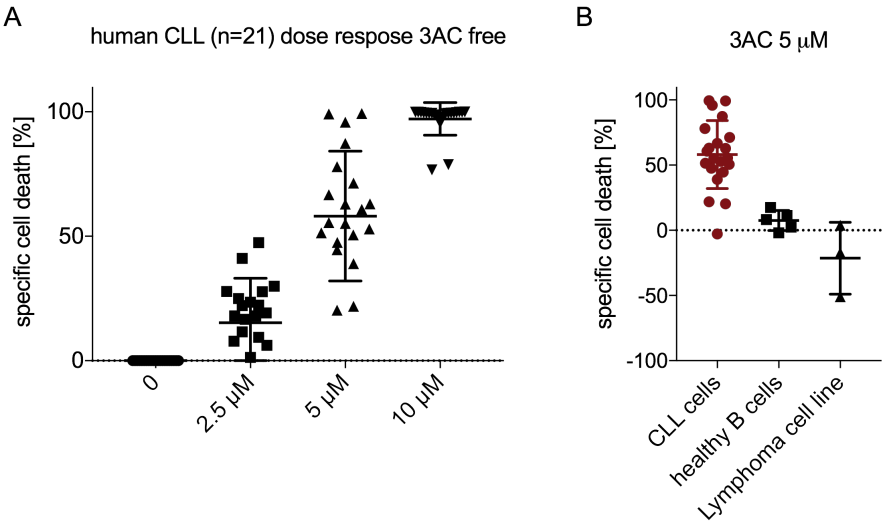

Figure 5.26: 3AC induces specific cell death in CLL samples. A) 21 patient-derived CLL samples, isolated from peripheral blood, were treated with 3AC for 48 h and viability was analyzed by DAPI exclusion via flow cytometry. B) Treatment of B lymphoma cell lines (SUDHL6, BJAB, Bal17), healthy B cells (n=4), and CLL cell lines (MEC-1, EHEB). All cells were treated and analyzed as described in A).

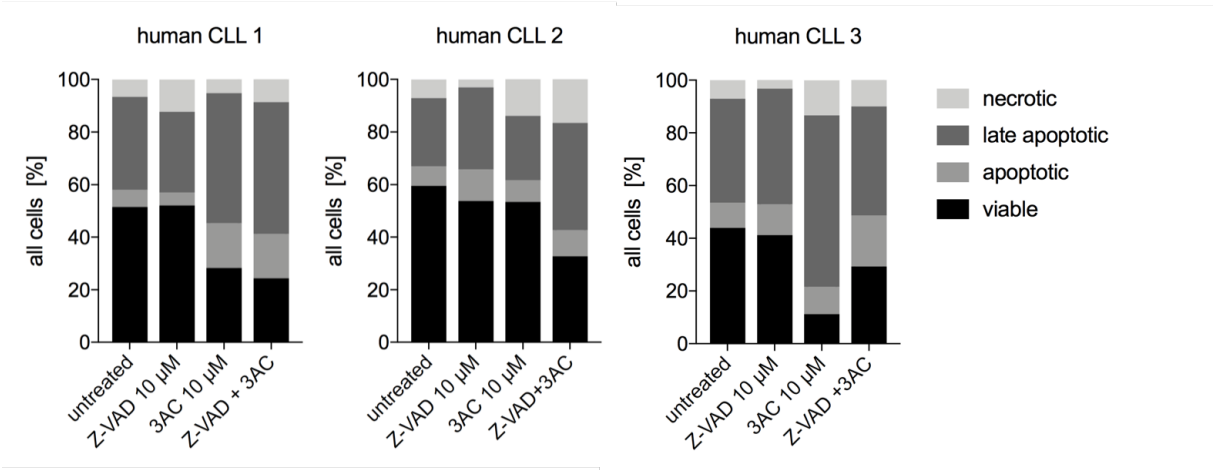

Figure 5.27: Apoptosis is barely involved in 3AC-mediated CLL cell death. AnxV stainings and flow cytometric analysis of CLL patient cells (n=3) treated for 48 h with 3AC. Cells were pre-treated for 1 h with the pan-caspase inhibitor.

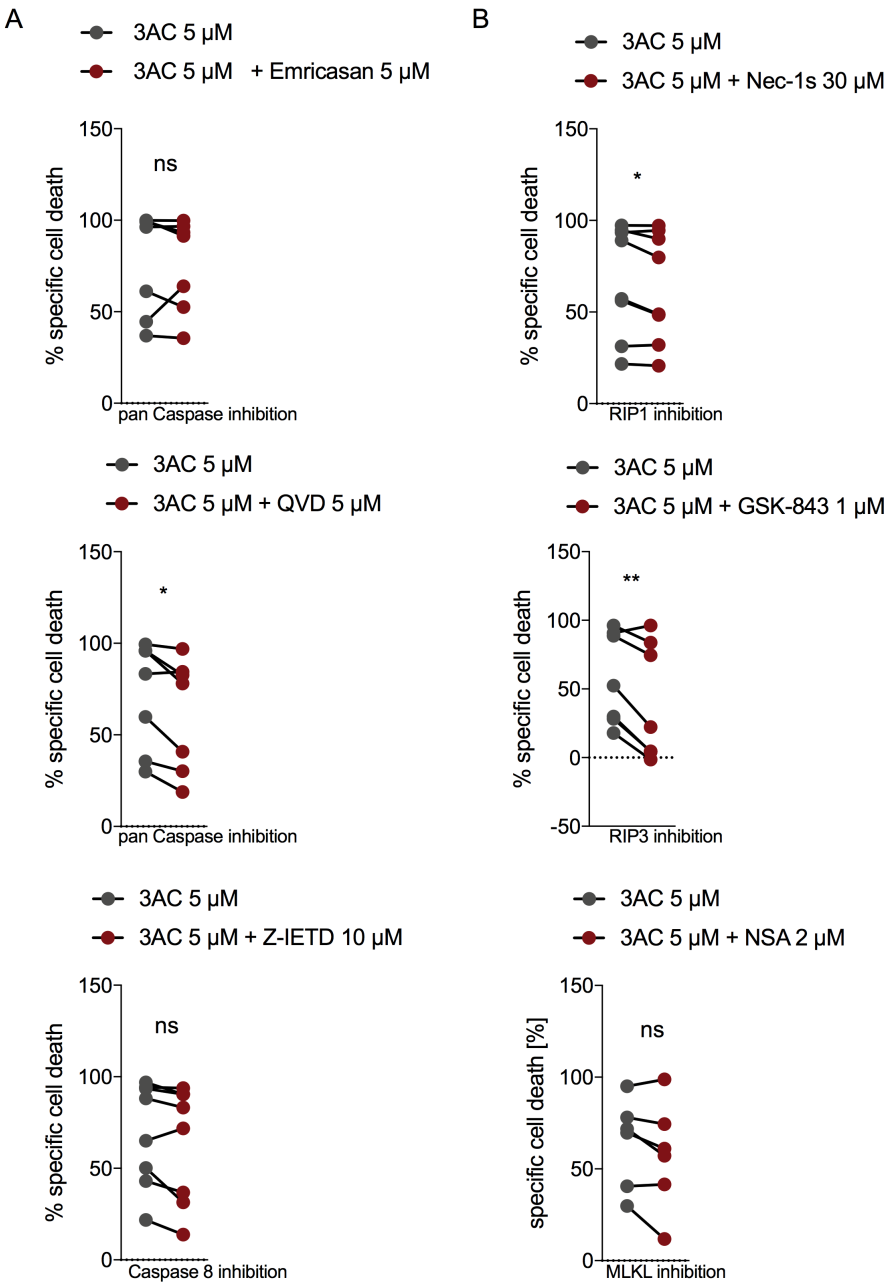

Figure 5.28: 3AC specifically decreases CLL viability with features of necroptosis. A) Patient-derived CLL cells (n=7) were 1 h pre-treated with respective caspase inhibitors, followed by 48 h combinatorial 3AC treatment and flow cytometric analysis of DAPI exclusion. B) 1 h pre-incubation with 3 distinct necroptosis inhibitors followed by 48 h 3AC treatment. Paired Student‘s t-Test was applied for statistical analysis. *, $p<0.05$; **, $p<0.01$.

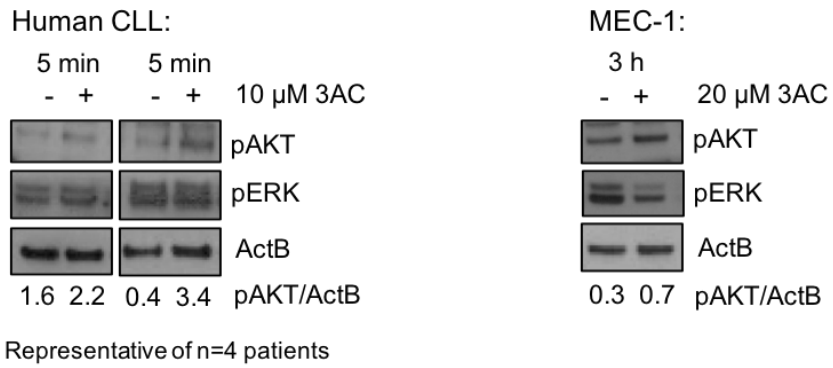

Figure 5.29: SHIP1 inhibition induces fast phosphorylation of AKT (pAKT). Primary patient-derived CLL cells or MEC-1 cells were treated with 10 or 20 µM 3AC for 5 min or 3 h and protein lysates were prepared for Western Blot analysis. Quantification was performed with ImageJ and is depicted below the Western Blots.

5.3.2.2 Small molecule inhibition of SHIP1 *in vivo* decreases disease progression.

Next, we wanted to test the effects of SHIP1 inhibition on CLL cell survival *in vivo*. In need of a potent and well-tolerated SHIP1 inhibitor, we tested the water soluble 3AC derivative K118 *in vitro* [Brooks et al., 2015]. Even at lower concentrations, K118 compared to 3AC induced high levels of specific cell death in all CLL patient (n=7) cells tested (figure 5.30). To study its potency *in vivo*, we then started to xenograft MEC-1 Luc CLL cells in immunocompromized NSG mice and initiated treatment on d 2 (daily, 10 doses) with 10 mg/kg K118 (n=4) or H_2O control (n=4), as described. Bioimaging on d 0 upon transplantation confirmed equal injection of MEC-1 Luc cells in all mice (figure 5.31B). In line with our *in vitro* findings, K118 reduced the tumor burden, as depicted by bioimaging over time, and increased the overall survival of the mice (figure 5.31A+B). To evaluate whether K118 has equal effects on primary patient-derived CLL cells *in vivo*, we then xenografted primary patient-derived CLL cells (n=3 patient-derived CLL cells) into immunocompromised NSG mice and treated them daily with 10 mg/kg K118, starting on day 1 post injection [Brooks et al., 2015]. Upon 5 to 9 days, depending on the engraftment of patient cells, we harvested the spleens and analyzed the human CLL content. We found significantly less CLL cells as compared to the control groups (figure 5.32) in

2 out of 3 tested CLL patients, which most likely reflects patient heterogeneity. To better reflect therapeutic approaches in CLL patients and in an immuno-competent system, we continued and isolated diseased splenocytes of an aged TCL1tg mouse and transplanted 10 C57BL/6 recipient mice and waited for the CLL to expand until it has reached an average of 60% CLL of PBMCs. We initiated treatment (d 11 upon transplantation) and mice received 10 mg/kg K118 (n=5) or vehicle (n=5) by intraperitoneal (i.p.) injections. Two treatment cycles with in total 8 doses (day 11, 12, 13, 14 and day 17, 18, 19, 20) were undertaken. Strikingly, on day 22, we found a reduction in the tumor burden in the spleens in the K118 cohort. Total cell numbers confirmed a strong reduction of CLL cell count upon K118 treatment. To note, also the overall spleen size was decreased upon K118 treatment (figure 5.33A-C). Taken together, we could confirm efficacy of SHIP1 inhibition *in vivo* in both immuno-competent and supressed mouse models.

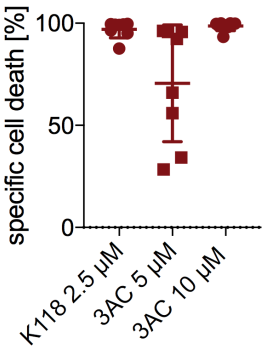

Figure 5.30: The water soluble 3AC-derivative K118 effectively kills CLL cells *in vitro*. Patient-derived CLL cells (n=7 patients) were treated for 48 h with indicated concentrations of K118 or 3AC. Flow cytometric analysis of DAPI exclusion was used to measure viability and induction of specific cell death is depicted.

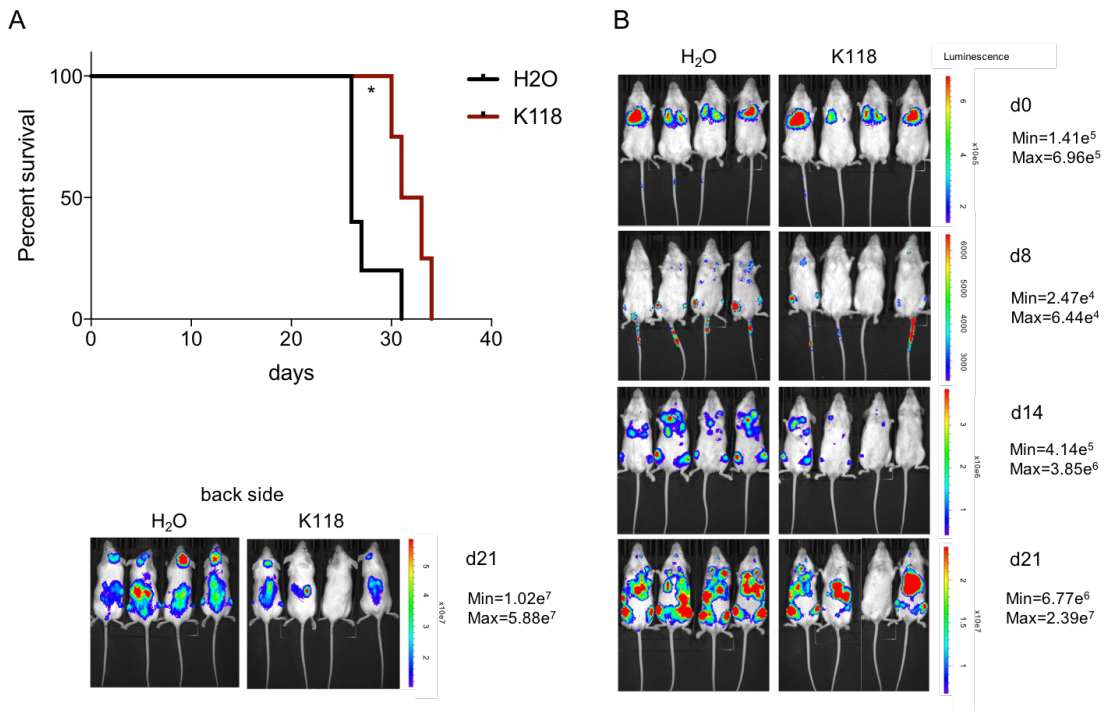

Figure 5.31: SHIP1 inhibition in MEC-1 CLL xenografts *in vivo* results in decreased tumor burden and increased overall survival. 2x10e^6 MEC-1 Luc cells were applied for xenotransplantation and were injected i.v. in NSG mice (n=9) and treatment with 10 mg/kg K118 (n=4) or H_2O (n=5) was started on day 2 after transplantation. A) Upon 10 days of daily treatment the CLL content was followed by bioimaging. Photon emission is measured as radiance (photons/second/cm^2/steradian) and minimum and maximum values are depicted for each time point. (B) Overall survival of mice is depicted in a Kaplan-Meier plot. To test significance, Log-Rank (Mantel-Cox) test, was applied. *, $p<0.05$.

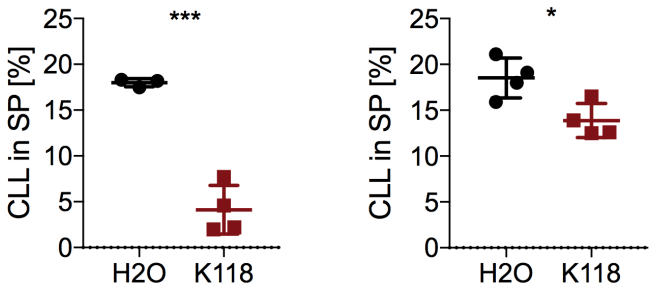

Figure 5.32: SHIP1 inhibition in patient-derived CLL xenografts *in vivo* results in reduced CLL counts in spleens. PBMCs were isolated from CLL patient-derived blood samples and samples with >80% CLL content were applied for xenotransplantation. 1x10e^8 patient CLL cells (n=3) were injected i.v. in NSG mice and treatment with 10 mg/kg K118 or H_2O was started on day 1 after transplantation. Upon 4-9 days of daily treatment the CLL content in the spleens was measured by flow cytometric analysis of viable human CD45$^+$, murine CD45$^-$, human CD19$^+$, and CD5$^+$ cells. To test significance, unpaired Student's t-Test was applied. *, p<0.05; ***, p<0.001.

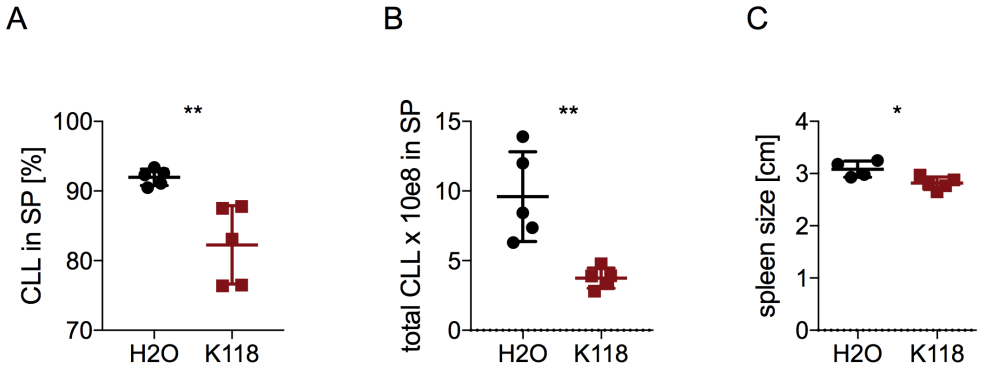

Figure 5.33: SHIP1 inhibition *in vivo* reduces TCL1tg CLL burden. A-C) Diseased splenocytes (92% CLL) of a TCL1tg mouse were transplanted in 12 C57BL/6 wt mice. On day 11 upon transplantation, mice were treated with 10 mg/kg K118 (n=5) or H_2O (n=5) daily for 4 consecutive days. After two days the same 4-day treatment cycle was repeated and upon 2 days end analysis of total splenocytes was performed. Flow cytometric analysis of CD19$^+$ CD5$^+$ cells depicts the percentage of CLL cells among viable splenocytes (A) in the respective groups. In addition, total CLL cell numbers (B) and spleen sizes upon K118 treatment (C) are depicted. Unpaired Student's t-Test was applied. *, p<0.05; **, p<0.01.

5.3.3 Genetic confirmation of small molecule inhibitor (3AC) effects

As particularly phosphatases are challenging to inhibit with small molecules [Zhang et al., 2013], to confirm the results obtained upon SHIP1 small molecule inhibition and to proof on-target specificity, we continued to genetically modify SHIP1 expression in CLL.

5.3.3.1 SHIP1 knockdown in MEC-1 CLL cells decreases viability

We used the CLL-like cell line MEC-1 expressing ecotropic receptor Slc7a (MEC-1 Eco), since primary CLL cells are very difficult to manipulate. We generated stable shRNA mediated SHIP1 knockdowns and used scramble control shRNA as a control. All vectors were kindly provided by Manfred Jücker (UKE Hamburg). First, we confirmed that SHIP1-targeting shRNAs (KD1 and KD2) downregulate SHIP1 protein levels in MEC-1 cells as compared to scramble shRNA control cells by Western blotting (figure 5.34 B). Then, we analyzed the viability of MEC-1 cells upon SHIP1 knockdown. Indeed, SHIP1 knockdown reduced MEC-1 cell survival *in vitro* in line with the induction of cell death observed upon SHIP1 inhibition. This was evident by a reduction of cell viability and cell count in the SHIP1 knockdown MEC1 cells, shown in 2 independent experiments (figure 5.34A). To test the relevance of SHIP1 knockdown *in vivo*, we transplanted both MEC-1 Eco and MEC-1 Luc cells, carrying scramble or SHIP1 targeting shRNAs (scr/KD1/KD2), into immuno-deficient NSG recipients. To ensure the initial injection of equal amounts of viable cells, bioimaging of xenotransplanted NSG mice was performed directly on day 0, 1 h post transplantation (figure 5.35 B). Again, in line with K118 treatment effects *in vivo*, SHIP1 knockdown significantly prolonged the survival of tumor-bearing mice (figure 5.35A). Bioimaging confirmed the reduction of engraftment and progression of leukemic cells (figure 5.35B) in the MEC-1 Luc setting.

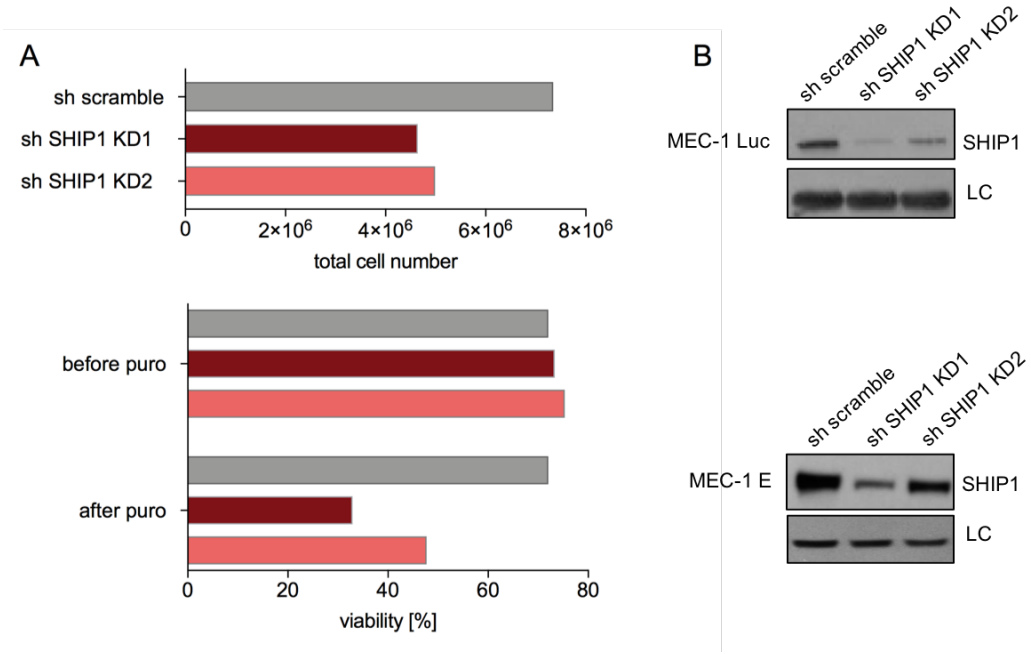

Figure 5.34: SHIP1 knockdown in MEC-1 Eco and MEC-1 Luc cells decreases cell viability *in vitro*. A) 5 days upon spin infection, Puromycin (2 μg/ml) selection was performed for 2 days and viability, measured by flow cytometric DAPI exclusion, is depicted before and after selection. In addition, total cell numbers were counted upon completed selection. B) Western Blot validation of successful SHIP1 knockdown in MEC-1 cells.

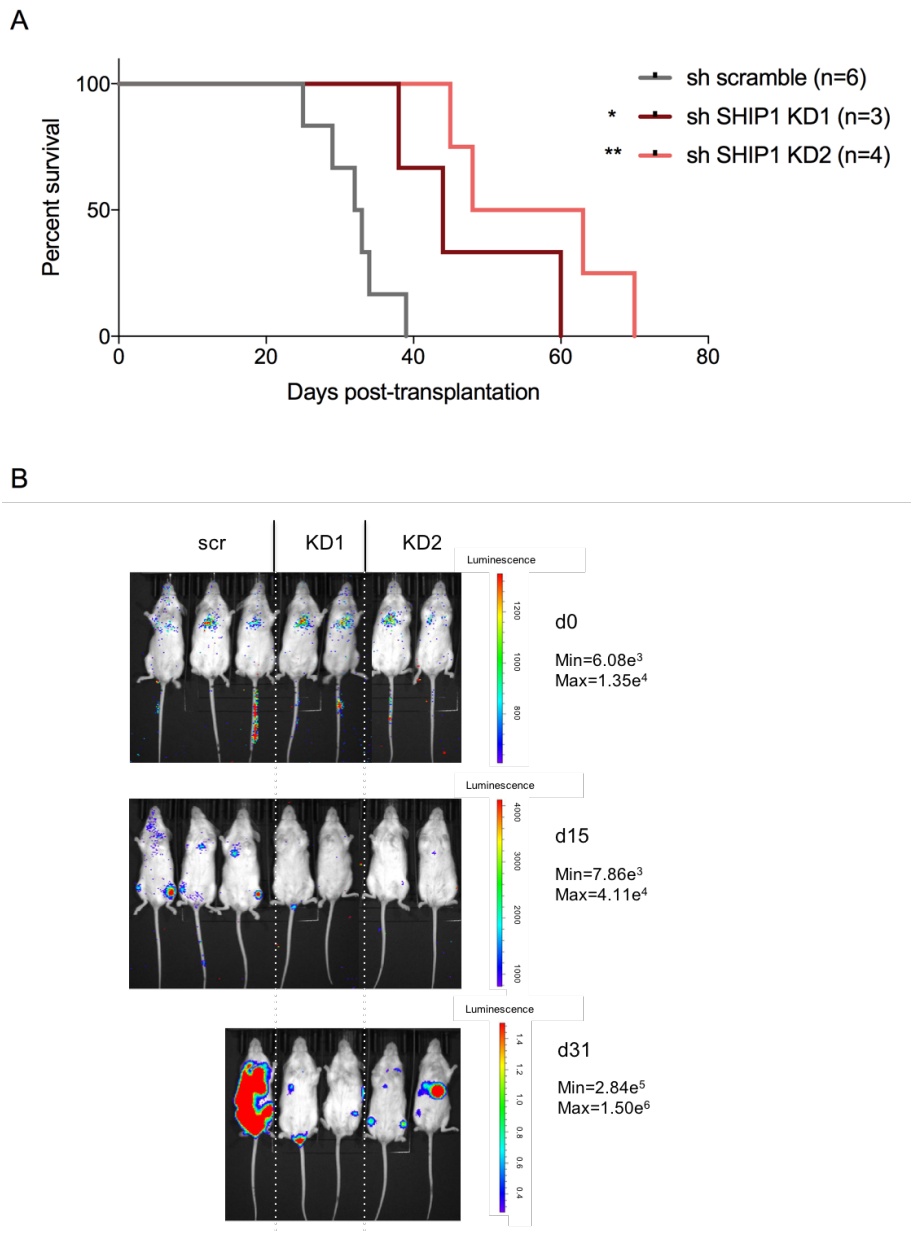

Figure 5.35: SHIP1 knockdown in xenotransplanted MEC-1 Eco and MEC-1 Luc cells increases survival of recipient NSG mice. A) Kaplan-Meier plot depicting survival of NSG mice xenotransplanted with 1x10e^6 MEC-1 cells bearing SHIP1 knockdowns or scramble control. To test significance, Log-Rank (Mantel-Cox) test was applied. *, $p<0.05$; **, $p<0.01$. B) Bioimaging of xenotransplanted NSG mice on day 0, 15, and 31 was undertaken by IVIS Spectrum in vivo imaging system (Perkin Elmer and Living Image software). Photon emission is measured as radiance (photons/second/cm^2/steradian) and minimum and maximum values are depicted for each time point.

5.3.3.2 *SHIP1* knockout in MEC-1 CLL cells confirms growth disadvantage

In addition, we generated *SHIP1* knockout clones of the MEC-1 cell line by the CRISPR/Cas9 technique. Four distinct sgRNA-MSCV-Puro vectors were applied and retroviraly introduced into stable Cas9 (GFP^+) expressing MEC-1 cells. Upon Puromycin selection, MEC-1 cells were single cell sorted and outgrowing clones were further expanded. Figure 5.36A confirms *SHIP1* knockout by Western Blot and sequencing results are shown for one representative ko (mismatches, compared to wt *SHIP1* are depicted in red). Figure 5.36C shows competition assays where GFP^+ successful *SHIP1* knockouts were co-cultivated in 1:1 ratios with GFP^- wt MEC-1 cells. The ratio of GFP-expressing cells was followed over time. A strong decline in GFP-expressing cells was noted when *SHIP1* ko GFP^+, however not *SHIP1* wt GFP^+, cells were mixed with wt GFP^- cells. Strikingly, and in line with our previous results of SHIP1 inhibition and knockdown, *SHIP1* knockout in MEC-1 cells resulted in a selective growth disadvantage shown for 4 independent clones, each resulting from a distinct sgRNA against *SHIP1*.

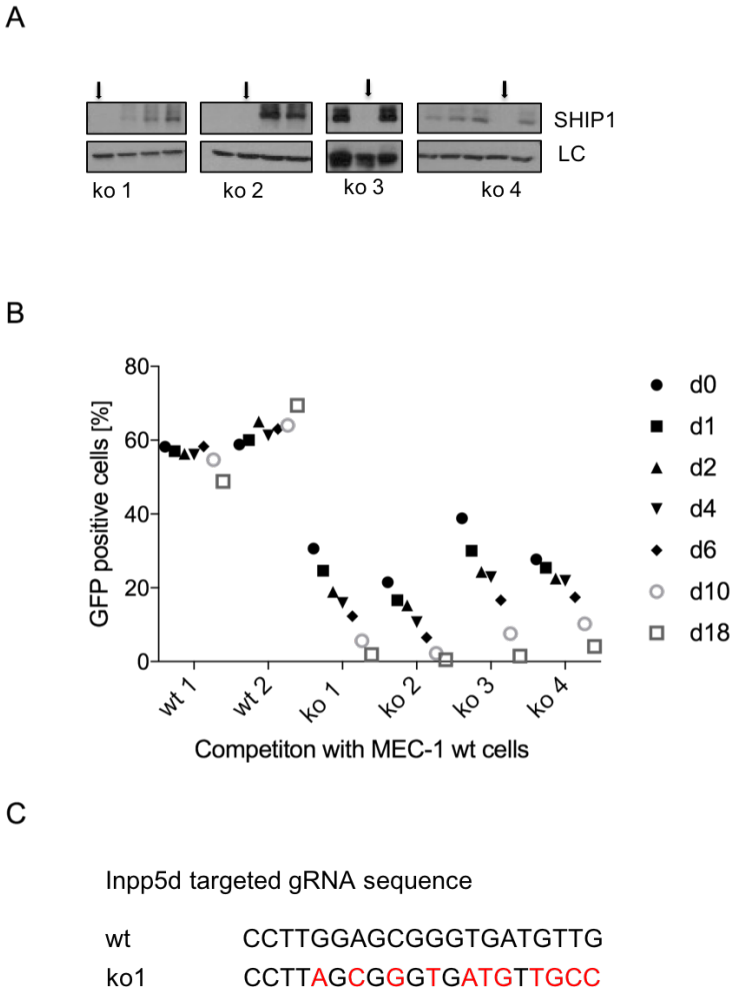

Figure 5.36: *SHIP1* knockout in MEC-1 results in a growth disadvantage. A) Western Blot validation of *SHIP1* knockouts in MEC-1 cells. B) Competitor assay of *SHIP1* ko and wt MEC-1 cells. Equal amounts of *SHIP1* ko/wt (GFP^+) and wt (GFP^-) cells were mixed on day 0 and GFP percentage was followed over time by flow cytometry. C) Sequencing results of one representative *SHIP1* knockout (ko1) compared to the wildtype sequence. Mutations are depicted in red.

5.3.3.3 Constitutive AKT activation is detrimental for MEC-1 CLL cells

In order to determine whether AKT hyperactivation can mimic the effect of SHIP1 inhibition in CLL, we first introduced a constitutively active form of AKT (myristoylated AKT (myrAKT)) into the MEC-1 Eco cell line. The empty GFP vector served as a control (plasmid MSCV IRES GFP (pMIG)). We followed the percentage of pMIG-myrAKT- and pMIG-empty-expressing MEC-1 cells over time and observed a decrease of GFP in myrAKT-carrying cells, whereas empty vector control cells

maintained stable GFP expression over time (figure 5.37A). AKT overexpression and activation was confirmed by Western blot analysis (figure 5.37B). Together, this data implicates that AKT activation is detrimental for MEC-1 CLL cells.

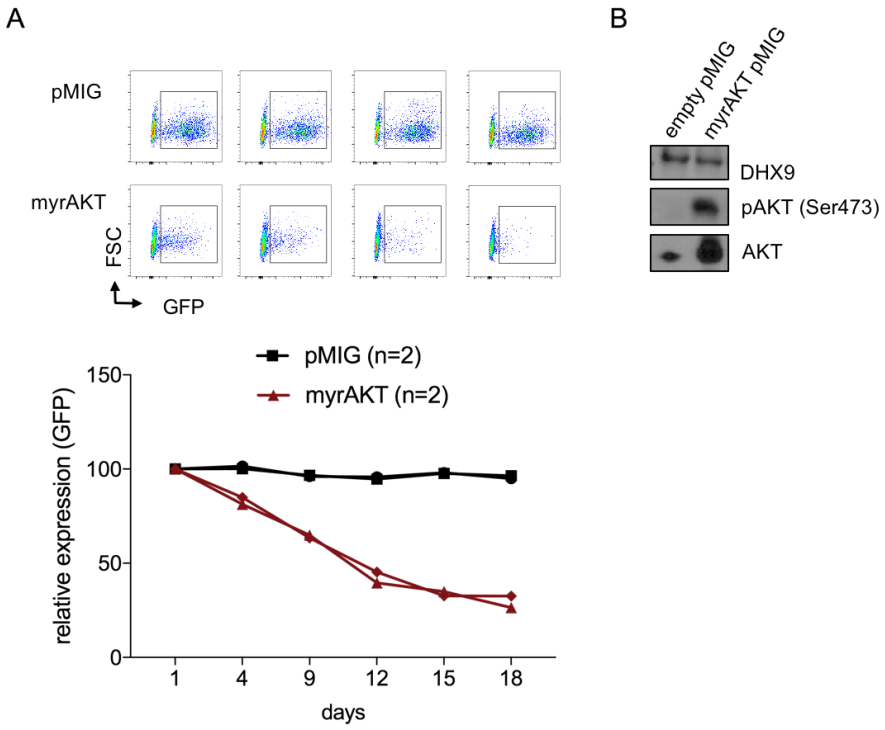

Figure 5.37: myrAKT is detrimental for MEC-1 CLL cells. A) Western Blot confirmation of MEC-1 cells expressing activated myrAKT versus empty pMIG. B) Flow cytometric analysis of GFP expression in pMIG-expressing MEC-1 compared to pMIG-myrAKT-expressing cells. GFP content was analyzed over time by flow cytometric measurement.

5.3.3.4 Constitutive AKT activation in the murine TCL1tg CLL mouse model decreases tumor burden

We further set off to investigate the effects of AKT activation in primary CLL cells and most importantly within the immunocompetent microenvironment. As a CLL mouse model, we choose the commonly applied TCL1tg mouse model [Bichi et al., 2002]. It is currently the best mouse model for CLL that expresses human TCL1 under the promoter of the μ heavy chain and induces a CLL-like disease after 8-12 months of age. It mainly represents the more aggressive, unmutated CLL [Bichi et al., 2002]. Interestingly, the emerging murine CLL largely reveals the characteristics of the human disease with microenvironmental alterations and immunosuppression and

similar BCR signaling activity [Dühren-von Minden et al., 2012].
A mouse line has been previously generated that carries an inducible, active version of AKT glutamine to lysine mutation at position 17 (AKT(E17K)) found in solid tumors, such as breast and ovarian cancer [Carpten et al., 2007]. The inducible expression was chosen to mimic a therapeutic approach. A complementary deoxyribonucleic acid (cDNA) encoding AKT(E17K) together with an IRES-GFP preceded by a loxP-flanked STOP cassette was introduced into the ubiquitously expressed murine ROSA26 locus (Doctoral Thesis Stefan Wanninger, 2014 TUM). The resulting mouse line is referred to as Gt(ROSA)26Sortm2(AKT*E17K)Jrld and from here on named AKT(E17K)tg. Crossing AKT(E17K)tg to the Mb1CreERT2 strain [Hug et al., 2014] results in STOP cassette excision specifically in the B cell-lineage upon tamoxifen treatment and AKT(E17K) expression can be measured by GFP expression. This line was further crossed to the TCL1tg CLL model and resulting triple transgenic animals carrying TCL1tg, AKT(E17K)tg, and Mb1CreERT2 were grown until the age of 12-14 months, until CLL developed without induction of the AKT transgene.

Upon signs of illness and CLL infiltration, we harvested splenocytes of the TCL1tg, AKT(E17K)tg, Mb1CreERT2 mice. We first of all tested proper AKT(E17K)-GFP expression in vitro by 4-OHT or TAT-Cre administration depending on the available genotypes. We could detect GFP positive cells and thus AKT(E17K) expression, which peaked around day 3-4 and comprised up to 40% of CLL splenocytes. Strikingly, the GFP content declined thereafter and cells died *in vitro*. We tested splenocytes of n=3 different donor mice and found smiliar kinetics in all 3 samples, comprising quick recombination of AKT (E17K) GFP^+ cells, and a drop in viability and decline in GFP^+ cells thereafter (figure 5.38A). In contrast, when healthy B cells, that resulted from crossed AKT(E17K) with Mb1CreERT2 mice, were induced with 4-OHT *in vitro*, cells started to express GFP with slower kinetics, but also reached up to 40% starting at day 7 and GFP content as well as viability stayed constant for a prolonged time compared to CLL cells (figure 5.38 A+B). Strikingly, by directly comparing the induction in CLL versus healthy B cells, we found a decrease in viability in CLL cells, but an increased viability in B cells compared to respective non-induced cells (figure 5.38 B).

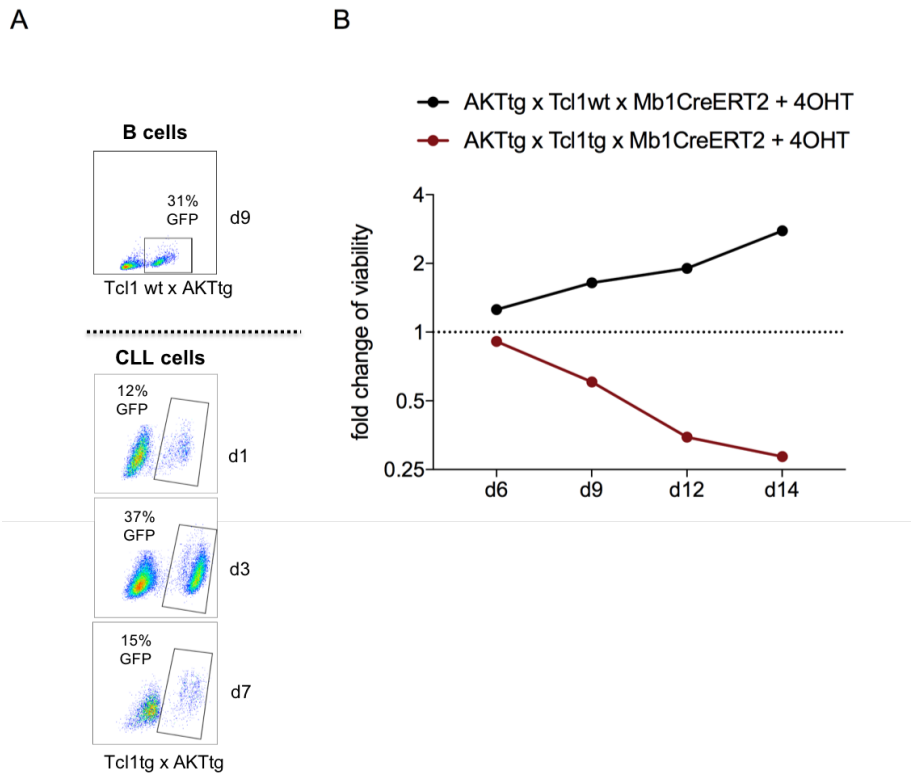

Figure 5.38: Induction of constitutive active AKT(E17K) in diseased TCL1tg CLL cells *in vitro* induces cell death. A) AKT(E17K)tg bearing CLL and wt B cells were induced *in vitro* by TAT-Cre treatment and GFP expression and viability was followed by flow cytometric DAPI exclusion over time. B) Fold change of viability of AKT(E17K)tg induced (versus non-induced) cells by 4-OHT addition. Depicted is the induction of CLL (TCL1tg) versus healthy B cells and viability was analyzed by flow cytometric DAPI exclusion.

To investigate whether CLL cell death induction can also be observed *in vivo*, we transplanted splenocytes of the above described aged TCL1tg, AKT(E17K)tg, Mb1CreERT2 mice into wt C57Bl/6 recipients. Induction of AKT(E17K) expression was achieved by tamoxifen (TAM)-enriched or control chow for two weeks. To capture early effects, we tracked CLL content in the peripheral blood over time. A significant decrease in the percentage of $CD19^+$ $CD5^+$ CLL cells in the PB in the TAM group as compared to the control mice could be detected (figure 5.39A). To note, no GFP^+ cells were detected at any time point, pointing towards a disadvantage of AKT(E17K) expression for CLL survival that we had observed *in vitro*. 8 weeks post transplantation, we sacrificed all animals to analyze whether any GFP^+ AKT(E17K) CLL cells can be detected in the lymphoid organs. Again, we did not find AKT(E17K)-

GFP-expressing CLL cells in the spleens and lymph nodes of the mice (figure 5.39B). Regarding organ morphology, we found a minor reduction of spleen sizes and a strong difference in the axillary lymph node sizes that was also reflected by flow cytometric analysis of immune cell composition of the LNs. TAM group mice possessed reduced numbers of CLL cells and a percentage increase in T cells (figure 5.39B). To determine the activation status of these T cells, we performed a multiparametric flow cytometric analysis comprising distinct T cell activation markers and cytokines. Interestingly, we found a significant decrease in two immunosuppressive modulators, programmed cell death protein 1 (PD-1) and IL-10, in TAM-induced mice (figure 5.39C).

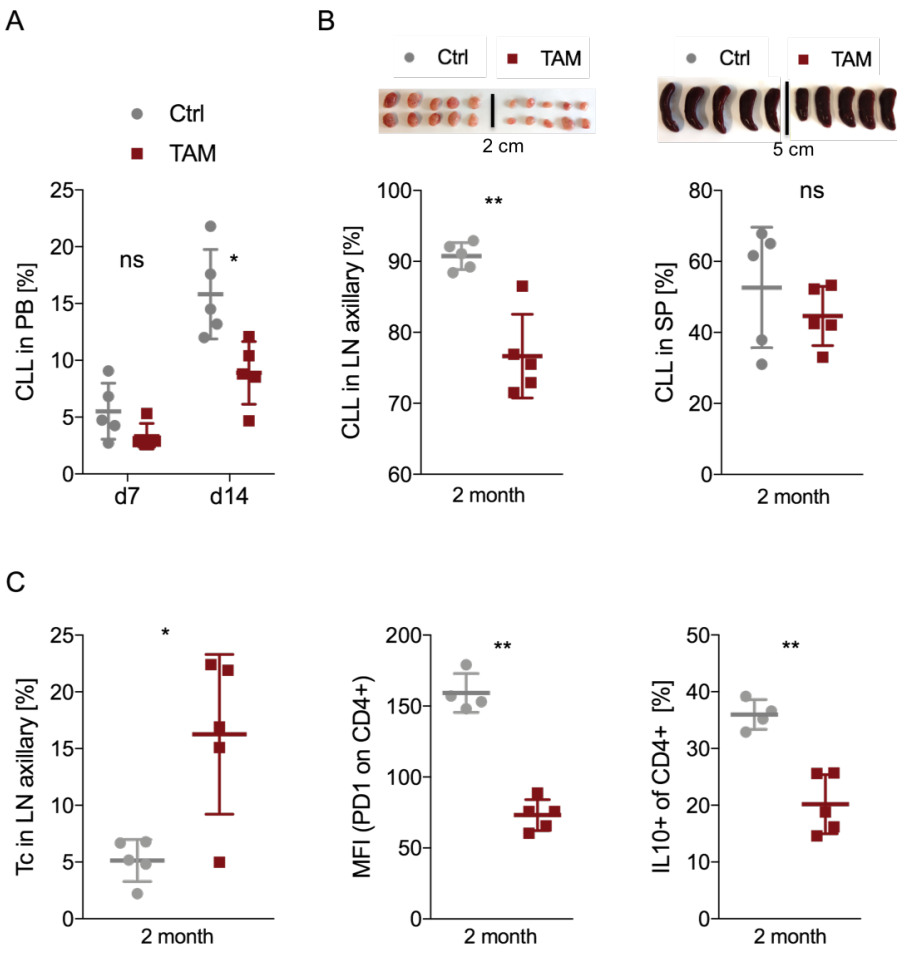

Figure 5.39: Induction of constitutive active AKT(E17K) in diseased TCL1tg CLL cells *in vivo* reduces tumor cell count. Diseased splenocytes of an aged AKT(E17K)tg, TCL1tg, Mb1CreERT2 mouse were transplanted in C57BL/6 wt mice and AKT(E17K) expression was induced by TAM chow for 2 weeks. A) PB was analyzed at day 7 and 14 upon transplantation and induction to evaluate CLL content in PB over time by flow cytometric analysis of $CD5^{+}CD19^{+}$ and GFP^{+} content. B) Pictures and flow cytometric end analysis (2 month upon TAM induction) of CLL content of spleen and axillary lymphnodes are depicted. C) T cell flow cytometric analysis of axillary lymphnodes comprising overall T cell percentage and intracellular staining of PD1 and IL10 gated on CD4+ T cells. A+B+C) Paired Student's t-Test was applied for statistical analysis. *, $p<0.05$; **, $p<0.01$.

This, together with recents findings of induced T cell responses upon SHIP1 *in vivo* inhibition [Gumbleton et al., 2017], encouraged us to study the effects of SHIP1 inhibition with regard to T cell activation more in detail, as described in the following section.

5.3.4 SHIP1 phosphatase activity is critical for CLL immunosurveillance

We further continued to study the role of SHIP1 inhibition not only in CLL cells, but also in T cells. First, we made use of a hybridoma T cell reporter line that carries a nuclear factor of activated T-cells (NFAT) cassette fused to GFP ([Neumann et al., 2014] adapted from [Bot et al., 1996]). When we applied *in vitro* a suboptimal dose (to mimic tumor associated antigens) of CD3 stimulation together with 3AC, we could detect increased T cell activation (figure 5.40A).
To mimic more complex microenvironmental settings and the interplay between CLL and T cells, we further set out and fed murine CLL (TCL1tg) cells with Ovalbumin, to allow endocytosis of the protein and processing of the protein into peptides over night. We continued to treat the cells for 48 h with 3AC, or chemotherapeutics as a reference (Doxorubicin and Oxaliplatin), to induce cell death. To investigate whether CLL cells themselves are sufficient as APCs to induce T cell activation, we co-cultivated the CLL cells directly with isolated OT-I $CD8^+$-CFSE labeled T cells and measured T cell proliferation after 72 h co-cultivation. OT-I T cells can specifically recognize the OVA-derived SINFEKL peptide presented by the H-2Kb MHCI molecule. Strikingly, we could detect an increase in T cell proliferation when CLL cells were treated with 3AC (figure 5.40B). However, both chemotherapeutics were unable to increase the proliferation significantly. In addition, we also tested only the supernatants of 3AC treated OVA fed CLL cells in co-culture with OT-I T cells and again obtained a trend of increased T cell proliferation, suggesting the involvement of exosomal delivery of MHC-I bound peptides (figure 5.40C). Taken together, those results imply the induction of an immunogenic form of cell death upon SHIP1 inhibition.

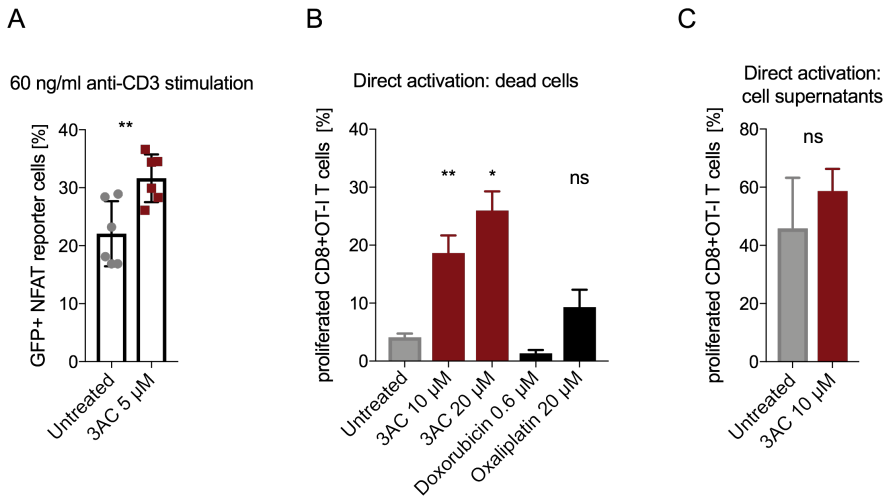

Figure 5.40: SHIP1 inhibition can increase T cell activation. A) NFAT reporter T cells were directly treated with 3AC upon pre-stimulation with anti-CD3 antibody. Activation of T cells was measured by flow cytometry after 72 h. Data summarizes two independent experiments (n=2). B) Murine CLL cells (>70% CLL) were fed with Ovalbumin for 24 hours and then treated with 3AC, Oxaliplatin, or Doxorubicin for 48 hours to induce cell death. Complete induction of cell death was confirmed by flow cytometric analysis of DAPI exclusion. CLL cells were then co-cultivated with isolated OT-I $CD8^+$ T cells that were CFSE-labeled. T cell proliferation was measured upon 72 h co-cultivation by flow cytometry. C) Same setting as described in B) however only CLL cell supernatants were transferred into the co-culture with OT-I T cells. Paired Student‘s t-Test was applied for statistical analysis and depicts technical replicates. Data is representative for 2 independent experiments each. *, $p<0.05$; **, $p<0.01$.

To study further stimulatory effects of SHIP1 inhibition in CLL cells on the immune system, we continued to apply more complex co-culture settings with DCs, as they comprise the most potent APCs. Again, CLL cells were fed for 24 h with Ovalbumin and then treated with 3AC for 48 h and in addition, when the co-culture with T cells was started, also bone marrow-derived dendritic cells (BMDCs), as potent APCs, were added. Strikingly, we found a strong increase in T cell proliferation when CLL cells were treated with 3AC. Again, the addition of OVA fed and 3AC treated CLL cell supernatants was tested in co-culture with BMDCs and T cells and revealed a trend of higher T cell proliferation(figure 5.41), in contrast to Oxaliplatin or Doxorubicin treated CLL supernatants.

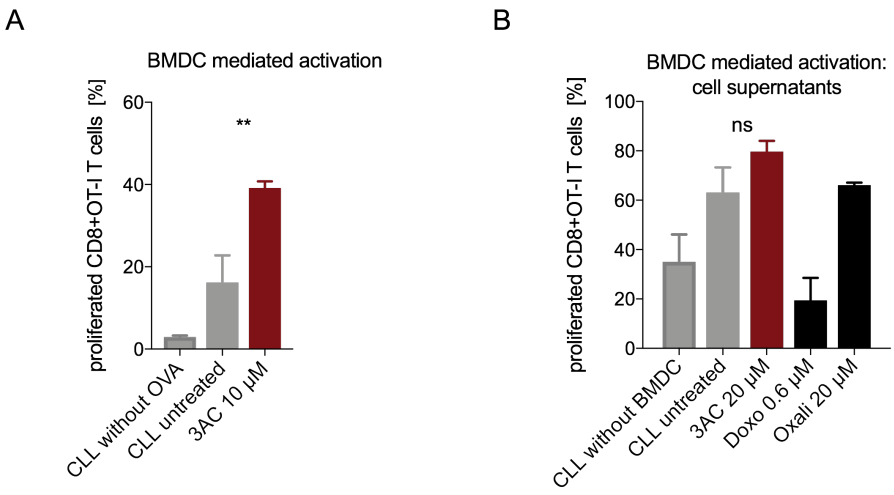

Figure 5.41: SHIP1 inhibition in Ovalbumin fed CLL cells induces ICD and increases dendritic cell mediated OT-I CD8$^+$ T cell proliferation. Murine CLL cells (>70% CLL) were fed with Ovalbumin for 24 hours and then treated with 3AC or distinct chemotherapeutics for 48 hours to induce cell death. CLL cells were then co-cultivated with BMDCs and isolated OT-I CD8$^+$ T cells that were CFSE-labeled. T cell proliferation was measured upon 72 h co-cultivation by flow cytometry. For statistical analysis paired Student's t-Test was applied on technical triplicates and one representative for two independent experiments is depicted. **, $p<0.01$.

We continued to explore the potential of ICD induction upon SHIP1 inhibition in CLL cells. ICD is characterized by the secretion of damage-associated molecular patterns (DAMPs), namely CALR exposure on the outer membrane, which serves as an "eat me" signal to professional phagozytes when translocated from the lumen of the endoplasmic reticulum to the membrane surface [Kroemer et al., 2013]. Further important DAMPs comprise secreted HMGB1 and ATP, whereas HMGB1 is considered to be a late marker of ICD induction and its extracellular release seems to be required for the optimal presentation of antigens by dendritic cells, as it binds to several pattern recognition receptors expressed on APCs. Released ATP functions as a "find-me" signal for phagocytes and can also bind to purinergic receptors on target cells and initiate inflammasome activation [Kroemer et al., 2013]. First, we studied CALR exposure on the membrane as an early described event for ICD and found, consistent for all patients (n=8), an increase in the MFI of CALR upon 4 hours of 3AC treatment (figure 5.42).

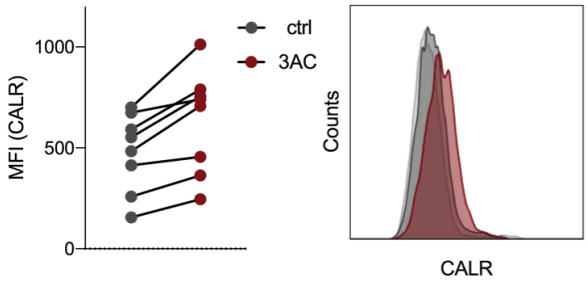

Figure 5.42: CALR is exposed to the cell surface early upon SHIP1 inhibition. Patient-derived CLL cells (n=8) were treated for 4 h with 15 μM 3AC and CALR was stained on the cell surface and analyzed by flow cytometry.

Next, we evaluated the potential extracellular release of ATP upon SHIP1 inhibition and could also confirm an increase of ATP in supernatants from patient-derived CLL cells treated with 3AC (figure 5.43).

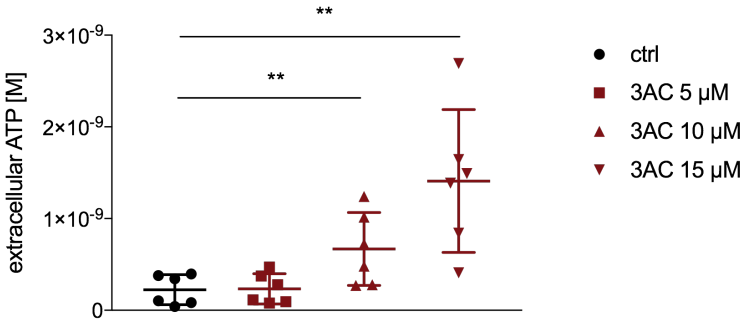

Figure 5.43: ATP is released from the cells early upon SHIP1 inhibition. Patient-derived CLL cells (n=6) were treated for 4 hours with 5, 10, and 15 μM 3AC and ATP was measured in the supernatants by luminescent read-out (ATP Enliten, Promega). To test significance paired Student's t-Test was applied on biological replicates (n=6). *, $p<0.05$; **, $p<0.01$.

Finally, figure 5.44A shows supernatants of patient-derived CLL cells treated for 48 h with K118, 3AC, or left untreated. Indeed, with increasing doses of K118 and 3AC striking amounts of HMGB1 were released from the cells. This was consistent within all patients tested (figure 5.44A). Since we found the involvement of necroptosis upon SHIP1 inhibition, we further set out to study the link between necroptosis and ICD. As in particular MLKL is responsible for pore formation upon activation of the necroptosome, we co-treated CLL cells with a MLKL inhibitor together with K118 or 3AC for 48 hours as depicted in figure 5.44B. Clearly, co-inhibition of MLKL

strongly decreased the release of HMGB1, relating the induction of necroptosis to ICD. In conclusion, our data strongly suggest the immunogenic potential of SHIP1 inhibition in CLL cells.

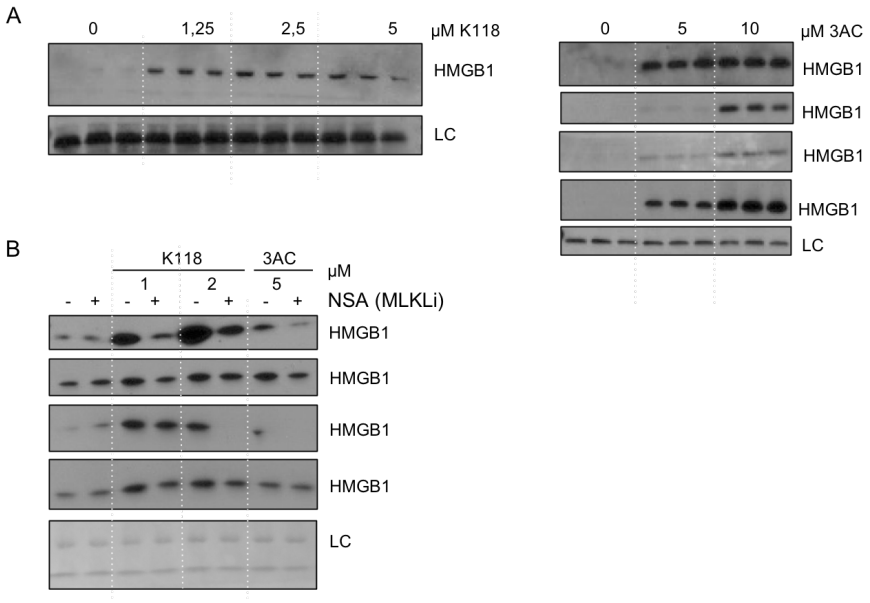

Figure 5.44: HMGB1 is released upon K118/3AC treatment by a mechanism involving necroptosis. A) Patient-derived CLL cells (n=2; K118/n=5; 3AC) were treated for 48 h with indicated concentrations of K118/3AC and supernatants were analyzed by Western Blot. B) Patient-derived CLL cells (n=4) were pre-treated for 1 h with 2 μM of a MLKL (NSA) inhibitor and then 3AC/K118 were added for 48 h. Again supernatants were analyzed by Western Blot for HMGB1 release. One loading control (LC) is shown each as representative for equal loading.

5.3.5 SHIP1 inhibition in drug-resistant CLL

As Ibrutinib-resistant cases are emerging in clinical patients care and challenging to treat, we aimed to investigate SHIP1 inhibition in Ibrutinib resistance. As already described in the previous chapter (DUSP1/6 in CLL), for this purpose MEC-1 resistant cells were generated. When MEC-1 wt and Ibrutinib- or Idelalisib-resistant cells were synchronized and treated simultaneously with 3AC for 48 hours, we found increased sensitivity and induction of specific cell death in resistant cells (figure 5.41A+B). To further study a clinical relevance, Ibrutinib-resistant patient-derived CLL samples are planned to be treated with the SHIP1 inhibitor 3AC and compared to treatment naive patient-derived cells.

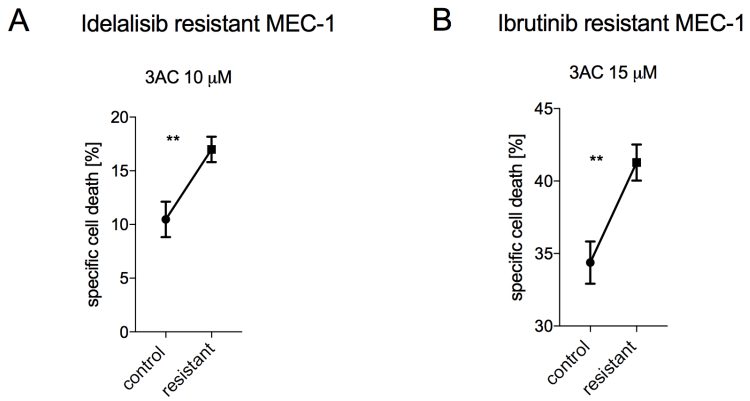

Figure 5.45: Idelalisib- and Ibrutinib-resistant MEC-1 cells are more sensitive for SHIP1 inhibition. A) Treatment naive and Idelalisib-resistent MEC-1 cells were incubated in two independent experiments (technical triplicates) with 3AC for 48 h and viability was measured by flow cytometry and DAPI exclusion. One representative is shown. B) Same setting as described in A) with Ibrutinib-resistant MEC-1 cells compared to treatment naive MEC-1. Cell lines treated with Idelalisib and Ibrutinib to confirm successful resistance generation are already depicted in the Chapter: DUSP1/6 in CLL, figure 5.24. Paired Student‘s t-Test was applied for statistical analysis. *, $p<0.05$; **, $p<0.01$.

Chapter 6

Discussion

Pathological RANK signaling in CLL

Our analysis of a genetic mouse model with enforced conditional RANK(K240E) expression in early pre-B cells reveals that deregulated RANK signaling does not only drive lymphoproliferation followed by an SLE-like autoimmune disorder, but also has the potential to promote transformation of B1 B cells *in vivo*. A clonal CLL-like disease develops in aged RANK(K240E) expressing mice and thus highlights the relevance of this signaling network for malignant transformation and CLL development.

As it was shown by Begüm Alankus, RANK(K240E) expression in early B cells leads to a premature activation of B cells (increased MHC-II and CD86) in the bone marrow, where RANKL is provided by stromal cells. Such an B cell activation is absent in wt cells to avoid autoimmunity, however it might mediate the escape of negative selection of RANK(K240E) B cells [Nemazee, 2017]. Under physiological conditions, the vast majority of newly generated pre-B cells carry autoreactive BCRs and are negatively selected at central tolerance checkpoints in the bone marrow, or later on at peripheral checkpoints ([Pelanda and Torres, 2012]; [Shlomchik et al., 2019]; [Wardemann et al., 2003]. Thus, RANK(K240E) expressing B cells in the bone marrow most likely obtain an initial survival advantage to overcome the central tolerance checkpoint and induce the SLE-like phenotype. Defects at central tolerance checkpoints are described in several autoimmunity disorders, includ-

ing SLE, linking early, aberrant B cell activation with autoimmunity [Nemazee, 2017]. To note, different other members of the TNFRSF (APRIL/BAFF system) are well described to be involved in SLE pathogenesis [Vincent et al., 2014] and other studies directly link the involvement of RANK/RANKL in human autoimmune disorders [Carmona-Fernandes et al., 2011]. Previously, it could be shown by B. Alankus (doctoral thesis) that upon RANKL stimulation of RANK(K240E) B cells, PI3K signaling was upregulated. Interestingly, mice lacking PTEN, a negative regulator of PI3K, possessed increased PI3K activity in B cells, which then lost self-tolerance and mice presented with increased serum autoantibodies [Suzuki et al., 2003]. In line with that, human autoimmune patients benefit from PI3K inhibition, which emphasizes the role of PI3K activity during the disease course [Banham-Hall et al., 2012]; [Boyle et al., 2014]. RANK(K240E)$^{\text{CD19-Cre}}$ mice that survive longer than 8 - 10 months confirm the malignant potential of the RANK(K240E) mutation. We observed a clonal expansion of CD19^{+}CD5^{+}GFP^{+} B cells that closely resemble the disease CLL in RANK(K240E)$^{\text{CD19-Cre}}$ mice, indicating that several mice survive despite the strong autoimmune phenotype and develop an indolent leukemia. A link between autoimmunity and CLL is well established. For example the B cell receptor of CLL cells itself recognizes autoantigen, linking also defects in B cell selection with CLL pathogenesis [Burger and Chiorazzi, 2013]. Besides, 40% of CLL patients carry positive serum markers for autoimmune diseases and autoimmune cytopenias frequently occur [Duek et al., 2006]; [Barcellini et al., 2006]; [Vanura et al., 2008].
In line with the human course of the disease, as well as other murine CLL mouse models (e.g. TCL1tg), RANK(K240E) CLL cell expansion is slow and only present in aged mice (older than 8-10 months). The mechanism behind lymphoma development in aged RANK(K240E) expressing B cells is not yet fully resolved. The PI3K signaling pathway promotes the development and progression of human B cell lymphomas, including CLL and ABC-DLBCL [Fruman et al., 2017]. Previous reports unraveled that high PI3K signaling promotes B1 cell development. In line with that, B. Alankus could show that RANK(K240E) B cells display PI3K activation. Thus, mutant RANK-driven PI3K activation might promote the B1 cell lineage decision and consequently promote the transformation of B1 cells [Calamito et al., 2010].
Although the RANK(K240E) mutation is derived from DLBCL, we did not ob-

serve the transformation to an aggressive phenotype resembling DLBCL. To note, in DLBCL the malignant cells are of post-germinal B cell origin. In this study, we however investigated enforced RANK(K240E) expression starting in the early pre-B cell stage and not specifically in the post-germinal center B cell. B. Alankus could show that several B2 cells have undergone a germinal center reaction, as indicated by class-switch-recombination and somatic hypermutation of some cells in RANK(K240E)$^{\text{CD19-Cre}}$ mice. However, this was not sufficient to drive their transformation, since only CD5^{+} cells of the B1 lineage progressed (upon transplantation). This suggests that certain additional alterations seem to be required to mediate transformation of RANK(K240E) expressing B cells to an aggressive phenotype. In ABC DLBCL patients, BCL2 amplifications and genes involved in terminal B cell differentiation (B-cell lymphoma 6 (BCL6) translocation or B lymphocyte-induced maturation protein-1 (BLIMP-1) mutations) are among the most frequent genetic alterations [Bea et al., 2005]; [Iqbal et al., 2007]; [Mandelbaum et al., 2010]. Previous studies have shown that the RANK mutation still relies on RANKL in order to provide a sufficient survival and proliferation signal to result in an growth advantage over time. Since the aged RANK(K240E) CLL cells present still ligand dependence and anti-RANKL blockage can interfere with the RANK/RANKL axis, new therapeutic options appear. In human CLL, the addition of RANKL blocking antibody alone was sufficient to reduce CLL survival, a finding that confirmed the autocrine loop of both RANK and RANKL expression on CLL cells [Schmiedel et al., 2013]. Of importance, the food and drug administration (FDA) approved antibody Denosumab blocks RANKL. It is currently in clinical application for the treatment of osteoporosis and skeleton-related events in the context of bone metastasis and giant cell tumor of bone. Recently, Marini and collegues could show that human CLL xenotransplanted mice benefited from Denosumab treatment in terms of bone descruction. However, these mice also had decreased CLL burden in spleen and bone marrow [Marini et al., 2017]. To note, in contrast to our direct therapeutical approach, the focus of their study was to reduce bone erosion that occurs in treatment naive patients and throughout all stages of CLL, which could be achieved by intervention with the RANK/RANKL signaling axis. We could confirm *in vivo* efficacy and observed a significant difference in overall survival by interfering with RANK/RANKL signaling.

To what extent the increased survival is related to the murine microenvironmental or human autocrine RANKL blockage still needs further investigation. As residual leukemic cells that may represent the starting point of relapse survive in the bone marrow, targeting the CLL-stroma crosstalk might be of particular interest.

DUSP1/6 inhibition in CLL as novel therapeutic approach

In our second approach to dissect CLL specific signaling processes, we focused on the negative feedback regulation of the MAPK pathway. Whole-exome sequencing of CLL and matched germline DNA sampes revealed MAPK signaling as central pathway involved in CLL [Landau et al., 2015]. The current clincial landscape includes two approved MEK1/2 inhibitors (Trametinib, Cobimetinib), yet poor, insufficient responses have been described for CLL, mainly attributed to upregulation of alternative pro-survival pathways upon MEK inhibitor application [Chen et al., 2018]. Interestingly, ERK1/2 regulate their own dual specificity phosphatases, namely DUSP1 (more active against p38 and JNK) and DUSP6 (rather specific for ERK), which are expressed as immediate early genes following MAPK stimulation [Groom et al., 1996];[Farooq and Zhou, 2004]. In line with that, we oberved increased DUSP6 levels in more aggressive RAS/BRAF mutant CLL samples [Zenz et al., 2019]. Despite the unquestionable relevance of MAPK signaling for CLL progression, here, we show that DUSP1/6 inhibition by small molecule inhibitor BCI and also genetic *DUSP1/6* deletion result in a strong and selective growth disadvantage for CLL cells and implicate that enhanced MAPK signaling is detrimental for CLL. The induction of cell death is accompanied by features of apoptosis, such as involvement of caspases, phophatidylserine exposure on the outer cell membrane, and poly(ADP-ribose)-polymerase 1 (PARP) cleavage. Besides, we found the induction of several regulators of the DNA damage response. The central question is what renders CLL cells more sensitive towards DUSP1/6 inhibition and induces programmed cell death in usually apoptosis resistant clones. By analyzing downstream MAPK signaling changes upon BCI treatment of primary CLL cells, we found a transient and very fast increase in pERK. We hypothesize that sustained hypersignaling leads to an unbearable signaling level for CLL cells and induces negative selection via presumably activation induced

cell death. Clonal deletion in physiological B cell development is of high importance to eliminate, for example autoreactive B cells and to prevent autoimmunity. Limnander and collegues found a calcium-driven pathway that leads to activation of ERK and results in the pro-apoptotic process of negative selection [Limnander et al., 2011]. Also in pre-B cells it was shown that DUSP6 provides negative feedback for ERK which regulates the signal strength and enables the development of malignant acute lymphoblastic leukemia (ALL) cells that evolve from intermediate signals, whereas cells experiencing too strong signals become deleted early on [Shojaee et al., 2015]. To mention, Shojaee and collegues report that upon DUSP6 inhibition, the increase in pERK was only minor and thus propose human ALL cells to be highly sensitive to very small imbalances in ERK signaling, a phenomenon we also observe in CLL cells. A multitude of further pro-apoptotic signaling pathways that involve ERK activation are described, whereas both subcellular localization of ERK, mediated through sequestration by subcellular anchors, (e.g. phospho-enriched protein in astrocytes 15 kDa (PEA15) in the cytosol) and prolonged activation seem to mediate the respective outcome [Cagnol and Chambard, 2010]. Sustained cytoplasmatic pERK is discussed to rather promote senescence or autophagy, while prolonged nuclear activity of ERK is thought to trigger apoptosis. To mention, DUSP6 functions in the cytoplasm, whereas, DUSP1 is operating in the nucleus [Farooq and Zhou, 2004]. Thus it is most likely the combinatorial inhibition of both phosphatases that results in the observed mode of cell death with apoptotic features and the induction of a DNA damage response. Besides, we observed growth inhibitory effects for both *DUSP1* and *DUSP6* single knockout, however we were unable to create double knock outs, possibly implicating their lethality. The involvement of DUSP6 and DUSP1 in DNA damage has already been described in other tumor entities [Bagnyukova et al., 2013]; [Fang et al., 2018]. To what extent the DDR is involved in the pro-apoptotic process, or results as a secondary effect upon cell death, remains still unclear. The application of a selective CHK1 inhibitor (LY2603618) revealed a trend towards decreased specific cell death induction in combination with BCI. This would rather suggest the involvement of a DDR response to be directly involved in the induction of cell death. Besides our phosphoproteome analysis upon BCI treatment predicted several AMPK-regulated phopsho sites in CLL cells. Apart from its essential role

in regulating metabolism, AMPK has been described as genomic stress sensor that is involved in the DDR pathway [Sanli et al., 2014]. Application of Compound C (AMPK inhibitor) in combination with BCI significantly increased the induction of CLL cell death, which rather points towards an anti-apoptotic role of the induced DDR response. Those conflicting results need further investigation. Besides, the involvement of AMPK upon DUSP1/6 inhibition might also link the observed DDR response to autophagy. To what extent autophagy is participating in CLL cell death upon DUSP1/6 inhibition requires further investigation. Yet, participation at some degree is likely since we observed the occurance of a DNA damage response upon BCI treatment and it is well established that autophagy is activated by DNA damage and is required for several functional outcomes of DDR signaling, including repair of DNA lesions, senescence, cell death, and cytokine secretion [Eliopoulos et al., 2016]. AMPK is connected to autophagy, as it gets activated under starvation conditions and is involved in the phagophore formation by interacting with autophagy-related (ATG) family proteins [Hardie, 2011]; [Lee et al., 2010]. Indeed, a direct role for DUSP1 in the regulation of autophagy has also previously been described [Wang et al., 2016]. During autophagy DUSP1 transcription is blocked, which results in increased JNK activation by releasing the inhibitory effects. In line with that, we also observed an increase in phosphorylated JNK upon DUSP1/6 inhibition in CLL. Active JNK in turn is well described to induce a variety of transciption factors including activator protein 1 (AP-1) [Eliopoulos et al., 2016]. To note, a very strong event upon BCI treatment in CLL cells was the increase in ATF2 and c-JUN phosphorylation, two members of the AP-1 heterodimer complex family. Particular interest is attributed to the fact that autophagy may link DDR to the generation of local and systemic immune responses via induction of "immunogenic cell death", a form of cell death that releases immunostimulatory DAMPs from dying tumor cells, as it is described that autophagy is inevitable to induce immunogenicity in distinct chemotherapy treated tumors. [Michaud et al., 2011]; [Eliopoulos et al., 2016]. Activation of autophagy is also known to contribute to DNA damage-induced senescence [Kang et al., 2015]. To study the involvement of senescence upon DUSP1/6 inhibition in CLL is still of future interest. Cellular senescence has been shown to be the outcome of prolonged oncogene signaling, which usually promotes tumori-

genesis. Courtois-Cox and collegues found that senescence sensitive cells rely on a negative feedback network including DUSP1 and DUSP6 among others, which can terminate aberrant signals [Courtois-Cox et al., 2006]. Based on a discovered novel role of autophagy to link DDR to the secretion of cytokines, chemokines and growth factors, known as senescence-associated secretory phenotype (SASP), that can establish an inflammatory environment and potentially induce immune responses, further studies of scenescence induction upon DUSP1/6 inhibition are of particular interest. [Kang et al., 2015]. Sustained therapeutic success requires the restoration of an intact immune system with functional T cell responses in the CLL setting. Rendering CLL cells immunogenic, to induce cytotoxic T cell responses, is hereby the major goal. In preliminary experiments (data not shown) we found T cells to be activated in different experimental settings upon DUSP1/6 inhibition. This is in line with previous studies that showed that DUSP6 plays an important role in T cells. An age associated increase in DUSP6, due to loss of miR-181a expression, is described to result in an increase in the activation threshold of naive T cells [Li et al., 2012]. To study the effects of DUSP1/6 inhibition with regard to the T cell compartment more in detail appears promising and is of future interest. Our concept of negative feedback inhibition in CLL challenges the role of DUSP1 and DUSP6 as tumorsupressors, as it is characterized in many solid tumors [Calvisi et al., 2008]; [Wong et al., 2012]; [Ma et al., 2013]. Such negative regulators are frequently deregulated in many cancer types, yet, ALL, and as we show also CLL cells, still exhibit intact negative control of ERK via DUSP1/6 [Pratilas et al., 2009]; [Frank et al., 2009]. In line with that, characterization of CLL patients revealed upregulation of DUSP6 mRNA in patients with MAPK mutations and thus more aggressive subtypes of CLL. This emphasizes the potential of DUSP1/6 as attractive therapeutic targets in CLL to induce non bearable hyperactivation. We thereby challenge the concept of kinase inhibition that is currently in clinical application and frequently results in resistance development with poor further treatment options. Recent reports have shown that Ibrutinib resistant clones have adapted to increased PI3K signaling [Woyach and Johnson, 2015]; [Woyach, 2015]. As we observed increased sensitivity of Ibrutinib and Idelalisib resistant MEC-1 cells to BCI, we hypothesize that resistant cells need a lower additional signal increase to enter activation-induced cell death. Evaluation of Ibrutinib resistent

patient samples will be essential to confirm our rationale, which might then open the opportunity for phosphatase inhibitors in clinical application. A recent study also provided evidence that DUSP1 upregulation (together with c-FOS) is involved in resistance mechanisms and its inhibition was able to overcome tyrosine kinase inhibitor generated resistance in acute myeloid leukemia [Kesarwani et al., 2017]. Apart from the potential of phophatase inhibitors in kinase inhibition resistant cells, importantly, novel perspectives are needed to avoid resistances in the first place. For example, sequential treatment regimens comprising targeted inhibition of increased kinase signaling (e.g. BTK inhibitor Ibrutinib) and pharmacological inhibition of negative control (e.g. DUSP1/6 inhibitor BCI) could prohibit selective pressures and clonal evolution that would favor outgrowth of drug-resistant clones with adaptive fitness that could evolve upon continuous single kinase or phosphatase inhibition.

SHIP1 inhibition is critical for CLL progression and immunosurveillance

To underline the concept of negative feedback inhibition in CLL, we aimed to broaden the application of phosphatase inhibition to further targets. Two kinase inhibitors in clinical application, namely Idelalisib and Duvelisib reflect the important role of PI3K signaling downstream the BCR for CLL survival, yet, face critical toxicities and side effects and lack the activation of sustained immune responses [Ortiz-Maldonado et al., 2015]. We show here that SHIP1, a negative regulator that dephosphorylates PI-3,4,5-P3 to PI-3,4-P2 at the plasma membrane, is highly active in CLL and provides negative regulation of PI3K signaling. We demonstrate that SHIP1 inhibition or genetic manipulation induces cell death specifically in CLL cells and leads to transient AKT activation. In line with that, AKT hyperactivation in diseased CLL can mimic the inhibitor effects.

We hereby challenge the current view of the tumor-promoting role of high levels of PI3K and AKT in CLL, which has been studied extensively in CLL. It has been shown by several groups that AKT is phosphorylated at both Ser473 and threonine site at position 308 (Thr308) sites in CLL cells, freshly isolated from patient-derived PBMCs [Zhuang et al., 2010]; [Barragán et al., 2006]. Inhibition of AKT in those samples led to induction of apoptosis, which mechanistically appeared in loss of

myeloid cell leukemia 1 (MCL1) and loss of MDM2 phosphorylation leading to increased p53 expression [de Frias et al., 2009]; [Zhuang et al., 2010].
Moreover, TCL1 is directly interacting with AKT and sensitizes its phosphorylation, whereas TCL1 levels predict the signaling intensity and high TCL1 levels are strongly associated with aggressive disease course [Schrader et al., 2014]; [Herling et al., 2009]. In line with that, transgenic mice over-expressing TCL1 develop a CLL-like disorder associated with TCL1-stimulated AKT activation [Bichi et al., 2002];
[Pekarsky et al., 2007].
It was previously shown that active AKT promotes the expression of cyclin A, a cell cycle promoter in CLL cells, when introduced via electroporation in primary blood derived CLL cells [Longo et al., 2007]. However, it is important to consider that Longo et al. (2008) measured viability and expression of antiapoptotic molecules in primary CLL cells only 48 h upon myrAKT introduction, which could be prior to the induction of hypersignaling. Furthermore, the increase in AKT phosphorylation was only minor, which could be due to weaker expression from the pCDNA plasmid used in the study by Longo et al., as compared to our MSVC-based transductions [Longo et al., 2008]. To note, in both our settings upon 3AC treatment of CLL cells and upon introduction of myrAKT in MEC-1 CLL cells, we observed phosphorylation of the Ser473, which is known to represent a strong AKT activation. It is also important to mention that our results were confirmed with an *in vivo* CLL model that allows enforced AKT signaling over a longer time period in mature CLL cells, where a functional microenvironment is present. In another study, AKT activation was shown to contribute to Richter Syndrome, an aggressive transformation of CLL to DLBCL [Nickel et al., 2016]. Here, myrAKT was induced early on in B cells by CD19Cre in the TCL1 mouse model and resulted in accelerated transformation into Richter syndrome. Again, it is important to discriminate the distinct roles of PI3K signaling during CLL pathogenesis and in mature, diseased CLL with functional BCR activity. As we have shown, in the scenario of enforced mutant RANK signaling early on in pre-B cells, PI3K activation clearly favors the development of hematological malignancies, in particular CLL. Similarly, the expression of human AKT1 containing an E17K mutation in the PH domain, which facilitates AKT activation by localization to the plasma membrane, promotes a myc-driven B-cell leukemia in mice

[Carpten et al., 2007]. In strong contrast, we therapeutically induced the expression of active AKT(E17K) in CLL cells, when mature, diseased CLL cells were already engrafted and proliferated in recipient mice. Consequently, in diseased, mature CLL cells we propose an upper signaling threshold with induction of activation induced cell death upon hypersignaling.

Evidence for the here proposed concept of a maximum tolerable signaling threshold was already described for pre-B ALL, where SHIP1 inhibition was strongly linked to SYK hyperactivation and the induction of cell death [Chen et al., 2015]. It clearly challenges the role of SHIP1 as tumor suppressor, as it is described for example in acute myeloid leukemia (AML). Täger and colleagues could show that SHIP1, but not an AML-derived SHIP1 tyrosine to histidine at position 643 (Y643H) mutant prolong the survival of AML (cell line) cells xenografted in a NSG mouse model. Also, an analysis of 290 AML patients revealed a correlation between expression of SHIP1 and overall survival of the AML patients [Täger et al., 2017].

Still, the question remains, what renders mature CLL cells susceptible to cell death upon SHIP1 inhibition or AKT hyperactivation, and avoids proliferation towards an aggressive lymphoma?

Exploring more in detail the signaling changes upon SHIP1 inhibition or AKT hyperactivation, we found an increase in pAKT Ser473. It is well known that for full AKT activation both sites need to be phosphorylated, yet, phosphorylation of Ser473 results in stronger activation. Several lines of evidence indicate that distinct cell types rely on specific AKT signaling thresholds.

First of all, recently, it has been published that AKT signaling is rewired in germinal center B cells compared to naïve B cells. In detail, PTEN activity restricts the phosphorylation of the Ser473 AKT site, which is mechanistically linked to the AKT-mechanistic target of rapamycin complex 1 (mTORC1)-S6 axis [Luo et al., 2019]. It is likely that differential phosphorylation of the two main activating sites on AKT (Thr308 and Ser473) are responsible to activate distinct target substrates and pathways. Thus, different signaling strengths, which are generated by respective amounts of PI-3,4,5-P3 generation, result in distinct biological outcomes. In DLBCL cells that originate from GC B cells, the miR-155 is often overexpressed leading to reduced amounts of SHIP1 [Pedersen et al., 2009]. The activated B cell subset of DL-

BCL consequently displays constitutive AKT signaling through chronic active BCR signaling [Davis et al., 2010]. This could explain the differences of SHIP1 inhibition sensitivity of CLL compared to DLBCL cells. In CLL, SHIP1 is readily expressed and active, thus, alterations in AKT signaling strength might be less well tolerated. Further detailed investigation is required to understand distinct signaling networks in healthy B, CLL and DLBCL cell subtypes.

Secondly, Tregs have a unique AKT network, as they possess a defect to phosphorylate AKT upon activation. This disability is largely due to decreased pAKT(Ser473) and not pAKT(Thr308) levels [Crellin et al., 2007]. To be noted, a stronger signal is needed for pAKT(S473). This unique AKT axis in Tregs is interesting from two different points of views. First, it suggests that cells of regulatory function might rely on different signaling thresholds and secondly, SHIP1 inhibition in Tregs might reprogram their immunosuppressive properties by AKT activation or eliminate them. Indeed, regulatory B10 cells, provide another example that supports this rationale. B10 cells exhibit immunosuppressive functions to downregulate inflammation via IL-10 production. Interestingly, B10 and CLL cells share phenotypical similarities comprising surface markers and both express IL-10, which in the CLL setting results in the established immunosuppressive phenotype [Alhakeem et al., 2018]. For B10 cells it could already be shown that *SHIP1* deletion results in reduced cell numbers and is accompanied by an increase in pAKT [Chen et al., 2017]. Although further studies will be needed to dissect the complex AKT signaling network downstream of SHIP1 inhibition, based on our data, AKT is involved in the observed induction of cell death and CLL cells seem to possess a unique AKT signaling network, similar to other regulatory, immunosupressive cell types.

As AKT constitutes the primary effector downstream of PI3K, we focused on AKT hyperactivation to mimic SHIP1 inhibition. In line with our results, a growing number of studies indicate that AKT activation can promote cell death under certain circumstances [Los et al., 2009]. For example upon glucose withdrawal, AKT is no longer able to maintain mitochondrial integrity and as a result AKT-expressing cells are more sensitive for cell death induction. [Gottlob et al., 2001]; [Elstrom et al., 2004]. Besides, eukaryotic translation initiation factor 2A (eIF2α) was proposed as potential molecular switch that decides over cell survival or death. Phosphorylated eIF2α is

known for its important role in the regulation of redox homeostasis and adaptation to oxidative stress and the authors suggested that inactivation of P-eIF2α might be a suitable approach to activate AKT in response to oxidative stress and induce cell death [Rajesh et al., 2015].

However, also AKT independent, yet PI3K dependent signaling networks might contribute to the observed effects comprising cell death induction and immunogenicity upon SHIP1 inhibition. Such branches might include the PDK1-mechanistic target of rapamycin complex 2 (mTORC2) axis, Rac signaling, or the kinase BTK, whose more detailed study is of future interest [Lien et al., 2017]. The appearance of Ser473 phosphorylation upon SHIP1 inhibition could also point to a functional role of mTORC2, which requires further investigation [Cosimo et al., 2019]. Attempts to understand the mechanism of cell death and immunogenicity upon SHIP1 inhibition revealed little participation of caspases in this process. We applied pan-caspase and caspase-8 inhibitors prior to SHIP1 inhibition and found no reversal of the induction of specific cell death. Thus, classical apoptosis is rather unlikely, which was underlined by inconsistent induction of phosphatidylserine on the outer membranes. Interestingly, both RIP1 and RIP3 inhibition partially but significantly reduced the induction of specific cell death induced by SHIP1 inhibition. It is well characterized that programmed cell death mechanisms are dysregulated in CLL and contribute to the accumulation of malignant clones and also mediate chemoresistence [Bagacean et al., 2019]. Apart from the defective apoptotic machinery that has been intensively investigated in CLL, in 2012 Liu and colleagues showed that CLL cells also fail to undergo necroptosis, a regulated inflammatory mode of cell death. Two main components of the necroptotic pathway, RIP3 and CYLD, are down regulated in CLL compared to normal B cells, both at protein and transcriptional level. In classical necroptosis, the necrosome complex is formed by heterodimerization of RIP3 and RIP1. This can only happen upon deubiquitination of RIP1 by CYLD. RIP1/RIP3 complex formation in the cytosol thereafter promotes the oligomerization of MLKL by phosphorylation, which results in MLKL plasma membrane translocation and subsequent formation of pores [Liu et al., 2012]. To note and in line with our observation of strong high-mobility-group-protein B1 (HMGB1) release upon SHIP1 inhibition, only necroptosis leads to secretion of DAMPs, in contrast to necrosis.

MLKL inhibition prior to SHIP1 inhibition did not result in altered CLL viability, however we found a partial reversion of HMGB1 release, which links necroptosis to the induction of ICD . The exact mechanism how SHIP1 inhibition is linked to the induction of the necrosome formation and subsequent ICD induction requires further investigation.

The involvement of RIP3 in the cascade of cell death could also point towards non-bearable metabolic alterations upon SHIP1 inhibition. The involvement of the aerobic mitochondrial respiration upon SHIP1 inhibition still needs to be further dissected, but initial experiments indicated increased oxidative phosphorylation upon SHIP1 inhibition. It is known that RIP3 can up regulate aerobic metabolism and that the enhanced respiration provides a feedback loop on the necrosome to promote necroptosis [Qiu et al., 2018]. Further studies are required to determine a possible link between necroptotic cell death and potential metabolic reprogramming [Zhang et al., 2009].

Durable therapeutic responses are rare in CLL and up to date the only curative approach is allogenic stem cell transplantation, which bears risks and is only available for a small, fit group of patients. It reflects the urgent need for options to re-activate immune responses in the strongly immunosuppressed microenvironment in CLL patients. In this context, literature provides already evidence that pulsatile SHIP1 inhibition has the potential to restore T cell responses in distinct lymphoma entities and colon cancer [Gumbleton et al., 2017]. Our data of involvement of necroptosis upon 3AC treatment bears great potential for the induction of ICD by SHIP1 inhibition. Indeed, we found strong HMGB1 release upon 3AC treatment of CLL cells that was inhibited by combinatorial MLKL inhibition. Besides, Calreticulin, another strong hallmark of ICD, was exposed on the outer cell surface and ATP was released early upon SHIP1 inhibition. Therefore, we tried to mimic complex microenvironmental settings *in vitro* by applying labeled cytotoxic T cells from the OT-I system in co-culture with either 3AC killed (Ovalbumin fed) CLL cells alone (direct activation) or in additional combination with antigen presenting wildtype BMDCs (BMDC-mediated activation). Direct activation and BMDC-mediated activation resulted both in increased T cell proliferation and confirmed the induction of immunogenic CLL cell death upon 3AC treatment. Strikingly, although unstimulated CLL cells

are described to be unable to initiate T cell proliferation, upon 3AC treatment, we found a very strong induction in proliferation of cytotoxic OT-I T cells in response to MHC-I presented SINFEKL. Interestingly, T cells showed increased proliferation also in the absence of BMDCs, confirming the functional presentation of antigens by CLL cells themselves. Surprisingly, even the transfer of CLL supernatants upon 3AC treatment partially increased T cell proliferation in the presence or absence of BMDCs. Most likely exosome-based transfer of MHC-I presented SINFEKL peptide is responsible for T cell activation. Exosomes are well characterized to modulate immune responses either directly by MHC-antigen exposure, or indirectly by offering antigens to surrounding cells [Clayton et al., 2001]; [André et al., 2004]. Although BMDCs and T cells were not derived from a CLL (TCL1tg background) microenvironment in our setting, it has been previously shown that primary patient CLL cells and also BMDCs pulsed with dead CLL cells are in general still capable to present antigen and induce allogeneic T cell responses in the immunosuppressive CLL setting [Krackhardt et al., 2002]. However, the major hurdle remains to obtain antitumor cytotoxic T cell responses in autologous settings, where immune responses in CLL are known to be absent. To this end, the characterization of ICD in an *in vivo* fully immunocompetent setup will be essential to study the immunomodulatory potential of 3AC. Overall, our here proposed concept of negative feedback inhibition provides a novel attractive therapy rationale for CLL, as it selectively eliminates malignant CLL cells and at the same time has potential to induce cytotoxic T cell responses.

Chapter 7

Summary and Outlook

Pathological RANK signaling in CLL

Taken together, our experiments show that enforced expression of the DLBCL-derived RANK(K240E) mutation in B cells can drive transformation of B1 B cells, resulting in the development of a monoclonal CLL-like disease in aged mice. This highlights the relevance of RANK signaling for malignant transformation and offers novel therapeutic approaches by targeting the RANK/RANKL signaling axis in CLL. Our mouse model of conditional RANK(K240E) expression early on in pre-B cells could emerge as a novel murine model for CLL development. As younger mice, that succumbed a strong autoimmune phenotype carried mutated BCR receptors, the analysis of the mutational status of aged mice with CLL phenotype is of future interest and it can be speculated that our model might provide a CLL mouse model for the less aggressive, IgVH mutated CLL, in contrast to the commonly applied aggressive TCL1tg model carrying unmutated IgVH.

We provide evidence for *in vivo* efficacy of RANKL blocking antibody administration in distinct CLL mouse models (TCL1tg and MEC-1 Xenograft). Our attempts to evaluate the clinical outcome of CLL for patients that receive Denosumab for the treatment of comorbidities were unsuccessful due to the low number of patients. However, further clinical assessment of Denosumab for CLL therapy, potentially in combination with standard therapies, is of interest. Similarly, the potential therapeutic options for RANK/RANKL blockage in autoimmune disorders, as well as

RANK-mutated DLBCL, require deeper investigation and are of future interest. The development of the more aggressive DLBCL was not observed in our murine model and its investigation is planned in the future. Our mouse model of inducible RANK(K240E) expression, crossed to a GC-specific Cre line, can provide a powerful tool. A potential combination with BCL2 overexpression and/or of loss of BLIMP-1 could promote a potential transformation to DLBCL and provide mechanistic insight into the gradual steps of DLBC pathogenesis.

DUSP1/6 inhibition in CLL as novel therapeutic approach

We provide here evidence for the concept of negative feedback inhibition in CLL as novel, promising therapeutic approach. DUSP1 and DUSP6 inhibition as well as genetic phosphatase knockout induces cell death in CLL cells. Of future interest is a better understanding of the involvement and potential interplay of DDR, autophagy, and senescence in the induction of activation induced cell death in CLL cells, which might be linked to the occurrence of an immunogenic form of cell death. Therapeutic success is strongly linked to the activation of proper immune responses and functional cytotoxic T cell responses. Since this needs to be evaluated in an *in vivo* setting, where CLL cells reside in their microenvironmental niches, the application and efficacy of BCI *in vivo* is the most important missing next step. A more stable formulation of BCI (BCI-215) is available and planned to be tested in CLL *in vivo* mouse models. Additional combination with improved nanomedicines might be beneficial and is planned.

SHIP1 inhibition is critical for CLL progression and immunosurveillance

In line with our concept of negative feedback inhibition, we further demonstrated that SHIP1 inhibition and genetic manipulation of SHIP1 or its downstream pathway confirm our hypothesis of activation induced cell death in CLL. We observed the involvement of necroptosis and the induction of ICD upon SHIP1 inhibition. The characterization of ICD in an *in vivo* setup is still missing and will be inevitable to study the immunomodulatory potential of SHIP1 inhibition for potential future clinical application. Besides, further studies are required to determine a possible

link between necroptotic cell death, subsequent ICD, and a potential metabolic reprogramming [Zhang et al., 2009]. Those new insights will help to further dissect the mechanism upon SHIP1 inhibition.

As AKT constitutes the primary effector downstream of PI3K, we focused on AKT hyperactivation to mimic SHIP1 inhibition. The study of further AKT downstream modules, such as FoxO transcription factors, and their interplay with potentially altered metabolic demands is of future interest. In line with this, functional metabolic analysis are planned upon SHIP1 inhibition and AKT activation in CLL cells.

Besides, also AKT independent, PI3K dependent signaling networks might contribute to the observed effects comprising cell death induction and immunogenicity upon SHIP1 inhibition. Investigation of the role of for example PDK1, mTORC2, Rac, and BTK, downstream of PI3K activation is still missing. For both attempts a comprehensive RNA sequencing analysis upon SHIP1 inhibition and AKT hyperactivation in CLL cells might be useful.

Given the current clinical situation with the onset of developing resistances upon Ibrutinib and Idelalisib therapy, our concept of negative feedback inhbition can provide a valuable alternative. In particular, the analysis of Ibrutinib resistant patient samples will evaluate whether negative feedback inhibition can help to treat developing resistances. Apart from an application in resistances, we recommend a fundamental rethinking of the current clinical landscape that is composed of kinase inhibitors. The development of safe and selective phosphatase inhibitors and in particular a sophisticated alternation of kinase and phosphatase inhibitors has the potential for improved clinical outcome with respect to sustained immune responses and avoidance of resistances.

Bibliography

[Abdelrasoul et al., 2018] Abdelrasoul, H., Werner, M., Setz, C. S., Okkenhaug, K., and Jumaa, H. (2018). Pi3k induces b-cell development and regulates b cell identity. *Sci Rep*, 8(1):1327.

[Alhakeem et al., 2018] Alhakeem, S. S., McKenna, M. K., Oben, K. Z., Noothi, S. K., Rivas, J. R., Hildebrandt, G. C., Fleischman, R. A., Rangnekar, V. M., Muthusamy, N., and Bondada, S. (2018). Chronic lymphocytic leukemia-derived il-10 suppresses antitumor immunity. *J Immunol*, 200(12):4180–4189.

[Allam and Marshall, 2005] Allam, A. and Marshall, A. J. (2005). Role of the adaptor proteins bam32, tapp1 and tapp2 in lymphocyte activation. *Immunol Lett*, 97(1):7–17.

[Alt et al., 1984] Alt, F. W., Yancopoulos, G. D., Blackwell, T. K., Wood, C., Thomas, E., Boss, M., Coffman, R., Rosenberg, N., Tonegawa, S., and Baltimore, D. (1984). Ordered rearrangement of immunoglobulin heavy chain variable region segments. *EMBO J*, 3(6):1209–19.

[Anderson et al., 1997] Anderson, D. M., Maraskovsky, E., Billingsley, W. L., Dougall, W. C., Tometsko, M. E., Roux, E. R., Teepe, M. C., DuBose, R. F., Cosman, D., and Galibert, L. (1997). A homologue of the tnf receptor and its ligand enhance t-cell growth and dendritic-cell function. *Nature*, 390(6656):175–9.

[André et al., 2004] André, F., Chaput, N., Schartz, N. E. C., Flament, C., Aubert, N., Bernard, J., Lemonnier, F., Raposo, G., Escudier, B., Hsu, D.-H., Tursz, T., Amigorena, S., Angevin, E., and Zitvogel, L. (2004). Exosomes as potent cell-free peptide-based vaccine. i. dendritic cell-derived exosomes transfer functional mhc class i/peptide complexes to dendritic cells. *J Immunol*, 172(4):2126–36.

[Bagacean et al., 2019] Bagacean, C., Tomuleasa, C., Tempescul, A., Grewal, R., Brooks, W. H., Berthou, C., and Renaudineau, Y. (2019). Apoptotic resistance in chronic lymphocytic leukemia and therapeutic perspectives. *Crit Rev Clin Lab Sci*, 56(5):321–332.

[Bagnyukova et al., 2013] Bagnyukova, T. V., Restifo, D., Beeharry, N., Gabitova, L., Li, T., Serebriiskii, I. G., Golemis, E. A., and Astsaturov, I. (2013). Dusp6 regulates drug sensitivity by modulating dna damage response. *Br J Cancer*, 109(4):1063–71.

[Bair and Porter, 2019] Bair, S. M. and Porter, D. L. (2019). Accelerating chimeric antigen receptor therapy in chronic lymphocytic leukemia: The development and challenges of chimeric antigen receptor t-cell therapy for chronic lymphocytic leukemia. *Am J Hematol*, 94(S1):S10–S17.

[Banham-Hall et al., 2012] Banham-Hall, E., Clatworthy, M. R., and Okkenhaug, K. (2012). The therapeutic potential for pi3k inhibitors in autoimmune rheumatic diseases. *Open Rheumatol J*, 6:245–58.

[Bannard and Cyster, 2017] Bannard, O. and Cyster, J. G. (2017). Germinal centers: programmed for affinity maturation and antibody diversification. *Curr Opin Immunol*, 45:21–30.

[Barcellini et al., 2006] Barcellini, W., Capalbo, S., Agostinelli, R. M., Mauro, F. R., Ambrosetti, A., Calori, R., Cortelezzi, A., Laurenti, L., Pogliani, E. M., Pedotti, P., Liso, V., Girelli, G., Mandelli, F., Zanella, A., and GIMEMA Chronic Lymphocytic Leukemia Group (2006). Relationship between autoimmune phenomena and disease stage and therapy in b-cell chronic lymphocytic leukemia. *Haematologica*, 91(12):1689–92.

[Barragán et al., 2006] Barragán, M., de Frias, M., Iglesias-Serret, D., Campàs, C., Castaño, E., Santidrián, A. F., Coll-Mulet, L., Cosialls, A. M., Domingo, A., Pons, G., and Gil, J. (2006). Regulation of akt/pkb by phosphatidylinositol 3-kinase-dependent and -independent pathways in b-cell chronic lymphocytic leukemia cells: role of protein kinase cbeta. *J Leukoc Biol*, 80(6):1473–9.

[Batten et al., 2004] Batten, M., Fletcher, C., Ng, L. G., Groom, J., Wheway, J., Laâbi, Y., Xin, X., Schneider, P., Tschopp, J., Mackay, C. R., and Mackay, F. (2004). Tnf deficiency fails to protect baff transgenic mice against autoimmunity and reveals a predisposition to b cell lymphoma. *J Immunol*, 172(2):812–22.

[Baumgarth, 2011] Baumgarth, N. (2011). The double life of a b-1 cell: self-reactivity selects for protective effector functions. *Nat Rev Immunol*, 11(1):34–46.

[Bea et al., 2005] Bea, S., Zettl, A., Wright, G., Salaverria, I., Jehn, P., Moreno, V., Burek, C., Ott, G., Puig, X., Yang, L., Lopez-Guillermo, A., Chan, W. C., Greiner, T. C., Weisenburger, D. D., Armitage, J. O., Gascoyne, R. D., Connors, J. M., Grogan, T. M., Braziel, R., Fisher, R. I., Smeland, E. B., Kvaloy, S., Holte, H., Delabie, J., Simon, R., Powell, J., Wilson, W. H., Jaffe, E. S., Montserrat, E., Muller-Hermelink, H.-K., Staudt, L. M., Campo, E., Rosenwald, A., and Lymphoma/Leukemia Molecular Profiling Project (2005). Diffuse large b-cell lymphoma subgroups have distinct genetic profiles that influence tumor biology and improve gene-expression-based survival prediction. *Blood*, 106(9):3183–90.

[Benkisser-Petersen et al., 2016] Benkisser-Petersen, M., Buchner, M., Dörffel, A., Dühren-von Minden, M., Claus, R., Kläsener, K., Leberecht, K., Burger, M., Dierks, C., Jumaa, H., Malavasi, F., Reth, M., Veelken, H., Duyster, J., and Zirlik, K. (2016). Spleen tyrosine kinase is involved in the cd38 signal transduction pathway in chronic lymphocytic leukemia. *PLoS One*, 11(12):e0169159.

[Berland and Wortis, 2002] Berland, R. and Wortis, H. H. (2002). Origins and functions of b-1 cells with notes on the role of cd5. *Annu Rev Immunol*, 20:253–300.

[Bichi et al., 2002] Bichi, R., Shinton, S. A., Martin, E. S., Koval, A., Calin, G. A., Cesari, R., Russo, G., Hardy, R. R., and Croce, C. M. (2002). Human chronic lymphocytic leukemia modeled in mouse by targeted tcl1 expression. *Proc Natl Acad Sci U S A*, 99(10):6955–60.

[Bot et al., 1996] Bot, A., Bot, S., Antohi, S., Karjalainen, K., and Bona, C. (1996). Kinetics of generation and persistence on membrane class ii molecules of a viral peptide expressed on foreign and self proteins. *J Immunol*, 157(8):3436–42.

[Boyle et al., 2014] Boyle, D. L., Kim, H.-R., Topolewski, K., Bartok, B., and Firestein, G. S. (2014). Novel phosphoinositide 3-kinase , inhibitor: potent anti-inflammatory effects and joint protection in models of rheumatoid arthritis. *J Pharmacol Exp Ther*, 348(2):271–80.

[Brooks et al., 2010] Brooks, R., Fuhler, G. M., Iyer, S., Smith, M. J., Park, M.-Y., Paraiso, K. H. T., Engelman, R. W., and Kerr, W. G. (2010). Ship1 inhibition increases immunoregulatory capacity and triggers apoptosis of hematopoietic cancer cells. *J Immunol*, 184(7):3582–9.

[Brooks et al., 2015] Brooks, R., Iyer, S., Akada, H., Neelam, S., Russo, C. M., Chisholm, J. D., and Kerr, W. G. (2015). Coordinate expansion of murine hematopoietic and mesenchymal stem cell compartments by shipi. *Stem Cells*, 33(3):848–58.

[Buchner et al., 2009] Buchner, M., Fuchs, S., Prinz, G., Pfeifer, D., Bartholomé, K., Burger, M., Chevalier, N., Vallat, L., Timmer, J., Gribben, J. G., Jumaa, H., Veelken, H., Dierks, C., and Zirlik, K. (2009). Spleen tyrosine kinase is overexpressed and represents a potential therapeutic target in chronic lymphocytic leukemia. *Cancer Res*, 69(13):5424–32.

[Buchner and Müschen, 2014] Buchner, M. and Müschen, M. (2014). Targeting the b-cell receptor signaling pathway in b lymphoid malignancies. *Curr Opin Hematol*, 21(4):341–9.

[Burger and Chiorazzi, 2013] Burger, J. A. and Chiorazzi, N. (2013). B cell receptor signaling in chronic lymphocytic leukemia. *Trends Immunol*, 34(12):592–601.

[Byrd et al., 2013] Byrd, J. C., Furman, R. R., Coutre, S. E., Flinn, I. W., Burger, J. A., Blum, K. A., Grant, B., Sharman, J. P., Coleman, M., Wierda, W. G., Jones, J. A., Zhao, W., Heerema, N. A., Johnson, A. J., Sukbuntherng, J., Chang, B. Y., Clow, F., Hedrick, E., Buggy, J. J., James, D. F., and O'Brien, S. (2013). Targeting btk with ibrutinib in relapsed chronic lymphocytic leukemia. *N Engl J Med*, 369(1):32–42.

[Cagnol and Chambard, 2010] Cagnol, S. and Chambard, J.-C. (2010). Erk and cell death: mechanisms of erk-induced cell death–apoptosis, autophagy and senescence. *FEBS J*, 277(1):2–21.

[Calamito et al., 2010] Calamito, M., Juntilla, M. M., Thomas, M., Northrup, D. L., Rathmell, J., Birnbaum, M. J., Koretzky, G., and Allman, D. (2010). Akt1 and akt2 promote peripheral b-cell maturation and survival. *Blood*, 115(20):4043–50.

[Calvisi et al., 2008] Calvisi, D. F., Pinna, F., Meloni, F., Ladu, S., Pellegrino, R., Sini, M., Daino, L., Simile, M. M., De Miglio, M. R., Virdis, P., Frau, M., Tomasi, M. L., Seddaiu, M. A., Muroni, M. R., Feo, F., and Pascale, R. M. (2008). Dual-specificity phosphatase 1 ubiquitination in extracellular signal-regulated kinase-mediated control of growth in human hepatocellular carcinoma. *Cancer Res*, 68(11):4192–200.

[Cambier et al., 1994] Cambier, J. C., Pleiman, C. M., and Clark, M. R. (1994). Signal transduction by the b cell antigen receptor and its coreceptors. *Annu Rev Immunol*, 12:457–86.

[Carmona-Fernandes et al., 2011] Carmona-Fernandes, D., Santos, M. J., Perpétuo, I. P., Fonseca, J. E., and Canhão, H. (2011). Soluble receptor activator of nuclear factor b ligand/osteoprotegerin ratio is increased in systemic lupus erythematosus patients. *Arthritis Res Ther*, 13(5):R175.

[Carpten et al., 2007] Carpten, J. D., Faber, A. L., Horn, C., Donoho, G. P., Briggs, S. L., Robbins, C. M., Hostetter, G., Boguslawski, S., Moses, T. Y., Savage, S., Uhlik, M., Lin, A., Du, J., Qian, Y.-W., Zeckner, D. J., Tucker-Kellogg, G., Touchman, J., Patel, K., Mousses, S., Bittner, M., Schevitz, R., Lai, M.-H. T., Blanchard, K. L., and Thomas, J. E. (2007). A transforming mutation in the pleckstrin homology domain of akt1 in cancer. *Nature*, 448(7152):439–44.

[Carrà et al., 2017] Carrà, G., Panuzzo, C., Torti, D., Parvis, G., Crivellaro, S., Familiari, U., Volante, M., Morena, D., Lingua, M. F., Brancaccio, M., Guerrasio, A., Pandolfi, P. P., Saglio, G., Taulli, R., and Morotti, A. (2017). Therapeutic inhibition of usp7-pten network in chronic lymphocytic leukemia: a strategy to overcome tp53 mutated/deleted clones. *Oncotarget*, 8(22):35508–35522.

[Caunt and Keyse, 2013] Caunt, C. J. and Keyse, S. M. (2013). Dual-specificity map kinase phosphatases (mkps): shaping the outcome of map kinase signalling. *FEBS J*, 280(2):489–504.

[Chalhoub and Baker, 2009] Chalhoub, N. and Baker, S. J. (2009). Pten and the pi3-kinase pathway in cancer. *Annu Rev Pathol*, 4:127–50.

[Chantry et al., 1997] Chantry, D., Vojtek, A., Kashishian, A., Holtzman, D. A., Wood, C., Gray, P. W., Cooper, J. A., and Hoekstra, M. F. (1997). p110delta, a novel phosphatidylinositol 3-kinase catalytic subunit that associates with p85 and is expressed predominantly in leukocytes. *J Biol Chem*, 272(31):19236–41.

[Chen et al., 2018] Chen, Y., Germano, S., Shelmani, G., Kluczna, D., Jayne, S., Dyer, M. J. S., and Macip, S. (2018). Paradoxical activation of alternative pro-survival pathways determines resistance to mek inhibitors in chronic lymphocytic leukaemia. *Br J Haematol*, 182(6):921–924.

[Chen et al., 2017] Chen, Y., Hu, F., Dong, X., Zhao, M., Wang, J., Sun, X., Kim, T. J., Li, Z., and Liu, W. (2017). Ship-1 deficiency in aid+ b cells leads to the impaired function of b10 cells with spontaneous autoimmunity. *J Immunol*, 199(9):3063–3073.

[Chen et al., 2015] Chen, Z., Shojaee, S., Buchner, M., Geng, H., Lee, J. W., Klemm, L., Titz, B., Graeber, T. G., Park, E., Tan, Y. X., Satterthwaite, A., Paietta, E., Hunger, S. P., Willman, C. L., Melnick, A., Loh, M. L., Jung, J. U., Coligan, J. E., Bolland, S., Mak, T. W., Limnander, A., Jumaa, H., Reth, M., Weiss, A., Lowell, C. A., and Müschen, M. (2015). Signalling thresholds and negative b-cell selection in acute lymphoblastic leukaemia. *Nature*, 521(7552):357–61.

[Chiorazzi et al., 2005] Chiorazzi, N., Rai, K. R., and Ferrarini, M. (2005). Chronic lymphocytic leukemia. *N Engl J Med*, 352(8):804–15.

[Christopoulos et al., 2011] Christopoulos, P., Pfeifer, D., Bartholomé, K., Follo, M., Timmer, J., Fisch, P., and Veelken, H. (2011). Definition and characterization of the systemic t-cell dysregulation in untreated indolent b-cell lymphoma and very early cll. *Blood*, 117(14):3836–46.

[Chung et al., 2002] Chung, J. B., Sater, R. A., Fields, M. L., Erikson, J., and Monroe, J. G. (2002). Cd23 defines two distinct subsets of immature b cells which differ in their responses to t cell help signals. *Int Immunol*, 14(2):157–66.

[Clayton et al., 2001] Clayton, A., Court, J., Navabi, H., Adams, M., Mason, M. D., Hobot, J. A., Newman, G. R., and Jasani, B. (2001). Analysis of antigen presenting cell derived exosomes, based on immuno-magnetic isolation and flow cytometry. *J Immunol Methods*, 247(1-2):163–74.

[Compagno et al., 2009] Compagno, M., Lim, W. K., Grunn, A., Nandula, S. V., Brahmachary, M., Shen, Q., Bertoni, F., Ponzoni, M., Scandurra, M., Califano, A., Bhagat, G., Chadburn, A., Dalla-Favera, R., and Pasqualucci, L. (2009). Mutations of multiple genes cause deregulation of nf-kappab in diffuse large b-cell lymphoma. *Nature*, 459(7247):717–21.

[Cosimo et al., 2019] Cosimo, E., Tarafdar, A., Moles, M. W., Holroyd, A. K., Malik, N., Catherwood, M. A., Hay, J., Dunn, K. M., Macdonald, A. M., Guichard, S. M., O'Rourke, D., Leach, M. T., Sansom, O. J., Cosulich, S. C., McCaig, A. M., and Michie, A. M. (2019). Akt/mtorc2 inhibition activates foxo1 function in cll cells reducing b-cell receptor-mediated survival. *Clin Cancer Res*, 25(5):1574–1587.

[Courtois-Cox et al., 2006] Courtois-Cox, S., Genther Williams, S. M., Reczek, E. E., Johnson, B. W., McGillicuddy, L. T., Johannessen, C. M., Hollstein, P. E., MacCollin, M., and Cichowski, K. (2006). A negative feedback signaling network underlies oncogene-induced senescence. *Cancer Cell*, 10(6):459–72.

[Crellin et al., 2007] Crellin, N. K., Garcia, R. V., and Levings, M. K. (2007). Altered activation of akt is required for the suppressive function of human cd4+cd25+ t regulatory cells. *Blood*, 109(5):2014–22.

[Damle et al., 1999] Damle, R. N., Wasil, T., Fais, F., Ghiotto, F., Valetto, A., Allen, S. L., Buchbinder, A., Budman, D., Dittmar, K., Kolitz, J., Lichtman, S. M., Schulman, P., Vinciguerra, V. P., Rai, K. R., Ferrarini, M., and Chiorazzi, N. (1999). Ig v gene mutation status and cd38 expression as novel prognostic indicators in chronic lymphocytic leukemia. *Blood*, 94(6):1840–7.

[Damm et al., 2014] Damm, F., Mylonas, E., Cosson, A., Yoshida, K., Della Valle, V., Mouly, E., Diop, M., Scourzic, L., Shiraishi, Y., Chiba, K., Tanaka, H., Miyano, S., Kikushige, Y., Davi, F., Lambert, J., Gautheret, D., Merle-Béral, H., Sutton, L., Dessen, P., Solary, E., Akashi, K., Vainchenker, W., Mercher, T., Droin, N., Ogawa, S., Nguyen-Khac, F., and Bernard, O. A. (2014). Acquired initiating mutations in early hematopoietic cells of cll patients. *Cancer Discov*, 4(9):1088–101.

[Davis et al., 2010] Davis, R. E., Ngo, V. N., Lenz, G., Tolar, P., Young, R. M., Romesser, P. B., Kohlhammer, H., Lamy, L., Zhao, H., Yang, Y., Xu, W., Shaffer, A. L., Wright, G., Xiao, W., Powell, J., Jiang, J.-K., Thomas, C. J., Rosenwald, A., Ott, G., Muller-Hermelink, H. K., Gascoyne, R. D., Connors, J. M., Johnson, N. A., Rimsza, L. M., Campo, E., Jaffe, E. S., Wilson, W. H., Delabie, J., Smeland, E. B., Fisher, R. I., Braziel, R. M., Tubbs, R. R., Cook, J. R., Weisenburger, D. D., Chan, W. C., Pierce, S. K., and Staudt, L. M. (2010). Chronic active b-cell-receptor signalling in diffuse large b-cell lymphoma. *Nature*, 463(7277):88–92.

[de Frias et al., 2009] de Frias, M., Iglesias-Serret, D., Cosialls, A. M., Coll-Mulet, L., Santidrián, A. F., González-Gironès, D. M., de la Banda, E., Pons, G., and Gil, J. (2009). Akt inhibitors induce apoptosis in chronic lymphocytic leukemia cells. *Haematologica*, 94(12):1698–707.

[DeFranco, 1996] DeFranco, A. L. (1996). The two-headed antigen. b-cell co-receptors. *Curr Biol*, 6(5):548–50.

[Deshantri et al., 2018] Deshantri, A. K., Varela Moreira, A., Ecker, V., Mandhane, S. N., Schiffelers, R. M., Buchner, M., and Fens, M. H. A. M. (2018). Nanomedicines for the treatment of hematological malignancies. *J Control Release*, 287:194–215.

[Doench et al., 2016] Doench, J. G., Fusi, N., Sullender, M., Hegde, M., Vaimberg, E. W., Donovan, K. F., Smith, I., Tothova, Z., Wilen, C., Orchard, R., Virgin, H. W., Listgarten, J., and Root, D. E. (2016). Optimized sgrna design to maximize activity and minimize off-target effects of crispr-cas9. *Nat Biotechnol*, 34(2):184–191.

[Döhner et al., 2000] Döhner, H., Stilgenbauer, S., Benner, A., Leupolt, E., Kröber, A., Bullinger, L., Döhner, K., Bentz, M., and Lichter, P. (2000). Genomic aberrations and survival in chronic lymphocytic leukemia. *N Engl J Med*, 343(26):1910–6.

[Dreger et al., 2010] Dreger, P., Döhner, H., Ritgen, M., Böttcher, S., Busch, R., Dietrich, S., Bunjes, D., Cohen, S., Schubert, J., Hegenbart, U., Beelen, D., Zeis, M., Stadler, M., Hasenkamp, J., Uharek, L., Scheid, C., Humpe, A., Zenz, T., Winkler, D., Hallek, M., Kneba, M., Schmitz, N., Stilgenbauer, S., and German CLL Study Group (2010). Allogeneic stem cell transplantation provides durable disease control in poor-risk chronic lymphocytic leukemia: long-term clinical and mrd results of the german cll study group cll3x trial. *Blood*, 116(14):2438–47.

[Duan and Morel, 2006] Duan, B. and Morel, L. (2006). Role of b-1a cells in autoimmunity. *Autoimmun Rev*, 5(6):403–8.

[Duek et al., 2006] Duek, A., Shvidel, L., Braester, A., and Berrebi, A. (2006). Clinical and immunologic aspects of b chronic lymphocytic leukemia associated with autoimmune disorders. *Isr Med Assoc J*, 8(12):828–31.

[Dühren-von Minden et al., 2012] Dühren-von Minden, M., Übelhart, R., Schneider, D., Wossning, T., Bach, M. P., Buchner, M., Hofmann, D., Surova, E., Follo, M., Köhler, F., Wardemann, H., Zirlik, K., Veelken, H., and Jumaa, H. (2012). Chronic lymphocytic leukaemia is driven by antigen-independent cell-autonomous signalling. *Nature*, 489(7415):309–12.

[Eeva and Pelkonen, 2004] Eeva, J. and Pelkonen, J. (2004). Mechanisms of b cell receptor induced apoptosis. *Apoptosis*, 9(5):525–31.

[Eliopoulos et al., 2016] Eliopoulos, A. G., Havaki, S., and Gorgoulis, V. G. (2016). Dna damage response and autophagy: A meaningful partnership. *Front Genet*, 7:204.

[Elstrom et al., 2004] Elstrom, R. L., Bauer, D. E., Buzzai, M., Karnauskas, R., Harris, M. H., Plas, D. R., Zhuang, H., Cinalli, R. M., Alavi, A., Rudin, C. M., and Thompson, C. B. (2004). Akt stimulates aerobic glycolysis in cancer cells. *Cancer Res*, 64(11):3892–9.

[Fabbri et al., 2011] Fabbri, G., Rasi, S., Rossi, D., Trifonov, V., Khiabanian, H., Ma, J., Grunn, A., Fangazio, M., Capello, D., Monti, S., Cresta, S., Gargiulo, E., Forconi, F., Guarini, A., Arcaini, L., Paulli, M., Laurenti, L., Larocca, L. M., Marasca, R., Gattei, V., Oscier, D., Bertoni, F., Mullighan, C. G., Foá, R., Pasqualucci, L., Rabadan, R., Dalla-Favera, R., and Gaidano, G. (2011). Analysis of the chronic lymphocytic leukemia coding genome: role of notch1 mutational activation. *J Exp Med*, 208(7):1389–401.

[Fais et al., 1998] Fais, F., Ghiotto, F., Hashimoto, S., Sellars, B., Valetto, A., Allen, S. L., Schulman, P., Vinciguerra, V. P., Rai, K., Rassenti, L. Z., Kipps, T. J., Dighiero, G., Schroeder, Jr, H. W., Ferrarini, M., and Chiorazzi, N. (1998). Chronic lymphocytic leukemia b cells express restricted sets of mutated and unmutated antigen receptors. *J Clin Invest*, 102(8):1515–25.

[Falchi et al., 2016] Falchi, L., Baron, J. M., Orlikowski, C. A., and Ferrajoli, A. (2016). Bcr signaling inhibitors: an overview of toxicities associated with ibrutinib and idelalisib in patients with chronic lymphocytic leukemia. *Mediterr J Hematol Infect Dis*, 8(1):e2016011.

[Fang et al., 2018] Fang, J., Ye, Z., Gu, F., Yan, M., Lin, Q., Lin, J., Wang, Z., Xu, Y., and Wang, Y. (2018). Dusp1 enhances the chemoresistance of gallbladder cancer via the modulation of the p38 pathway and dna damage/repair system. *Oncol Lett*, 16(2):1869–1875.

[Farooq and Zhou, 2004] Farooq, A. and Zhou, M.-M. (2004). Structure and regulation of mapk phosphatases. *Cell Signal*, 16(7):769–79.

[Figgett et al., 2014] Figgett, W. A., Vincent, F. B., Saulep-Easton, D., and Mackay, F. (2014). Roles of ligands from the tnf superfamily in b cell development, function, and regulation. *Semin Immunol*, 26(3):191–202.

[Fiumara et al., 2001] Fiumara, P., Snell, V., Li, Y., Mukhopadhyay, A., Younes, M., Gillenwater, A. M., Cabanillas, F., Aggarwal, B. B., and Younes, A. (2001). Functional expression of receptor activator of nuclear factor kappab in hodgkin disease cell lines. *Blood*, 98(9):2784–90.

[Fleiss and Sarkisyan, 2019] Fleiss, A. and Sarkisyan, K. S. (2019). A brief review of bioluminescent systems (2019). *Curr Genet*, 65(4):877–882.

[Frank et al., 2009] Frank, M. J., Dawson, D. W., Bensinger, S. J., Hong, J. S., Knosp, W. M., Xu, L., Balatoni, C. E., Allen, E. L., Shen, R. R., Bar-Sagi, D., Martin, G. R., and Teitell, M. A. (2009). Expression of sprouty2 inhibits b-cell proliferation and is epigenetically silenced in mouse and human b-cell lymphomas. *Blood*, 113(11):2478–87.

[Frenzel et al., 2016] Frenzel, L. P., Reinhardt, H. C., and Pallasch, C. P. (2016). Concepts of chronic lymphocytic leukemia pathogenesis: Dna damage response and tumor microenvironment. *Oncol Res Treat*, 39(1-2):9–16.

[Fruman et al., 2017] Fruman, D. A., Chiu, H., Hopkins, B. D., Bagrodia, S., Cantley, L. C., and Abraham, R. T. (2017). The pi3k pathway in human disease. *Cell*, 170(4):605–635.

[Furman, 2010] Furman, R. R. (2010). Prognostic markers and stratification of chronic lymphocytic leukemia. *Hematology Am Soc Hematol Educ Program*, 2010:77–81.

[Furman et al., 2014] Furman, R. R., Cheng, S., Lu, P., Setty, M., Perez, A. R., Perez, A. R., Guo, A., Racchumi, J., Xu, G., Wu, H., Ma, J., Steggerda, S. M., Coleman, M., Leslie, C., and Wang, Y. L. (2014). Ibrutinib resistance in chronic lymphocytic leukemia. *N Engl J Med*, 370(24):2352–4.

[Garibyan and Avashia, 2013] Garibyan, L. and Avashia, N. (2013). Polymerase chain reaction. *J Invest Dermatol*, 133(3):1–4.

[Getahun and Cambier, 2015] Getahun, A. and Cambier, J. C. (2015). Of itims, itams, and itamis: revisiting immunoglobulin fc receptor signaling. *Immunol Rev*, 268(1):66–73.

[Godin et al., 1993] Godin, I. E., Garcia-Porrero, J. A., Coutinho, A., Dieterlen-Lièvre, F., and Marcos, M. A. (1993). Para-aortic splanchnopleura from early mouse embryos contains b1a cell progenitors. *Nature*, 364(6432):67–70.

[Goede et al., 2014] Goede, V., Fischer, K., Busch, R., Engelke, A., Eichhorst, B., Wendtner, C. M., Chagorova, T., de la Serna, J., Dilhuydy, M.-S., Illmer, T., Opat, S., Owen, C. J., Samoylova, O., Kreuzer, K.-A., Stilgenbauer, S., Döhner, H., Langerak, A. W., Ritgen, M., Kneba, M., Asikanius, E., Humphrey, K., Wenger, M., and Hallek, M. (2014). Obinutuzumab plus chlorambucil in patients with cll and coexisting conditions. *N Engl J Med*, 370(12):1101–10.

[Gottlob et al., 2001] Gottlob, K., Majewski, N., Kennedy, S., Kandel, E., Robey, R. B., and Hay, N. (2001). Inhibition of early apoptotic events by akt/pkb is dependent on the first committed step of glycolysis and mitochondrial hexokinase. *Genes Dev*, 15(11):1406–18.

[Greaves and Maley, 2012] Greaves, M. and Maley, C. C. (2012). Clonal evolution in cancer. *Nature*, 481(7381):306–13.

[Gref et al., 2000] Gref, Lück, Quellec, Marchand, Dellacherie, Harnisch, Blunk, and Müller (2000). 'stealth' corona-core nanoparticles surface modified by polyethylene glycol (peg): influences of the corona (peg chain length and surface density) and of the core composition on phagocytic uptake and plasma protein adsorption. *Colloids Surf B Biointerfaces*, 18(3-4):301–313.

[Groom et al., 1996] Groom, L. A., Sneddon, A. A., Alessi, D. R., Dowd, S., and Keyse, S. M. (1996). Differential regulation of the map, sap and rk/p38 kinases by pyst1, a novel cytosolic dual-specificity phosphatase. *EMBO J*, 15(14):3621–32.

[Guerrini et al., 2008] Guerrini, M. M., Sobacchi, C., Cassani, B., Abinun, M., Kilic, S. S., Pangrazio, A., Moratto, D., Mazzolari, E., Clayton-Smith, J., Orchard, P., Coxon, F. P., Helfrich, M. H., Crockett, J. C., Mellis, D., Vellodi, A., Tezcan, I., Notarangelo, L. D., Rogers, M. J., Vezzoni, P., Villa, A., and Frattini, A. (2008). Human osteoclast-poor osteopetrosis with hypogammaglobulinemia due to tnfrsf11a (rank) mutations. *Am J Hum Genet*, 83(1):64–76.

[Gumbleton et al., 2017] Gumbleton, M., Sudan, R., Fernandes, S., Engelman, R. W., Russo, C. M., Chisholm, J. D., and Kerr, W. G. (2017). Dual enhancement of t and nk cell function by pulsatile inhibition of ship1 improves antitumor immunity and survival. *Sci Signal*, 10(500).

[Gutierrez et al., 2010] Gutierrez, Jr, A., Tschumper, R. C., Wu, X., Shanafelt, T. D., Eckel-Passow, J., Huddleston, 3rd, P. M., Slager, S. L., Kay, N. E., and Jelinek, D. F. (2010). Lef-1 is a prosurvival factor in chronic lymphocytic leukemia and is expressed in the preleukemic state of monoclonal b-cell lymphocytosis. *Blood*, 116(16):2975–83.

[Hallek et al., 2018] Hallek, M., Cheson, B. D., Catovsky, D., Caligaris-Cappio, F., Dighiero, G., Döhner, H., Hillmen, P., Keating, M., Montserrat, E., Chiorazzi, N., Stilgenbauer, S., Rai, K. R., Byrd, J. C., Eichhorst, B., O'Brien, S., Robak, T., Seymour, J. F., and Kipps, T. J. (2018). iwcll guidelines for diagnosis, indications for treatment, response assessment, and supportive management of cll. *Blood*, 131(25):2745–2760.

[Hallek et al., 2010] Hallek, M., Fischer, K., Fingerle-Rowson, G., Fink, A. M., Busch, R., Mayer, J., Hensel, M., Hopfinger, G., Hess, G., von Grünhagen, U., Bergmann, M., Catalano, J., Zinzani, P. L., Caligaris-Cappio, F., Seymour, J. F., Berrebi, A., Jäger, U., Cazin, B., Trneny, M., Westermann, A., Wendtner, C. M., Eichhorst, B. F., Staib, P., Bühler, A., Winkler, D., Zenz, T., Böttcher, S., Ritgen, M., Mendila, M., Kneba, M., Döhner, H., Stilgenbauer, S., International Group of Investigators, and German Chronic Lymphocytic Leukaemia Study Group (2010). Addition of rituximab to fludarabine and cyclophosphamide in patients with chronic lymphocytic leukaemia: a randomised, open-label, phase 3 trial. *Lancet*, 376(9747):1164–74.

[Hamblin et al., 1999] Hamblin, T. J., Davis, Z., Gardiner, A., Oscier, D. G., and Stevenson, F. K. (1999). Unmutated ig v(h) genes are associated with a more aggressive form of chronic lymphocytic leukemia. *Blood*, 94(6):1848–54.

[Hardie, 2011] Hardie, D. G. (2011). Ampk and autophagy get connected. *EMBO J*, 30(4):634–5.

[Hardy, 2006] Hardy, R. R. (2006). B-1 b cell development. *J Immunol*, 177(5):2749–54.

[Hay and Cheung, 2019] Hay, A. E. and Cheung, M. C. (2019). Car t-cells: costs, comparisons, and commentary. *J Med Econ*, 22(7):613–615.

[Hayakawa et al., 1983] Hayakawa, K., Hardy, R. R., Parks, D. R., and Herzenberg, L. A. (1983). The "ly-1 b" cell subpopulation in normal immunodefective, and autoimmune mice. *J Exp Med*, 157(1):202–18.

[He et al., 2013] He, R., Zeng, L.-F., He, Y., Zhang, S., and Zhang, Z.-Y. (2013). Small molecule tools for functional interrogation of protein tyrosine phosphatases. *FEBS J*, 280(2):731–50.

[Herishanu et al., 2011] Herishanu, Y., Pérez-Galán, P., Liu, D., Biancotto, A., Pittaluga, S., Vire, B., Gibellini, F., Njuguna, N., Lee, E., Stennett, L., Raghavachari, N., Liu, P., McCoy, J. P., Raffeld, M., Stetler-Stevenson, M., Yuan, C., Sherry, R., Arthur, D. C., Maric, I., White, T., Marti, G. E., Munson, P., Wilson, W. H., and Wiestner, A. (2011). The lymph node microenvironment promotes b-cell receptor signaling, nf-kappab activation, and tumor proliferation in chronic lymphocytic leukemia. *Blood*, 117(2):563–74.

[Herling et al., 2009] Herling, M., Patel, K. A., Weit, N., Lilienthal, N., Hallek, M., Keating, M. J., and Jones, D. (2009). High tcl1 levels are a marker of b-cell receptor pathway responsiveness and adverse outcome in chronic lymphocytic leukemia. *Blood*, 114(21):4675–86.

[Hofbauer et al., 2011] Hofbauer, J. P., Heyder, C., Denk, U., Kocher, T., Holler, C., Trapin, D., Asslaber, D., Tinhofer, I., Greil, R., and Egle, A. (2011). Development of cll in the tcl1 transgenic mouse model is associated with severe skewing of the t-cell compartment homologous to human cll. *Leukemia*, 25(9):1452–8.

[Hogquist et al., 2003] Hogquist, K. A., Starr, T. K., and Jameson, S. C. (2003). Receptor sensitivity: when t cells lose their sense of self. *Curr Biol*, 13(6):R239–41.

[Holler et al., 2009] Holler, C., Piñón, J. D., Denk, U., Heyder, C., Hofbauer, S., Greil, R., and Egle, A. (2009). Pkcbeta is essential for the development of chronic lymphocytic leukemia in the tcl1 transgenic mouse model: validation of pkcbeta as a therapeutic target in chronic lymphocytic leukemia. *Blood*, 113(12):2791–4.

[Huang et al., 2011] Huang, W., Moisini, I., Bethunaickan, R., Sahu, R., Akerman, M., Eilat, D., Lesser, M., and Davidson, A. (2011). Baff/april inhibition decreases

selection of naive but not antigen-induced autoreactive b cells in murine systemic lupus erythematosus. *J Immunol*, 187(12):6571–80.

[Hug et al., 2014] Hug, E., Hobeika, E., Reth, M., and Jumaa, H. (2014). Inducible expression of hyperactive syk in b cells activates blimp-1-dependent terminal differentiation. *Oncogene*, 33(28):3730–41.

[Ibrahim et al., 2001] Ibrahim, S., Keating, M., Do, K. A., O'Brien, S., Huh, Y. O., Jilani, I., Lerner, S., Kantarjian, H. M., and Albitar, M. (2001). Cd38 expression as an important prognostic factor in b-cell chronic lymphocytic leukemia. *Blood*, 98(1):181–6.

[Iqbal et al., 2007] Iqbal, J., Greiner, T. C., Patel, K., Dave, B. J., Smith, L., Ji, J., Wright, G., Sanger, W. G., Pickering, D. L., Jain, S., Horsman, D. E., Shen, Y., Fu, K., Weisenburger, D. D., Hans, C. P., Campo, E., Gascoyne, R. D., Rosenwald, A., Jaffe, E. S., Delabie, J., Rimsza, L., Ott, G., Müller-Hermelink, H. K., Connors, J. M., Vose, J. M., McKeithan, T., Staudt, L. M., Chan, W. C., and Leukemia/Lymphoma Molecular Profiling Project (2007). Distinctive patterns of bcl6 molecular alterations and their functional consequences in different subgroups of diffuse large b-cell lymphoma. *Leukemia*, 21(11):2332–43.

[Jacob et al., 1991] Jacob, J., Kassir, R., and Kelsoe, G. (1991). In situ studies of the primary immune response to (4-hydroxy-3-nitrophenyl)acetyl. i. the architecture and dynamics of responding cell populations. *J Exp Med*, 173(5):1165–75.

[Jain and Stylianopoulos, 2010] Jain, R. K. and Stylianopoulos, T. (2010). Delivering nanomedicine to solid tumors. *Nat Rev Clin Oncol*, 7(11):653–64.

[Janeway et al., 1996] Janeway, C. A., Travers, P., Walport, M., Shlomchik, M., et al. (1996). *Immunobiology: the immune system in health and disease*, volume 7. Current Biology London.

[Jitschin et al., 2014] Jitschin, R., Braun, M., Büttner, M., Dettmer-Wilde, K., Bricks, J., Berger, J., Eckart, M. J., Krause, S. W., Oefner, P. J., Le Blanc, K., Mackensen, A., and Mougiakakos, D. (2014). Cll-cells induce idohi cd14+hla-drlo myeloid-derived suppressor cells that inhibit t-cell responses and promote tregs. *Blood*, 124(5):750–60.

[Jules et al., 2010] Jules, J., Ashley, J. W., and Feng, X. (2010). Selective targeting of rank signaling pathways as new therapeutic strategies for osteoporosis. *Expert Opin Ther Targets*, 14(9):923–34.

[Kamentsky et al., 1965] Kamentsky, L. A., Melamed, M. R., and Derman, H. (1965). Spectrophotometer: new instrument for ultrarapid cell analysis. *Science*, 150(3696):630–1.

[Kang et al., 2015] Kang, C., Xu, Q., Martin, T. D., Li, M. Z., Demaria, M., Aron, L., Lu, T., Yankner, B. A., Campisi, J., and Elledge, S. J. (2015). The dna damage response induces inflammation and senescence by inhibiting autophagy of gata4. *Science*, 349(6255):aaa5612.

[Kawabe et al., 1994] Kawabe, T., Naka, T., Yoshida, K., Tanaka, T., Fujiwara, H., Suematsu, S., Yoshida, N., Kishimoto, T., and Kikutani, H. (1994). The immune responses in cd40-deficient mice: impaired immunoglobulin class switching and germinal center formation. *Immunity*, 1(3):167–78.

[Keating et al., 1991] Keating, M. J., Kantarjian, H., O'Brien, S., Koller, C., Talpaz, M., Schachner, J., Childs, C. C., Freireich, E. J., and McCredie, K. B. (1991). Fludarabine: a new agent with marked cytoreductive activity in untreated chronic lymphocytic leukemia. *J Clin Oncol*, 9(1):44–9.

[Kesarwani et al., 2017] Kesarwani, M., Kincaid, Z., Gomaa, A., Huber, E., Rohrabaugh, S., Siddiqui, Z., Bouso, M. F., Latif, T., Xu, M., Komurov, K., Mulloy, J. C., Cancelas, J. A., Grimes, H. L., and Azam, M. (2017). Targeting c-fos and dusp1 abrogates intrinsic resistance to tyrosine-kinase inhibitor therapy in bcr-abl-induced leukemia. *Nat Med*, 23(4):472–482.

[Kikushige et al., 2011] Kikushige, Y., Ishikawa, F., Miyamoto, T., Shima, T., Urata, S., Yoshimoto, G., Mori, Y., Iino, T., Yamauchi, T., Eto, T., Niiro, H., Iwasaki, H., Takenaka, K., and Akashi, K. (2011). Self-renewing hematopoietic stem cell is the primary target in pathogenesis of human chronic lymphocytic leukemia. *Cancer Cell*, 20(2):246–59.

[Kil et al., 2012] Kil, L. P., Yuvaraj, S., Langerak, A. W., and Hendriks, R. W. (2012). The role of b cell receptor stimulation in cll pathogenesis. *Curr Pharm Des*, 18(23):3335–55.

[Kitamura et al., 1992] Kitamura, D., Kudo, A., Schaal, S., Müller, W., Melchers, F., and Rajewsky, K. (1992). A critical role of lambda 5 protein in b cell development. *Cell*, 69(5):823–31.

[Klein et al., 2010] Klein, U., Lia, M., Crespo, M., Siegel, R., Shen, Q., Mo, T., Ambesi-Impiombato, A., Califano, A., Migliazza, A., Bhagat, G., and Dalla-Favera, R. (2010). The dleu2/mir-15a/16-1 cluster controls b cell proliferation and its deletion leads to chronic lymphocytic leukemia. *Cancer Cell*, 17(1):28–40.

[Klein et al., 2001] Klein, U., Tu, Y., Stolovitzky, G. A., Mattioli, M., Cattoretti, G., Husson, H., Freedman, A., Inghirami, G., Cro, L., Baldini, L., Neri, A., Califano, A., and Dalla-Favera, R. (2001). Gene expression profiling of b cell chronic lymphocytic leukemia reveals a homogeneous phenotype related to memory b cells. *J Exp Med*, 194(11):1625–38.

[Krackhardt et al., 2002] Krackhardt, A. M., Harig, S., Witzens, M., Broderick, R., Barrett, P., and Gribben, J. G. (2002). T-cell responses against chronic lymphocytic leukemia cells: implications for immunotherapy. *Blood*, 100(1):167–73.

[Kroemer et al., 2013] Kroemer, G., Galluzzi, L., Kepp, O., and Zitvogel, L. (2013). Immunogenic cell death in cancer therapy. *Annu Rev Immunol*, 31:51–72.

[Kwak et al., 2019] Kwak, K., Akkaya, M., and Pierce, S. K. (2019). B cell signaling in context. *Nat Immunol*, 20(8):963–969.

[Lake et al., 2016] Lake, D., Corrêa, S. A. L., and Müller, J. (2016). Negative feedback regulation of the erk1/2 mapk pathway. *Cell Mol Life Sci*, 73(23):4397–4413.

[Landau et al., 2015] Landau, D. A., Tausch, E., Taylor-Weiner, A. N., Stewart, C., Reiter, J. G., Bahlo, J., Kluth, S., Bozic, I., Lawrence, M., Böttcher, S., Carter, S. L., Cibulskis, K., Mertens, D., Sougnez, C. L., Rosenberg, M., Hess, J. M., Edelmann, J., Kless, S., Kneba, M., Ritgen, M., Fink, A., Fischer, K., Gabriel, S., Lander, E. S., Nowak, M. A., Döhner, H., Hallek, M., Neuberg, D., Getz, G.,

Stilgenbauer, S., and Wu, C. J. (2015). Mutations driving cll and their evolution in progression and relapse. *Nature*, 526(7574):525–30.

[Lankester et al., 1995] Lankester, A. C., van Schijndel, G. M., van der Schoot, C. E., van Oers, M. H., van Noesel, C. J., and van Lier, R. A. (1995). Antigen receptor nonresponsiveness in chronic lymphocytic leukemia b cells. *Blood*, 86(3):1090–7.

[LeBien, 2000] LeBien, T. W. (2000). Fates of human b-cell precursors. *Blood*, 96(1):9–23.

[LeBien and Tedder, 2008] LeBien, T. W. and Tedder, T. F. (2008). B lymphocytes: how they develop and function. *Blood*, 112(5):1570–80.

[Lee et al., 2010] Lee, J. W., Park, S., Takahashi, Y., and Wang, H.-G. (2010). The association of ampk with ulk1 regulates autophagy. *PLoS One*, 5(11):e15394.

[Lemmon and Ferguson, 2000] Lemmon, M. A. and Ferguson, K. M. (2000). Signal-dependent membrane targeting by pleckstrin homology (ph) domains. *Biochem J*, 350 Pt 1:1–18.

[Lesley et al., 2004] Lesley, R., Xu, Y., Kalled, S. L., Hess, D. M., Schwab, S. R., Shu, H.-B., and Cyster, J. G. (2004). Reduced competitiveness of autoantigen-engaged b cells due to increased dependence on baff. *Immunity*, 20(4):441–53.

[Li et al., 2012] Li, G., Yu, M., Lee, W.-W., Tsang, M., Krishnan, E., Weyand, C. M., and Goronzy, J. J. (2012). Decline in mir-181a expression with age impairs t cell receptor sensitivity by increasing dusp6 activity. *Nat Med*, 18(10):1518–24.

[Lien et al., 2017] Lien, E. C., Dibble, C. C., and Toker, A. (2017). Pi3k signaling in cancer: beyond akt. *Curr Opin Cell Biol*, 45:62–71.

[Limnander et al., 2011] Limnander, A., Depeille, P., Freedman, T. S., Liou, J., Leitges, M., Kurosaki, T., Roose, J. P., and Weiss, A. (2011). Stim1, pkc- and rasgrp set a threshold for proapoptotic erk signaling during b cell development. *Nat Immunol*, 12(5):425–33.

[Liu et al., 2012] Liu, P., Xu, B., Shen, W., Zhu, H., Wu, W., Fu, Y., Chen, H., Dong, H., Zhu, Y., Miao, K., Xu, W., and Li, J. (2012). Dysregulation of tnf-induced

necroptotic signaling in chronic lymphocytic leukemia: suppression of cyld gene by lef1. *Leukemia*, 26(6):1293–300.

[Longo et al., 2007] Longo, P. G., Laurenti, L., Gobessi, S., Petlickovski, A., Pelosi, M., Chiusolo, P., Sica, S., Leone, G., and Efremov, D. G. (2007). The akt signaling pathway determines the different proliferative capacity of chronic lymphocytic leukemia b-cells from patients with progressive and stable disease. *Leukemia*, 21(1):110–20.

[Longo et al., 2008] Longo, P. G., Laurenti, L., Gobessi, S., Sica, S., Leone, G., and Efremov, D. G. (2008). The akt/mcl-1 pathway plays a prominent role in mediating antiapoptotic signals downstream of the b-cell receptor in chronic lymphocytic leukemia b cells. *Blood*, 111(2):846–55.

[Los et al., 2009] Los, M., Maddika, S., Erb, B., and Schulze-Osthoff, K. (2009). Switching akt: from survival signaling to deadly response. *Bioessays*, 31(5):492–5.

[Luo et al., 2019] Luo, W., Hawse, W., Conter, L., Trivedi, N., Weisel, F., Wikenheiser, D., Cattley, R. T., and Shlomchik, M. J. (2019). The akt kinase signaling network is rewired by pten to control proximal bcr signaling in germinal center b cells. *Nat Immunol*, 20(6):736–746.

[Luo et al., 2018] Luo, W., Weisel, F., and Shlomchik, M. J. (2018). B cell receptor and cd40 signaling are rewired for synergistic induction of the c-myc transcription factor in germinal center b cells. *Immunity*, 48(2):313–326.e5.

[Lutzny et al., 2013] Lutzny, G., Kocher, T., Schmidt-Supprian, M., Rudelius, M., Klein-Hitpass, L., Finch, A. J., Dürig, J., Wagner, M., Haferlach, C., Kohlmann, A., Schnittger, S., Seifert, M., Wanninger, S., Zaborsky, N., Oostendorp, R., Ruland, J., Leitges, M., Kuhnt, T., Schäfer, Y., Lampl, B., Peschel, C., Egle, A., and Ringshausen, I. (2013). Protein kinase c--dependent activation of nf-b in stromal cells is indispensable for the survival of chronic lymphocytic leukemia b cells in vivo. *Cancer Cell*, 23(1):77–92.

[Ma et al., 2013] Ma, J., Yu, X., Guo, L., and Lu, S. H. (2013). Dusp6, a tumor suppressor, is involved in differentiation and apoptosis in esophageal squamous cell carcinoma. *Oncol Lett*, 6(6):1624–1630.

[Mackay and Schneider, 2009] Mackay, F. and Schneider, P. (2009). Cracking the baff code. *Nat Rev Immunol*, 9(7):491–502.

[Mandelbaum et al., 2010] Mandelbaum, J., Bhagat, G., Tang, H., Mo, T., Brahmachary, M., Shen, Q., Chadburn, A., Rajewsky, K., Tarakhovsky, A., Pasqualucci, L., and Dalla-Favera, R. (2010). Blimp1 is a tumor suppressor gene frequently disrupted in activated b cell-like diffuse large b cell lymphoma. *Cancer Cell*, 18(6):568–79.

[Marini et al., 2017] Marini, C., Bruno, S., Fiz, F., Campi, C., Piva, R., Cutrona, G., Matis, S., Nieri, A., Miglino, M., Ibatici, A., Maria Orengo, A., Maria Massone, A., Neumaier, C. E., Totero, D. d., Giannoni, P., Bauckneht, M., Pennone, M., Tenca, C., Gugiatti, E., Bellini, A., Borra, A., Tedone, E., Efetürk, H., Rosa, F., Emionite, L., Cilli, M., Bagnara, D., Brucato, V., Bruzzi, P., Piana, M., Fais, F., and Sambuceti, G. (2017). Functional activation of osteoclast commitment in chronic lymphocytic leukaemia: a possible role for rank/rankl pathway. *Sci Rep*, 7(1):14159.

[Martin et al., 2001] Martin, F., Oliver, A. M., and Kearney, J. F. (2001). Marginal zone and b1 b cells unite in the early response against t-independent blood-borne particulate antigens. *Immunity*, 14(5):617–29.

[Mato et al., 2016] Mato, A. R., Nabhan, C., Barr, P. M., Ujjani, C. S., Hill, B. T., Lamanna, N., Skarbnik, A. P., Howlett, C., Pu, J. J., Sehgal, A. R., Strelec, L. E., Vandegrift, A., Fitzpatrick, D. M., Zent, C. S., Feldman, T., Goy, A., Claxton, D. F., Bachow, S. H., Kaur, G., Svoboda, J., Nasta, S. D., Porter, D., Landsburg, D. J., Schuster, S. J., Cheson, B. D., Kiselev, P., and Evens, A. M. (2016). Outcomes of cll patients treated with sequential kinase inhibitor therapy: a real world experience. *Blood*, 128(18):2199–2205.

[Mauerer et al., 2005] Mauerer, K., Zahrieh, D., Gorgun, G., Li, A., Zhou, J., Ansén, S., Rassenti, L. Z., and Gribben, J. G. (2005). Immunoglobulin gene segment usage, location and immunogenicity in mutated and unmutated chronic lymphocytic leukaemia. *Br J Haematol*, 129(4):499–510.

[Melchers, 2015] Melchers, F. (2015). Checkpoints that control b cell development. *J Clin Invest*, 125(6):2203–10.

[Messmer et al., 2004] Messmer, B. T., Albesiano, E., Efremov, D. G., Ghiotto, F., Allen, S. L., Kolitz, J., Foa, R., Damle, R. N., Fais, F., Messmer, D., Rai, K. R., Ferrarini, M., and Chiorazzi, N. (2004). Multiple distinct sets of stereotyped antigen receptors indicate a role for antigen in promoting chronic lymphocytic leukemia. *J Exp Med*, 200(4):519–25.

[Michaud et al., 2011] Michaud, M., Martins, I., Sukkurwala, A. Q., Adjemian, S., Ma, Y., Pellegatti, P., Shen, S., Kepp, O., Scoazec, M., Mignot, G., Rello-Varona, S., Tailler, M., Menger, L., Vacchelli, E., Galluzzi, L., Ghiringhelli, F., di Virgilio, F., Zitvogel, L., and Kroemer, G. (2011). Autophagy-dependent anticancer immune responses induced by chemotherapeutic agents in mice. *Science*, 334(6062):1573–7.

[Michigami et al., 2000] Michigami, T., Shimizu, N., Williams, P. J., Niewolna, M., Dallas, S. L., Mundy, G. R., and Yoneda, T. (2000). Cell-cell contact between marrow stromal cells and myeloma cells via vcam-1 and alpha(4)beta(1)-integrin enhances production of osteoclast-stimulating activity. *Blood*, 96(5):1953–60.

[Molina et al., 2009] Molina, G., Vogt, A., Bakan, A., Dai, W., Queiroz de Oliveira, P., Znosko, W., Smithgall, T. E., Bahar, I., Lazo, J. S., Day, B. W., and Tsang, M. (2009). Zebrafish chemical screening reveals an inhibitor of dusp6 that expands cardiac cell lineages. *Nat Chem Biol*, 5(9):680–7.

[Montecino-Rodriguez and Dorshkind, 2012] Montecino-Rodriguez, E. and Dorshkind, K. (2012). B-1 b cell development in the fetus and adult. *Immunity*, 36(1):13–21.

[Muramatsu et al., 2000] Muramatsu, M., Kinoshita, K., Fagarasan, S., Yamada, S., Shinkai, Y., and Honjo, T. (2000). Class switch recombination and hypermutation require activation-induced cytidine deaminase (aid), a potential rna editing enzyme. *Cell*, 102(5):553–63.

[Murray et al., 2008] Murray, F., Darzentas, N., Hadzidimitriou, A., Tobin, G., Boudjogra, M., Scielzo, C., Laoutaris, N., Karlsson, K., Baran-Marzsak, F., Tsaftaris,

A., Moreno, C., Anagnostopoulos, A., Caligaris-Cappio, F., Vaur, D., Ouzounis, C., Belessi, C., Ghia, P., Davi, F., Rosenquist, R., and Stamatopoulos, K. (2008). Stereotyped patterns of somatic hypermutation in subsets of patients with chronic lymphocytic leukemia: implications for the role of antigen selection in leukemogenesis. *Blood*, 111(3):1524–33.

[Nemazee, 2017] Nemazee, D. (2017). Mechanisms of central tolerance for b cells. *Nat Rev Immunol*, 17(5):281–294.

[Neumann et al., 2014] Neumann, K., Castiñeiras-Vilariño, M., Höckendorf, U., Hannesschläger, N., Lemeer, S., Kupka, D., Meyermann, S., Lech, M., Anders, H.-J., Kuster, B., Busch, D. H., Gewies, A., Naumann, R., Groß, O., and Ruland, J. (2014). Clec12a is an inhibitory receptor for uric acid crystals that regulates inflammation in response to cell death. *Immunity*, 40(3):389–99.

[Ng and Davids, 2014] Ng, S. Y. and Davids, M. S. (2014). Selective bcl-2 inhibition to treat chronic lymphocytic leukemia and non-hodgkin lymphoma. *Clin Adv Hematol Oncol*, 12(4):224–9.

[Nickel et al., 2016] Nickel, N., Al-Maarri, M., Pal, M., Roth, A., Knittel, G., Herling, C. D., Reinart, N., Schäfer, S., Hartmann, E. M., Rosenwald, A., Klapper, W., Büttner, R., Herling, M., Bruening, J., Reinhardt, C., Hallek, M., Wunderlich, T., and Pallasch, C. (2016). Transformation of Chronic Lymphocytic Leukemia Towards Richter´s Syndrome Is Induced By AKT Activation. *Blood*, 128(22):2031–2031.

[Nieuwenhuis and Opstelten, 1984] Nieuwenhuis, P. and Opstelten, D. (1984). Functional anatomy of germinal centers. *Am J Anat*, 170(3):421–35.

[Nitschke, 2005] Nitschke, L. (2005). The role of cd22 and other inhibitory coreceptors in b-cell activation. *Curr Opin Immunol*, 17(3):290–7.

[Nuñez et al., 1996] Nuñez, C., Nishimoto, N., Gartland, G. L., Billips, L. G., Burrows, P. D., Kubagawa, H., and Cooper, M. D. (1996). B cells are generated throughout life in humans. *J Immunol*, 156(2):866–72.

[O'Brien, 2008] O'Brien, S. (2008). New agents in the treatment of cll. *Hematology Am Soc Hematol Educ Program*, pages 457–64.

[Obukhanych and Nussenzweig, 2006] Obukhanych, T. V. and Nussenzweig, M. C. (2006). T-independent type ii immune responses generate memory b cells. *J Exp Med*, 203(2):305–10.

[Ochi and Watanabe, 2000] Ochi, H. and Watanabe, T. (2000). Negative regulation of b cell receptor-mediated signaling in b-1 cells through cd5 and ly49 co-receptors via lyn kinase activity. *Int Immunol*, 12(10):1417–23.

[Ortiz-Maldonado et al., 2015] Ortiz-Maldonado, V., García-Morillo, M., and Delgado, J. (2015). The biology behind pi3k inhibition in chronic lymphocytic leukaemia. *Ther Adv Hematol*, 6(1):25–36.

[Oscier et al., 1997] Oscier, D. G., Thompsett, A., Zhu, D., and Stevenson, F. K. (1997). Differential rates of somatic hypermutation in v(h) genes among subsets of chronic lymphocytic leukemia defined by chromosomal abnormalities. *Blood*, 89(11):4153–60.

[Palanichamy et al., 2009] Palanichamy, A., Barnard, J., Zheng, B., Owen, T., Quach, T., Wei, C., Looney, R. J., Sanz, I., and Anolik, J. H. (2009). Novel human transitional b cell populations revealed by b cell depletion therapy. *J Immunol*, 182(10):5982–93.

[Pauls and Marshall, 2017] Pauls, S. D. and Marshall, A. J. (2017). Regulation of immune cell signaling by ship1: A phosphatase, scaffold protein, and potential therapeutic target. *Eur J Immunol*, 47(6):932–945.

[Pedersen et al., 2009] Pedersen, I. M., Otero, D., Kao, E., Miletic, A. V., Hother, C., Ralfkiaer, E., Rickert, R. C., Gronbaek, K., and David, M. (2009). Onco-mir-155 targets ship1 to promote tnfalpha-dependent growth of b cell lymphomas. *EMBO Mol Med*, 1(5):288–95.

[Pekarsky et al., 2007] Pekarsky, Y., Zanesi, N., Aqeilan, R. I., and Croce, C. M. (2007). Animal models for chronic lymphocytic leukemia. *J Cell Biochem*, 100(5):1109–18.

[Pelanda and Torres, 2012] Pelanda, R. and Torres, R. M. (2012). Central b-cell tolerance: where selection begins. *Cold Spring Harb Perspect Biol*, 4(4):a007146.

[Pennycook et al., 1993] Pennycook, J. L., Chang, Y., Celler, J., Phillips, R. A., and Wu, G. E. (1993). High frequency of normal djh joints in b cell progenitors in severe combined immunodeficiency mice. *J Exp Med*, 178(3):1007–16.

[Perlot and Penninger, 2012] Perlot, T. and Penninger, J. M. (2012). Development and function of murine b cells lacking rank. *J Immunol*, 188(3):1201–5.

[Peterson and Kini, 2001] Peterson, L. and Kini, A. R. (2001). Angiogenesis is increased in b-cell chronic lymphocytic leukemia. *Blood*, 97(8):2529.

[Pinilla-Ibarz and Chavez, 2015] Pinilla-Ibarz, J. and Chavez, J. C. (2015). Life after ibrutinib? a new unmet need in cll. *Blood*, 125(13):2013–4.

[Pleasance et al., 2010] Pleasance, E. D., Cheetham, R. K., Stephens, P. J., McBride, D. J., Humphray, S. J., Greenman, C. D., Varela, I., Lin, M.-L., Ordóñez, G. R., Bignell, G. R., Ye, K., Alipaz, J., Bauer, M. J., Beare, D., Butler, A., Carter, R. J., Chen, L., Cox, A. J., Edkins, S., Kokko-Gonzales, P. I., Gormley, N. A., Grocock, R. J., Haudenschild, C. D., Hims, M. M., James, T., Jia, M., Kingsbury, Z., Leroy, C., Marshall, J., Menzies, A., Mudie, L. J., Ning, Z., Royce, T., Schulz-Trieglaff, O. B., Spiridou, A., Stebbings, L. A., Szajkowski, L., Teague, J., Williamson, D., Chin, L., Ross, M. T., Campbell, P. J., Bentley, D. R., Futreal, P. A., and Stratton, M. R. (2010). A comprehensive catalogue of somatic mutations from a human cancer genome. *Nature*, 463(7278):191–6.

[Porter et al., 2011] Porter, D. L., Levine, B. L., Kalos, M., Bagg, A., and June, C. H. (2011). Chimeric antigen receptor-modified t cells in chronic lymphoid leukemia. *N Engl J Med*, 365(8):725–33.

[Pratilas et al., 2009] Pratilas, C. A., Taylor, B. S., Ye, Q., Viale, A., Sander, C., Solit, D. B., and Rosen, N. (2009). (v600e)braf is associated with disabled feedback inhibition of raf-mek signaling and elevated transcriptional output of the pathway. *Proc Natl Acad Sci U S A*, 106(11):4519–24.

[Puente et al., 2015] Puente, X. S., Beà, S., Valdés-Mas, R., Villamor, N., Gutiérrez-Abril, J., Martín-Subero, J. I., Munar, M., Rubio-Pérez, C., Jares, P., Aymerich, M., Baumann, T., Beekman, R., Belver, L., Carrio, A., Castellano, G., Clot, G., Colado, E., Colomer, D., Costa, D., Delgado, J., Enjuanes, A., Estivill, X., Ferrando, A. A., Gelpí, J. L., González, B., González, S., González, M., Gut, M., Hernández-Rivas, J. M., López-Guerra, M., Martín-García, D., Navarro, A., Nicolás, P., Orozco, M., Payer, Á. R., Pinyol, M., Pisano, D. G., Puente, D. A., Queirós, A. C., Quesada, V., Romeo-Casabona, C. M., Royo, C., Royo, R., Rozman, M., Russiñol, N., Salaverría, I., Stamatopoulos, K., Stunnenberg, H. G., Tamborero, D., Terol, M. J., Valencia, A., López-Bigas, N., Torrents, D., Gut, I., López-Guillermo, A., López-Otín, C., and Campo, E. (2015). Non-coding recurrent mutations in chronic lymphocytic leukaemia. *Nature*, 526(7574):519–24.

[Puente et al., 2011] Puente, X. S., Pinyol, M., Quesada, V., Conde, L., Ordóñez, G. R., Villamor, N., Escaramis, G., Jares, P., Beà, S., González-Díaz, M., Bassaganyas, L., Baumann, T., Juan, M., López-Guerra, M., Colomer, D., Tubío, J. M. C., López, C., Navarro, A., Tornador, C., Aymerich, M., Rozman, M., Hernández, J. M., Puente, D. A., Freije, J. M. P., Velasco, G., Gutiérrez-Fernández, A., Costa, D., Carrió, A., Guijarro, S., Enjuanes, A., Hernández, L., Yagüe, J., Nicolás, P., Romeo-Casabona, C. M., Himmelbauer, H., Castillo, E., Dohm, J. C., de Sanjosé, S., Piris, M. A., de Alava, E., San Miguel, J., Royo, R., Gelpí, J. L., Torrents, D., Orozco, M., Pisano, D. G., Valencia, A., Guigó, R., Bayés, M., Heath, S., Gut, M., Klatt, P., Marshall, J., Raine, K., Stebbings, L. A., Futreal, P. A., Stratton, M. R., Campbell, P. J., Gut, I., López-Guillermo, A., Estivill, X., Montserrat, E., López-Otín, C., and Campo, E. (2011). Whole-genome sequencing identifies recurrent mutations in chronic lymphocytic leukaemia. *Nature*, 475(7354):101–5.

[Purroy and Wu, 2017] Purroy, N. and Wu, C. J. (2017). Coevolution of leukemia and host immune cells in chronic lymphocytic leukemia. *Cold Spring Harb Perspect Med*, 7(4).

[Qiu et al., 2018] Qiu, X., Zhang, Y., and Han, J. (2018). Rip3 is an upregulator of aerobic metabolism and the enhanced respiration by necrosomal rip3 feeds back on necrosome to promote necroptosis. *Cell Death Differ*, 25(5):821–824.

[Rai et al., 2000] Rai, K. R., Peterson, B. L., Appelbaum, F. R., Kolitz, J., Elias, L., Shepherd, L., Hines, J., Threatte, G. A., Larson, R. A., Cheson, B. D., and Schiffer, C. A. (2000). Fludarabine compared with chlorambucil as primary therapy for chronic lymphocytic leukemia. *N Engl J Med*, 343(24):1750–7.

[Rajesh et al., 2015] Rajesh, K., Krishnamoorthy, J., Kazimierczak, U., Tenkerian, C., Papadakis, A. I., Wang, S., Huang, S., and Koromilas, A. E. (2015). Phosphorylation of the translation initiation factor eif2 at serine 51 determines the cell fate decisions of akt in response to oxidative stress. *Cell Death Dis*, 6:e1591.

[Ran et al., 2013] Ran, F. A., Hsu, P. D., Wright, J., Agarwala, V., Scott, D. A., and Zhang, F. (2013). Genome engineering using the crispr-cas9 system. *Nat Protoc*, 8(11):2281–2308.

[Rassenti et al., 2004] Rassenti, L. Z., Huynh, L., Toy, T. L., Chen, L., Keating, M. J., Gribben, J. G., Neuberg, D. S., Flinn, I. W., Rai, K. R., Byrd, J. C., Kay, N. E., Greaves, A., Weiss, A., and Kipps, T. J. (2004). Zap-70 compared with immunoglobulin heavy-chain gene mutation status as a predictor of disease progression in chronic lymphocytic leukemia. *N Engl J Med*, 351(9):893–901.

[Rickert et al., 2011] Rickert, R. C., Jellusova, J., and Miletic, A. V. (2011). Signaling by the tumor necrosis factor receptor superfamily in b-cell biology and disease. *Immunol Rev*, 244(1):115–33.

[Rickert et al., 1997] Rickert, R. C., Roes, J., and Rajewsky, K. (1997). B lymphocyte-specific, cre-mediated mutagenesis in mice. *Nucleic Acids Res*, 25(6):1317–8.

[Rosenwald et al., 2001] Rosenwald, A., Alizadeh, A. A., Widhopf, G., Simon, R., Davis, R. E., Yu, X., Yang, L., Pickeral, O. K., Rassenti, L. Z., Powell, J., Botstein, D., Byrd, J. C., Grever, M. R., Cheson, B. D., Chiorazzi, N., Wilson, W. H., Kipps, T. J., Brown, P. O., and Staudt, L. M. (2001). Relation of gene expression phenotype to immunoglobulin mutation genotype in b cell chronic lymphocytic leukemia. *J Exp Med*, 194(11):1639–47.

[Rowley et al., 2007] Rowley, B., Tang, L., Shinton, S., Hayakawa, K., and Hardy, R. R. (2007). Autoreactive b-1 b cells: constraints on natural autoantibody b cell antigen receptors. *J Autoimmun*, 29(4):236–45.

[Ruprecht et al., 2015] Ruprecht, B., Koch, H., Medard, G., Mundt, M., Kuster, B., and Lemeer, S. (2015). Comprehensive and reproducible phosphopeptide enrichment using iron immobilized metal ion affinity chromatography (fe-imac) columns. *Mol Cell Proteomics*, 14(1):205–15.

[Sabattini et al., 2010] Sabattini, E., Bacci, F., Sagramoso, C., and Pileri, S. A. (2010). Who classification of tumours of haematopoietic and lymphoid tissues in 2008: an overview. *Pathologica*, 102(3):83–7.

[Saijo et al., 2002] Saijo, K., Mecklenbräuker, I., Santana, A., Leitger, M., Schmedt, C., and Tarakhovsky, A. (2002). Protein kinase c beta controls nuclear factor kappab activation in b cells through selective regulation of the ikappab kinase alpha. *J Exp Med*, 195(12):1647–52.

[Sanli et al., 2014] Sanli, T., Steinberg, G. R., Singh, G., and Tsakiridis, T. (2014). Amp-activated protein kinase (ampk) beyond metabolism: a novel genomic stress sensor participating in the dna damage response pathway. *Cancer Biol Ther*, 15(2):156–69.

[Savitsky et al., 1995] Savitsky, K., Bar-Shira, A., Gilad, S., Rotman, G., Ziv, Y., Vanagaite, L., Tagle, D. A., Smith, S., Uziel, T., Sfez, S., Ashkenazi, M., Pecker, I., Frydman, M., Harnik, R., Patanjali, S. R., Simmons, A., Clines, G. A., Sartiel, A., Gatti, R. A., Chessa, L., Sanal, O., Lavin, M. F., Jaspers, N. G., Taylor, A. M., Arlett, C. F., Miki, T., Weissman, S. M., Lovett, M., Collins, F. S., and Shiloh, Y. (1995). A single ataxia telangiectasia gene with a product similar to pi-3 kinase. *Science*, 268(5218):1749–53.

[Schambach et al., 2006] Schambach, A., Galla, M., Modlich, U., Will, E., Chandra, S., Reeves, L., Colbert, M., Williams, D. A., von Kalle, C., and Baum, C. (2006). Lentiviral vectors pseudotyped with murine ecotropic envelope: increased biosafety and convenience in preclinical research. *Exp Hematol*, 34(5):588–92.

[Schmiedel et al., 2013] Schmiedel, B. J., Scheible, C. A., Nuebling, T., Kopp, H.-G., Wirths, S., Azuma, M., Schneider, P., Jung, G., Grosse-Hovest, L., and Salih, H. R. (2013). Rankl expression, function, and therapeutic targeting in multiple myeloma and chronic lymphocytic leukemia. *Cancer Res*, 73(2):683–94.

[Schrader et al., 2014] Schrader, A., Popal, W., Lilienthal, N., Crispatzu, G., Mayer, P., Jones, D., Hallek, M., and Herling, M. (2014). Akt-pathway inhibition in chronic lymphocytic leukemia reveals response relationships defined by tcl1. *Curr Cancer Drug Targets*, 14(8):700–12.

[Schreiber et al., 2011] Schreiber, R. D., Old, L. J., and Smyth, M. J. (2011). Cancer immunoediting: integrating immunity's roles in cancer suppression and promotion. *Science*, 331(6024):1565–70.

[Secchiero et al., 2006] Secchiero, P., Corallini, F., Barbarotto, E., Melloni, E., di Iasio, M. G., Tiribelli, M., and Zauli, G. (2006). Role of the rankl/rank system in the induction of interleukin-8 (il-8) in b chronic lymphocytic leukemia (b-cll) cells. *J Cell Physiol*, 207(1):158–64.

[Seifert et al., 2012] Seifert, M., Sellmann, L., Bloehdorn, J., Wein, F., Stilgenbauer, S., Dürig, J., and Küppers, R. (2012). Cellular origin and pathophysiology of chronic lymphocytic leukemia. *J Exp Med*, 209(12):2183–98.

[Shehata et al., 2010] Shehata, M., Schnabl, S., Demirtas, D., Hilgarth, M., Hubmann, R., Ponath, E., Badrnya, S., Lehner, C., Hoelbl, A., Duechler, M., Gaiger, A., Zielinski, C., Schwarzmeier, J. D., and Jaeger, U. (2010). Reconstitution of pten activity by ck2 inhibitors and interference with the pi3-k/akt cascade counteract the antiapoptotic effect of human stromal cells in chronic lymphocytic leukemia. *Blood*, 116(14):2513–21.

[Shlomchik et al., 2019] Shlomchik, M. J., Luo, W., and Weisel, F. (2019). Linking signaling and selection in the germinal center. *Immunol Rev*, 288(1):49–63.

[Shojaee et al., 2015] Shojaee, S., Caeser, R., Buchner, M., Park, E., Swaminathan, S., Hurtz, C., Geng, H., Chan, L. N., Klemm, L., Hofmann, W.-K., Qiu, Y. H., Zhang, N., Coombes, K. R., Paietta, E., Molkentin, J., Koeffler, H. P., Willman,

C. L., Hunger, S. P., Melnick, A., Kornblau, S. M., and Müschen, M. (2015). Erk negative feedback control enables pre-b cell transformation and represents a therapeutic target in acute lymphoblastic leukemia. *Cancer Cell*, 28(1):114–28.

[Sindhava and Bondada, 2012] Sindhava, V. J. and Bondada, S. (2012). Multiple regulatory mechanisms control b-1 b cell activation. *Front Immunol*, 3:372.

[Sly et al., 2003] Sly, L. M., Rauh, M. J., Kalesnikoff, J., Büchse, T., and Krystal, G. (2003). Ship, ship2, and pten activities are regulated in vivo by modulation of their protein levels: Ship is up-regulated in macrophages and mast cells by lipopolysaccharide. *Exp Hematol*, 31(12):1170–81.

[Smulski and Eibel, 2018] Smulski, C. R. and Eibel, H. (2018). Baff and baff-receptor in b cell selection and survival. *Front Immunol*, 9:2285.

[Soneoka et al., 1995] Soneoka, Y., Cannon, P. M., Ramsdale, E. E., Griffiths, J. C., Romano, G., Kingsman, S. M., and Kingsman, A. J. (1995). A transient three-plasmid expression system for the production of high titer retroviral vectors. *Nucleic Acids Res*, 23(4):628–33.

[Song et al., 2005] Song, G., Ouyang, G., and Bao, S. (2005). The activation of akt/pkb signaling pathway and cell survival. *J Cell Mol Med*, 9(1):59–71.

[Stamatopoulos et al., 2007] Stamatopoulos, K., Belessi, C., Moreno, C., Boudjograh, M., Guida, G., Smilevska, T., Belhoul, L., Stella, S., Stavroyianni, N., Crespo, M., Hadzidimitriou, A., Sutton, L., Bosch, F., Laoutaris, N., Anagnostopoulos, A., Montserrat, E., Fassas, A., Dighiero, G., Caligaris-Cappio, F., Merle-Béral, H., Ghia, P., and Davi, F. (2007). Over 20% of patients with chronic lymphocytic leukemia carry stereotyped receptors: Pathogenetic implications and clinical correlations. *Blood*, 109(1):259–70.

[Stylianopoulos, 2013] Stylianopoulos, T. (2013). Epr-effect: utilizing size-dependent nanoparticle delivery to solid tumors. *Ther Deliv*, 4(4):421–3.

[Su et al., 1999] Su, L., Rickert, R. C., and David, M. (1999). Rapid stat phosphorylation via the b cell receptor. modulatory role of cd19. *J Biol Chem*, 274(45):31770–4.

[Suzuki et al., 2003] Suzuki, A., Kaisho, T., Ohishi, M., Tsukio-Yamaguchi, M., Tsubata, T., Koni, P. A., Sasaki, T., Mak, T. W., and Nakano, T. (2003). Critical roles of pten in b cell homeostasis and immunoglobulin class switch recombination. *J Exp Med*, 197(5):657–67.

[Swann and Smyth, 2007] Swann, J. B. and Smyth, M. J. (2007). Immune surveillance of tumors. *J Clin Invest*, 117(5):1137–46.

[Täger et al., 2017] Täger, M., Horn, S., Latuske, E., Ehm, P., Schaks, M., Nalaskowski, M., Fehse, B., Fiedler, W., Stocking, C., Wellbrock, J., and Jücker, M. (2017). Ship1, but not an aml-derived ship1 mutant, suppresses myeloid leukemia growth in a xenotransplantation mouse model. *Gene Ther*, 24(11):749–753.

[Tarlinton, 2006] Tarlinton, D. (2006). B-cell memory: are subsets necessary? *Nat Rev Immunol*, 6(10):785–90.

[Ten Hacken and Burger, 2016] Ten Hacken, E. and Burger, J. A. (2016). Microenvironment interactions and b-cell receptor signaling in chronic lymphocytic leukemia: Implications for disease pathogenesis and treatment. *Biochim Biophys Acta*, 1863(3):401–413.

[Tobón et al., 2013] Tobón, G. J., Izquierdo, J. H., and Cañas, C. A. (2013). B lymphocytes: development, tolerance, and their role in autoimmunity-focus on systemic lupus erythematosus. *Autoimmune Dis*, 2013:827254.

[Tonegawa, 1983] Tonegawa, S. (1983). Somatic generation of antibody diversity. *Nature*, 302(5909):575–81.

[Tsubata, 2012] Tsubata, T. (2012). Role of inhibitory bcr co-receptors in immunity. *Infect Disord Drug Targets*, 12(3):181–90.

[Turner et al., 2000] Turner, M., Schweighoffer, E., Colucci, F., Di Santo, J. P., and Tybulewicz, V. L. (2000). Tyrosine kinase syk: essential functions for immunoreceptor signalling. *Immunol Today*, 21(3):148–54.

[Vanhaesebroeck et al., 1997] Vanhaesebroeck, B., Welham, M. J., Kotani, K., Stein, R., Warne, P. H., Zvelebil, M. J., Higashi, K., Volinia, S., Downward, J., and

Waterfield, M. D. (1997). P110delta, a novel phosphoinositide 3-kinase in leukocytes. *Proc Natl Acad Sci U S A*, 94(9):4330–5.

[Vanura et al., 2008] Vanura, K., Le, T., Esterbauer, H., Späth, F., Porpaczy, E., Shehata, M., Eigenberger, K., Hauswirth, A., Skrabs, C., Krömer, E., Schwarzinger, I., Streubel, B., Steininger, C., Fonatsch, C., Stilgenbauer, S., Wagner, O., Gaiger, A., and Jäger, U. (2008). Autoimmune conditions and chronic infections in chronic lymphocytic leukemia patients at diagnosis are associated with unmutated igvh genes. *Haematologica*, 93(12):1912–6.

[Vincent et al., 2014] Vincent, F. B., Morand, E. F., Schneider, P., and Mackay, F. (2014). The baff/april system in sle pathogenesis. *Nat Rev Rheumatol*, 10(6):365–73.

[Wada et al., 2006] Wada, T., Nakashima, T., Hiroshi, N., and Penninger, J. M. (2006). Rankl-rank signaling in osteoclastogenesis and bone disease. *Trends Mol Med*, 12(1):17–25.

[Walsh and Choi, 2014] Walsh, M. C. and Choi, Y. (2014). Biology of the rankl-rank-opg system in immunity, bone, and beyond. *Front Immunol*, 5:511.

[Wang et al., 2016] Wang, J., Zhou, J.-Y., Kho, D., Reiners, Jr, J. J., and Wu, G. S. (2016). Role for dusp1 (dual-specificity protein phosphatase 1) in the regulation of autophagy. *Autophagy*, 12(10):1791–1803.

[Wang et al., 2011] Wang, L., Lawrence, M. S., Wan, Y., Stojanov, P., Sougnez, C., Stevenson, K., Werner, L., Sivachenko, A., DeLuca, D. S., Zhang, L., Zhang, W., Vartanov, A. R., Fernandes, S. M., Goldstein, N. R., Folco, E. G., Cibulskis, K., Tesar, B., Sievers, Q. L., Shefler, E., Gabriel, S., Hacohen, N., Reed, R., Meyerson, M., Golub, T. R., Lander, E. S., Neuberg, D., Brown, J. R., Getz, G., and Wu, C. J. (2011). Sf3b1 and other novel cancer genes in chronic lymphocytic leukemia. *N Engl J Med*, 365(26):2497–506.

[Wardemann et al., 2003] Wardemann, H., Yurasov, S., Schaefer, A., Young, J. W., Meffre, E., and Nussenzweig, M. C. (2003). Predominant autoantibody production by early human b cell precursors. *Science*, 301(5638):1374–7.

[Wierda et al., 2010] Wierda, W. G., Kipps, T. J., Mayer, J., Stilgenbauer, S., Williams, C. D., Hellmann, A., Robak, T., Furman, R. R., Hillmen, P., Trneny, M., Dyer, M. J. S., Padmanabhan, S., Piotrowska, M., Kozak, T., Chan, G., Davis, R., Losic, N., Wilms, J., Russell, C. A., Osterborg, A., and Hx-CD20-406 Study Investigators (2010). Ofatumumab as single-agent cd20 immunotherapy in fludarabine-refractory chronic lymphocytic leukemia. *J Clin Oncol*, 28(10):1749–55.

[Wilson et al., 2015] Wilson, W. H., Young, R. M., Schmitz, R., Yang, Y., Pittaluga, S., Wright, G., Lih, C.-J., Williams, P. M., Shaffer, A. L., Gerecitano, J., de Vos, S., Goy, A., Kenkre, V. P., Barr, P. M., Blum, K. A., Shustov, A., Advani, R., Fowler, N. H., Vose, J. M., Elstrom, R. L., Habermann, T. M., Barrientos, J. C., McGreivy, J., Fardis, M., Chang, B. Y., Clow, F., Munneke, B., Moussa, D., Beaupre, D. M., and Staudt, L. M. (2015). Targeting b cell receptor signaling with ibrutinib in diffuse large b cell lymphoma. *Nat Med*, 21(8):922–6.

[Wong et al., 2012] Wong, V. C. L., Chen, H., Ko, J. M. Y., Chan, K. W., Chan, Y. P., Law, S., Chua, D., Kwong, D. L.-W., Lung, H. L., Srivastava, G., Tang, J. C. O., Tsao, S. W., Zabarovsky, E. R., Stanbridge, E. J., and Lung, M. L. (2012). Tumor suppressor dual-specificity phosphatase 6 (dusp6) impairs cell invasion and epithelial-mesenchymal transition (emt)-associated phenotype. *Int J Cancer*, 130(1):83–95.

[Woyach, 2015] Woyach, J. A. (2015). Patterns of resistance to b cell-receptor pathway antagonists in chronic lymphocytic leukemia and strategies for management. *Hematology Am Soc Hematol Educ Program*, 2015:355–60.

[Woyach, 2017] Woyach, J. A. (2017). How i manage ibrutinib-refractory chronic lymphocytic leukemia. *Blood*, 129(10):1270–1274.

[Woyach et al., 2014] Woyach, J. A., Furman, R. R., Liu, T.-M., Ozer, H. G., Zapatka, M., Ruppert, A. S., Xue, L., Li, D. H.-H., Steggerda, S. M., Versele, M., Dave, S. S., Zhang, J., Yilmaz, A. S., Jaglowski, S. M., Blum, K. A., Lozanski, A., Lozanski, G., James, D. F., Barrientos, J. C., Lichter, P., Stilgenbauer, S., Buggy, J. J., Chang, B. Y., Johnson, A. J., and Byrd, J. C. (2014). Resistance mechanisms for the bruton's tyrosine kinase inhibitor ibrutinib. *N Engl J Med*, 370(24):2286–94.

[Woyach and Johnson, 2015] Woyach, J. A. and Johnson, A. J. (2015). Targeted therapies in cll: mechanisms of resistance and strategies for management. *Blood*, 126(4):471–7.

[Yun et al., 1998] Yun, T. J., Chaudhary, P. M., Shu, G. L., Frazer, J. K., Ewings, M. K., Schwartz, S. M., Pascual, V., Hood, L. E., and Clark, E. A. (1998). Opg/fdcr-1, a tnf receptor family member, is expressed in lymphoid cells and is up-regulated by ligating cd40. *J Immunol*, 161(11):6113–21.

[Zenz et al., 2019] Zenz, T., Luetge, A., Lu, J., Jennifer, H., Dietrich, S., Sellner, L., and Huber, W. (2019). Transcriptional Profiling Reveals Strong Impact of Major Molecular Disease Subgroups and Mixed Epistasis in Chronic Lymphocytic Leukemia. *Blood*, 134(Supplement$_1$) : 1742 − −1742.

[Zenz et al., 2010] Zenz, T., Vollmer, D., Trbusek, M., Smardova, J., Benner, A., Soussi, T., Helfrich, H., Heuberger, M., Hoth, P., Fuge, M., Denzel, T., Häbe, S., Malcikova, J., Kuglik, P., Truong, S., Patten, N., Wu, L., Oscier, D., Ibbotson, R., Gardiner, A., Tracy, I., Lin, K., Pettitt, A., Pospisilova, S., Mayer, J., Hallek, M., Döhner, H., Stilgenbauer, S., and European Research Initiative on CLL (ERIC) (2010). Tp53 mutation profile in chronic lymphocytic leukemia: evidence for a disease specific profile from a comprehensive analysis of 268 mutations. *Leukemia*, 24(12):2072–9.

[Zhang et al., 2009] Zhang, D.-W., Shao, J., Lin, J., Zhang, N., Lu, B.-J., Lin, S.-C., Dong, M.-Q., and Han, J. (2009). Rip3, an energy metabolism regulator that switches tnf-induced cell death from apoptosis to necrosis. *Science*, 325(5938):332–6.

[Zhang et al., 2013] Zhang, M., Yogesha, S. D., Mayfield, J. E., Gill, G. N., and Zhang, Y. (2013). Viewing serine/threonine protein phosphatases through the eyes of drug designers. *FEBS J*, 280(19):4739–60.

[Zhuang et al., 2010] Zhuang, J., Hawkins, S. F., Glenn, M. A., Lin, K., Johnson, G. G., Carter, A., Cawley, J. C., and Pettitt, A. R. (2010). Akt is activated in chronic lymphocytic leukemia cells and delivers a pro-survival signal: the therapeutic potential of akt inhibition. *Haematologica*, 95(1):110–8.

[Zou et al., 2015] Zou, Z.-J., Fan, L., Wang, L., Xu, J., Zhang, R., Tian, T., Li, J.-Y., and Xu, W. (2015). mir-26a and mir-214 down-regulate expression of the pten gene

in chronic lymphocytic leukemia, but not pten mutation or promoter methylation. *Oncotarget*, 6(2):1276–85.

Chapter 8

Acknowledgements

First and foremost, I would like to thank my supervisor Maike Buchner, for accepting me as PhD student and providing me with all the expertise and resources I needed. Maike, thank you for your trust and our side by side work during my start of the doctoral thesis that let me learn so quickly from you. Also for your open ear over the years and the freedom you provided me to follow my own interests and develop as person and researcher. Thank you for an unforgettable time and experience during the ASH conference in San Diego, for your support of my research stay at City of Hope, and other national and international conferences you encouraged and allowed me to join. Personally and professionally, I could not have wished for a better supervisor and friend during the last couple of years.

Moreover, I want to thank Jürgen Ruland and Bernhard Küster for being part of my thesis committee, for fruitful discussions and support throughout the years.

This whole work would have been impossible without the help and support of a great team, most importantly Martina Braun, Tanja Neumayer and Begüm Alankus. Thank you for our fantastic team work, for discussions, joint projects and experiments, and for our friendship that made the atmosphere in the laboratory so unique and enjoyable. Thank you Begüm for collaborating on the Rank project and for an unforgettable time we shared during our common time as PhDs. Tanja, thank you for excellent technical support and your contagous energy and good mood you shared with us. Martina, I cannot put in words the value you brought to our group, on a professional and friendship level. Thank you for our excellent working relationship

and our crazyness, that matched so perfectly to each other and lighted up even the difficult days - Grazie!

Thanks to all AG Buchner members, Lisa, Lotte and Sukanya for great help, team work and spirit. Moreover, I want to thank the whole AG Ruland and former members, in particular Lara, Marc, Andi, Ramona, Tim, Konsti, Zsuzsanna, Konstanze and Paul, for discussions and exchange of knowledge. A warm thanks goes to the original "AG Opelhalle", where everything started under an extraordinary environment to work. Thanks to the Elite Network of Bavaria and the iTarget community, for interesting seminars, workshops, conferences and constructive feedback, and for resulting collaborations.

Thanks to all our collaboration partners: Piero Giansanti (TUM) for performing the phosphoproteome analysis. Our collaboration partners and nanoparticle experts in Utrecht, Marcel Fens and Aida Varela-Moreira, who worked on optimizing the delivery of BCI. Heike Bittersohl (TUM) for the support with HPLC measurements. Manfred Jücker (UKE Hamburg) for providing the SHIP1 knockdown constructs and collaborating on SHIP1 activity measurements. Clemens Wendtner (München Klinik Schwabing), Thorsten Zenz (Universitätsspital Zürich) and Christian Bogner (TUM) for providing us with CLL patient samples and Junyan Lu (DKFZ Heidelberg) for sharing CLL patient RNA sequencing data.

Importantly, I want to thank all my friends, that supported me during the last couple of years. Especially my "family" and "Herzensmenschen". Thank you for not really knowing what a pipette is, and for reminding me that a life outside the lab exists. Thanks to my "Hubis" - with you everything began during our biomedical science studies in Marburg, where friendships for life started, and pipette boys were charged. It is impossible to mention every single support, but special thanks to: all recent hosts and couch provider, Yari, all Johanniscafe, Biergarten, Bartour friends, the "Donnerstag-los-Macher", the "little Friday" founder, the FC Stern family, the eastconnect crew and the "Stromstüberl". Not to forget: thank you coffee and road sandwich!

Zu guter Letzt, möchte ich mich bei meinen Eltern, Geschwistern und den Kaisers bedanken. Die gemeinsame Zeit in der Heimat war immer ein großartiger Ausgleich für mich und hat mir stets Energie gegeben um meine Arbeit fortzusetzen. Unser

Zusammenhalt als Familie in guten und schlechten Zeiten hat mich über die Zeit begleitet und uns näher zusammengebracht. Liebe Mama und lieber Papa, vielen Dank für eure grenzenlose Unterstützung über alle Jahre und euer Vertrauen in meine Entscheidungen. Ich bin unendlich dankbar, den Abschluss meiner Doktorarbeit mit euch gemeinsam zu erreichen und möchte euch von Herzen diese Arbeit widmen.